Thierry Roncalli

Handbook of Financial Risk Management

Chapter 1

Introduction

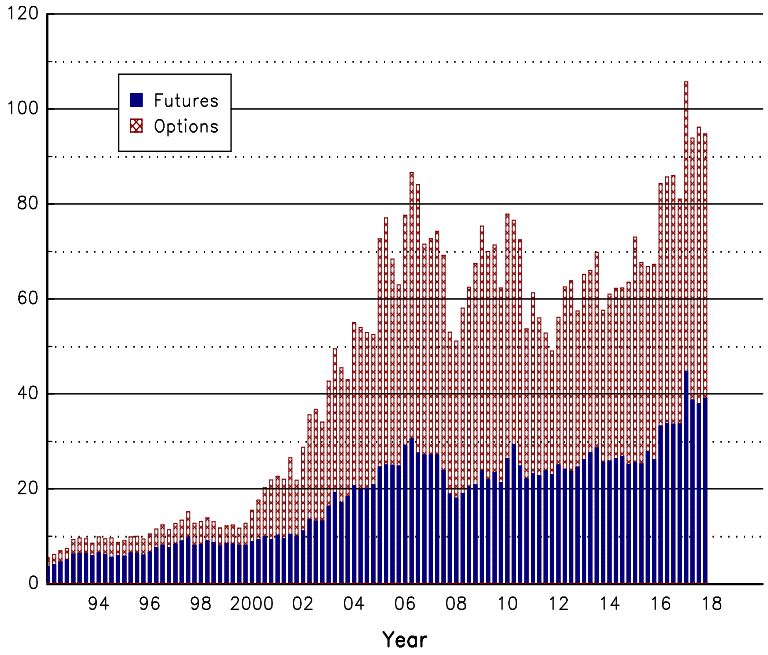

FIGURE 1.1: Notional outstanding amount of exchange-traded derivatives (in $ tn)

Source: Bank for International Settlement (2019) and author's calculations.

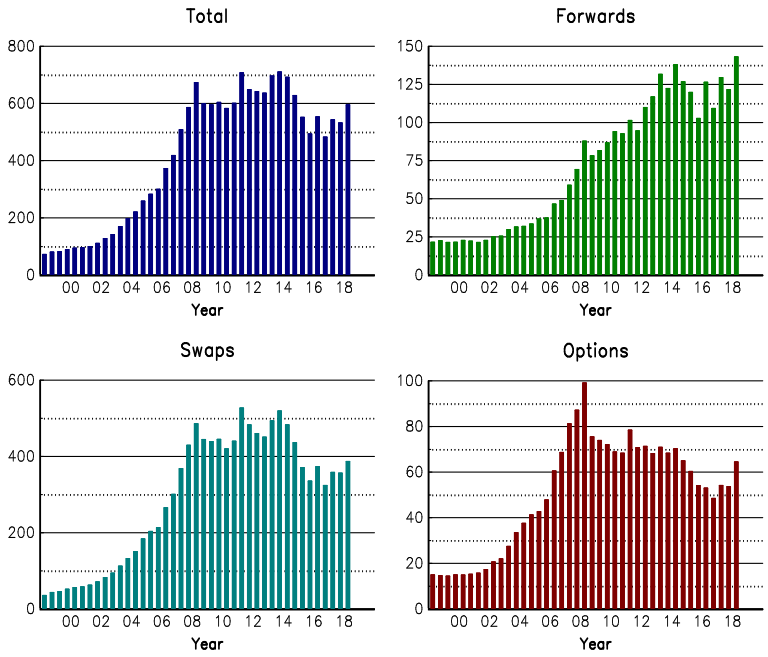

FIGURE 1.2: Notional outstanding amount of OTC derivatives (in $ tn)

Source: Bank for International Settlement (2019).

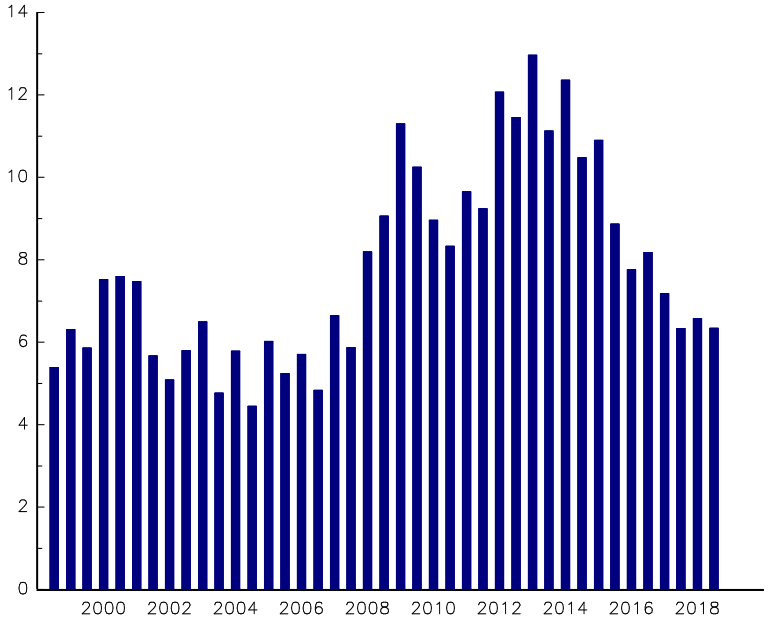

FIGURE 1.3: Ratio OTC derivatives/exchange-traded derivatives

Source: Bank for International Settlement (2019).

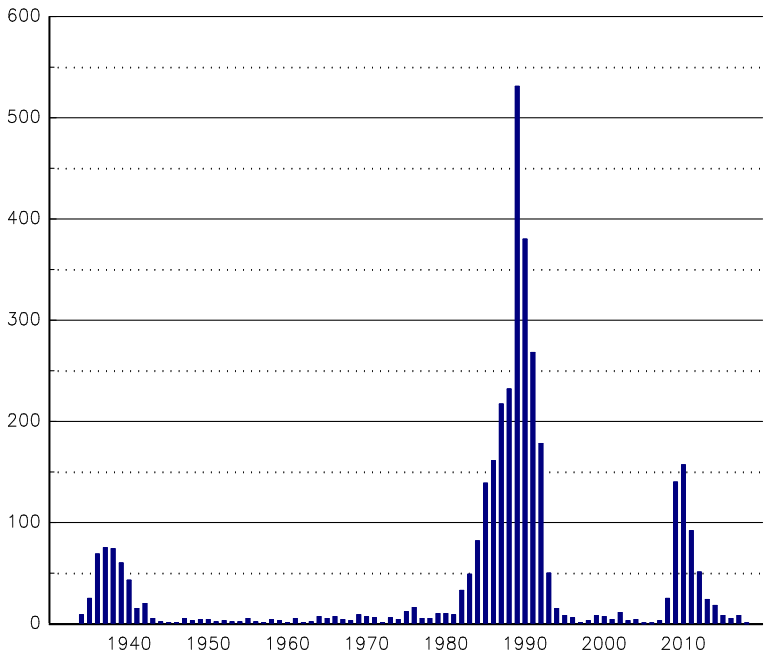

FIGURE 1.4: Number of bank defaults in the US

Source: Federal Deposit Insurance Corporation, Historical Statistics on Banking – Failures & Assistance Transactions, `www.fdic.gov/bank/individual/failed`.

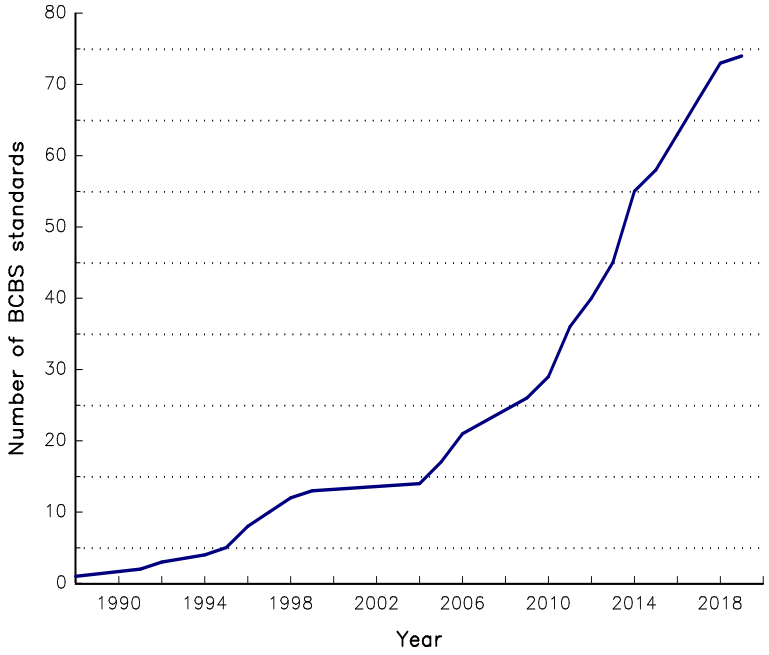

FIGURE 1.5: The huge increase of the number of banking supervision standards

Source: Basel Committee on Banking Supervision and author's calculations.

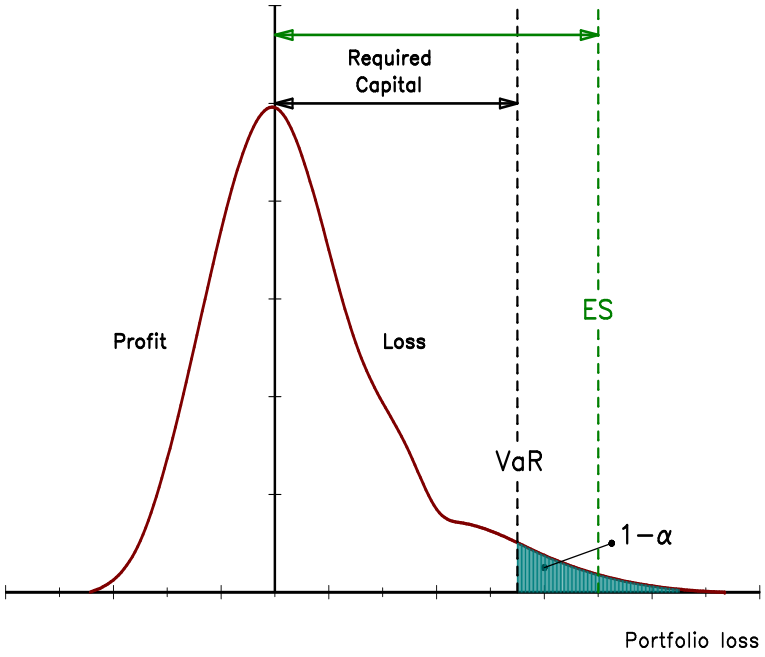

FIGURE 1.6: Probability distribution of the portfolio loss

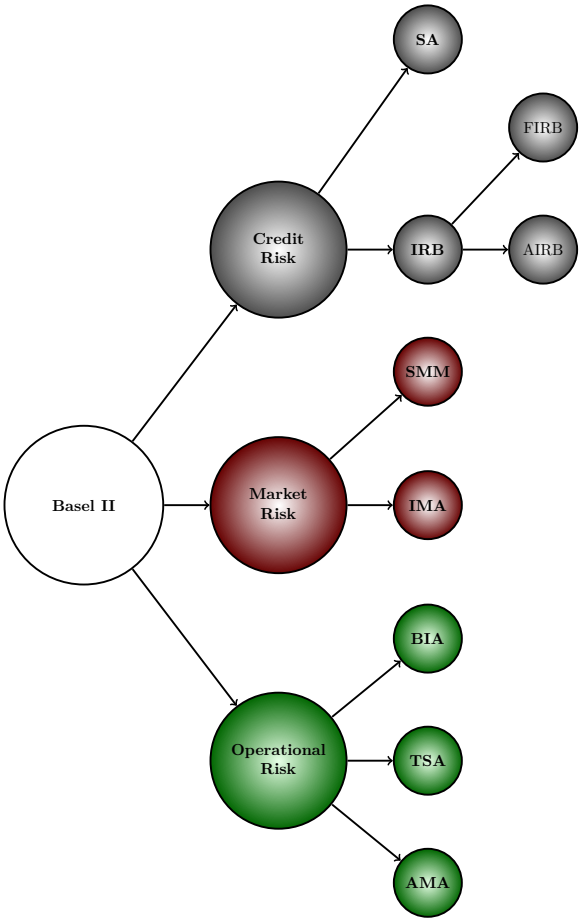

FIGURE 1.7: Minimum capital requirements in the Basel II framework

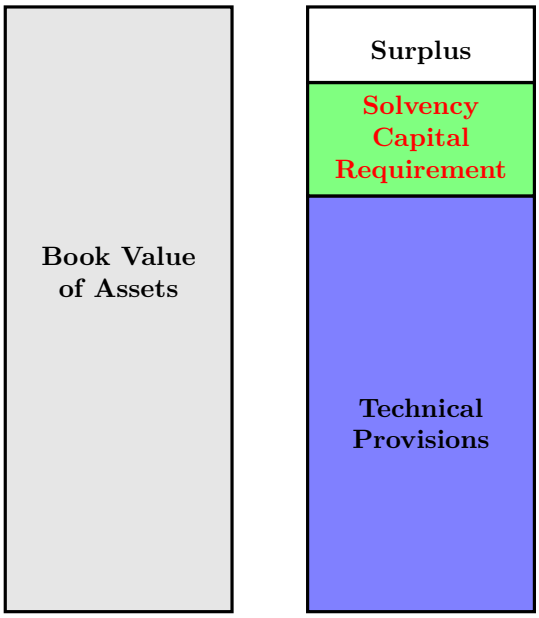

FIGURE 1.8: Solvency I capital requirement

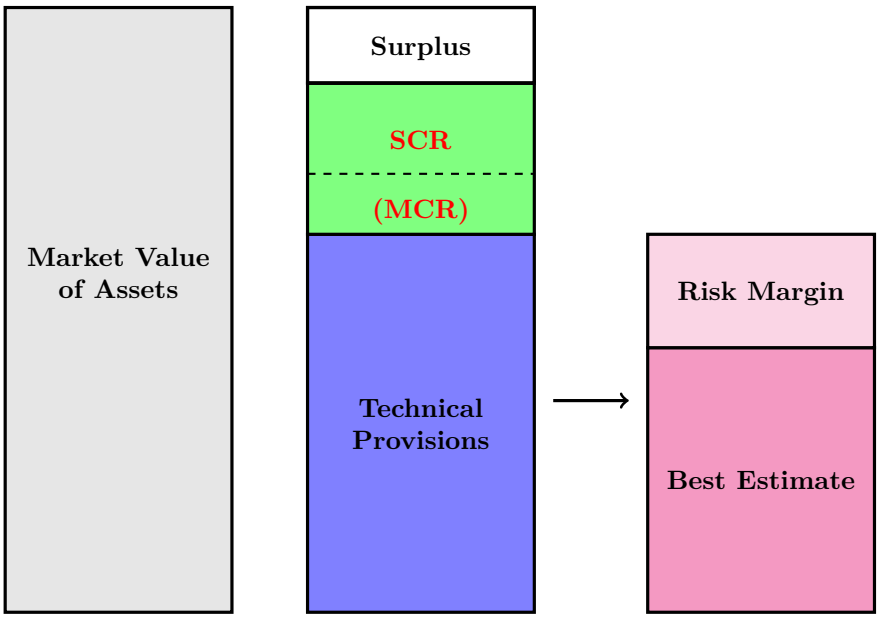

FIGURE 1.9: Solvency II capital requirement

Part I

Risk Management in the Financial Sector

Chapter 2

Market Risk

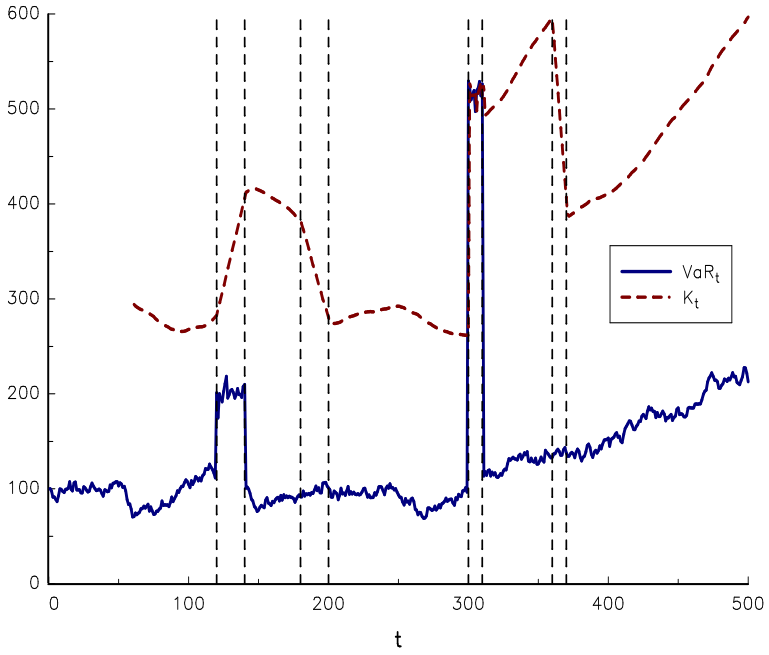

FIGURE 2.1: Calculation of the required capital with the VaR

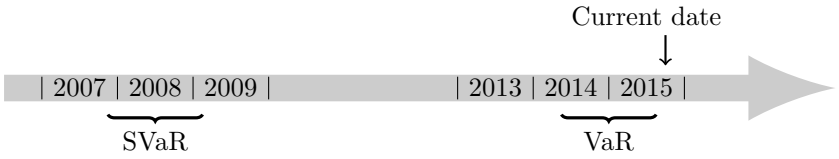

FIGURE 2.2: Two different periods to compute the VaR and the SVaR

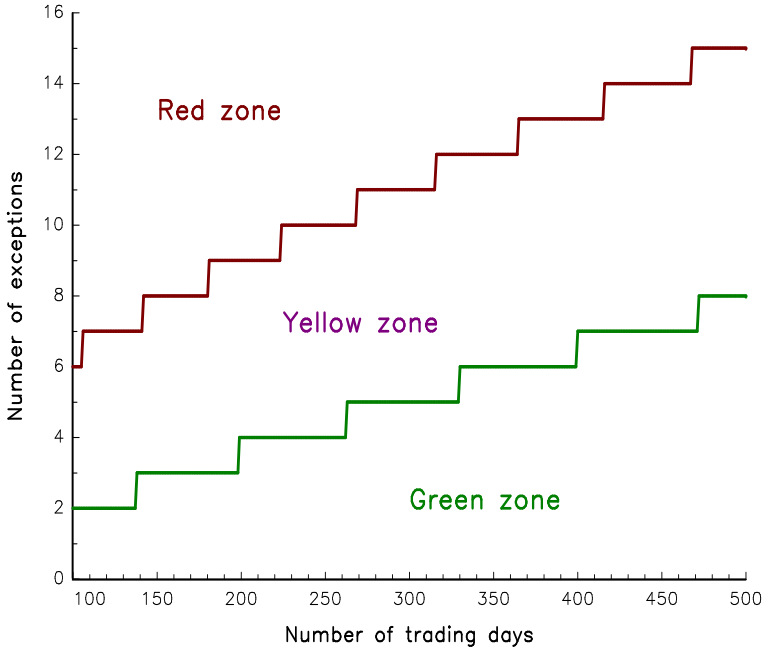

FIGURE 2.3: Color zones of the backtesting procedure ($\alpha = 99\%$)

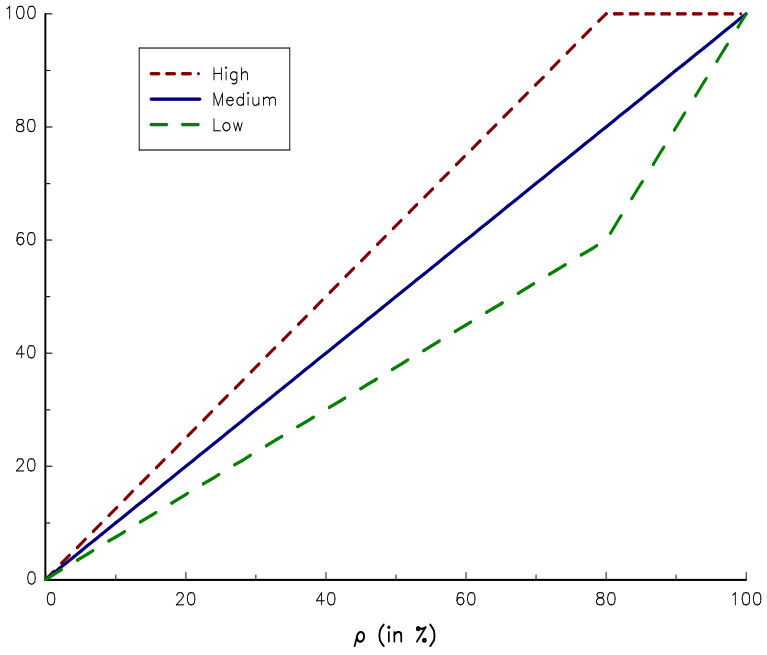

FIGURE 2.4: High, medium and low correlation scenarios

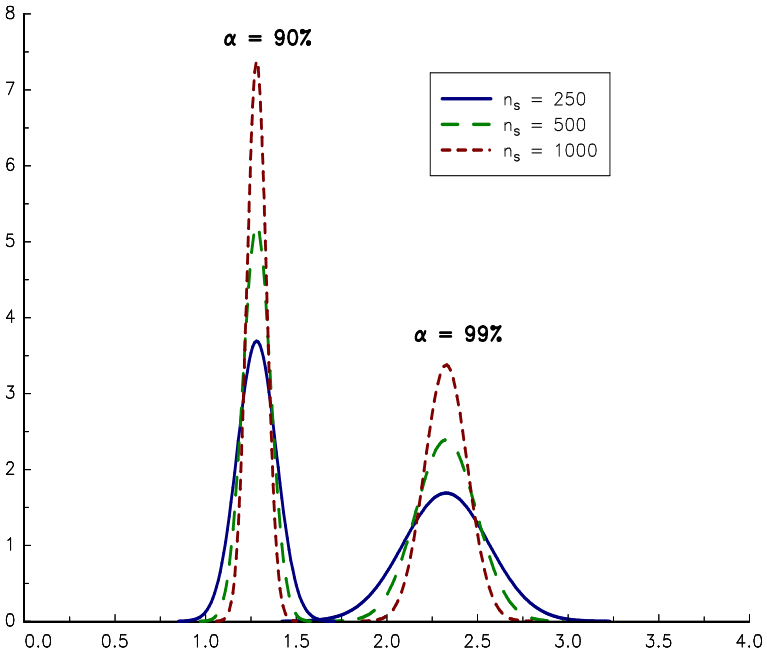

FIGURE 2.5: Density of the VaR estimator (Gaussian case)

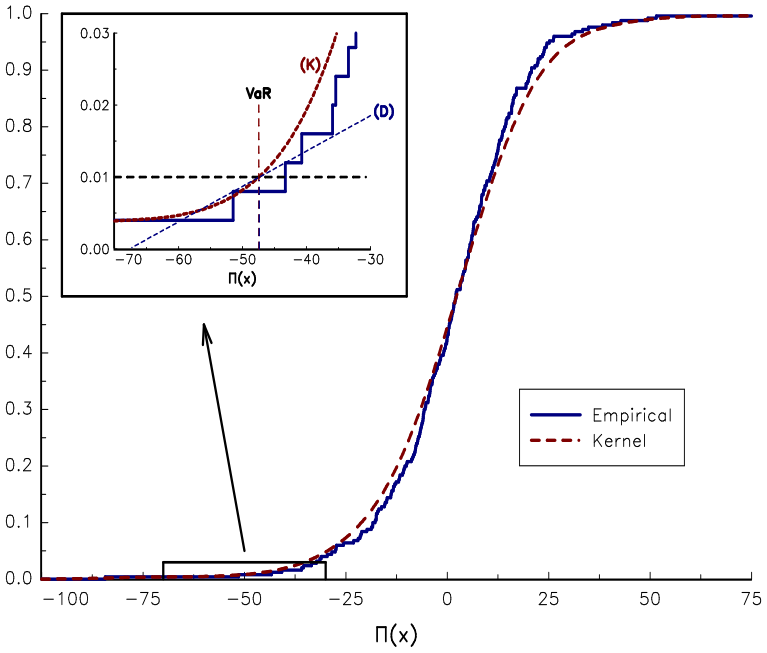

FIGURE 2.6: Kernel estimation of the historical VaR

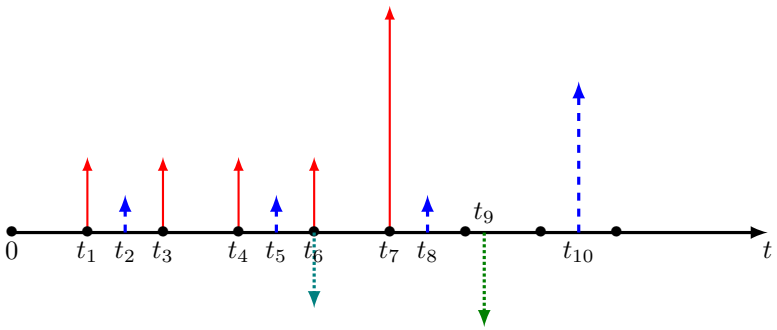

FIGURE 2.7: Cash flows of two bonds and two short exposures

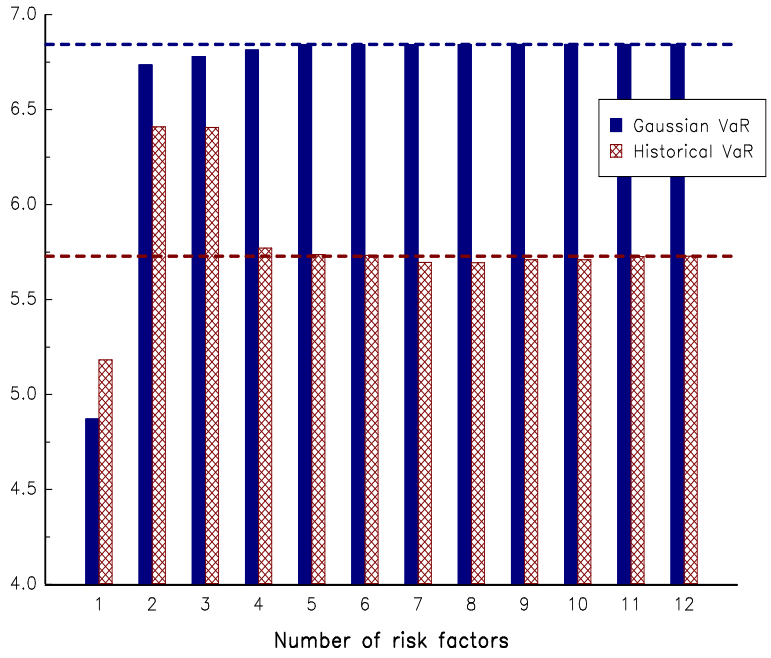

FIGURE 2.8: Convergence of the VaR with PCA risk factors

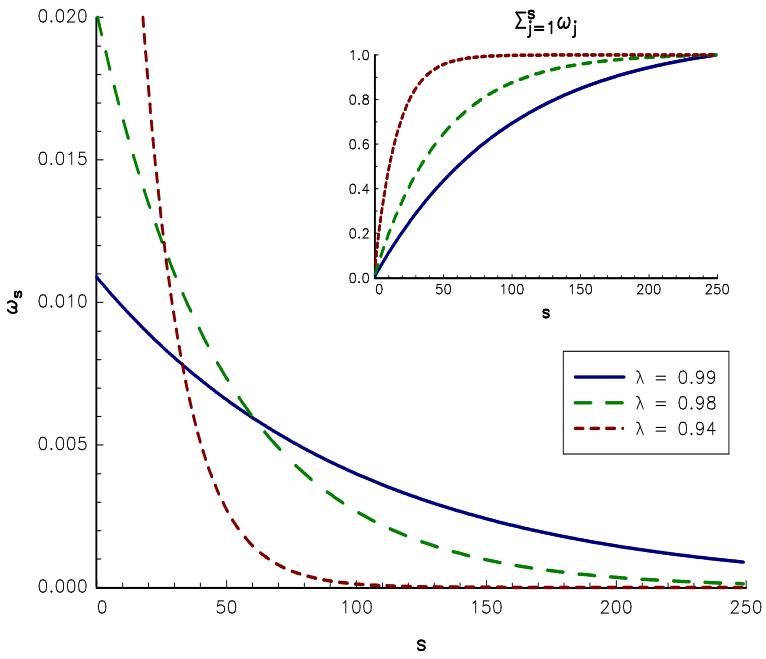

FIGURE 2.9: Weights of the EWMA estimator

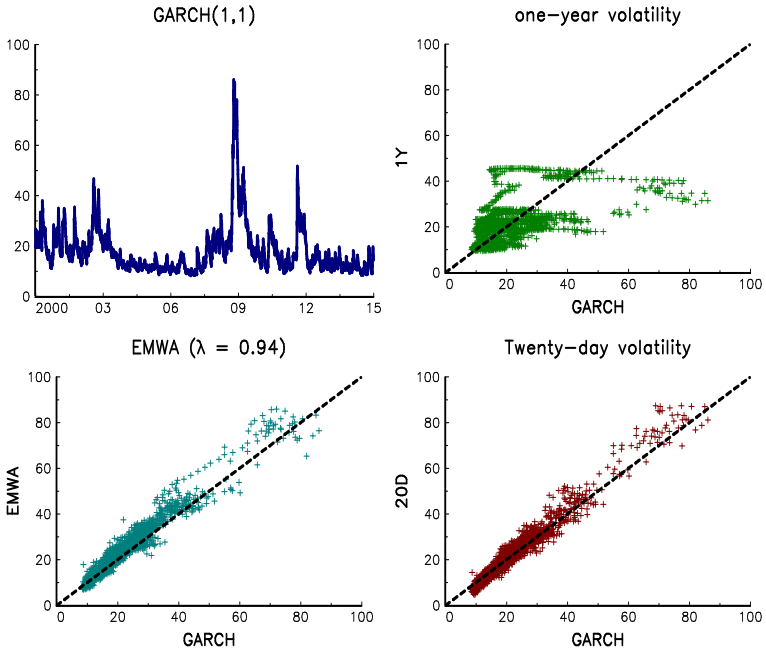

FIGURE 2.10: Comparison of GARCH and EWMA volatilities

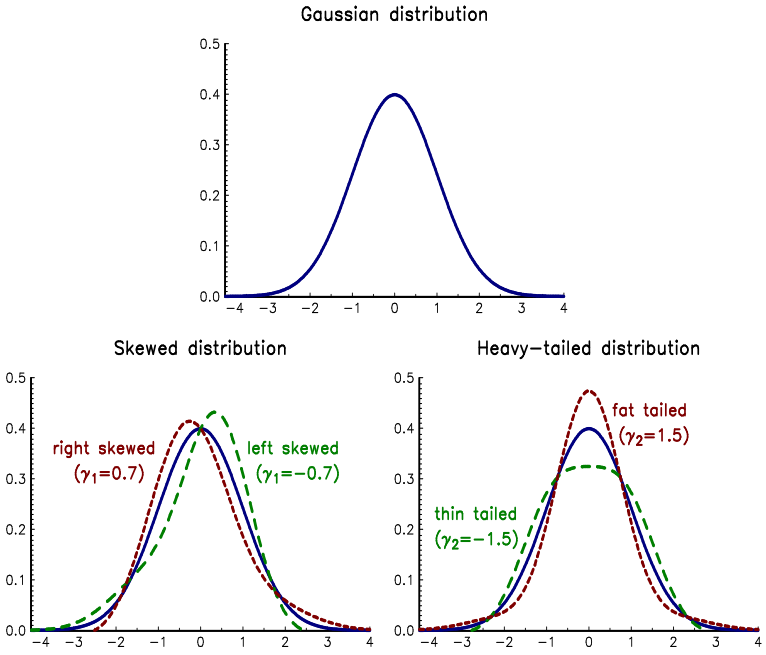

FIGURE 2.11: Examples of skewed and fat tailed distributions

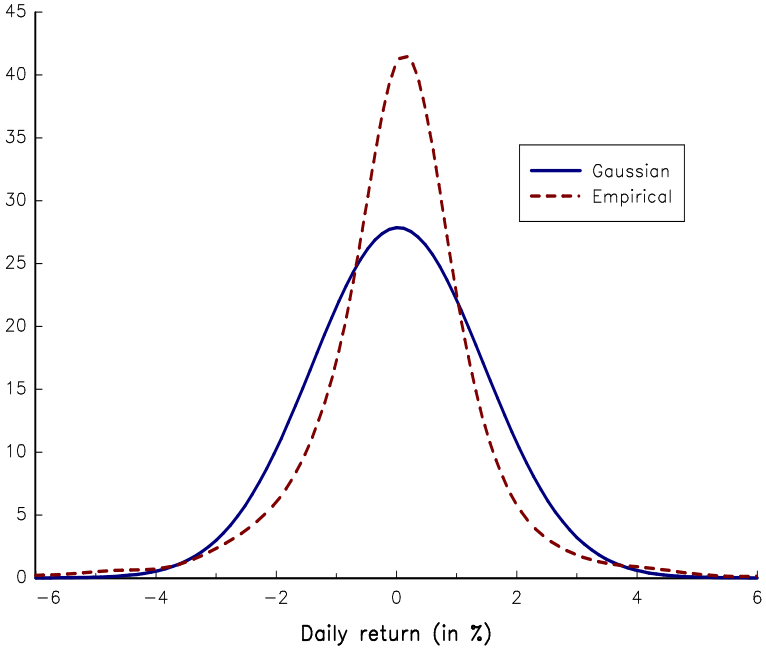

FIGURE 2.12: Estimated distribution of S&P 500 daily returns (2007-2014)

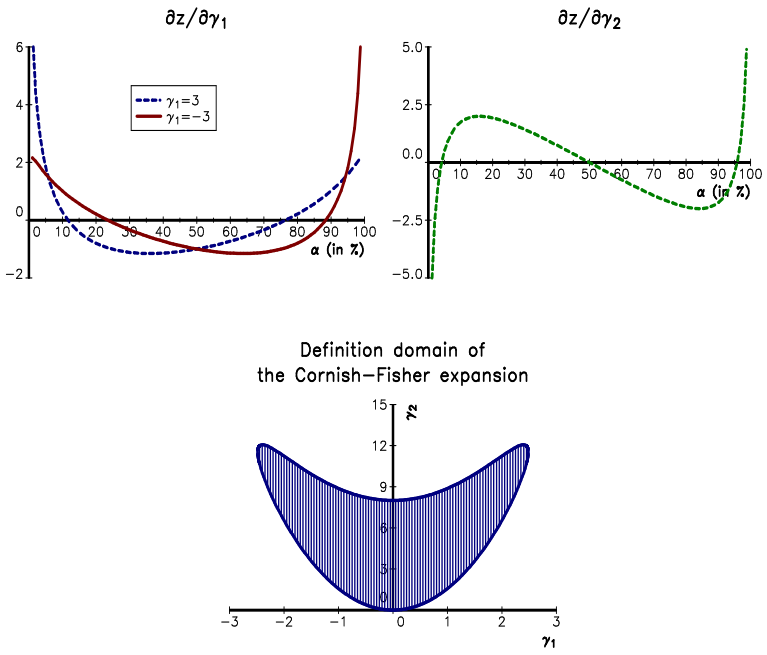

FIGURE 2.13: Derivatives and definition domain of the Cornish-Fisher expansion

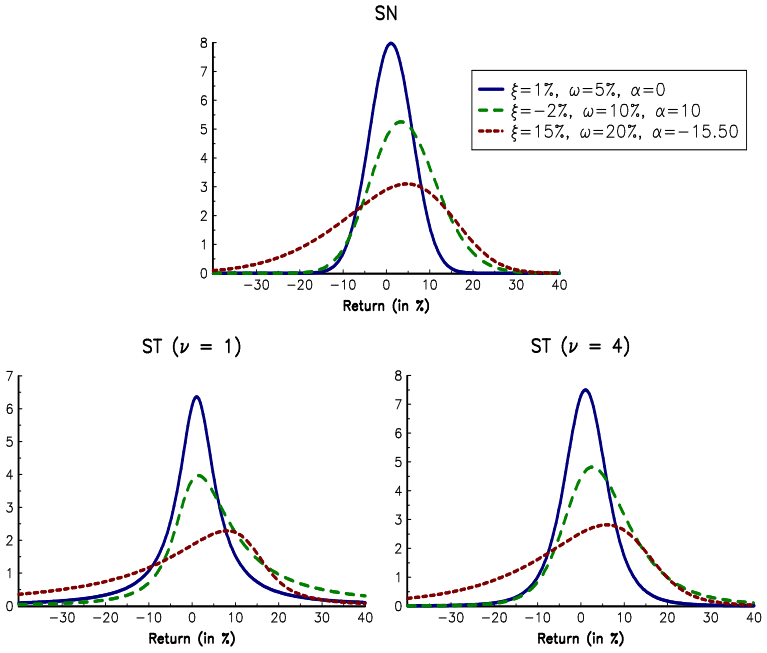

FIGURE 2.14: Skew normal and t distributions of asset returns

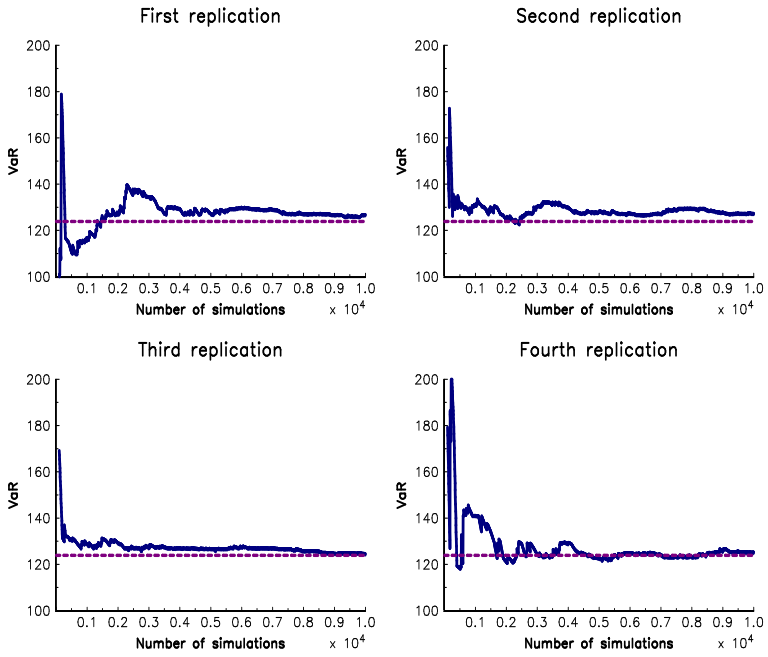

FIGURE 2.15: Convergence of the Monte Carlo VaR when asset returns are skew normal

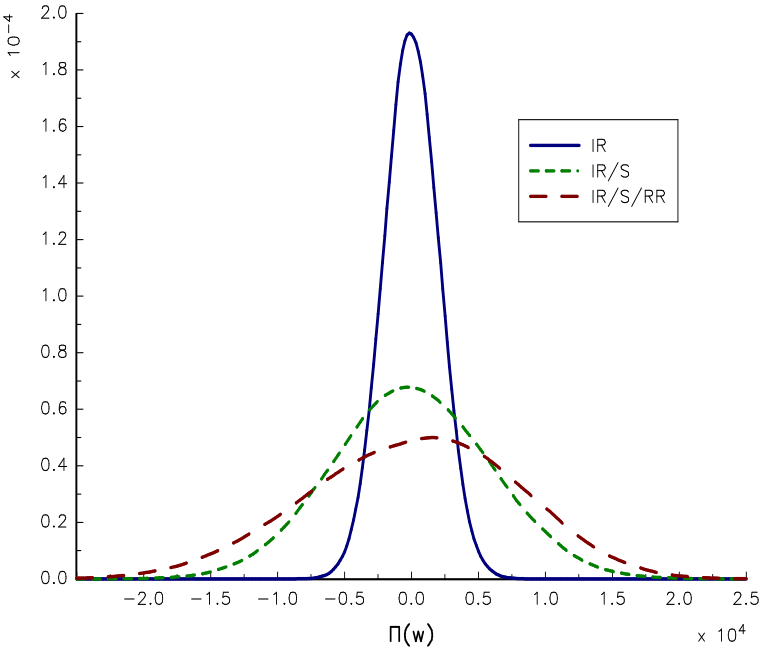

FIGURE 2.16: Probability density function of the daily P&L with credit risk

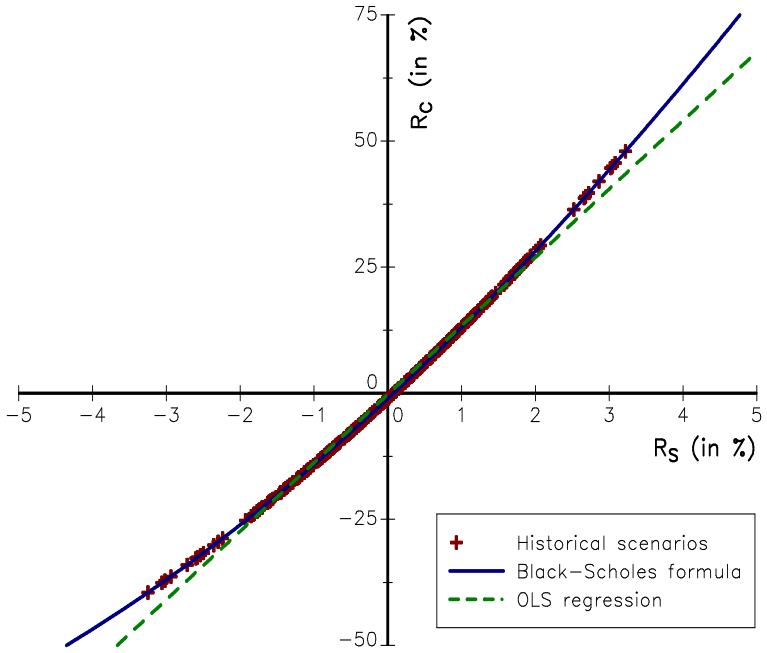

FIGURE 2.17: Relationship between the asset return R_S and the option return R_C

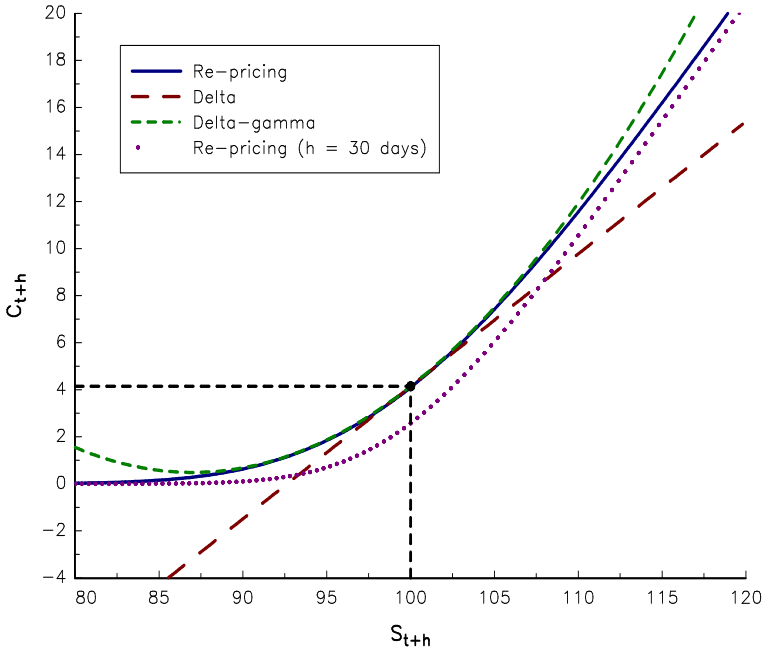

FIGURE 2.18: Approximation of the option price with the Greek coefficients

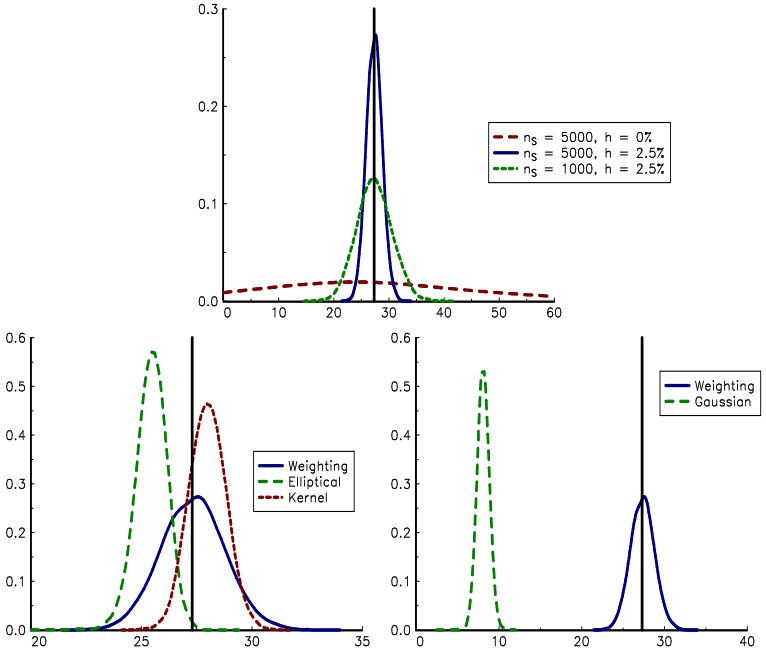

FIGURE 2.19: Density function of the different risk contribution estimators

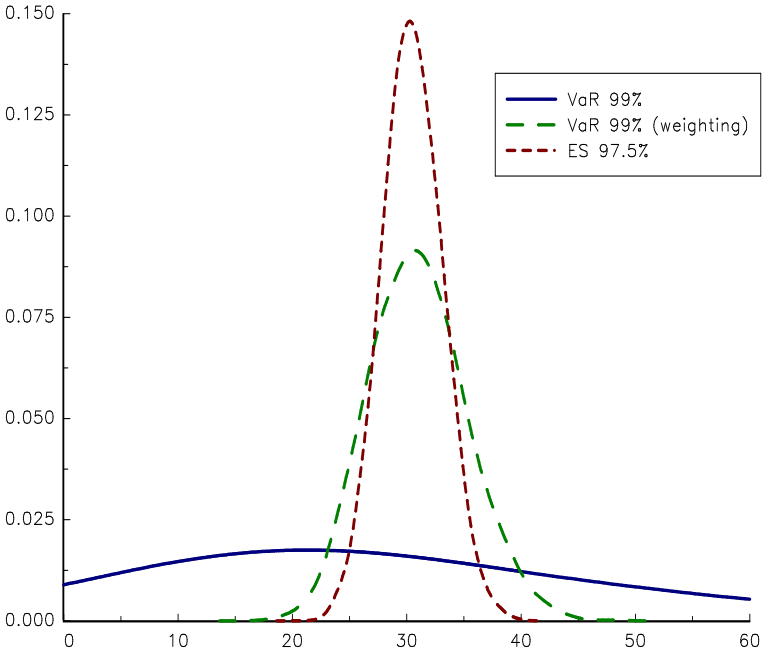

FIGURE 2.20: Probability density function of the $\mathcal{RC}_1$ estimator for the 99% VaR and 97.5% ES

Chapter 3

Credit Risk

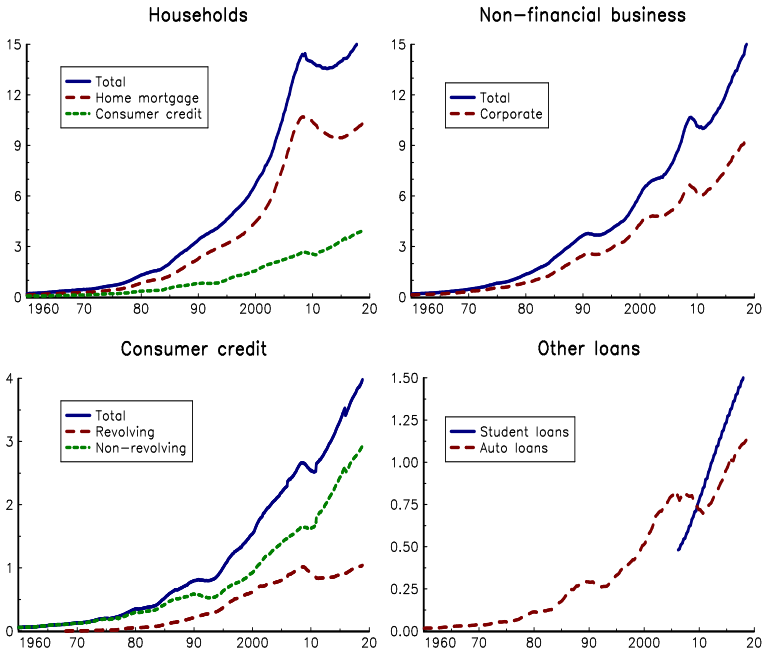

FIGURE 3.1: Credit debt outstanding in the United States (in $ tn)

Source: Board of Governors of the Federal Reserve System (2019).

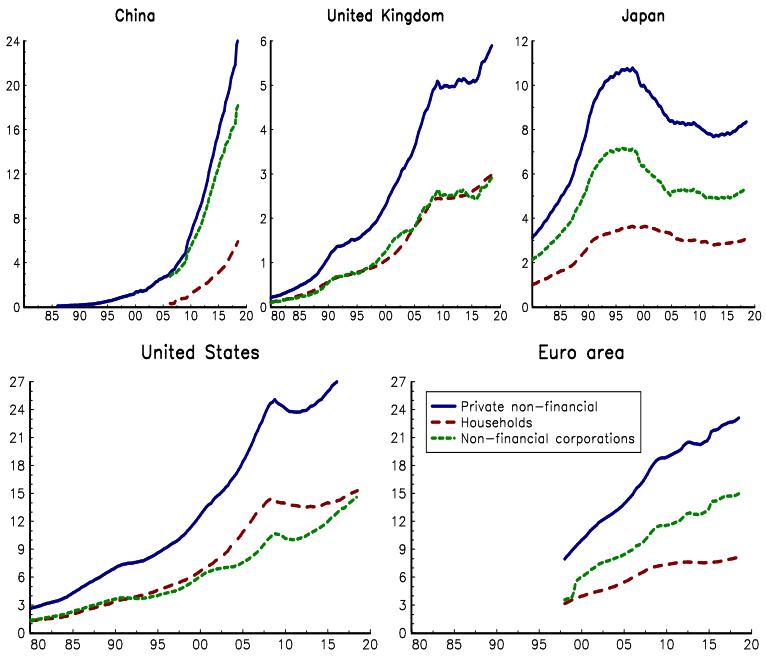

FIGURE 3.2: Credit to the private non-financial sector (in $ tn)

Source: Bank for International Settlement (2019) & author's calculations.

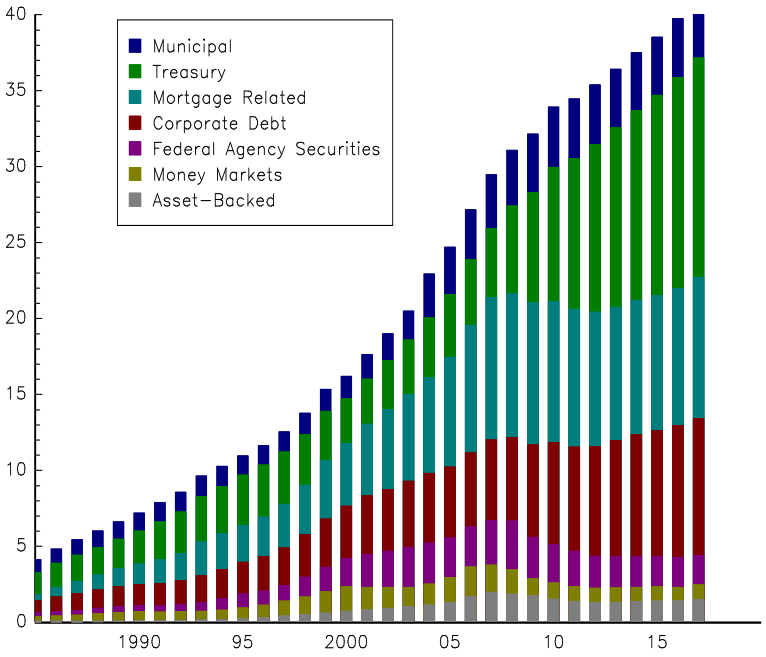

FIGURE 3.3: US bond market outstanding (in $ tn)

Source: Securities Industry and Financial Markets Association (2019a).

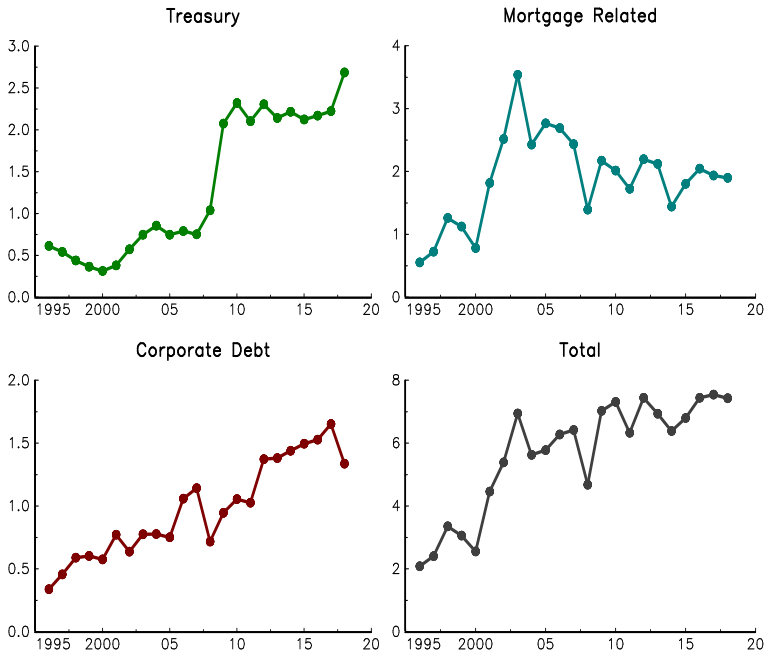

FIGURE 3.4: US bond market issuance (in $ tn)

Source: Securities Industry and Financial Markets Association (2019a).

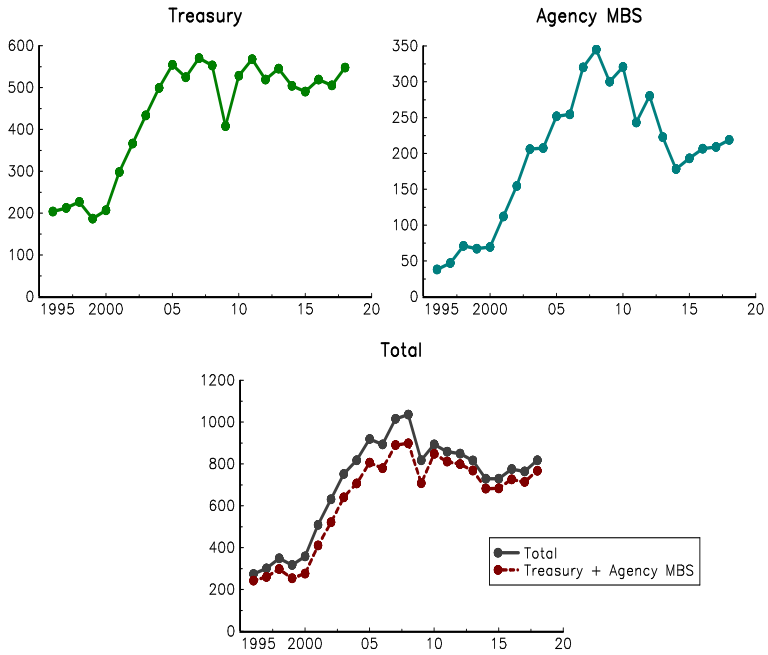

FIGURE 3.5: Average daily trading volume in US bond markets (in $ bn)

Source: Securities Industry and Financial Markets Association (2019a).

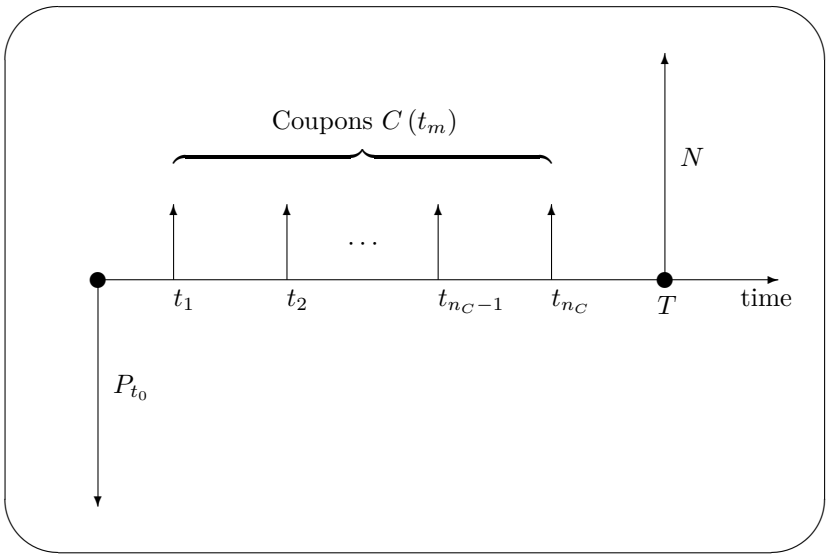

FIGURE 3.6: Cash flows of a bond with a fixed coupon rate

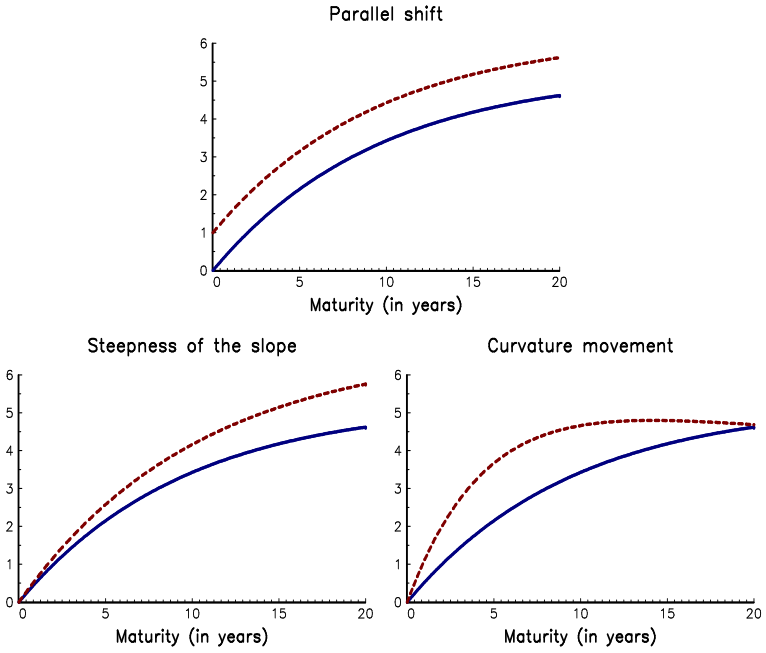

FIGURE 3.7: Movements of the yield curve

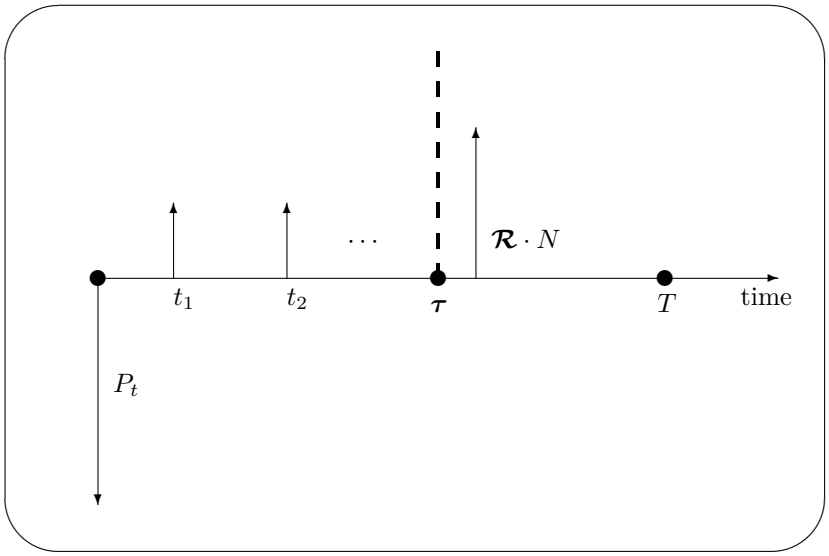

FIGURE 3.8: Cash flows of a bond with default risk

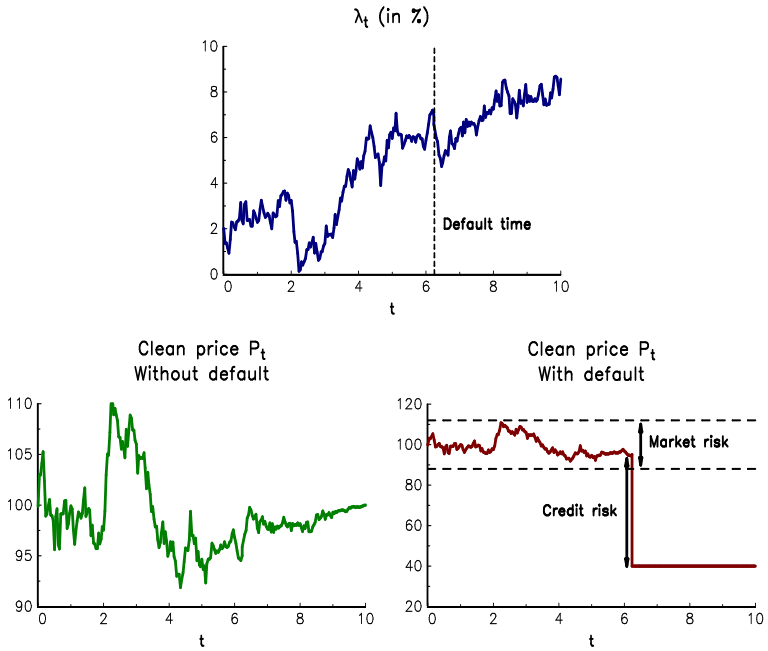

FIGURE 3.9: Difference between market and credit risks for a bond

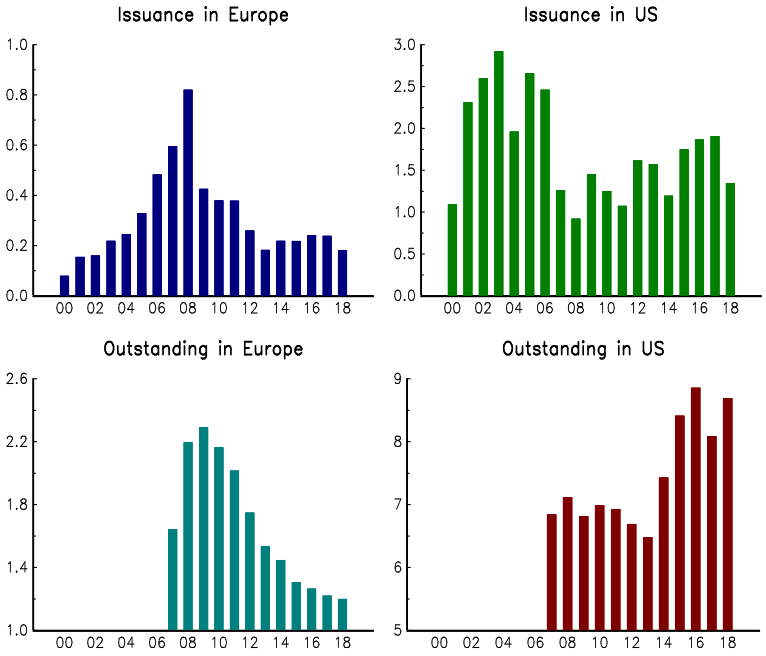

FIGURE 3.10: Securitization in Europe and US (in € tn)

Source: Association for Financial Markets in Europe (2019).

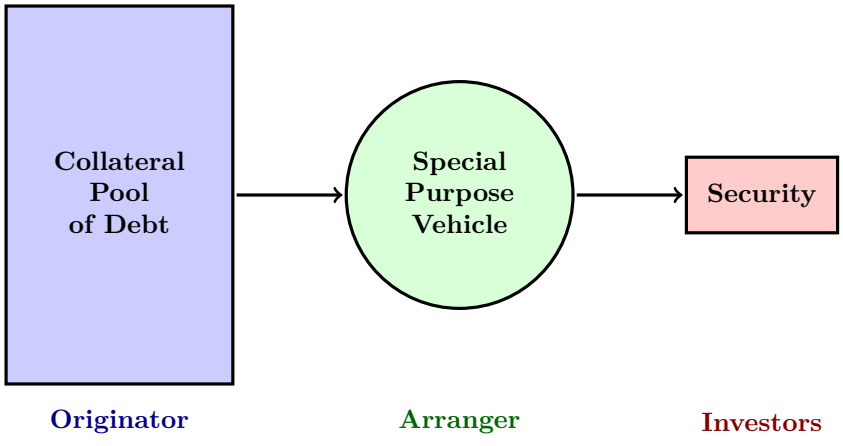

FIGURE 3.11: Structure of pass-through securities

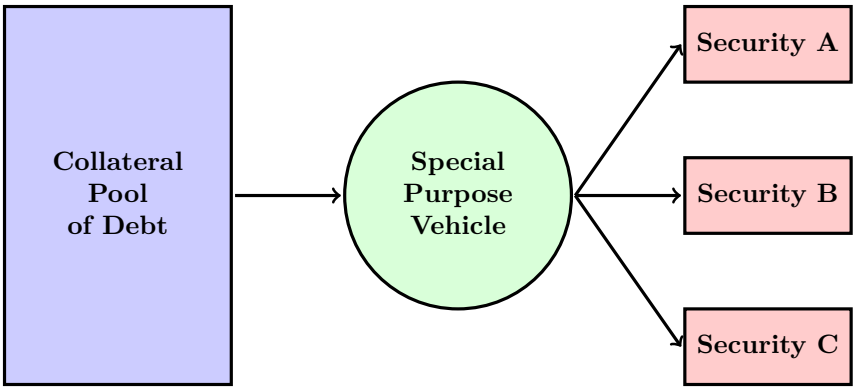

FIGURE 3.12: Structure of pay-through securities

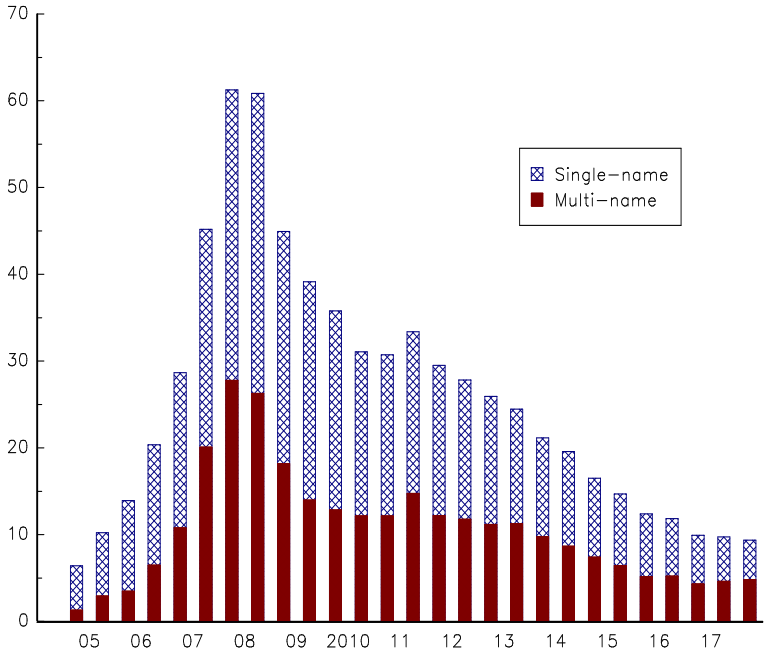

FIGURE 3.13: Outstanding amount of credit default swaps (in $ tn)

Source: Bank for International Settlement (2019).

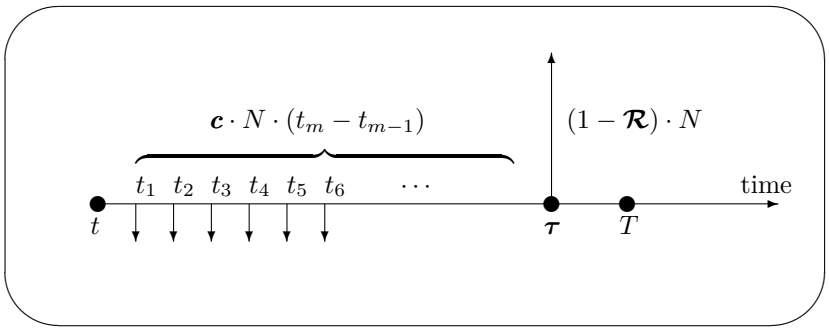

FIGURE 3.14: Cash flows of a single-name credit default swap

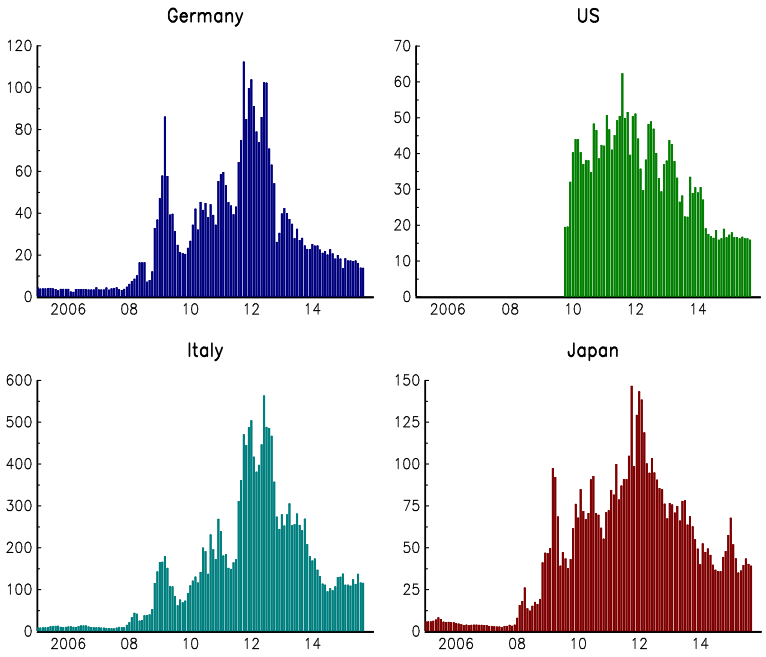

FIGURE 3.15: Evolution of some sovereign CDS spreads

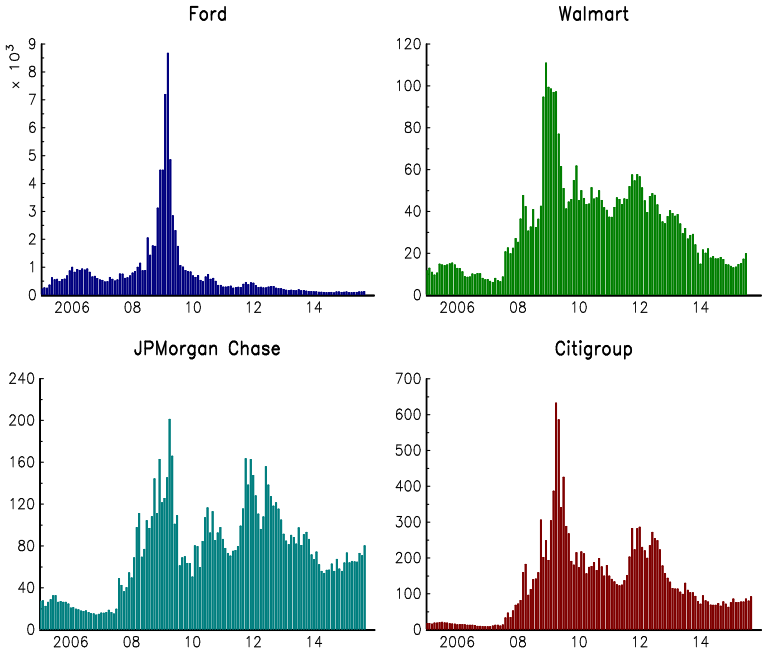

FIGURE 3.16: Evolution of some financial and corporate CDS spreads

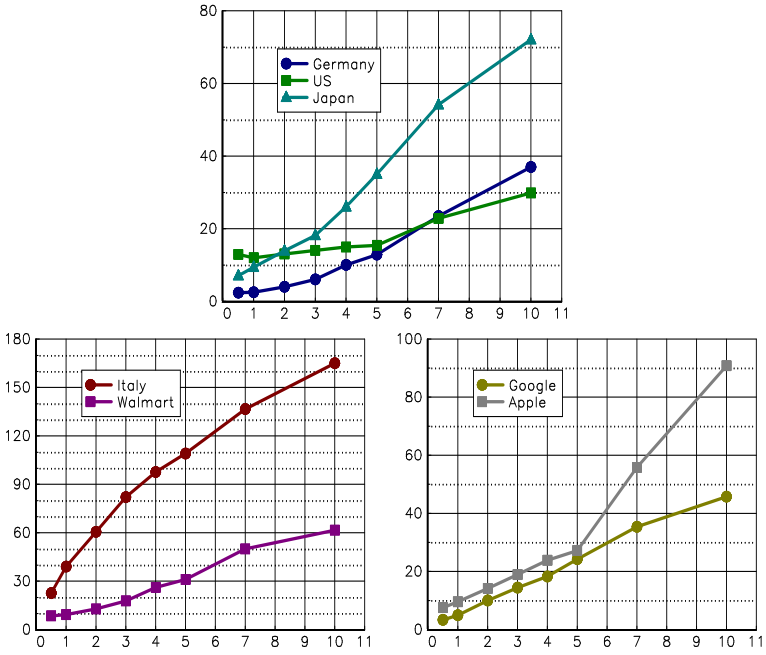

FIGURE 3.17: Example of CDS spread curves as of 2015-09-17

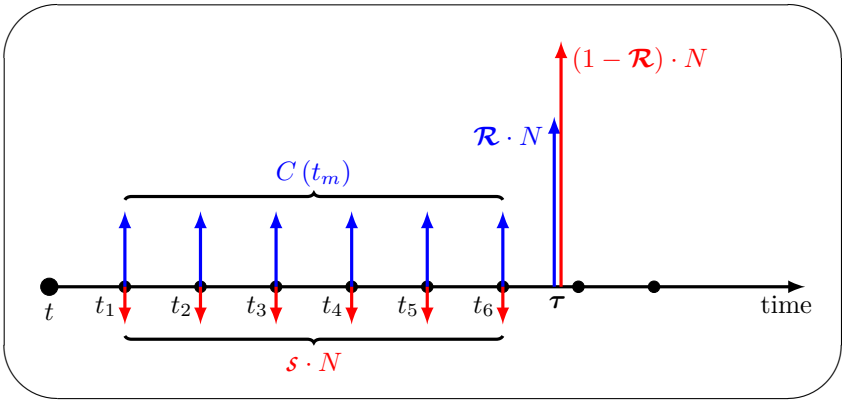

FIGURE 3.18: Hedging a defaultable bond with a credit default swap

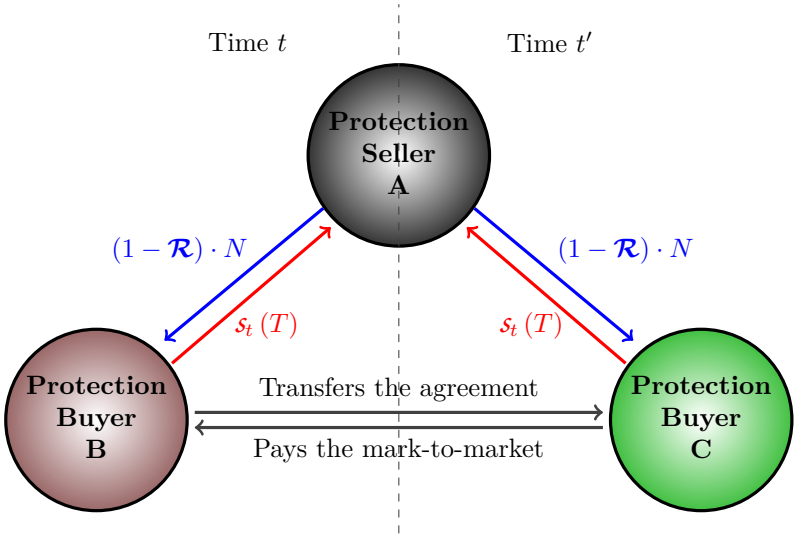

FIGURE 3.19: An example of CDS offsetting

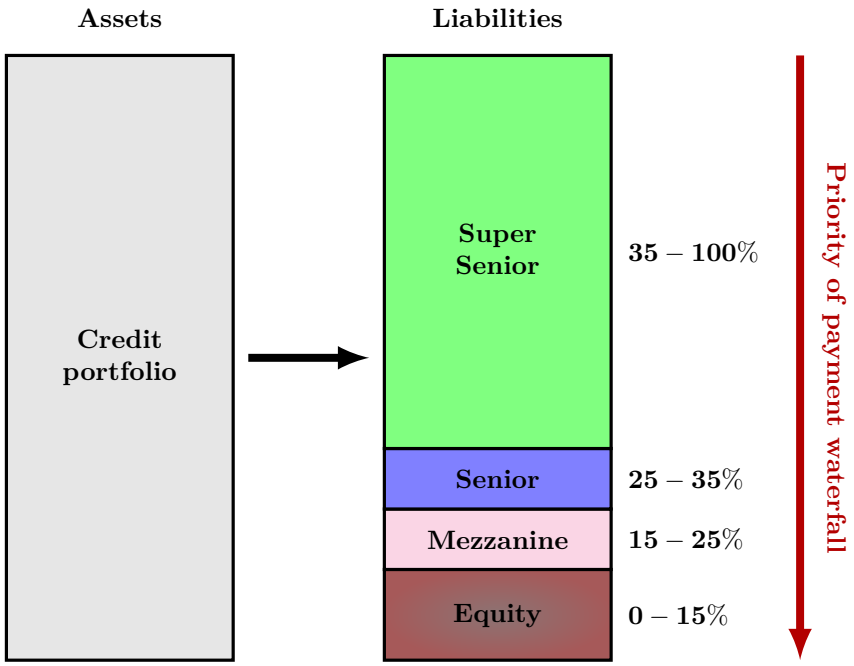

FIGURE 3.20: Structure of a collateralized debt obligation

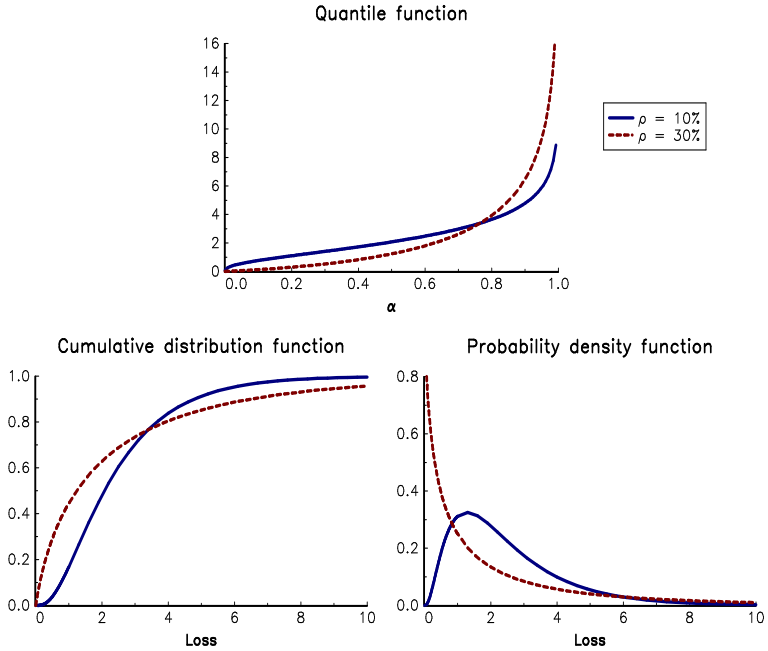

FIGURE 3.21: Probability functions of the credit portfolio loss

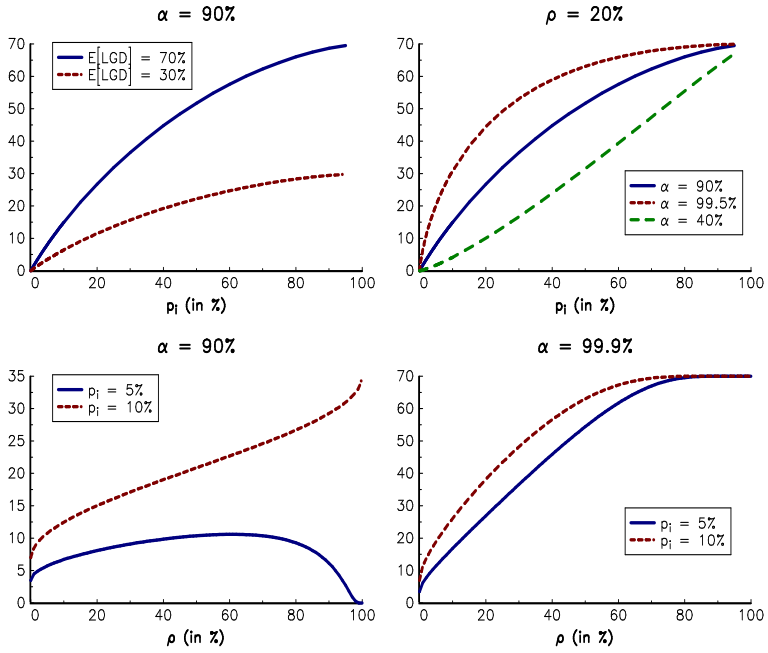

FIGURE 3.22: Relationship between the risk contribution $\mathcal{RC}_i$ and model parameters

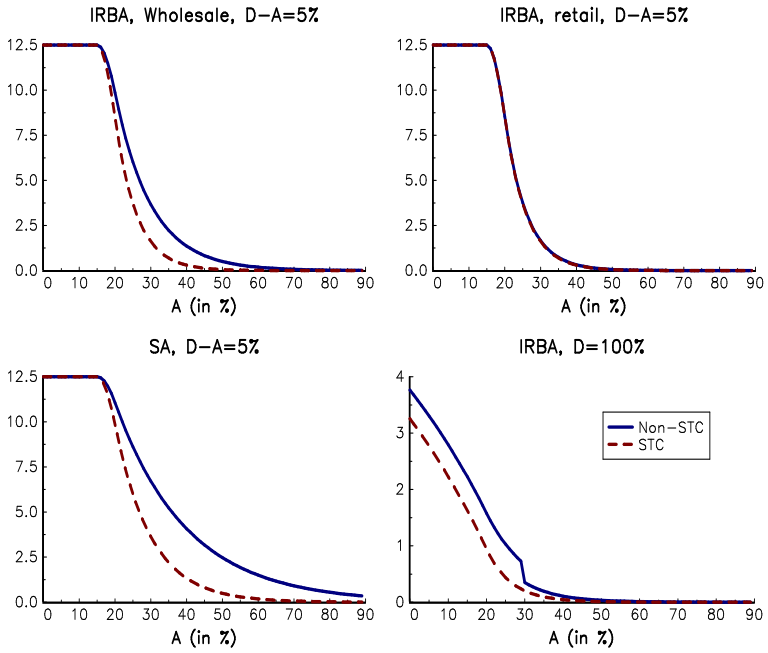

FIGURE 3.23: Risk weight of securitization exposures

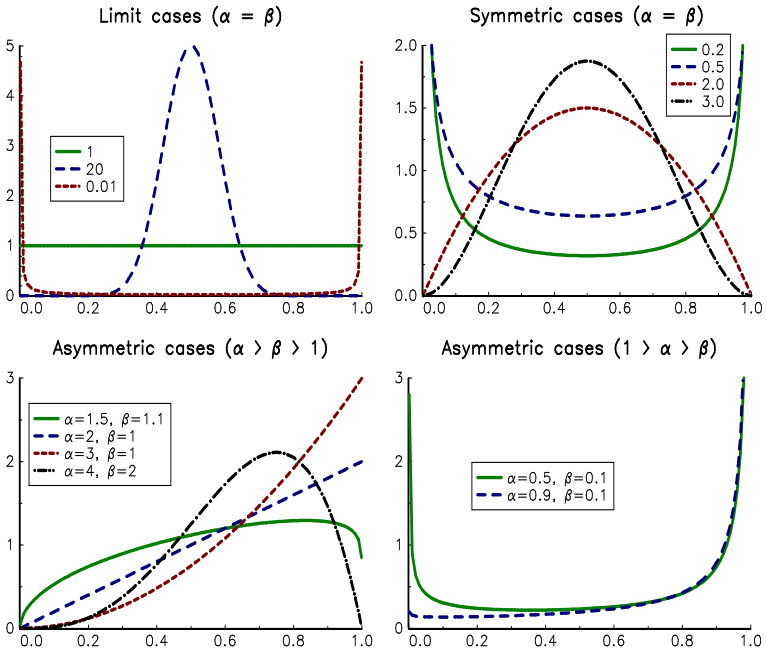

FIGURE 3.24: Probability density function of the beta distribution $\mathcal{B}(\alpha, \beta)$

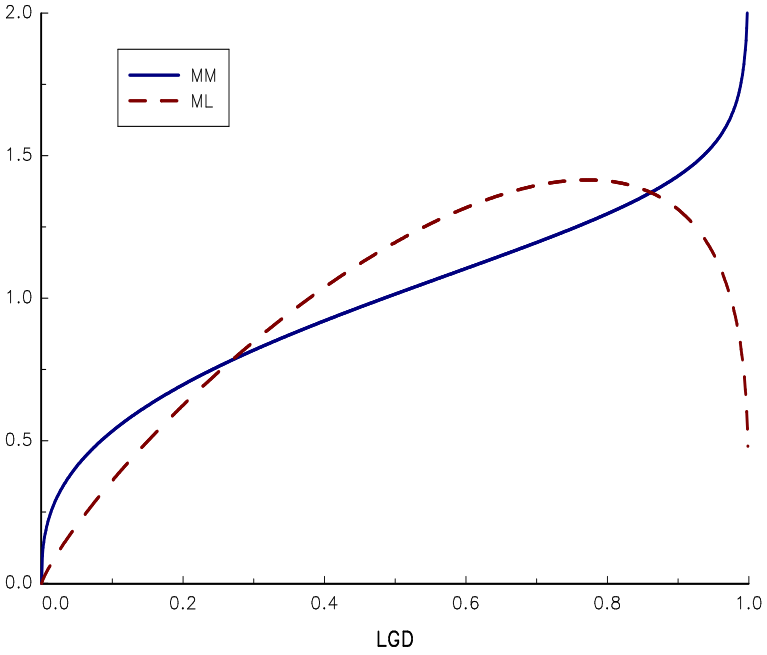

FIGURE 3.25: Calibration of the beta distribution

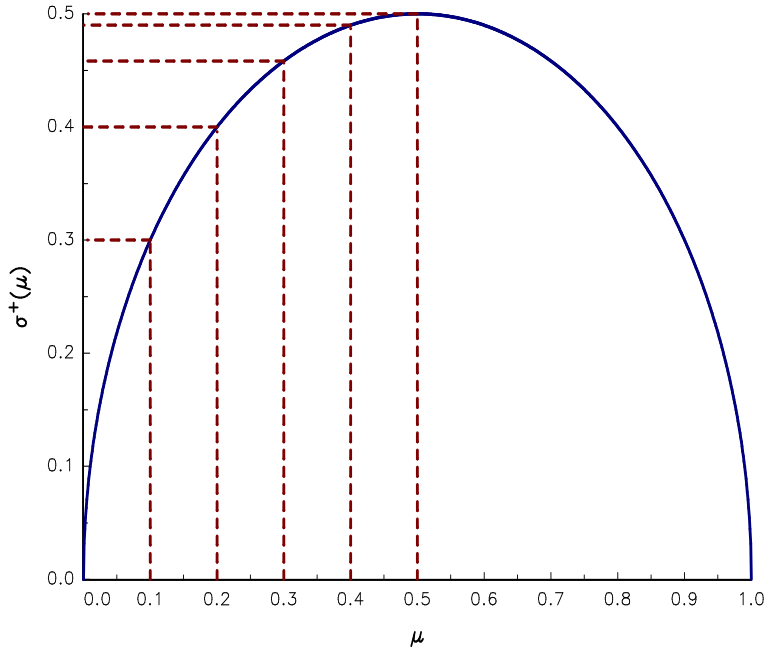

FIGURE 3.26: Maximum standard deviation $\sigma^+(\mu)$

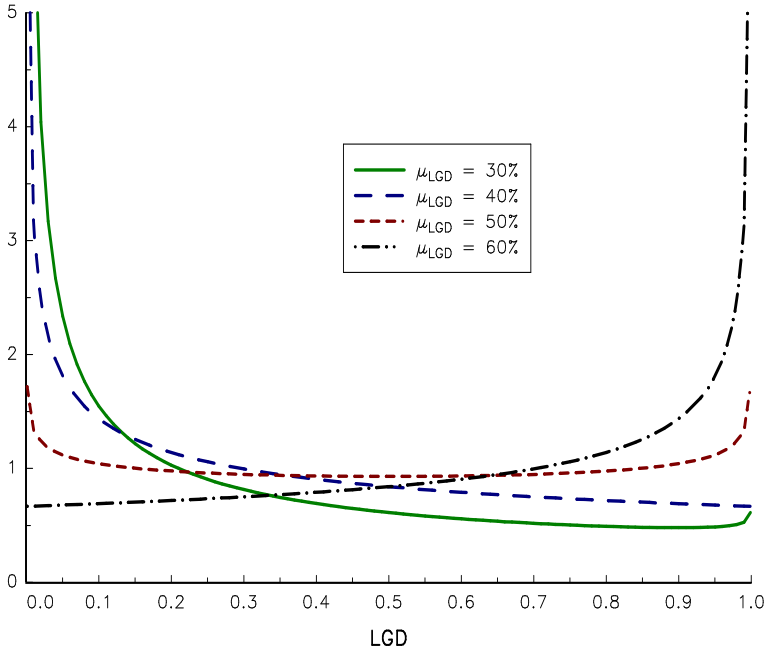

FIGURE 3.27: Calibration of the beta distribution when $\sigma_{\text{LGD}} = 30\%$

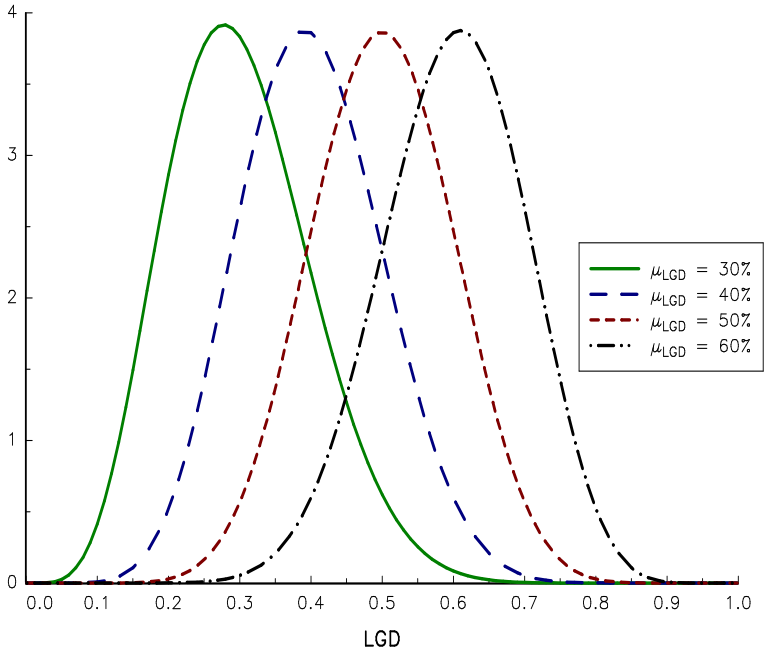

FIGURE 3.28: Calibration of the beta distribution when $\sigma_{\text{LGD}} = 10\%$

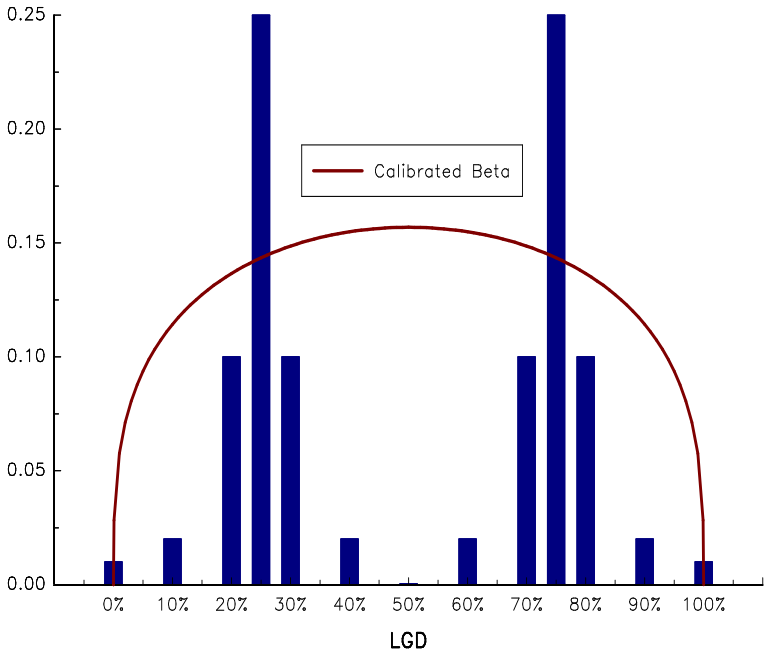

FIGURE 3.29: Calibration of a bimodal LGD distribution

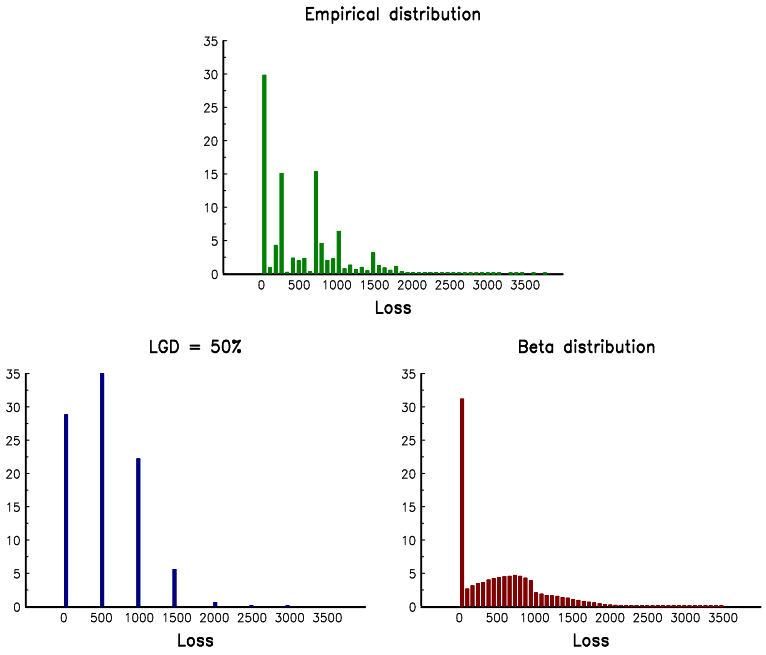

FIGURE 3.30: Loss frequency in % of the three LGD models

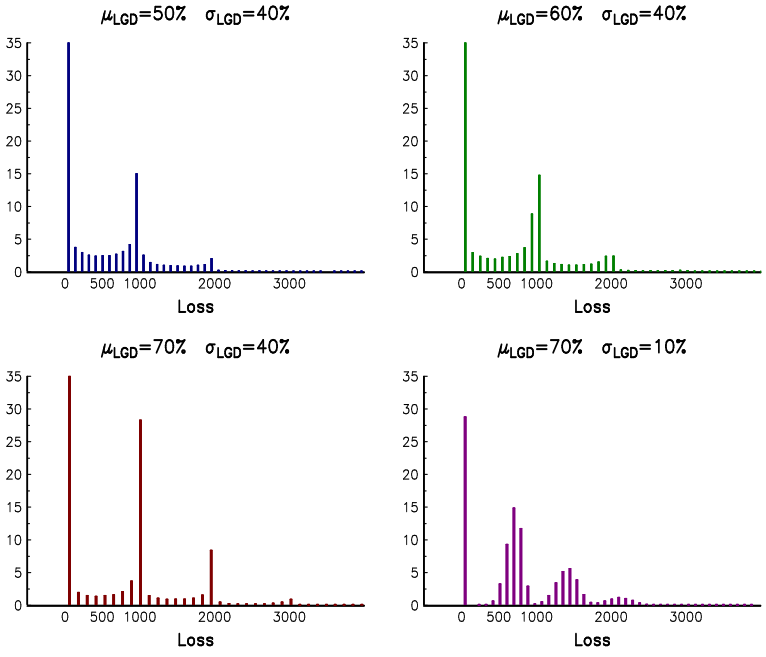

FIGURE 3.31: Loss frequency in % for different values of μ_{LGD} and σ_{LGD}

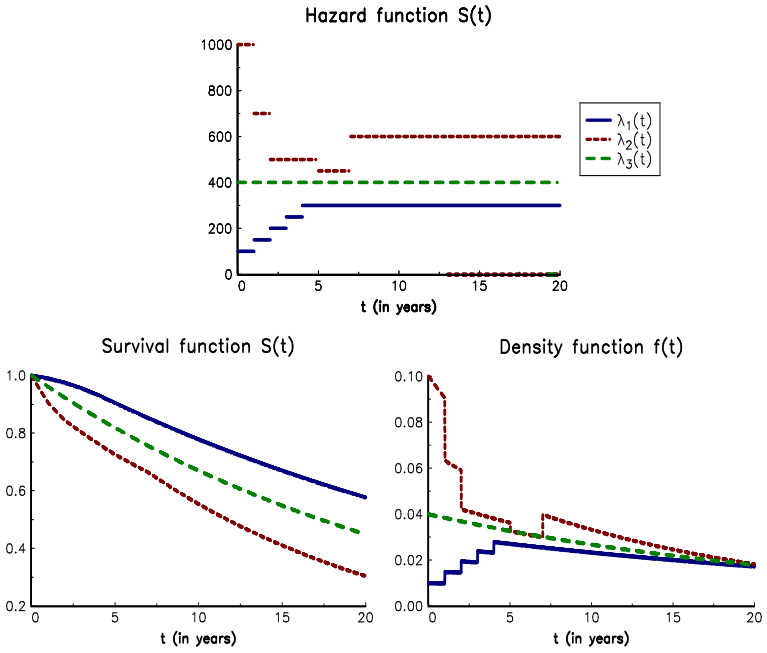

FIGURE 3.32: Example of the piecewise exponential model

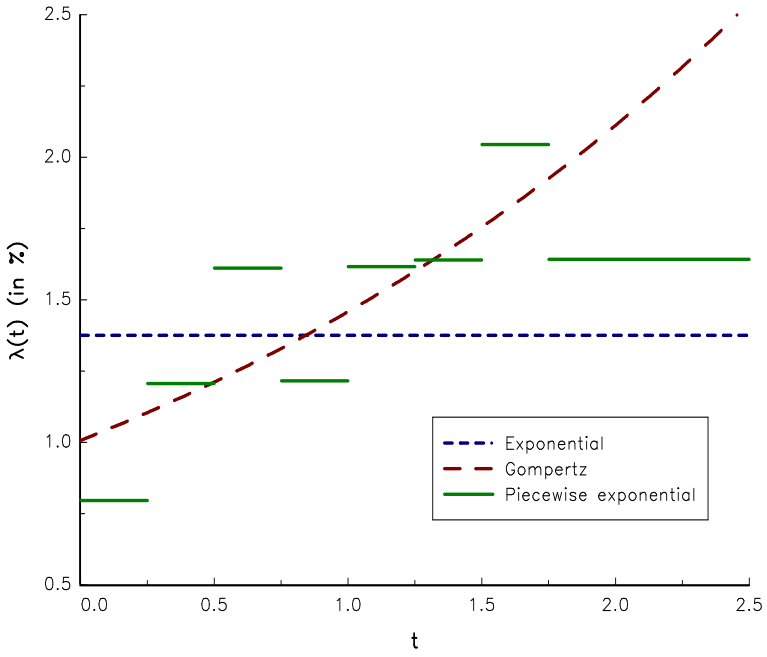

FIGURE 3.33: Estimated hazard function

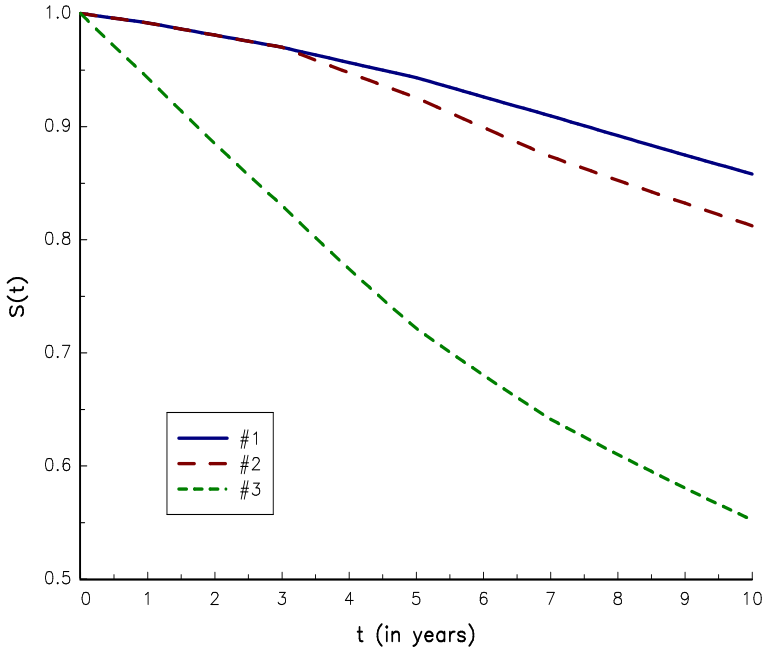

FIGURE 3.34: Calibrated survival function from CDS prices

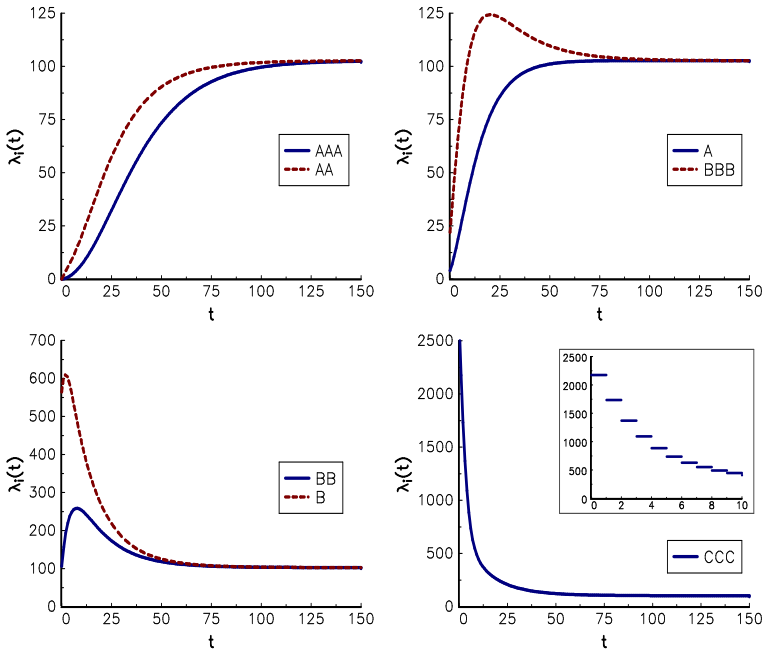

FIGURE 3.35: Estimated hazard function $\lambda_i(t)$ from the credit migration matrix

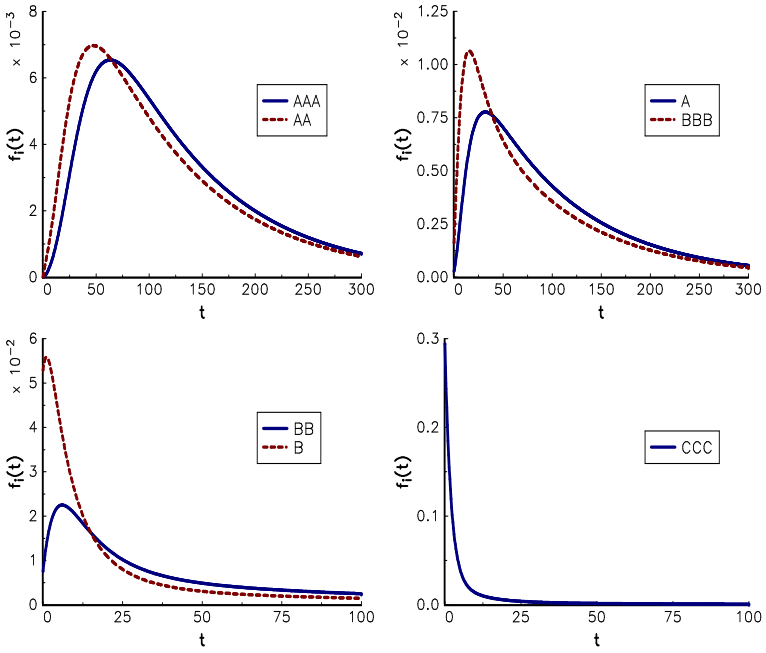

FIGURE 3.36: Probability density function $f_i(t)$ of S&P ratings

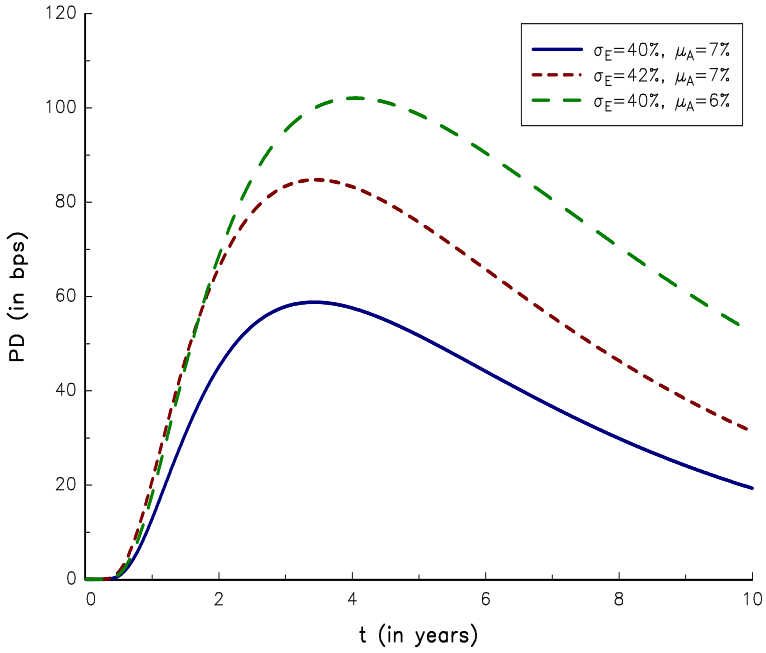

FIGURE 3.37: Probability of default in the KMV model

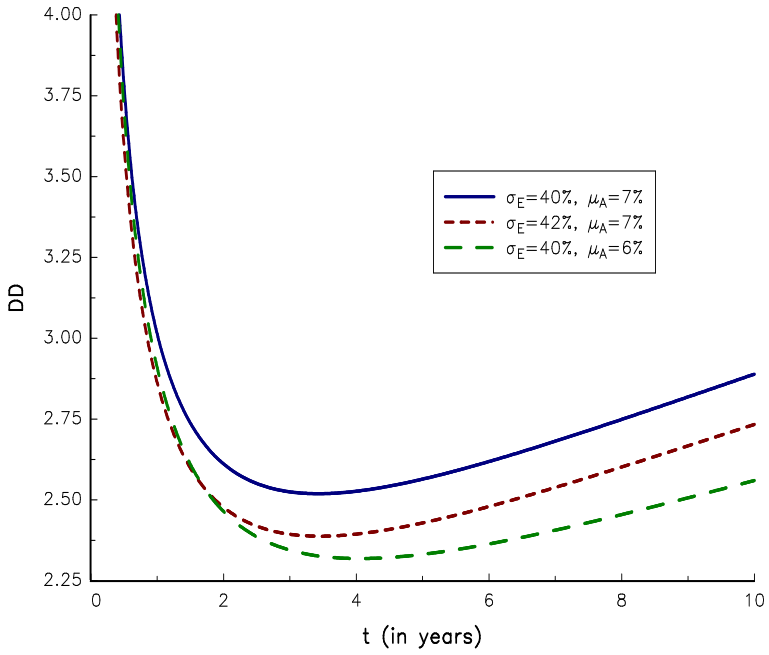

FIGURE 3.38: Distance-to-default in the KMV model

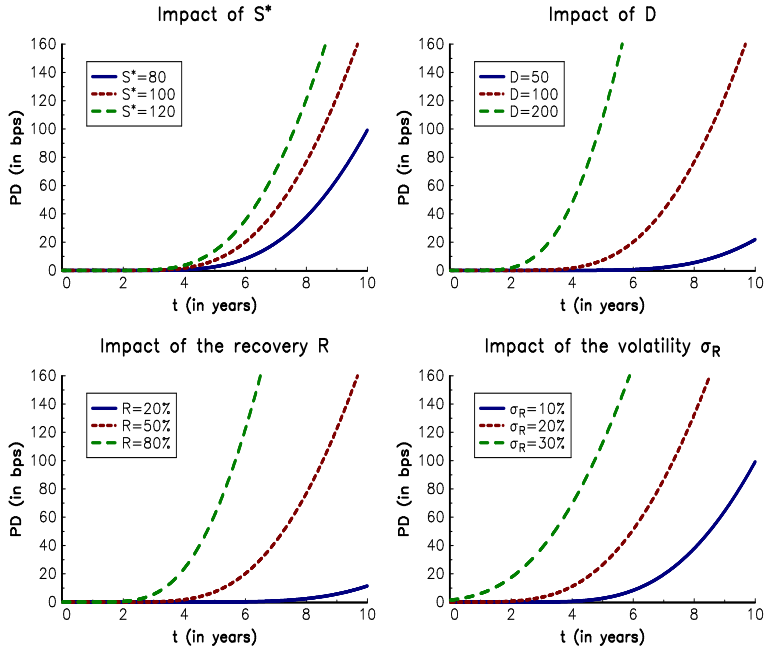

FIGURE 3.39: Probability of default in the CreditGrades model

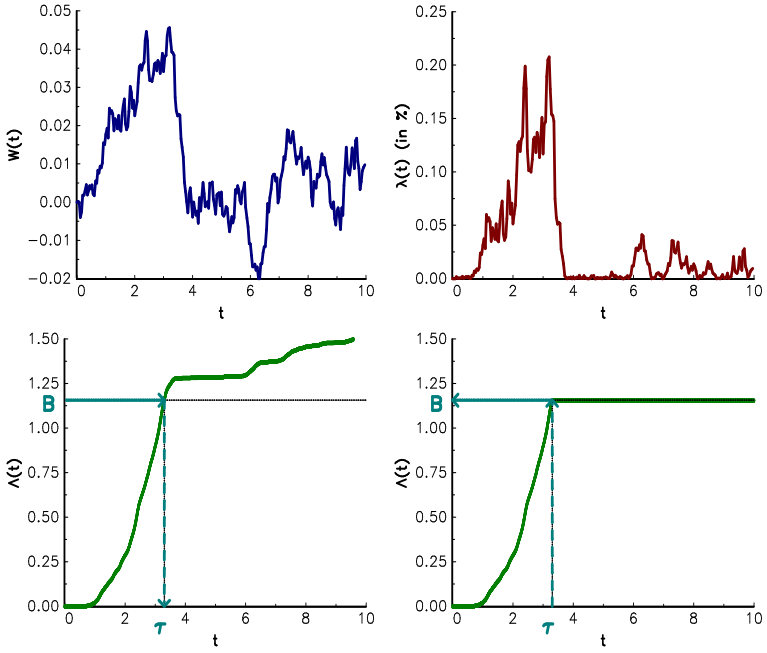

FIGURE 3.40: Intensity models and the default barrier issue

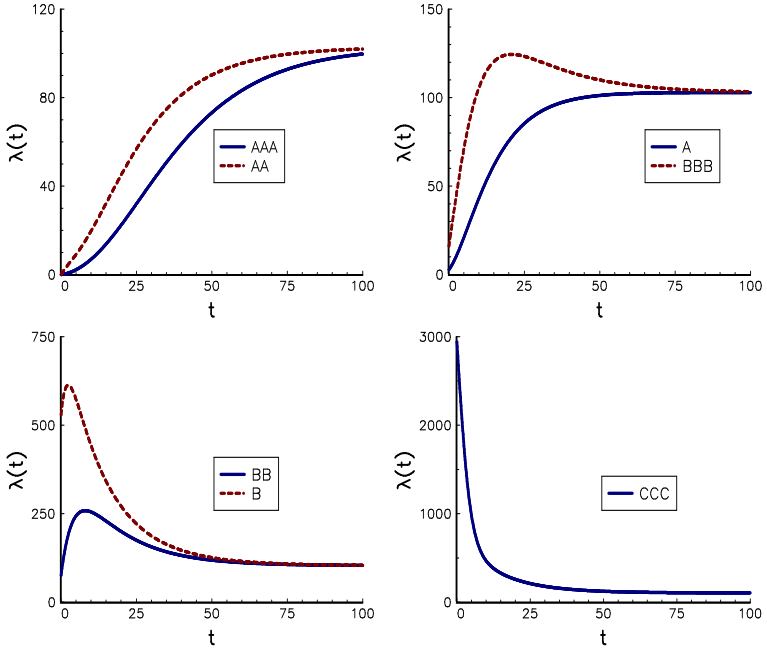

FIGURE 3.41: Hazard function $\lambda_i(t)$ (in bps)

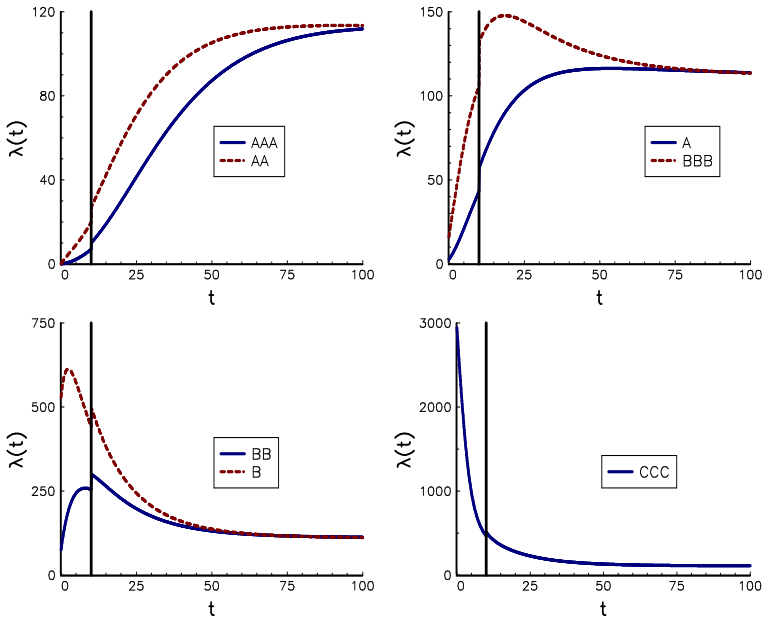

FIGURE 3.42: Hazard function $\lambda_i(t)$ (in bps) when a AAA-rated company defaults after 10 years ($\rho = 5\%$)

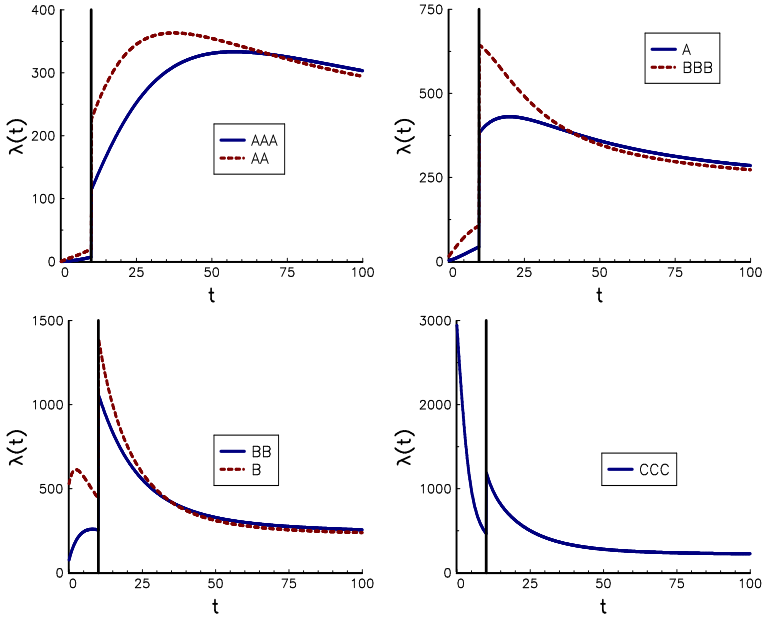

FIGURE 3.43: Hazard function $\lambda_i(t)$ (in bps) when a AAA-rated company defaults after 10 years ($\rho = 50\%$)

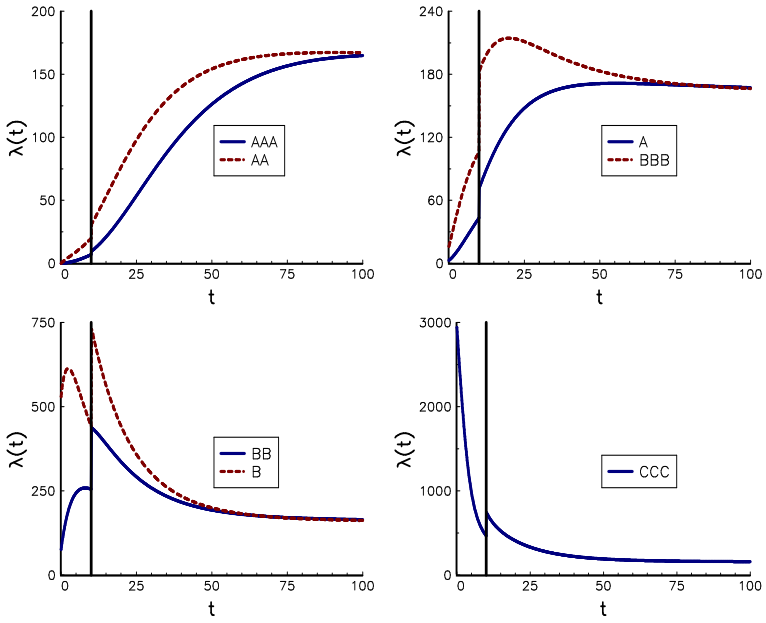

FIGURE 3.44: Hazard function $\lambda_i(t)$ (in bps) when a BB-rated company defaults after 10 years ($\rho = 50\%$)

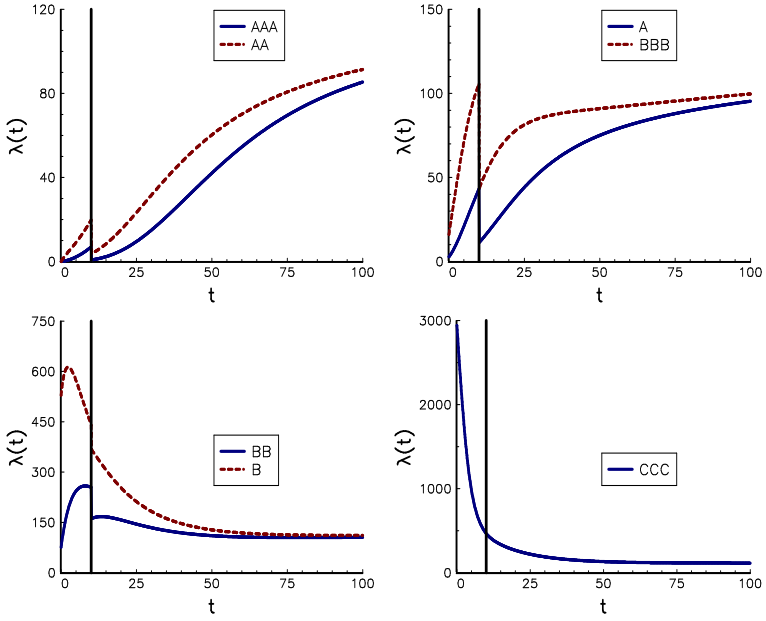

FIGURE 3.45: Hazard function $\lambda_i(t)$ (in bps) when a CCC-rated company defaults after 10 years ($\rho = 50\%$)

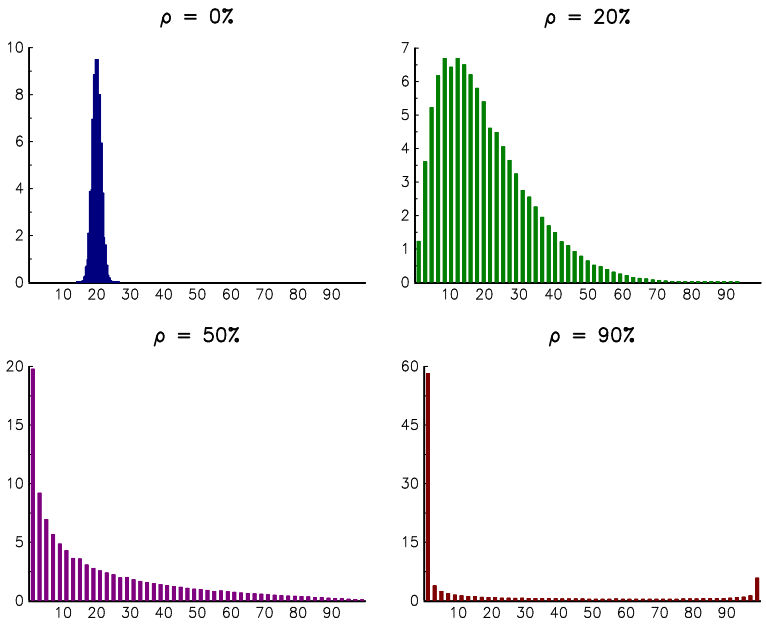

FIGURE 3.46: Distribution of the default rate (in %)

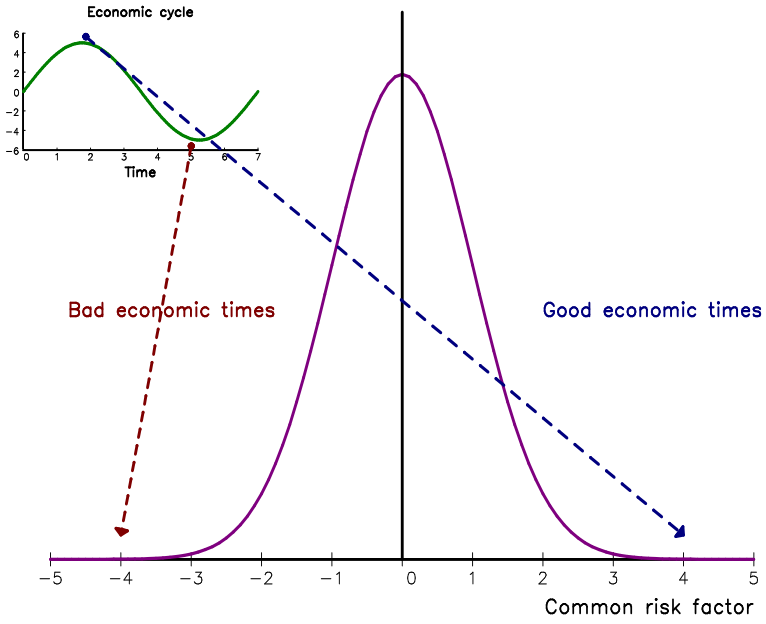

FIGURE 3.47: Economic interpretation of the common factor X

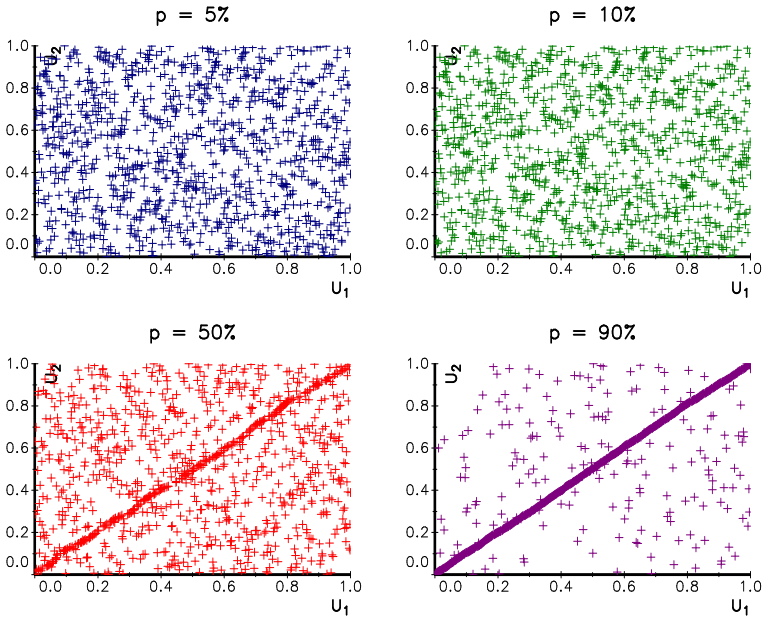

FIGURE 3.48: Dependogram of default times in the stochastic correlation model

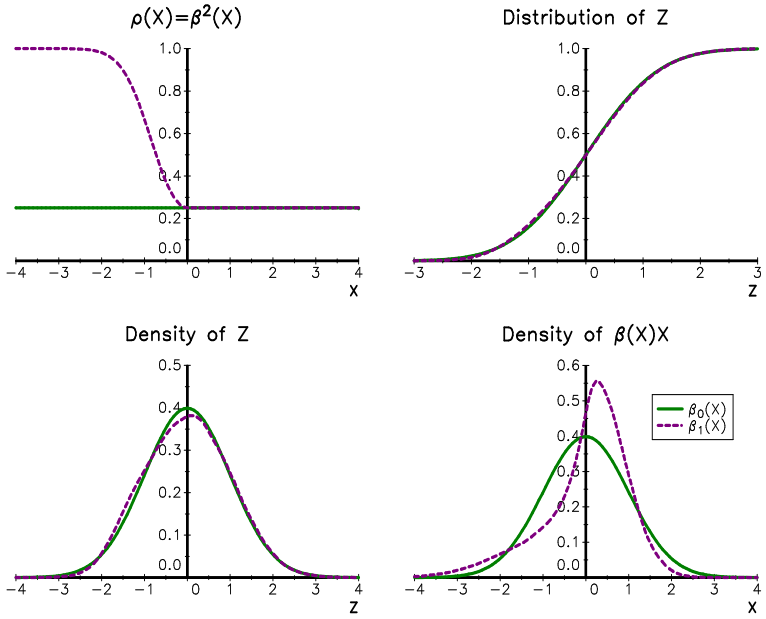

FIGURE 3.49: Distribution of the latent variable Z in the local correlation model

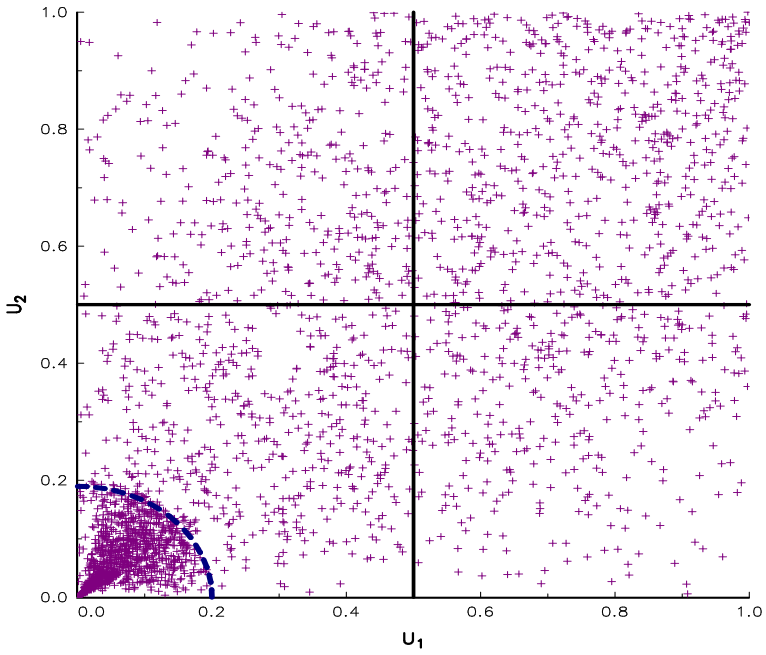

FIGURE 3.50: Dependogram of default times in the local correlation model

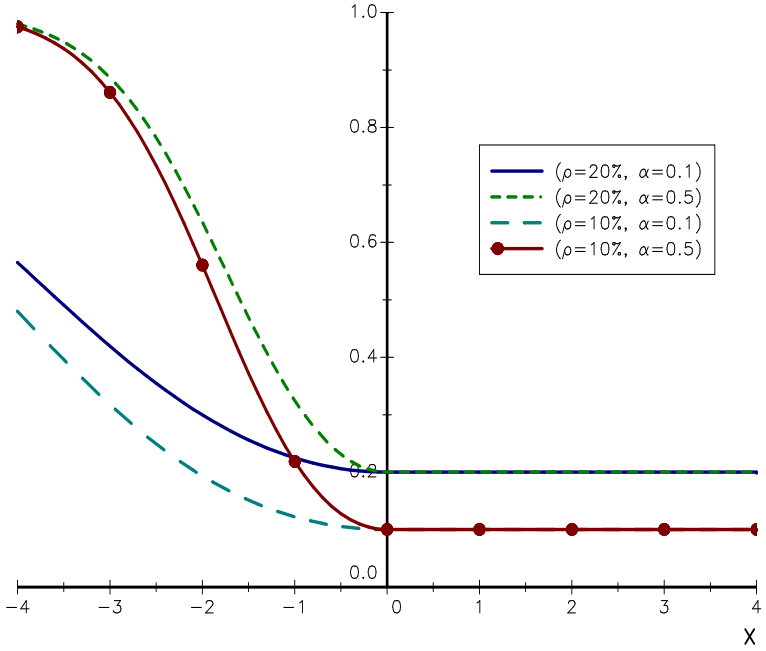

FIGURE 3.51: Local correlation $\rho(x) = \beta^2(x)$

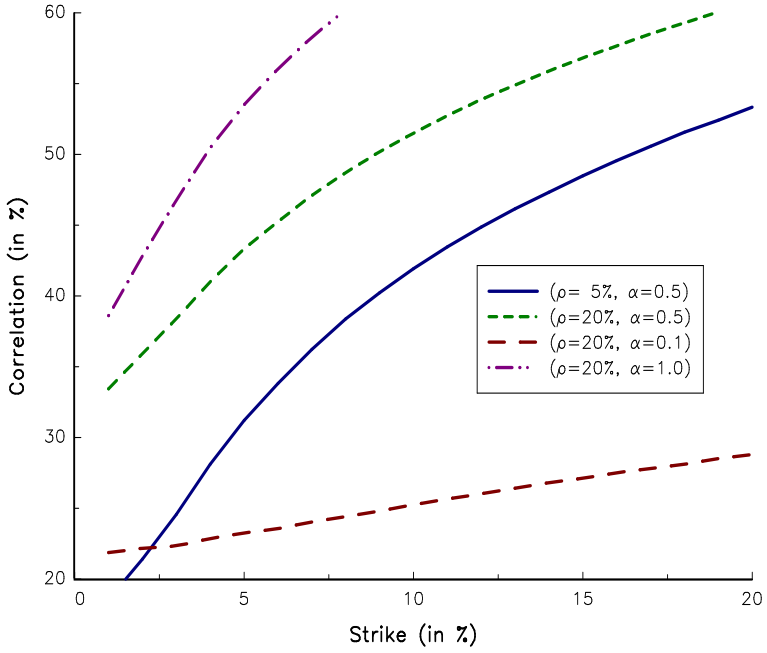

FIGURE 3.52: Correlation skew generated by the local correlation model

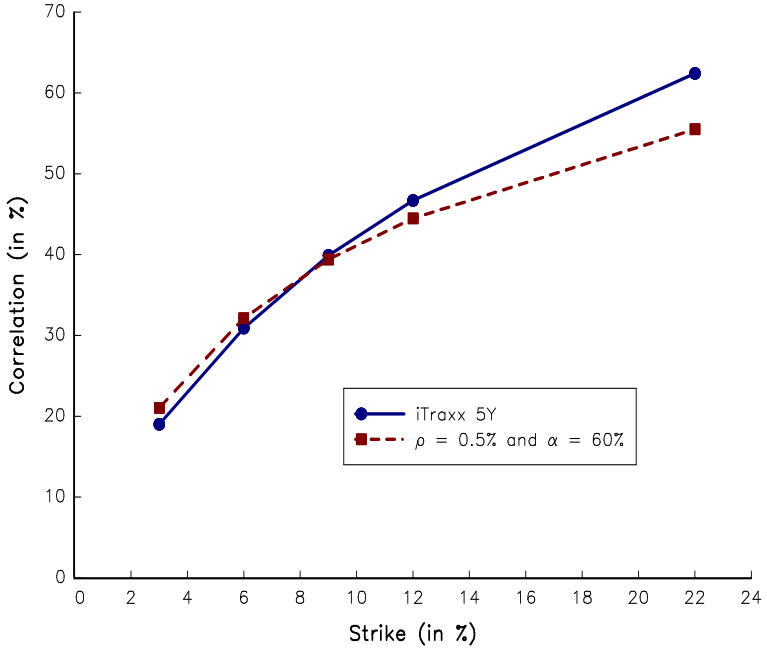

FIGURE 3.53: Calibration of the correlation skew (local correlation model)

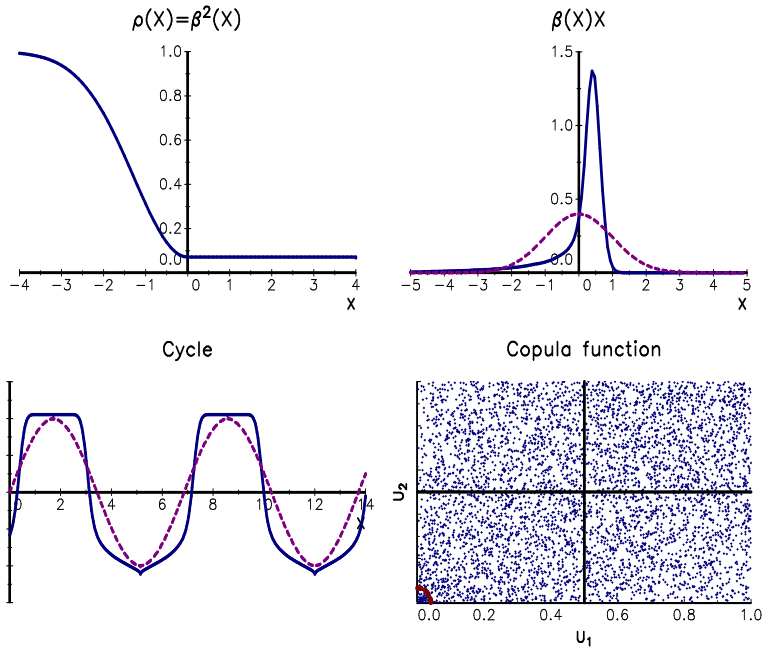

FIGURE 3.54: Implied local correlation model

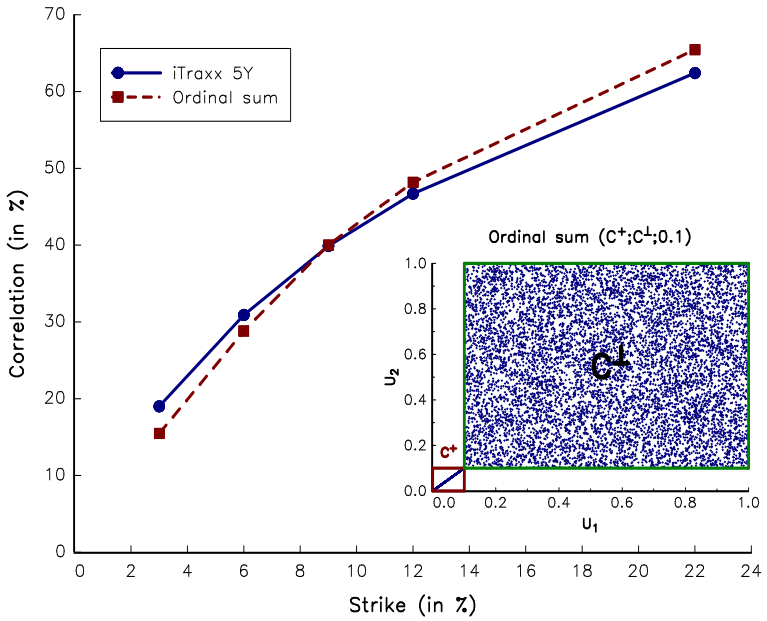

FIGURE 3.55: Calibration of the correlation skew (ordinal sum of $\mathbf{C}^{\perp}$ and $\mathbf{C}^{+}$)

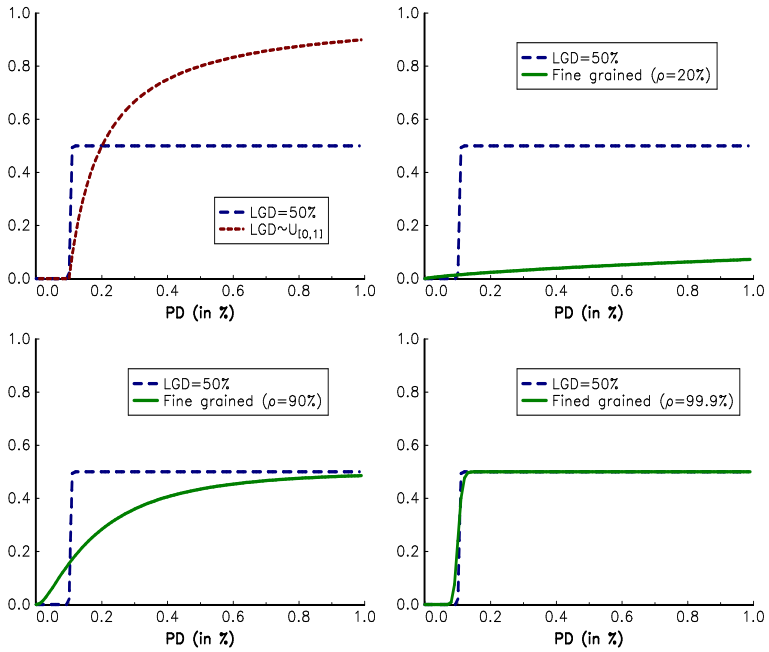

FIGURE 3.56: Comparison between the 99.9% value-at-risk of a loan and its risk contribution in an IFG portfolio

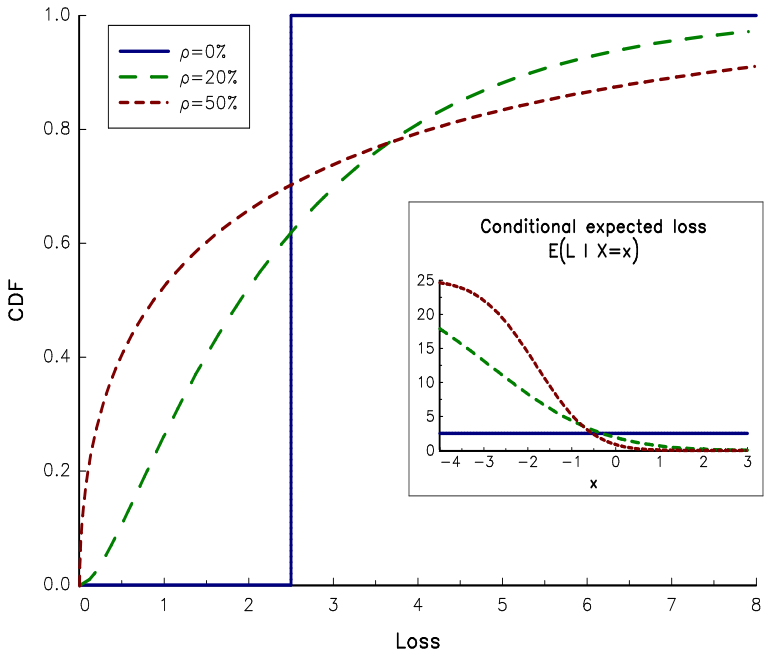

FIGURE 3.57: Loss distribution of an IFG portfolio

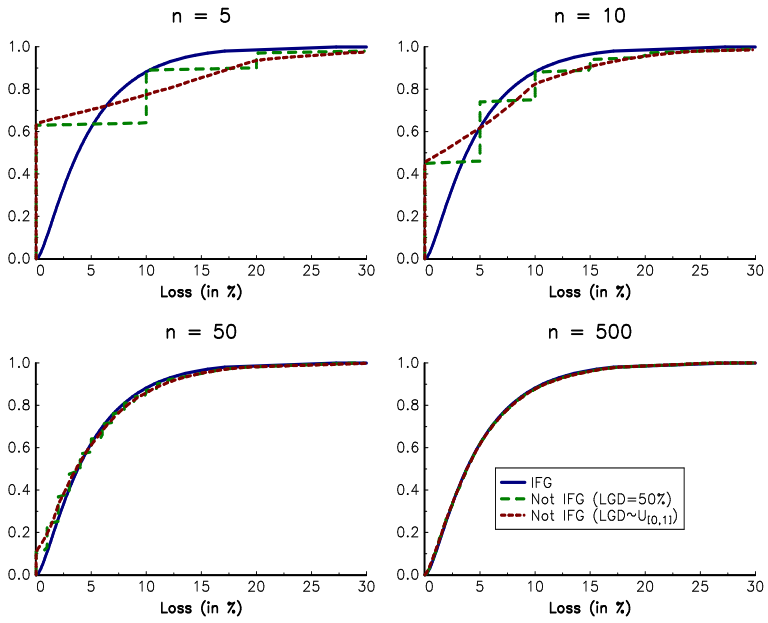

FIGURE 3.58: Comparison of the loss distribution of non-IFG and IFG portfolios

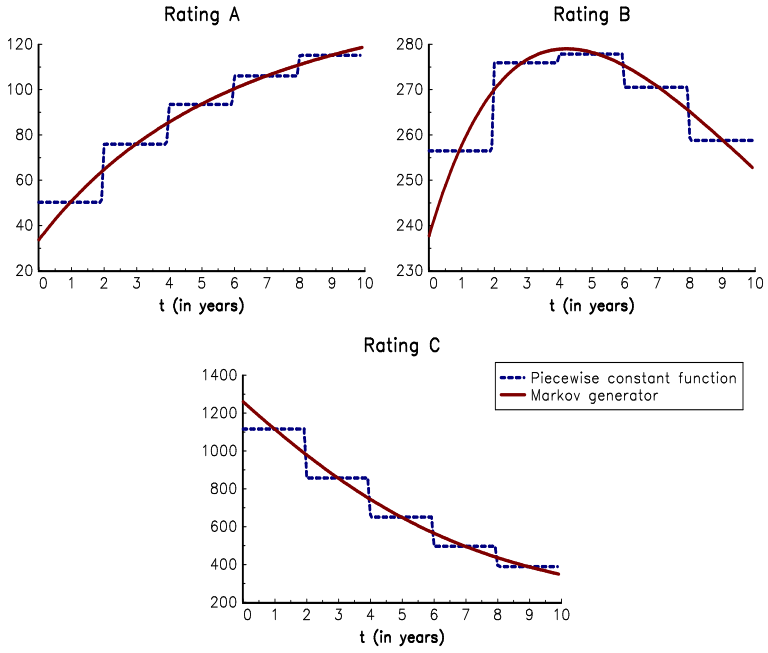

FIGURE 3.59: Hazard function $\lambda(t)$ (in bps) estimated respectively with the piecewise exponential model and the Markov generator

Chapter 4

Counterparty Credit Risk and Collateral Risk

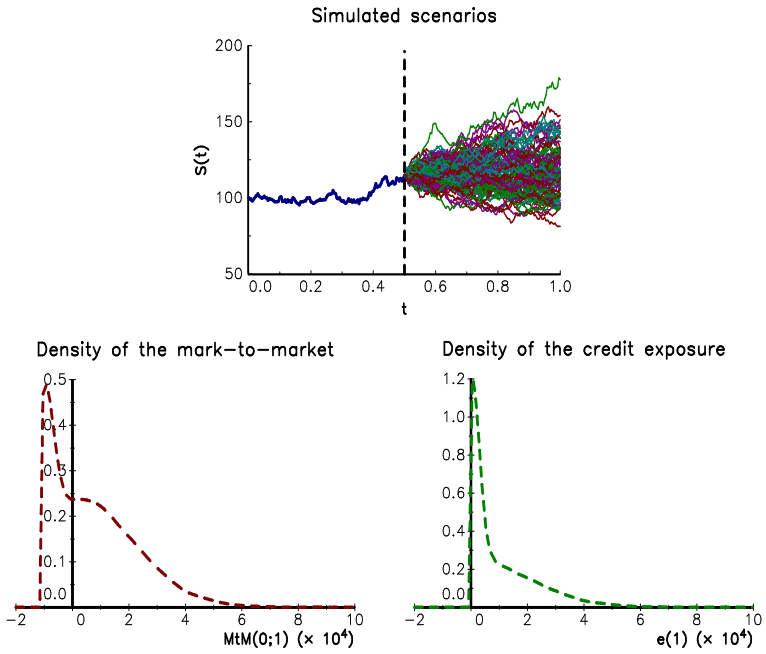

FIGURE 4.1: Probability density function of the counterparty exposure after six months

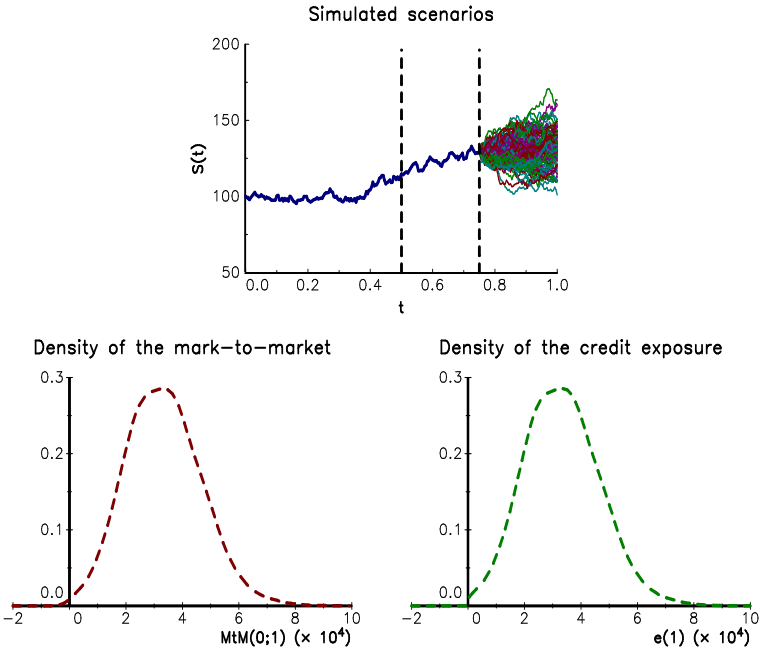

FIGURE 4.2: Probability density function of the counterparty exposure after nine months

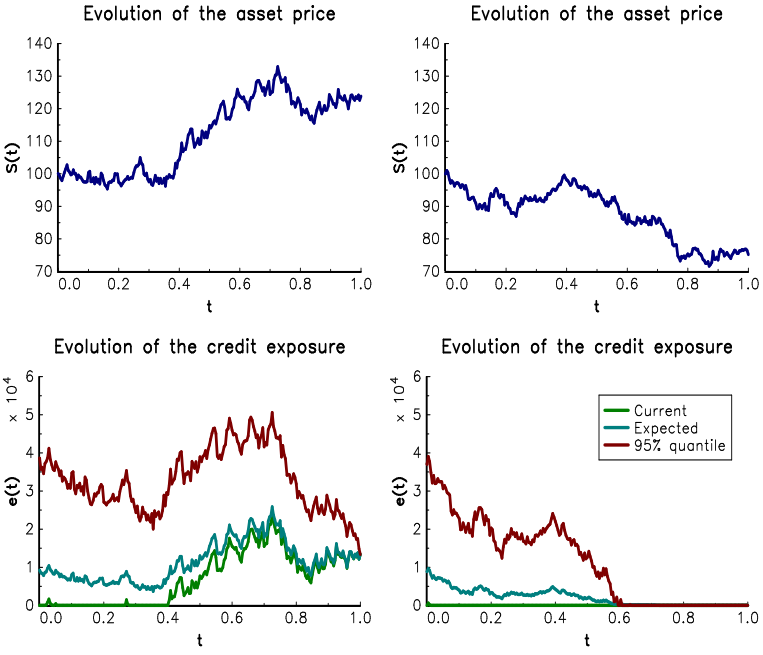

FIGURE 4.3: Evolution of the counterparty exposure

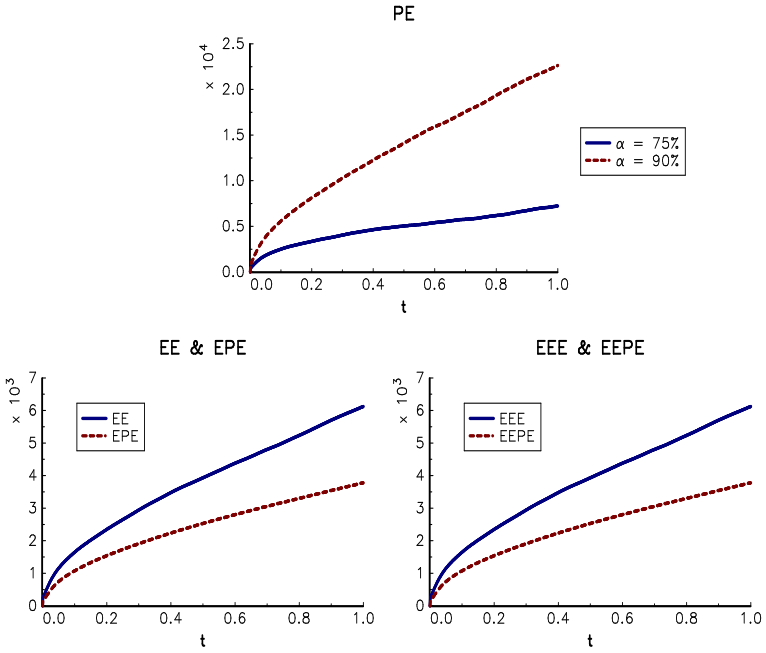

FIGURE 4.4: Counterparty exposure profile of option

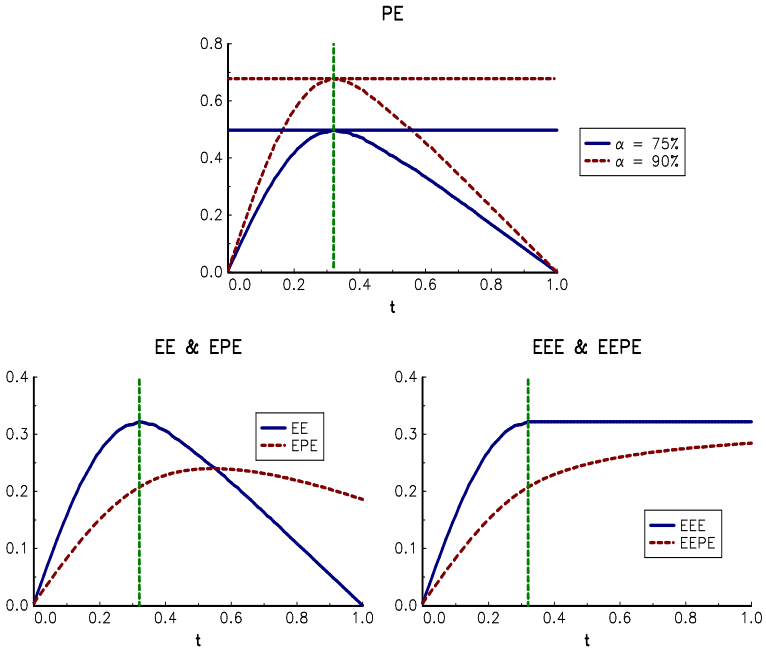

FIGURE 4.5: Counterparty exposure profile of interest rate swap

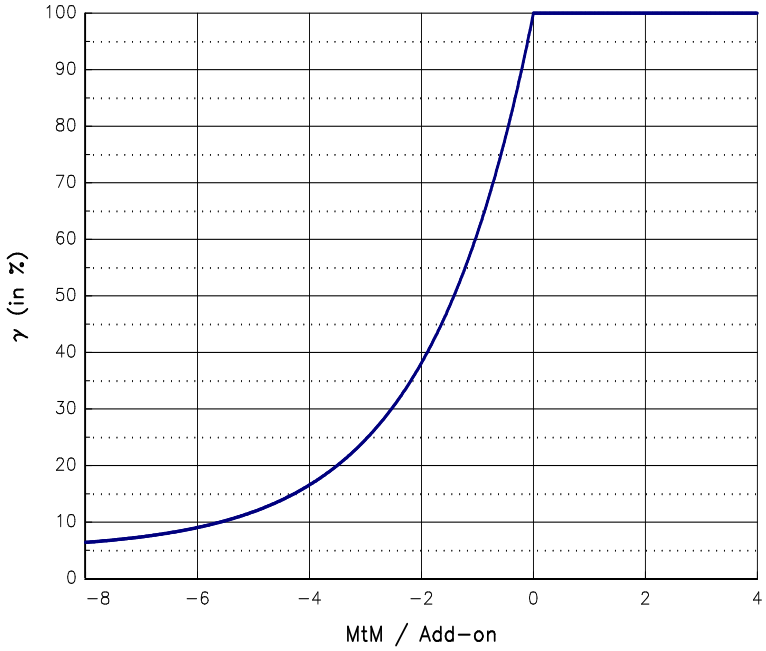

FIGURE 4.6: Impact of negative mark-to-market on the PFE multiplier

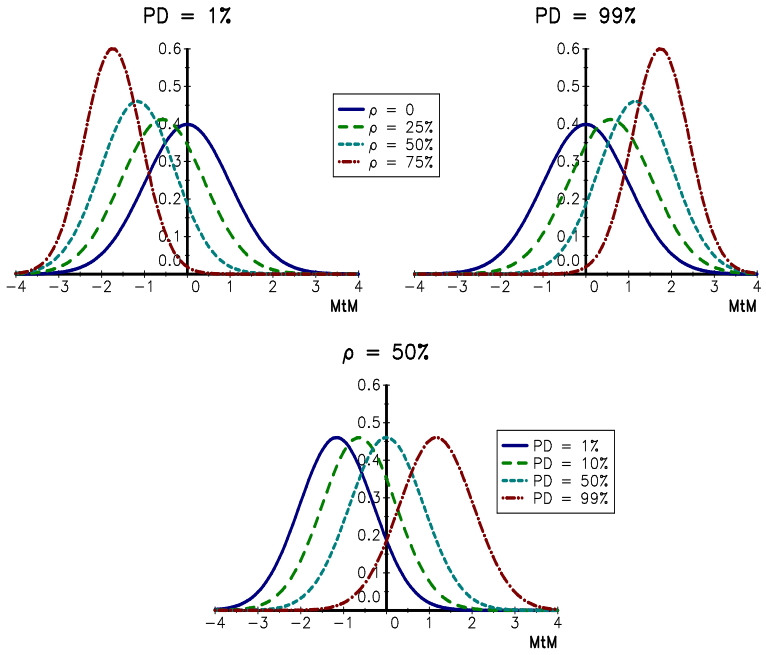

FIGURE 4.7: Conditional distribution of the mark-to-market

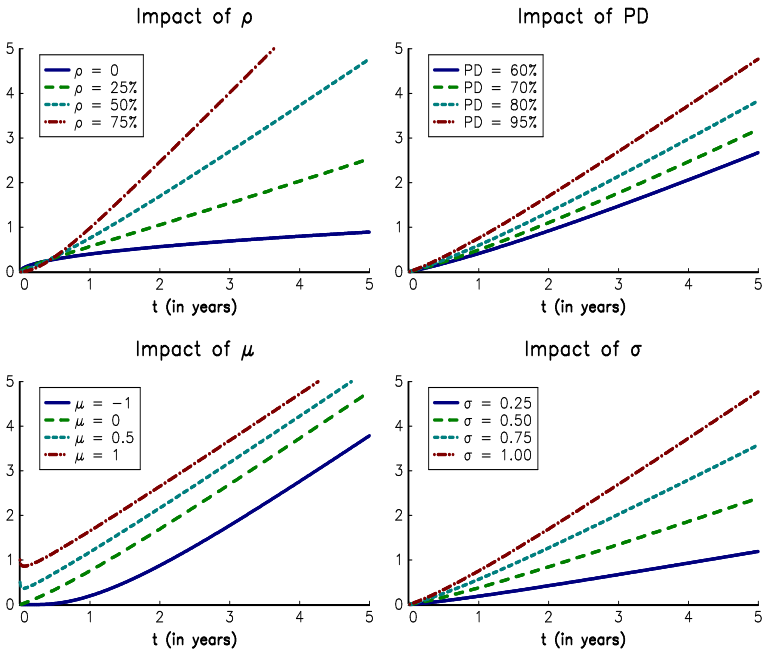

FIGURE 4.8: Conditional expectation of the exposure at default

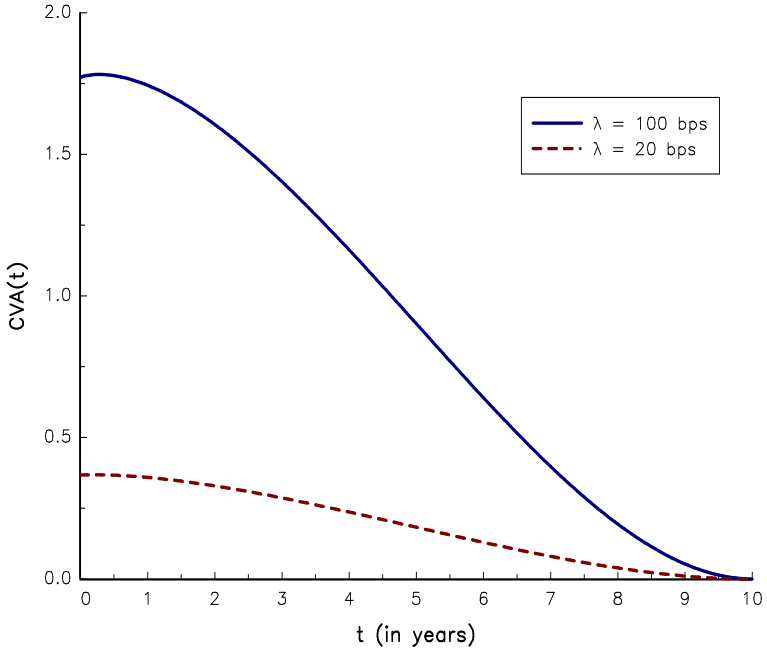

FIGURE 4.9: CVA of fixed-float swaps

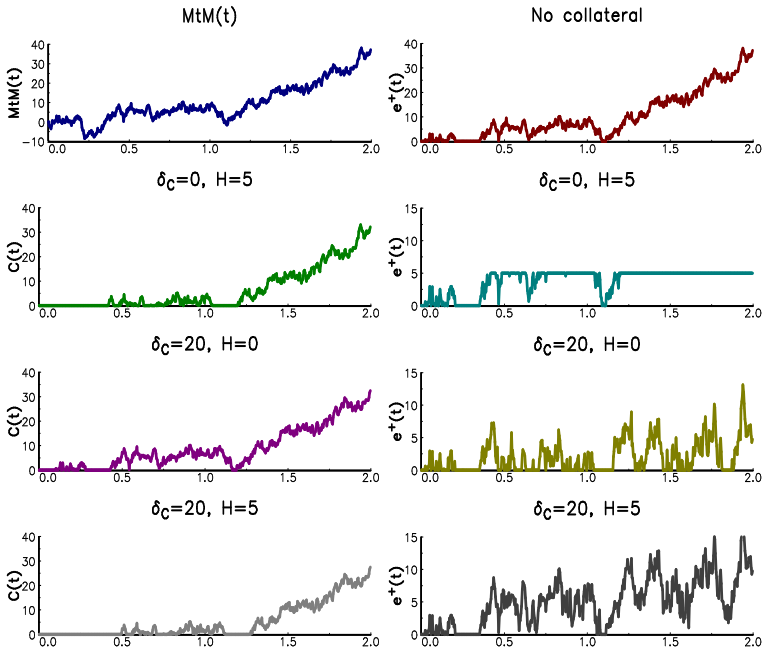

FIGURE 4.10: Impact of collateral on the counterparty exposure

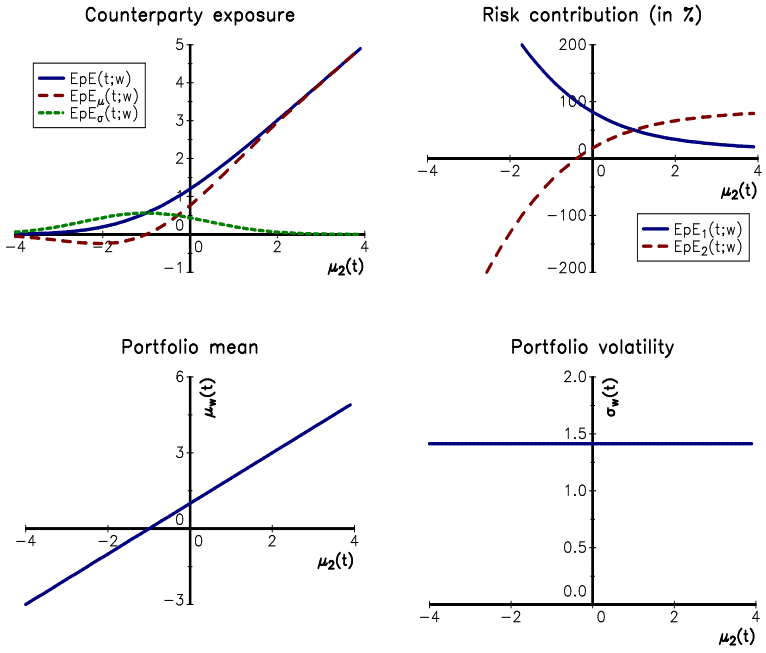

FIGURE 4.11: Impact of $\mu_i(t)/\sigma_i(t)$ on the counterparty exposure

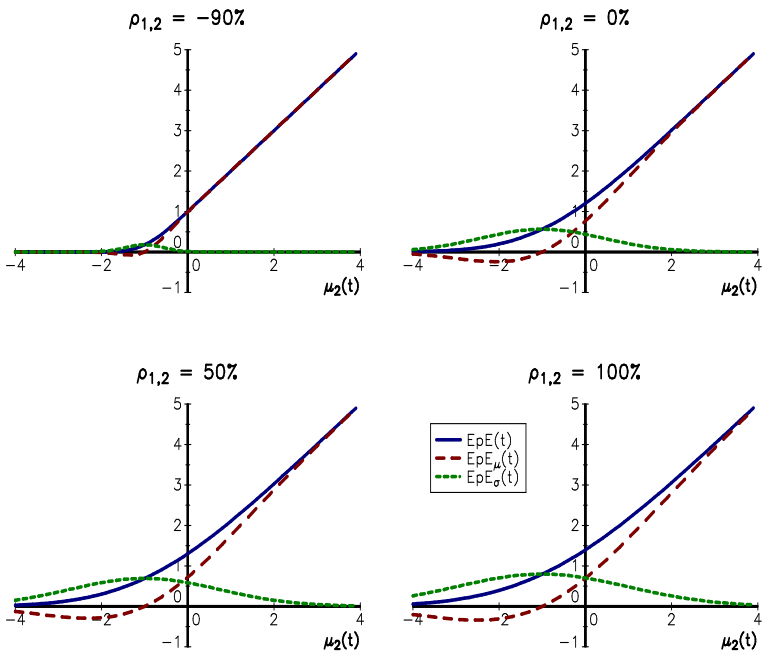

FIGURE 4.12: Impact of the correlation on the counterparty exposure

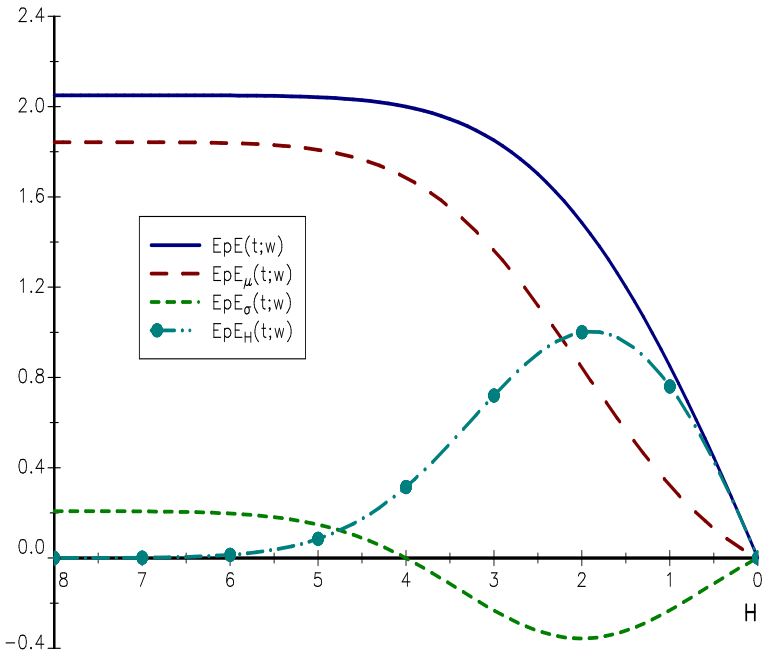

FIGURE 4.13: Decomposition of the counterparty exposure when there is a collateral agreement

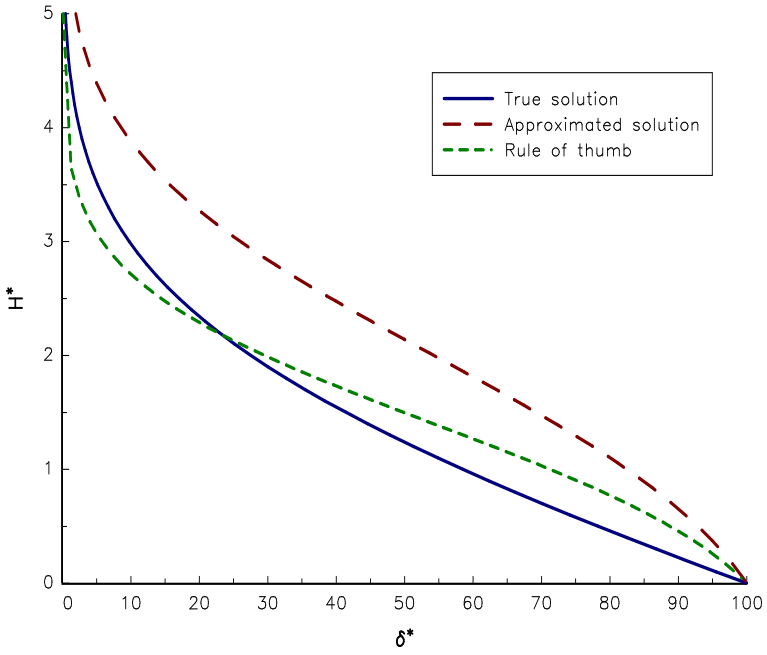

FIGURE 4.14: Optimal collateral threshold

Chapter 5

Operational Risk

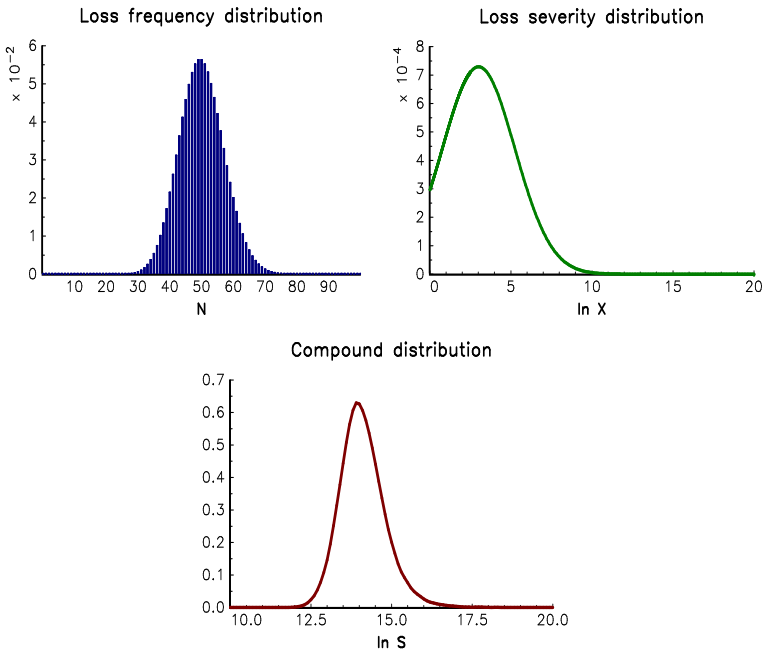

FIGURE 5.1: Compound distribution when $N \sim \mathcal{P}(50)$ and $X \sim \mathcal{LN}(8, 5)$

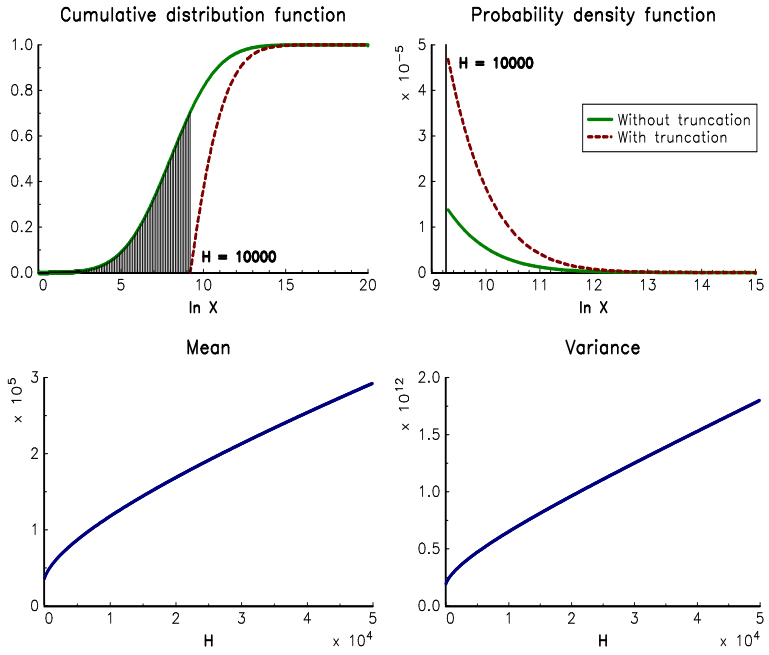

FIGURE 5.2: Impact of the threshold H on the severity distribution

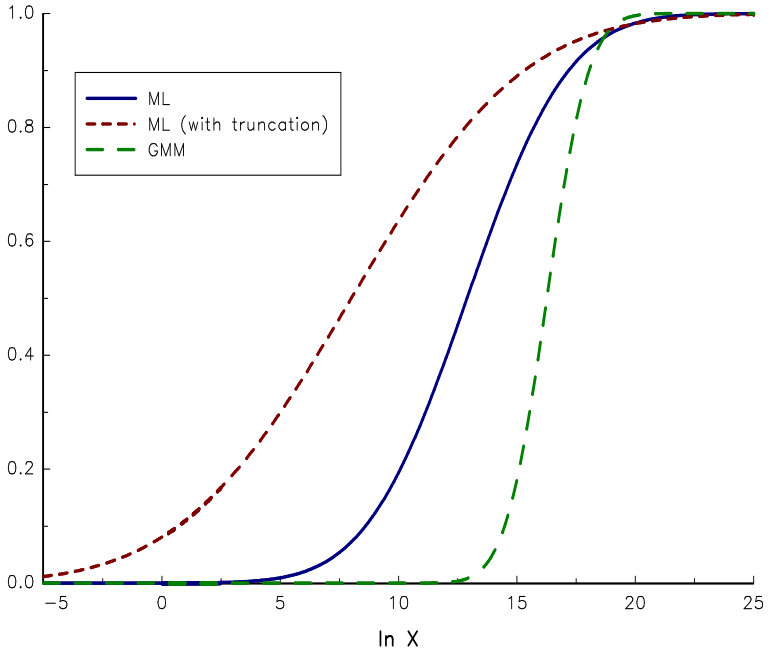

FIGURE 5.3: Comparison of the estimated severity distributions

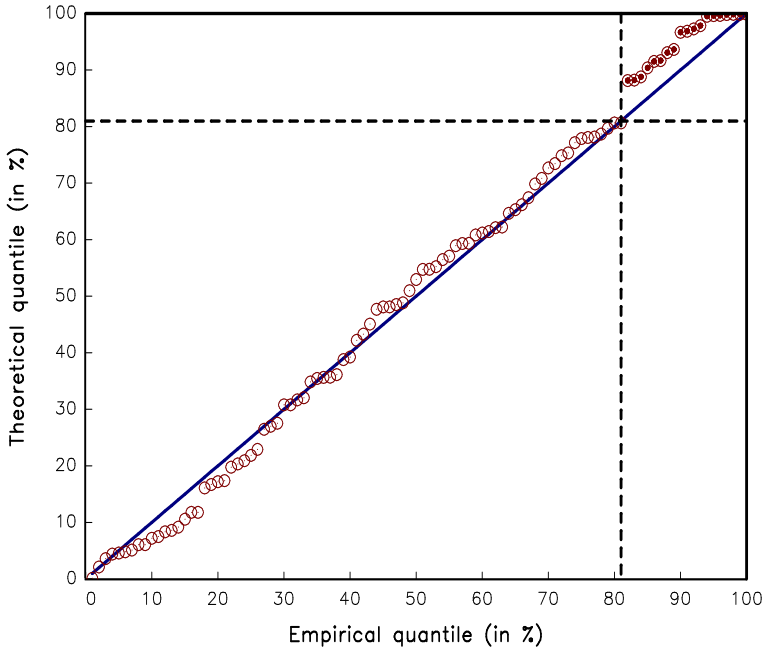

FIGURE 5.4: An example of QQ plot where extreme events are underestimated

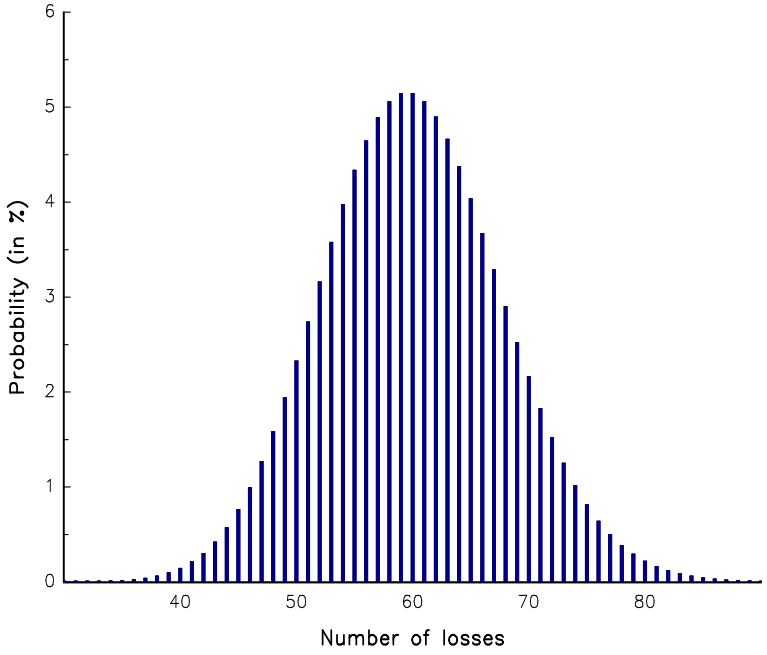

FIGURE 5.5: PMF of the Poisson distribution $\mathcal{P}(60)$

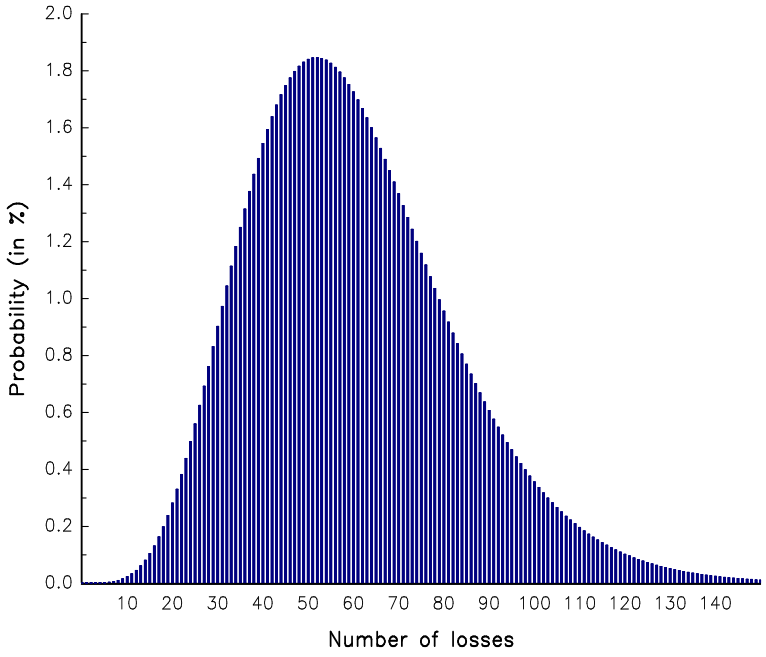

FIGURE 5.6: PMF of the negative binomial distribution

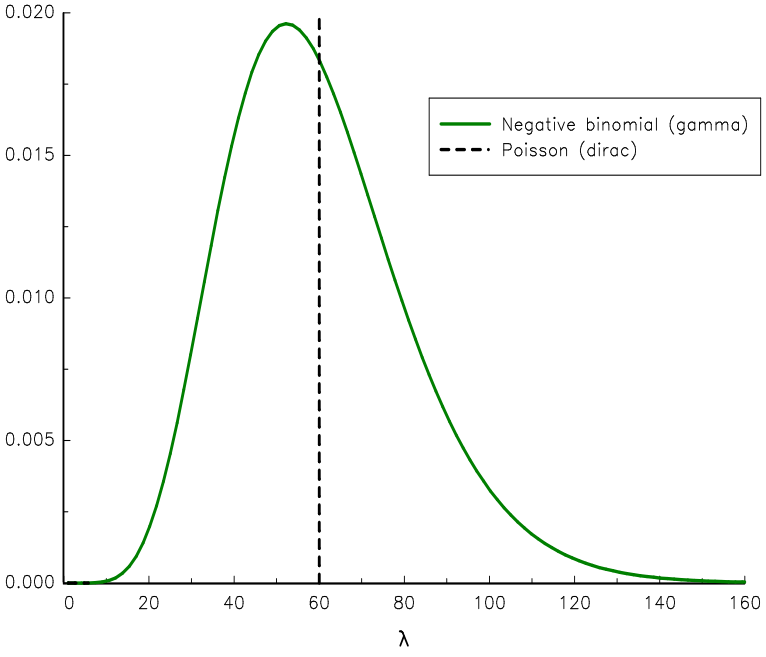

FIGURE 5.7: Probability density function of the parameter λ

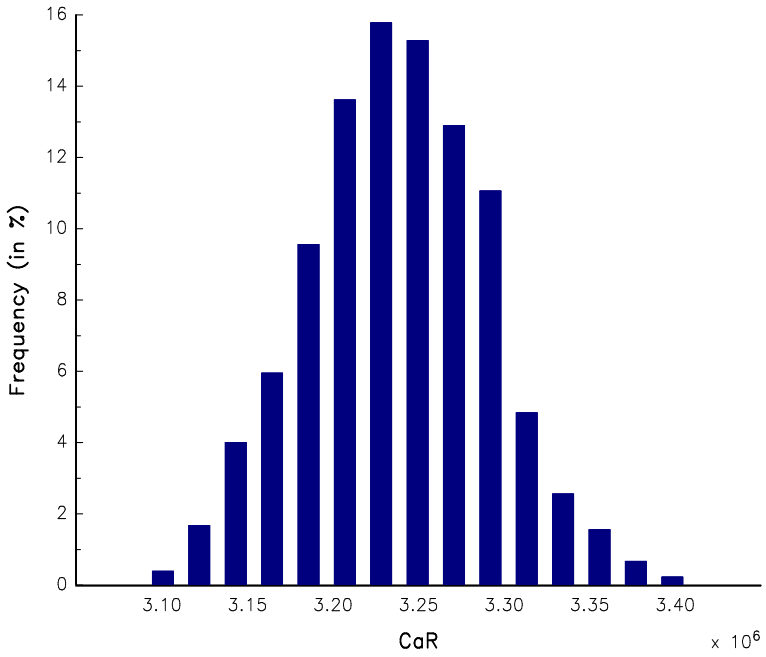

FIGURE 5.8: Histogram of the MC estimator $\widehat{\mathrm{CaR}}$

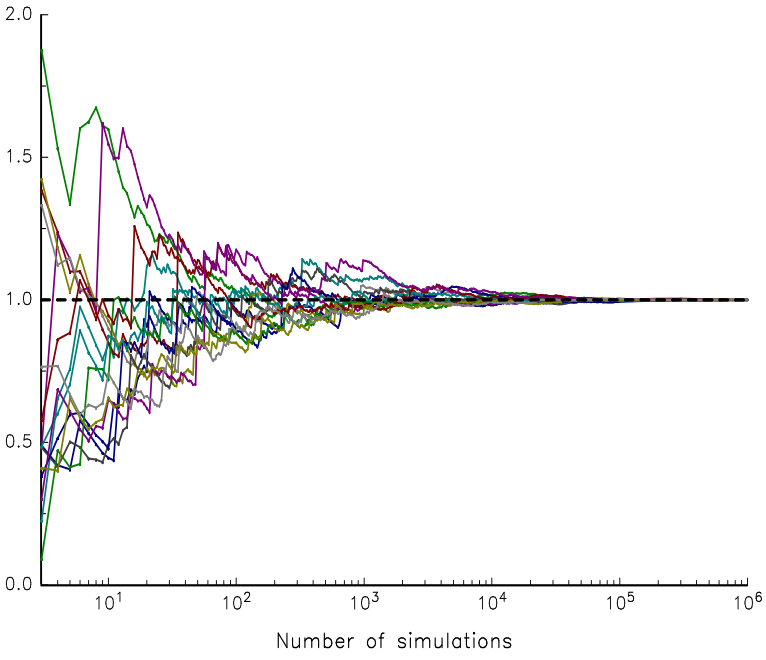

FIGURE 5.9: Convergence of the accuracy ratio $R(n_s)$ when $\sigma = 1$

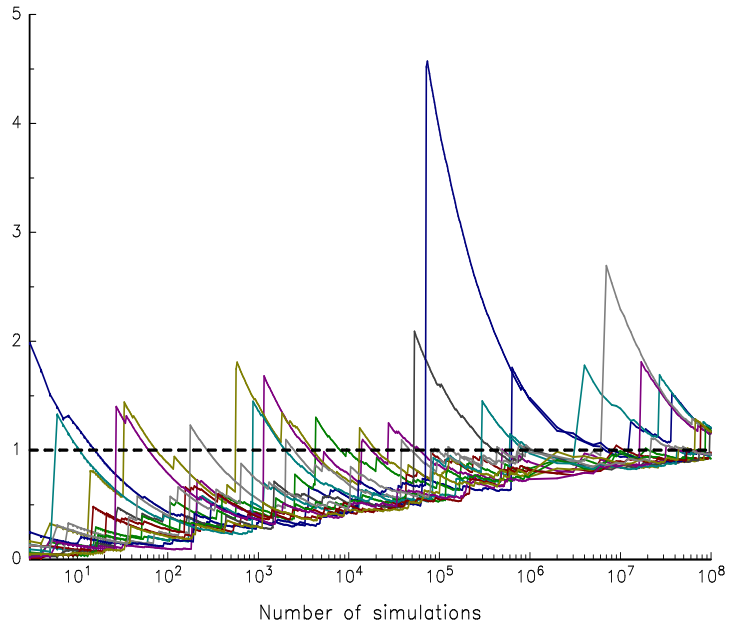

FIGURE 5.10: Convergence of the accuracy ratio $R(n_s)$ when $\sigma = 2.5$

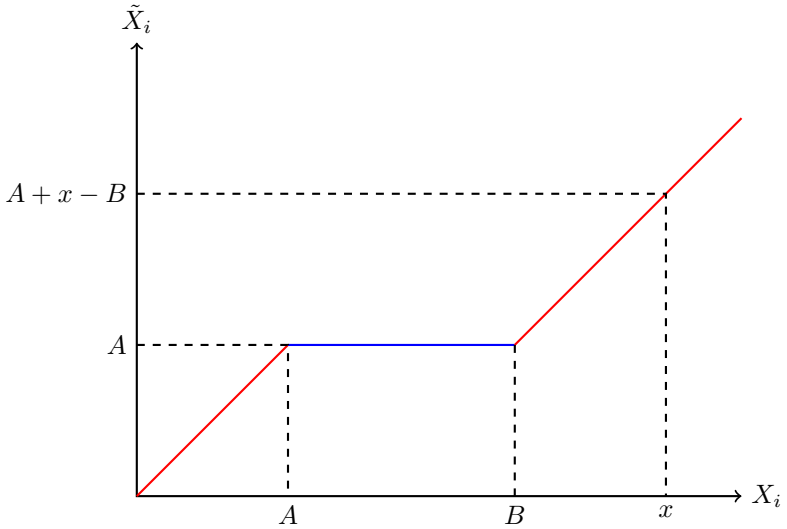

FIGURE 5.11: Impact of the insurance contract on the operational risk loss

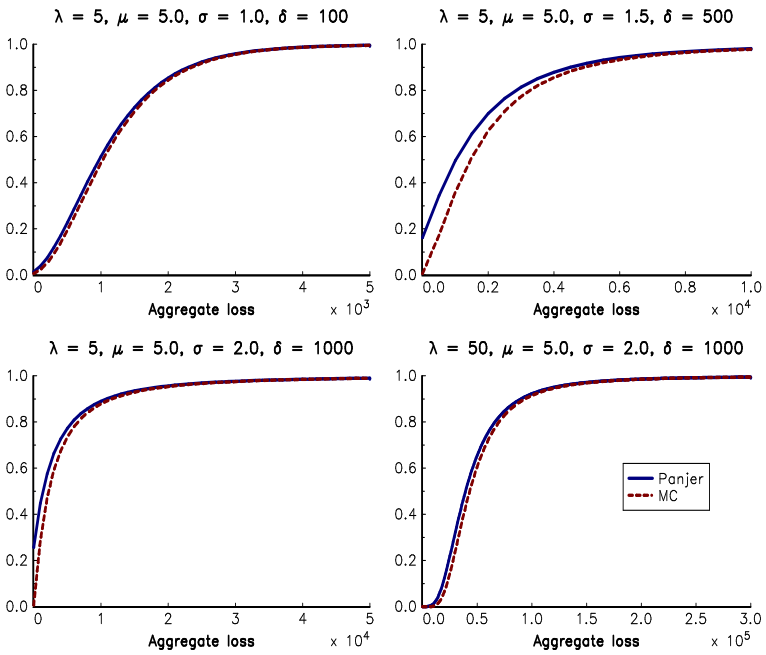

FIGURE 5.12: Comparison between the Panjer and MC compound distributions

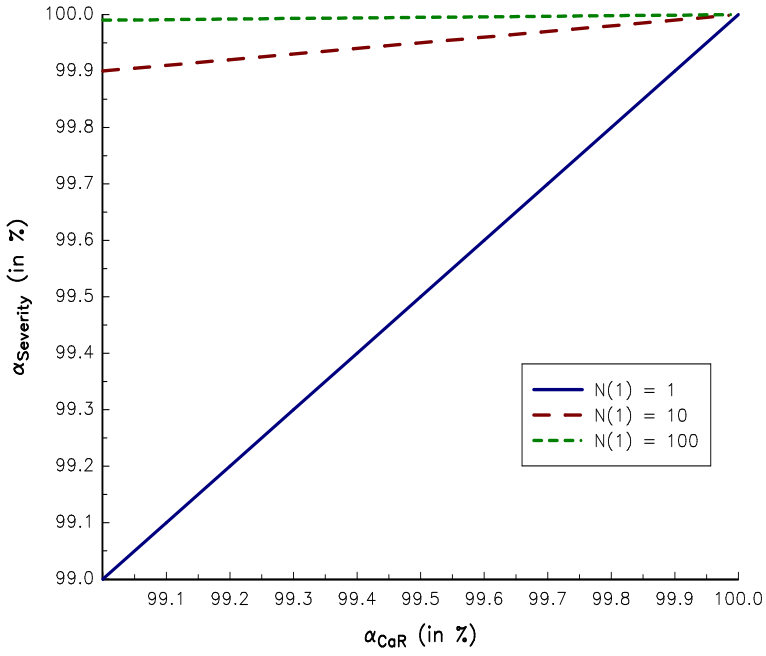

FIGURE 5.13: Relationship between α_{CaR} and α_{Severity}

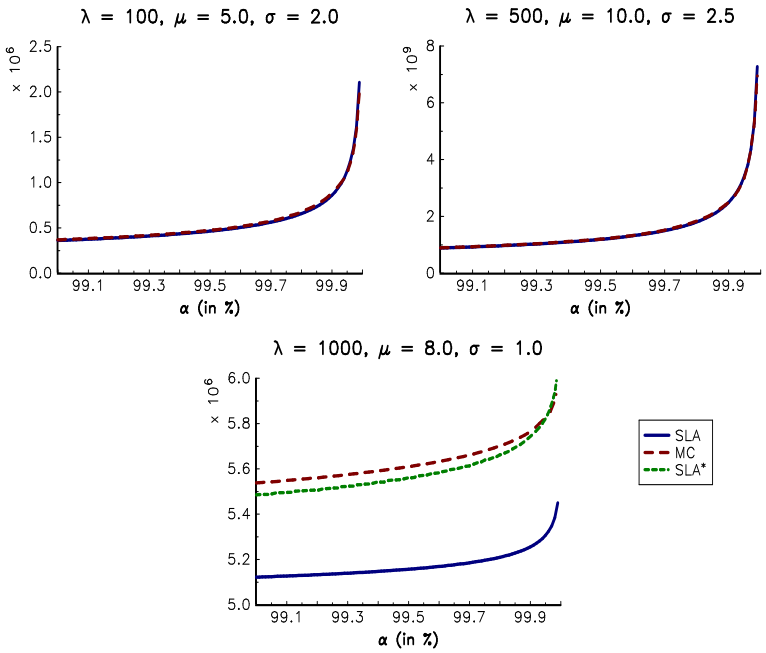

FIGURE 5.14: Numerical illustration of the single loss approximation

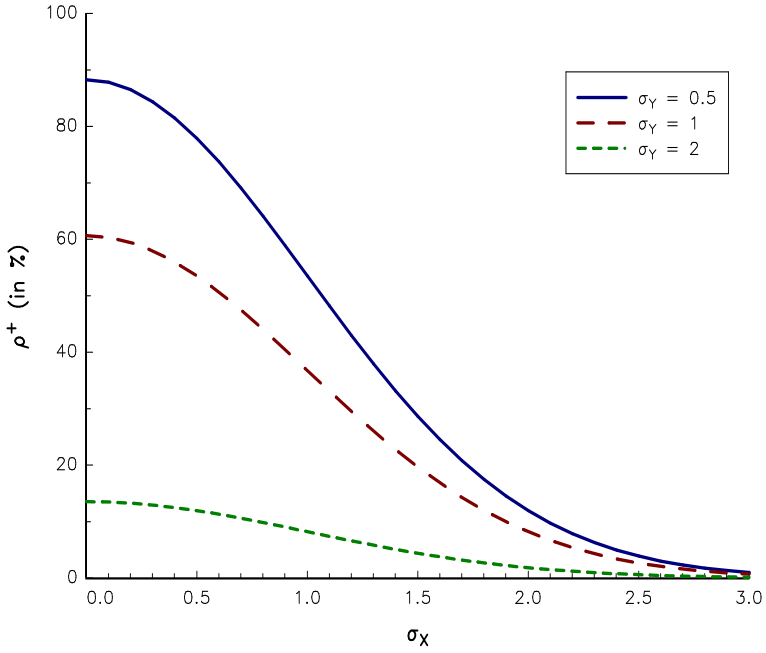

FIGURE 5.15: Upper bound ρ^+ of the aggregate loss correlation

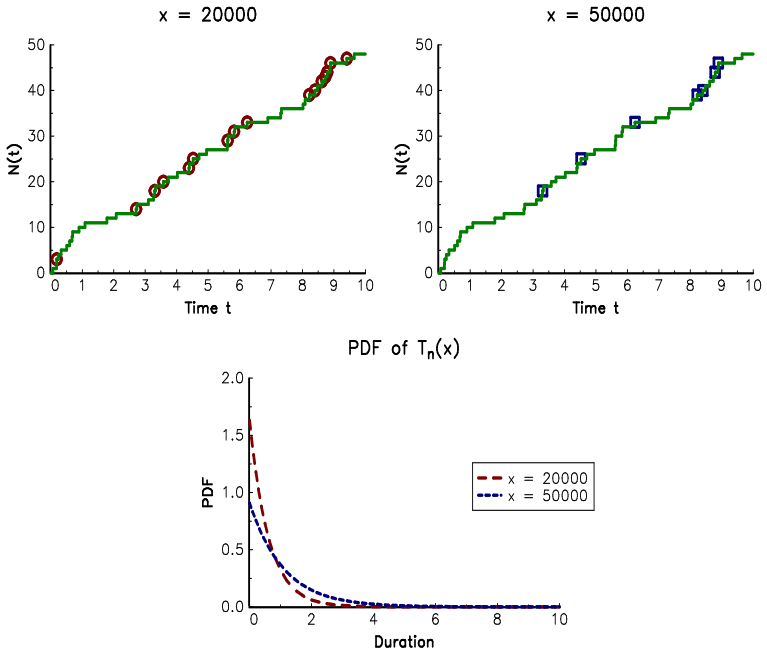

FIGURE 5.16: Simulation of the Poisson process $N(t)$ and peak over threshold events

Chapter 6

Liquidity Risk

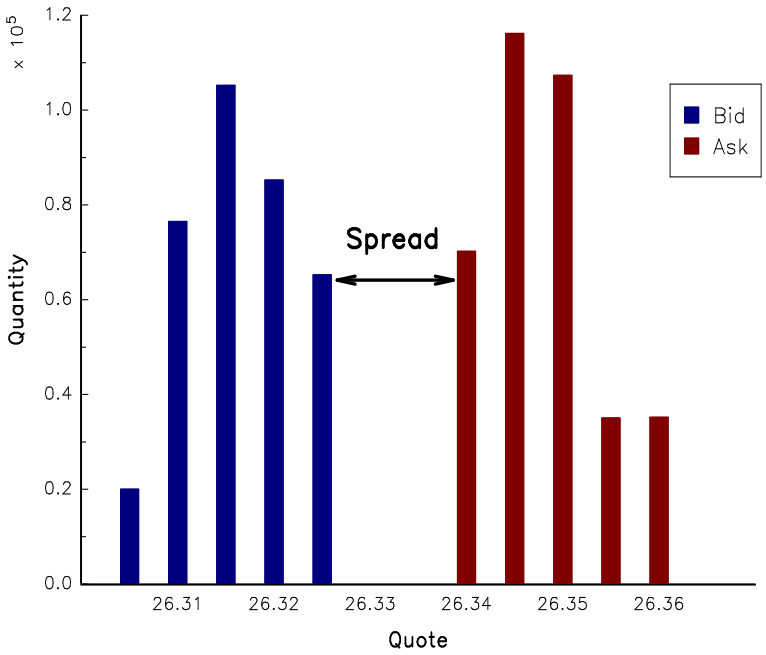

FIGURE 6.1: An example of a limit order book

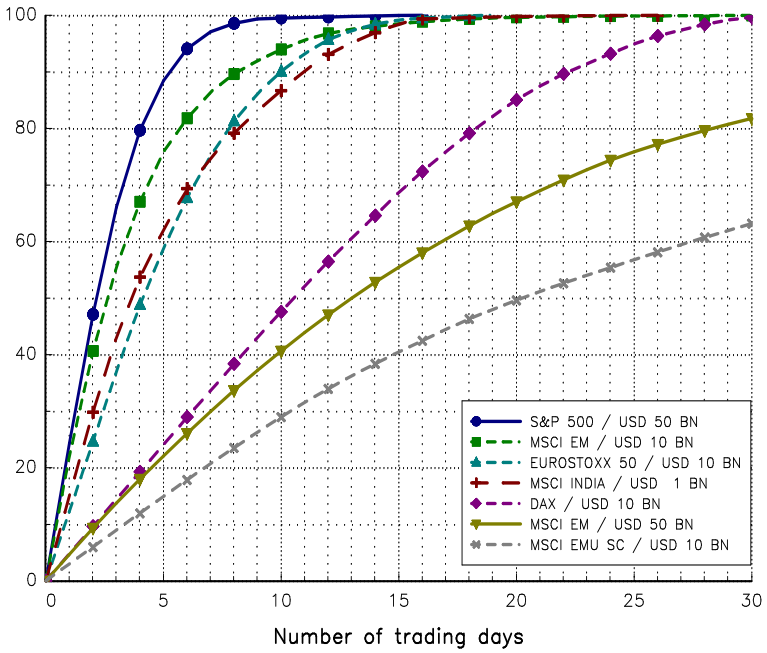

FIGURE 6.2: Comparing the liquidation ratio (in %) between index fund portfolios

Source: Roncalli and Weisang (2015).

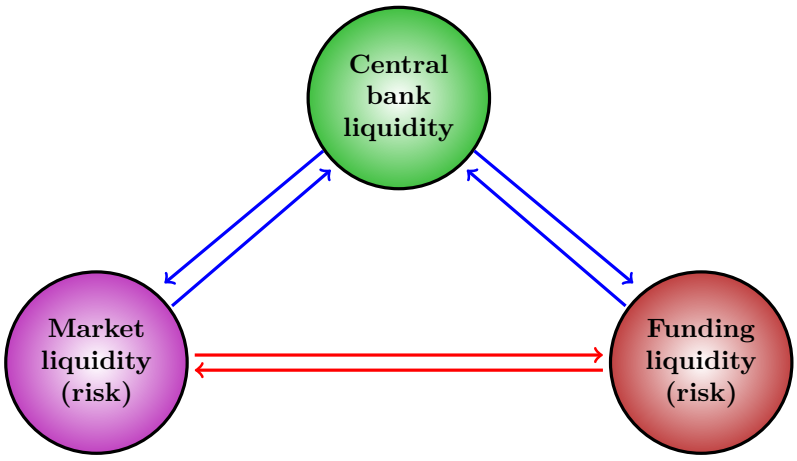

FIGURE 6.3: The liquidity nodes of the financial system

Source: Nikolaou (2009).

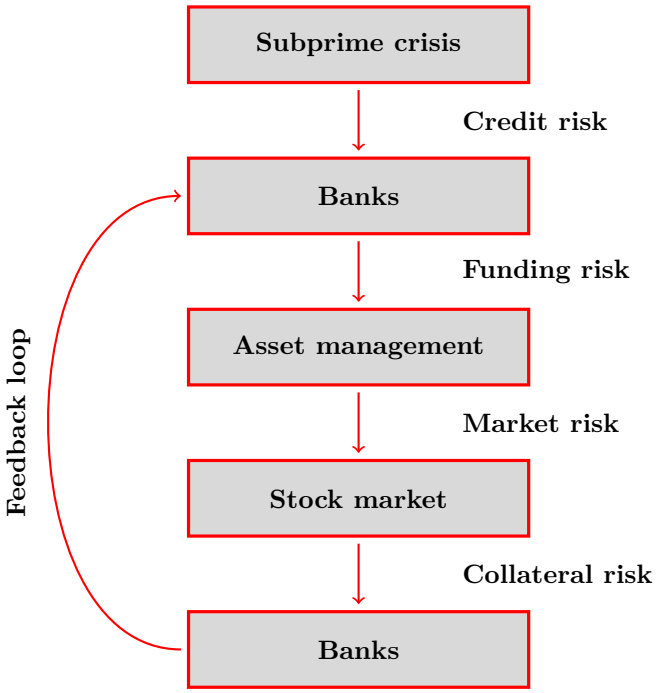

FIGURE 6.4: Spillover effects during the 2008 global financial crisis

Chapter 7

Asset Liability Management Risk

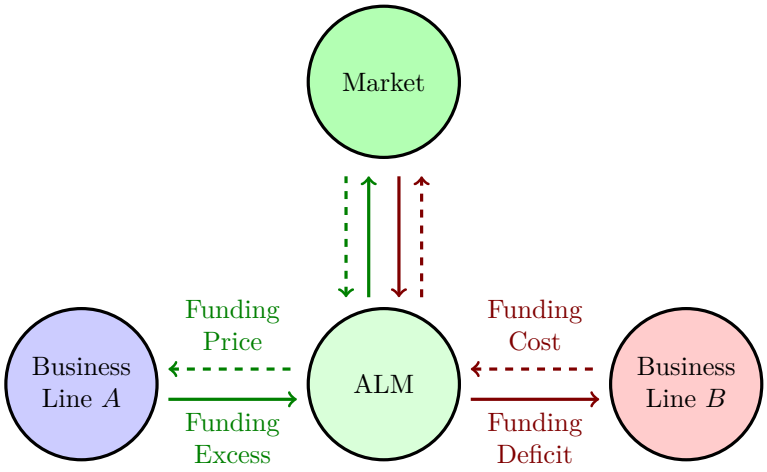

FIGURE 7.1: Internal and external funding transfer

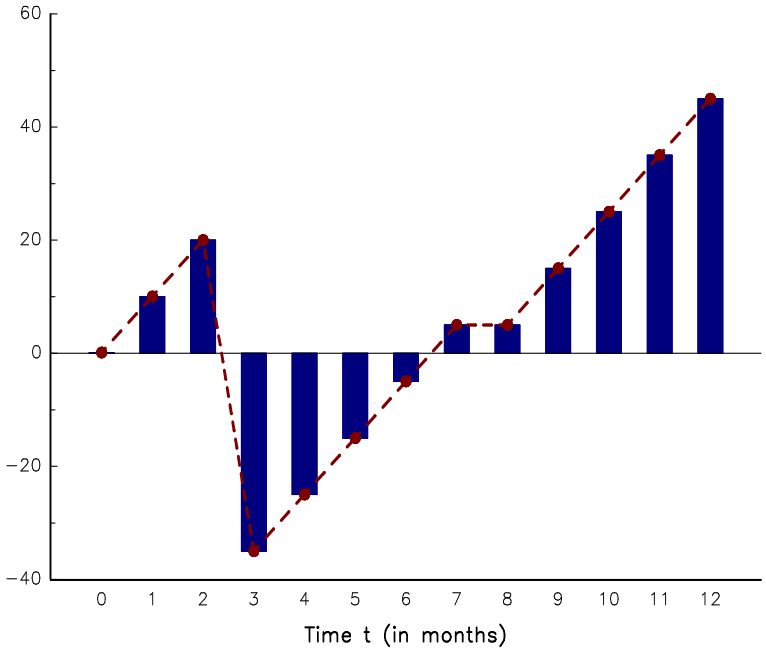

FIGURE 7.2: An example of liquidity gap

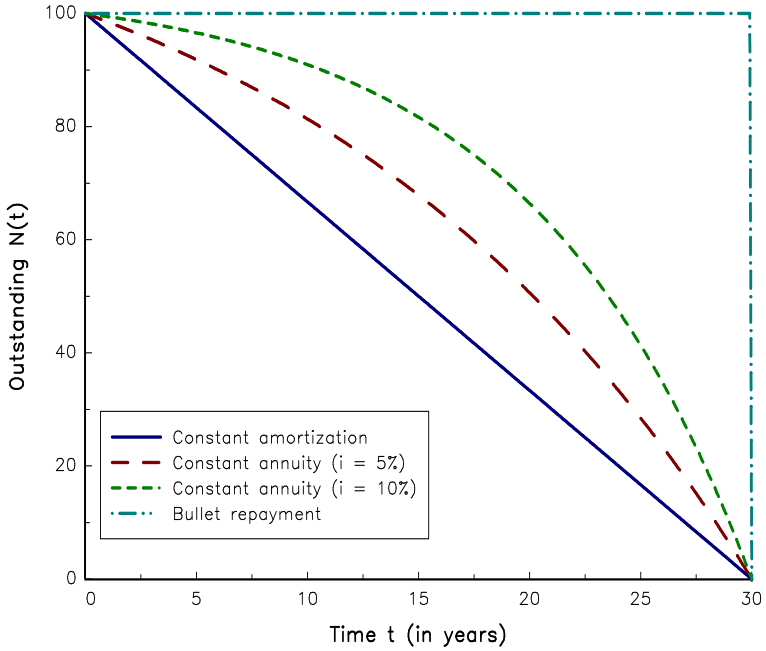

FIGURE 7.3: Amortization schedule of the 30-year mortgage

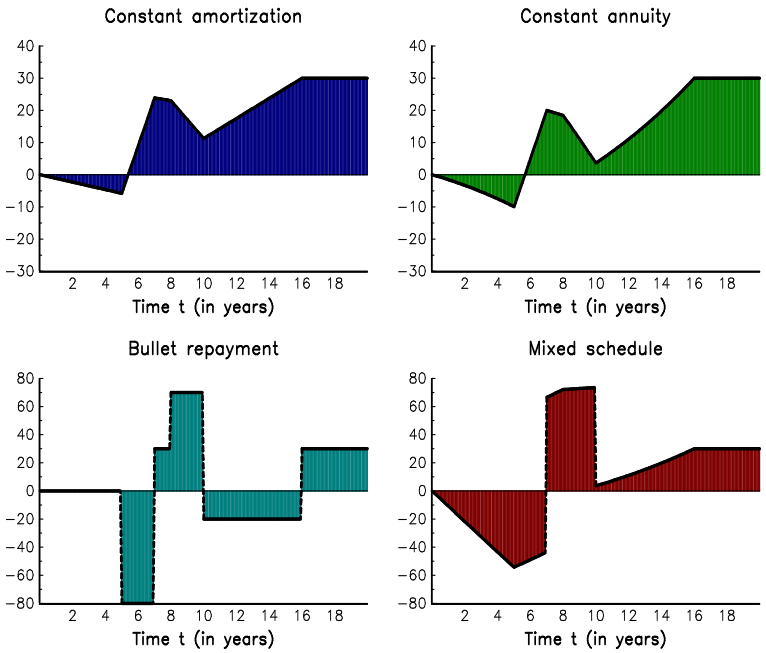

FIGURE 7.4: Impact of the amortization schedule on the liquidity gap

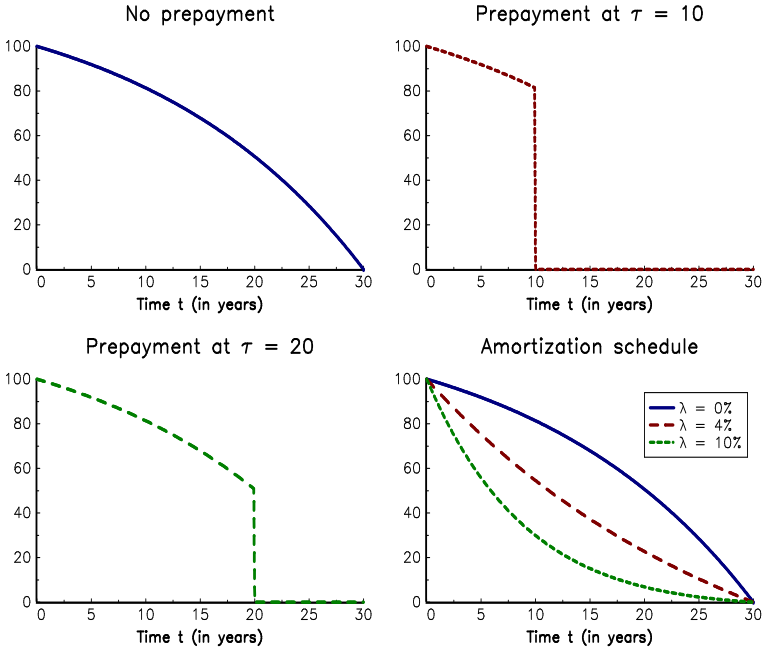

FIGURE 7.5: Conventional amortization schedule with prepayment risk

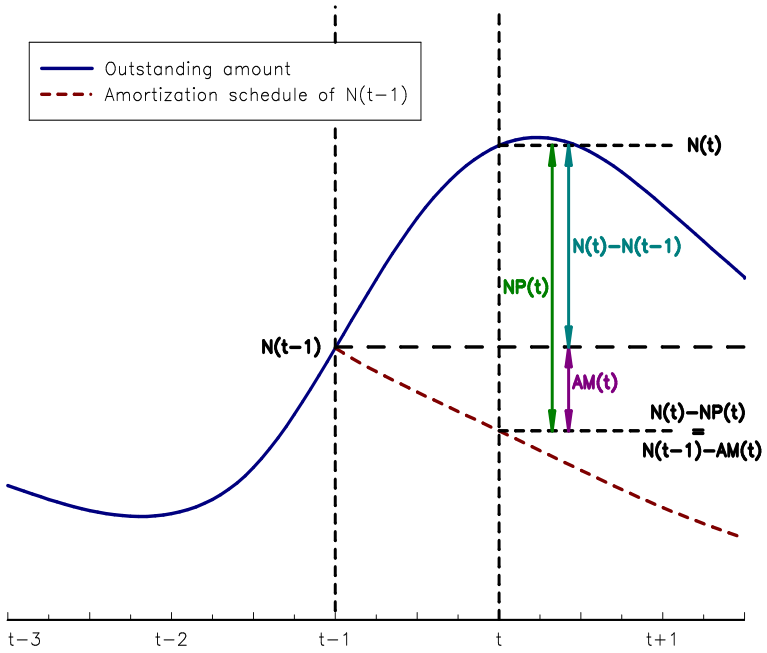

FIGURE 7.6: Impact of the new production on the outstanding amount

Source: Demey *et al.* (2003).

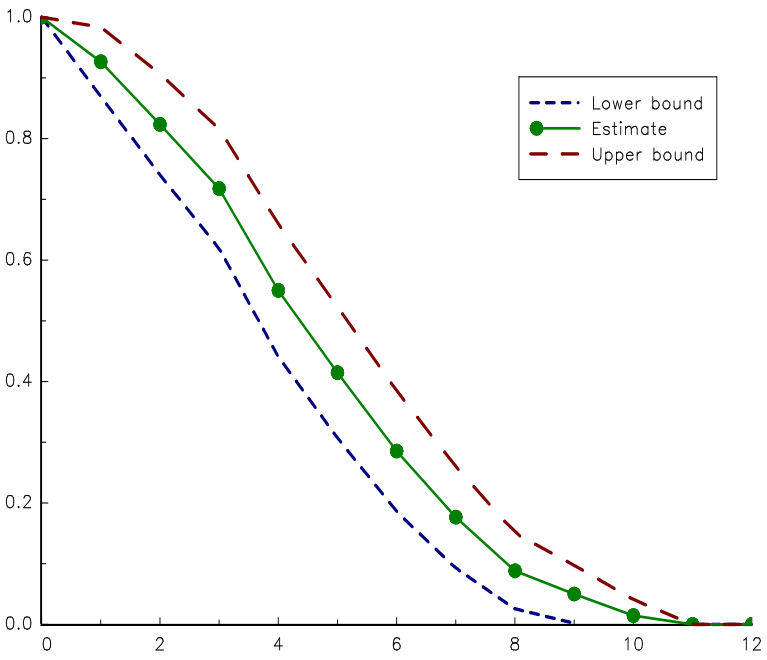

FIGURE 7.7: Estimation of the amortization function $\hat{\mathbf{S}}(u-t)$

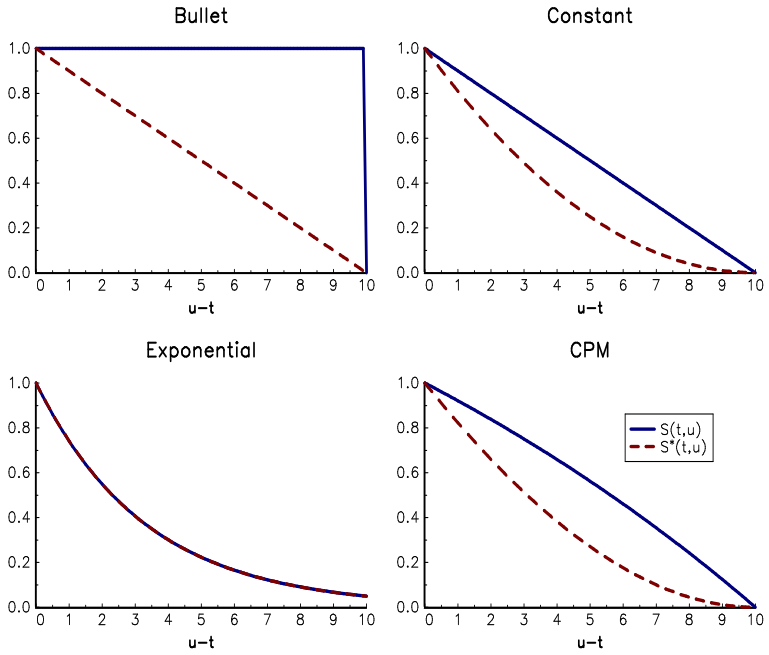

FIGURE 7.8: Amortization functions $\mathbf{S}(t,u)$ and $\mathbf{S}^{\star}(t,u)$

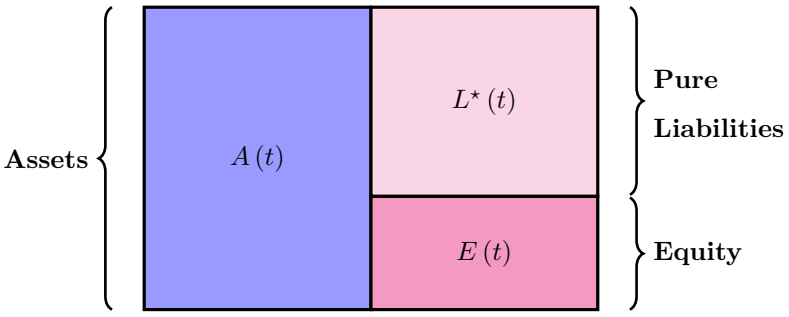

FIGURE 7.9: Relationship between $A(t)$, $L^{\star}(t)$ and $E(t)$

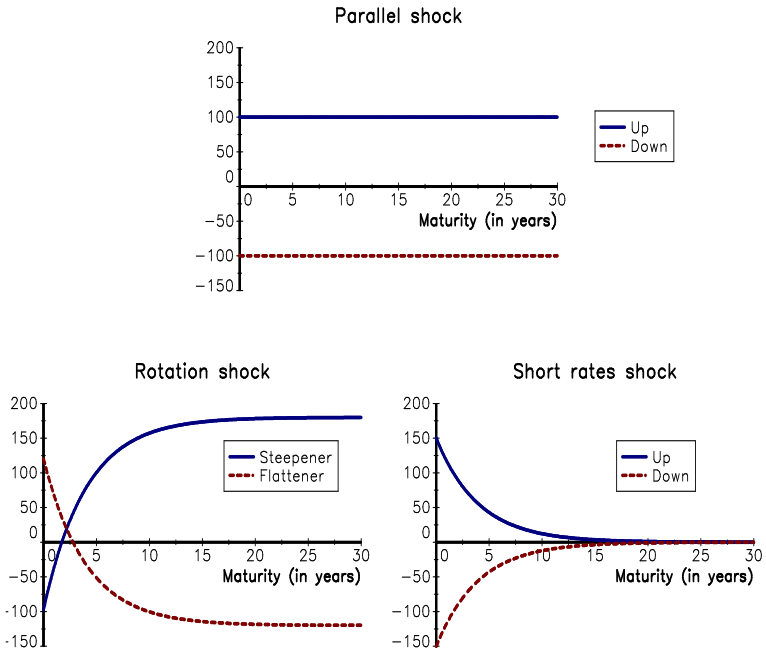

FIGURE 7.10: Interest rate shocks (in bps)

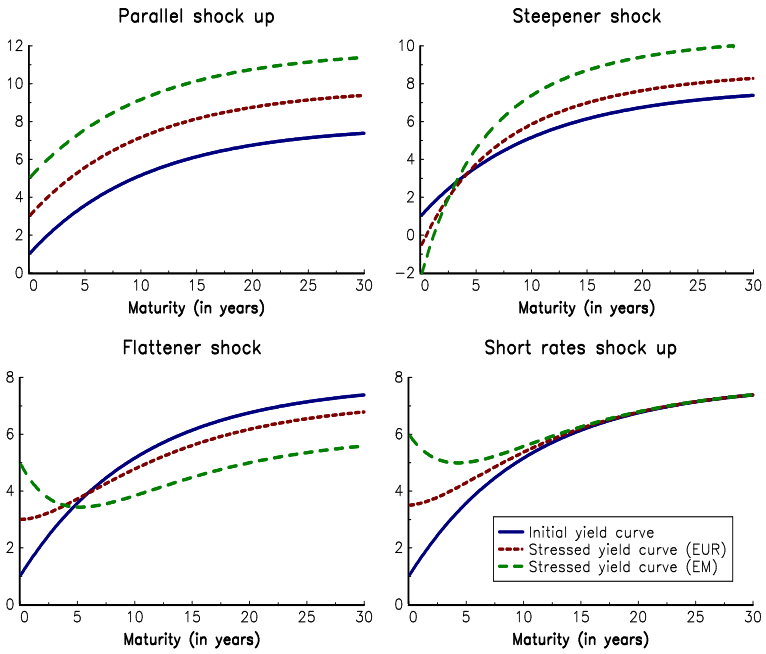

FIGURE 7.11: Stressed yield curve (in %)

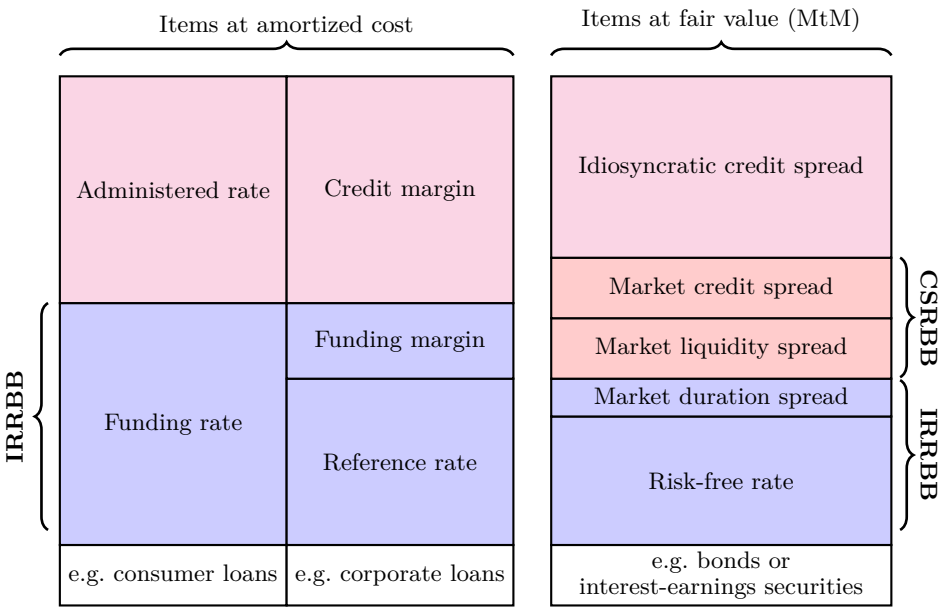

FIGURE 7.12: Components of interest rates

Source: BCBS (2016d, page 34).

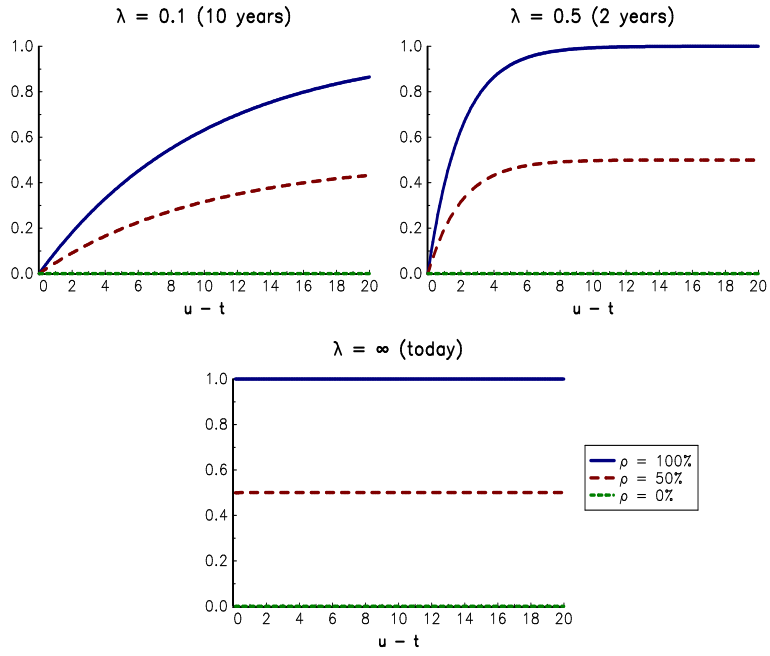

FIGURE 7.13: Sensitivity of the customer rate with respect to the market rate

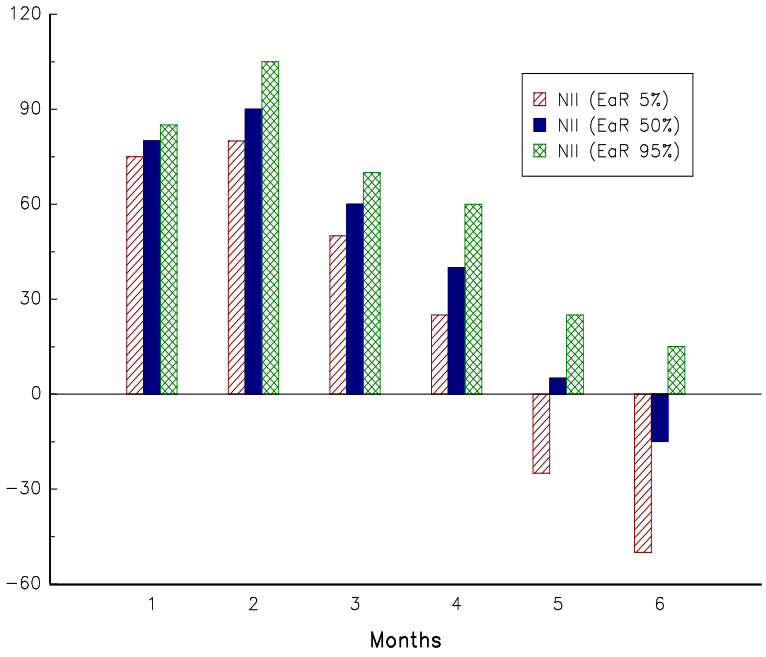

FIGURE 7.14: Earnings-at-risk analysis

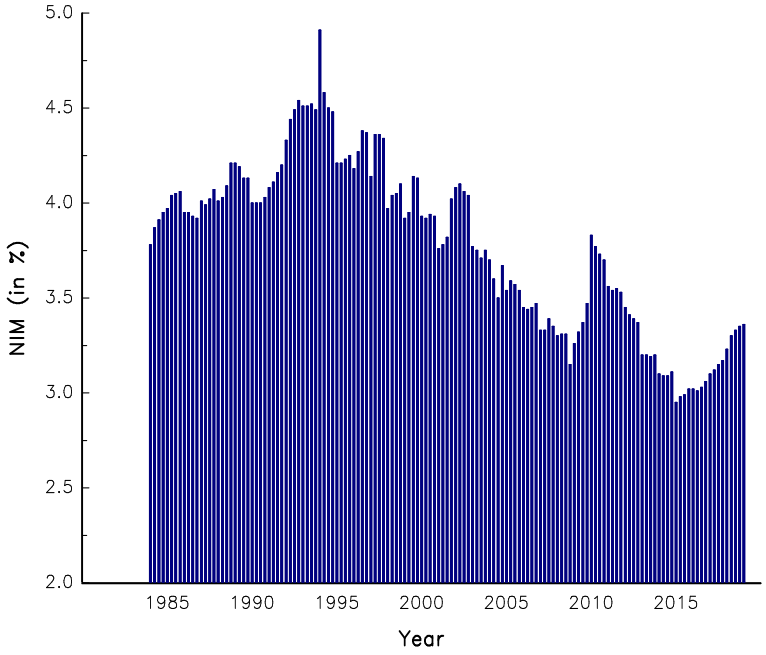

FIGURE 7.15: Evolution of the net interest margin in the US

Source: Federal Financial Institutions Examination Council (US), Net Interest Margin for all US Banks [USNIM], retrieved from FRED, Federal Reserve Bank of St. Louis; https://fred.stlouisfed.org/series/USNIM, July 9, 2019.

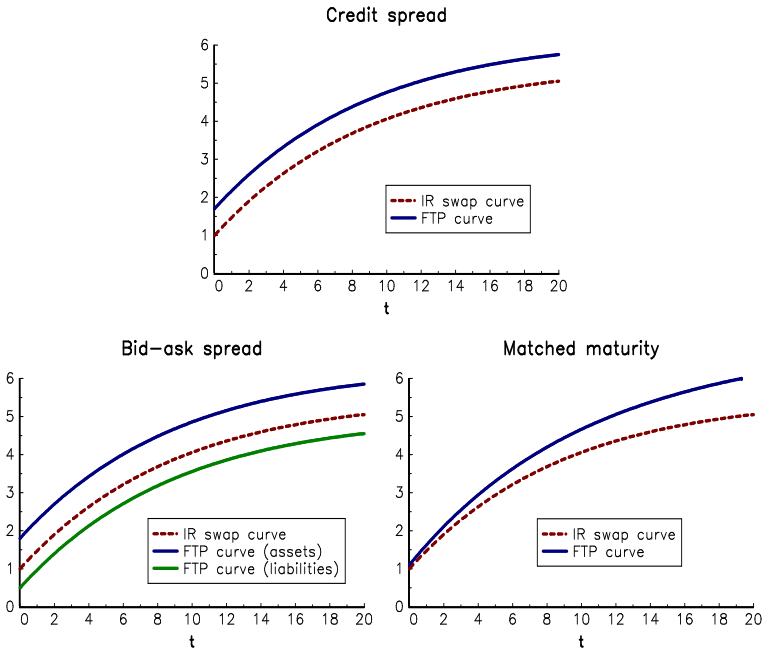

FIGURE 7.16: The term structure of FTP rates

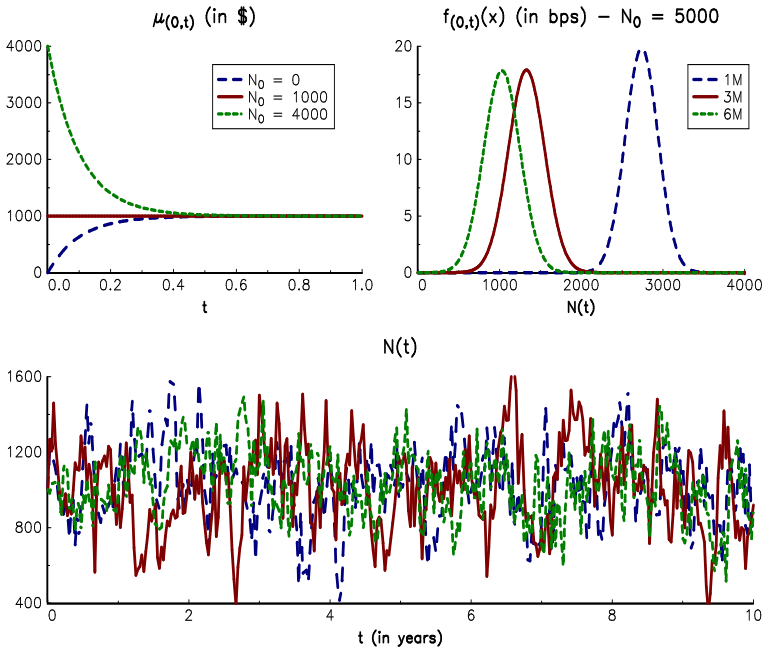

FIGURE 7.17: Statistics of the deposit amount $N(t)$

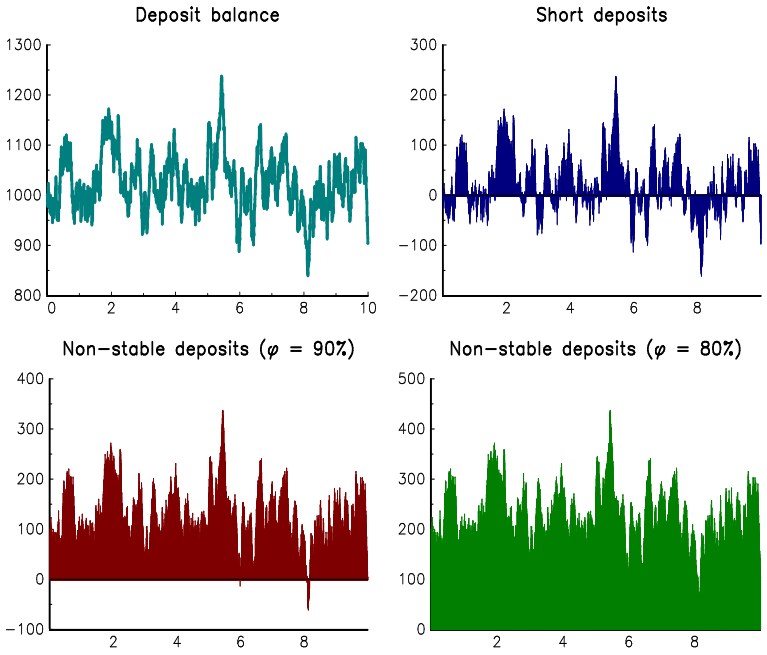

FIGURE 7.18: Stable and non-stable deposits

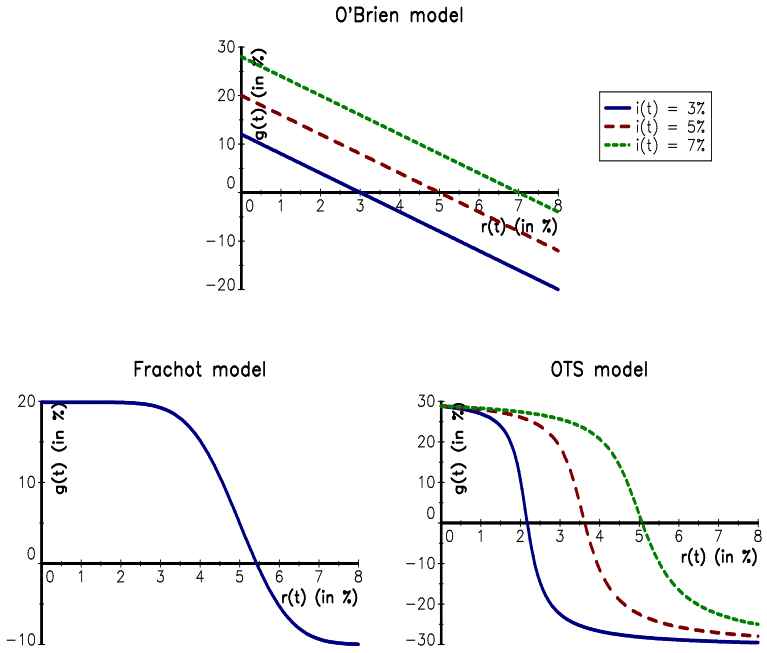

FIGURE 7.19: Impact of the market rate on the growth rate of deposits

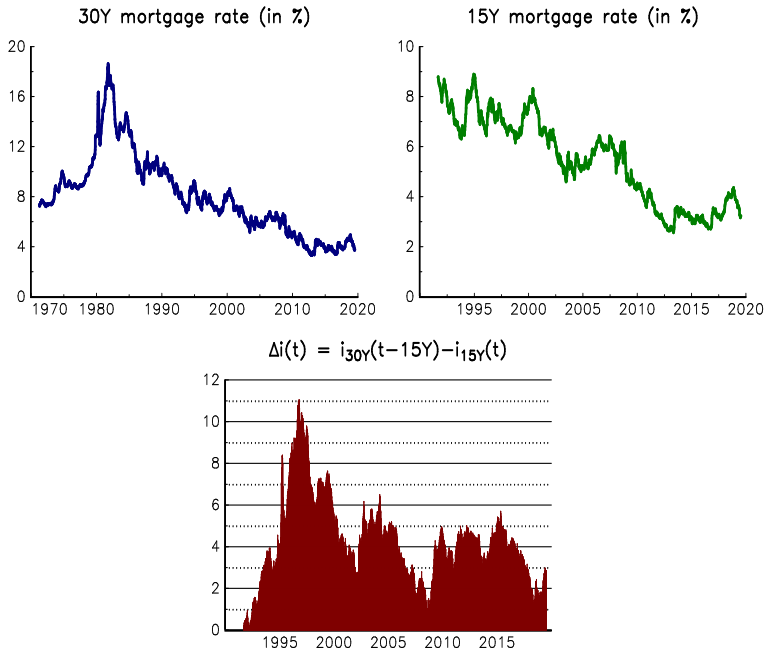

FIGURE 7.20: Evolution of 30-year and 10-year mortgage rates in the US

Source: Freddie Mac, 30Y/15Y Fixed Rate Mortgage Average in the United States [MORTGAGE30US/15US], retrieved from FRED, Federal Reserve Bank of St. Louis; https://fred.stlouisfed.org/series/MORTGAGE30US, July 24, 2019.

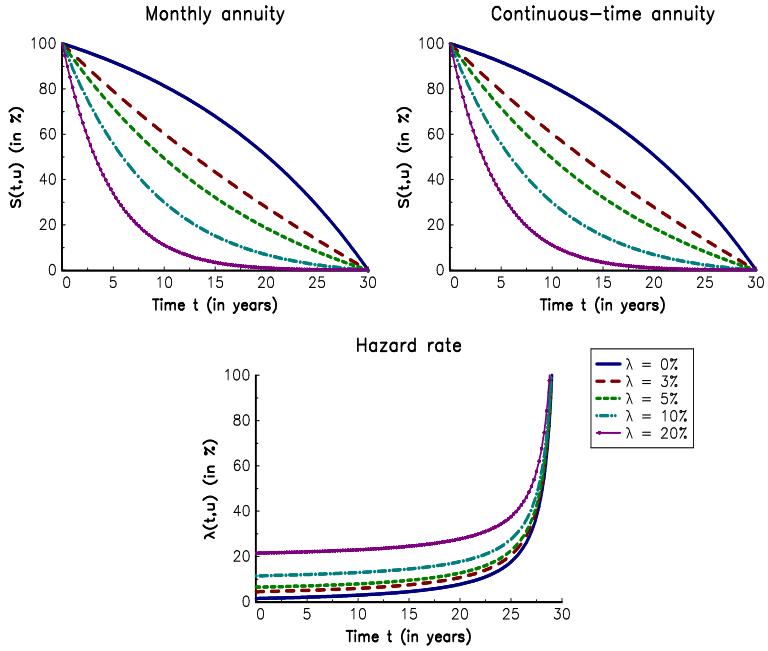

FIGURE 7.21: Survival function in the case of prepayment

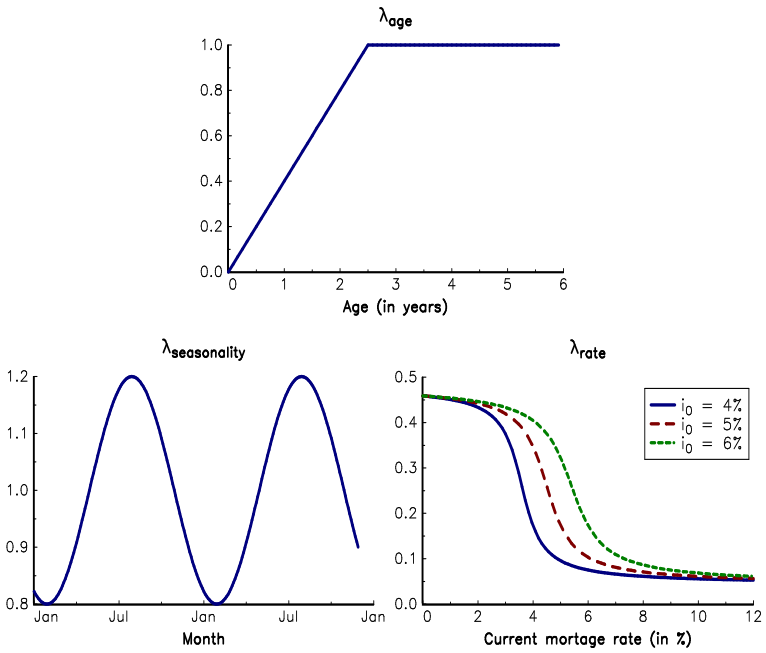

FIGURE 7.22: Components of the OTC model

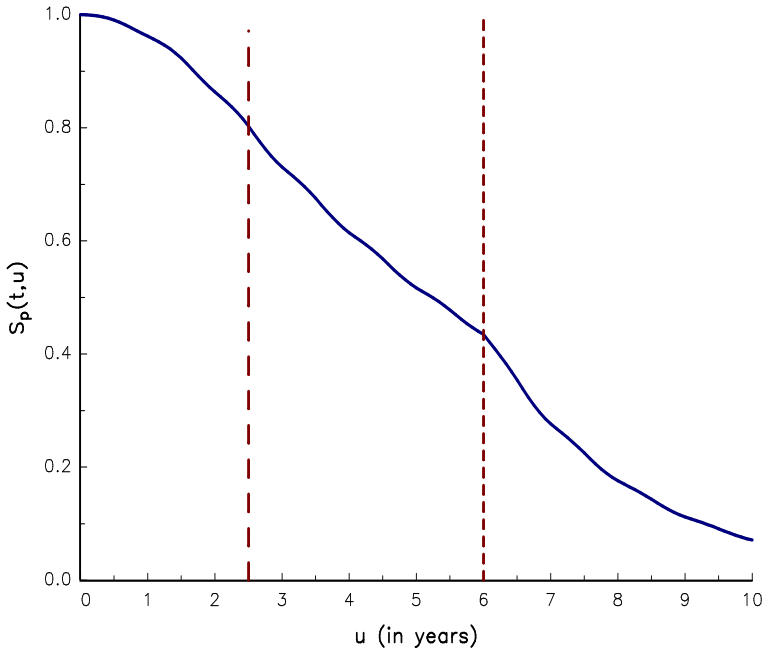

FIGURE 7.23: An example of survival function $\mathbf{S}_p(t,u)$ with a mortgage rate drop

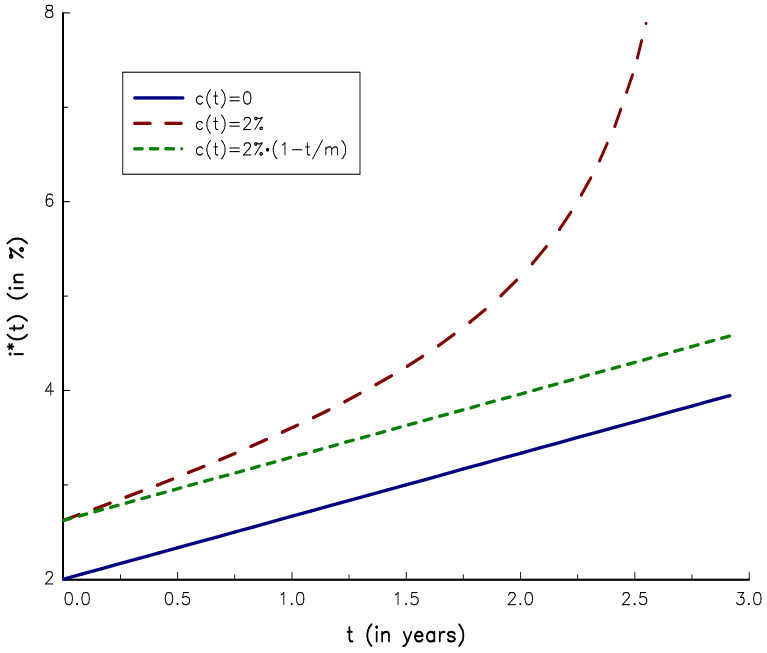

FIGURE 7.24: Refinancing incentive rule of term deposits

Chapter 8

Systemic Risk and Shadow Banking System

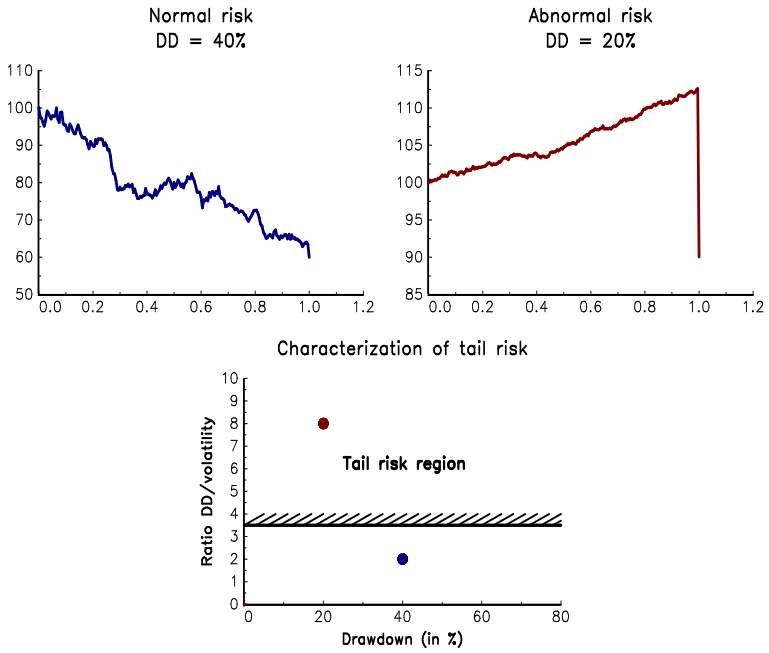

FIGURE 8.1: Illustration of tail risk

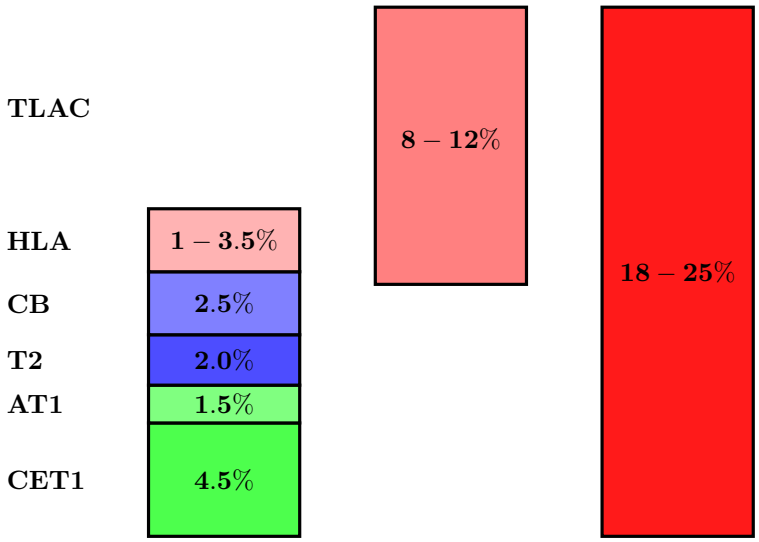

FIGURE 8.2: Impact of the TLAC on capital requirements

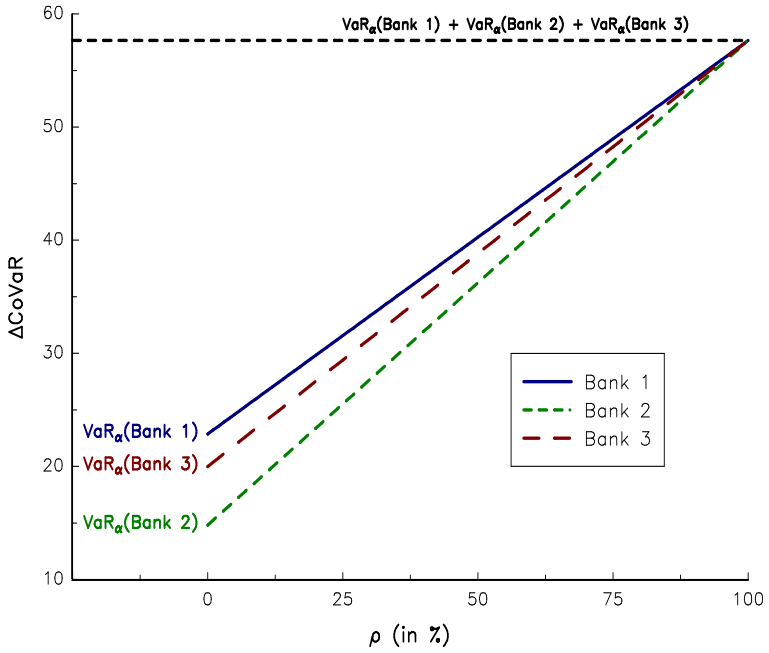

FIGURE 8.3: Impact of the uniform correlation on $\Delta\,\text{CoVaR}_i$

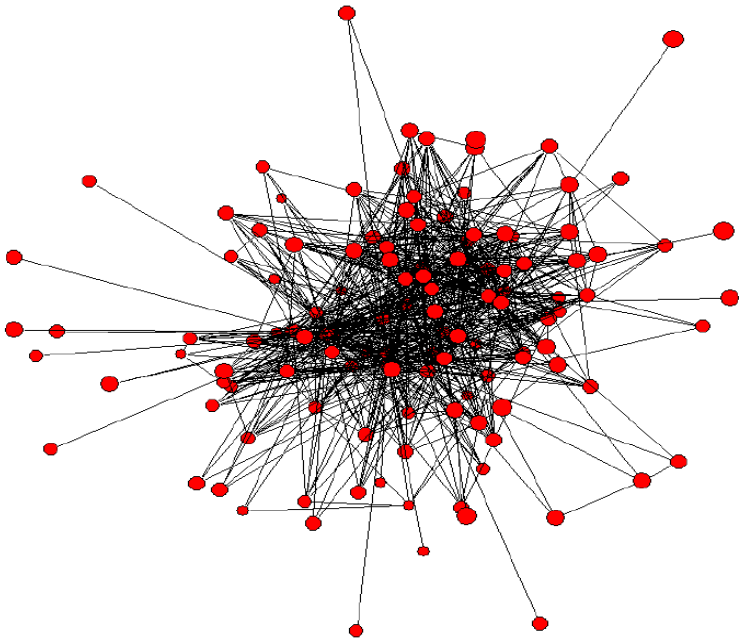

FIGURE 8.4: Network structure of the Brazilian banking system

Source: Cont *et al.* (2013).

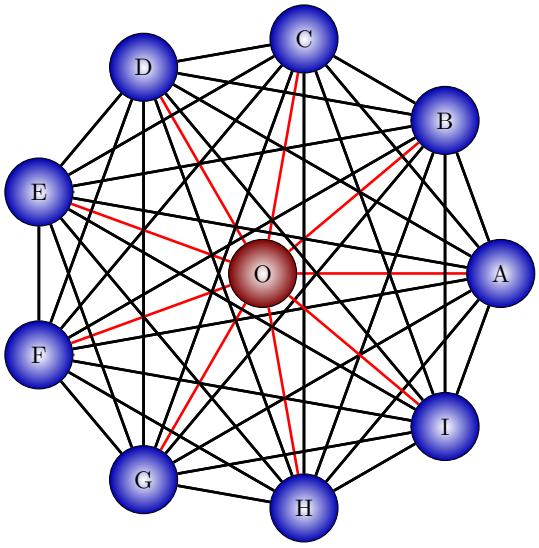

FIGURE 8.5: A completely connected network

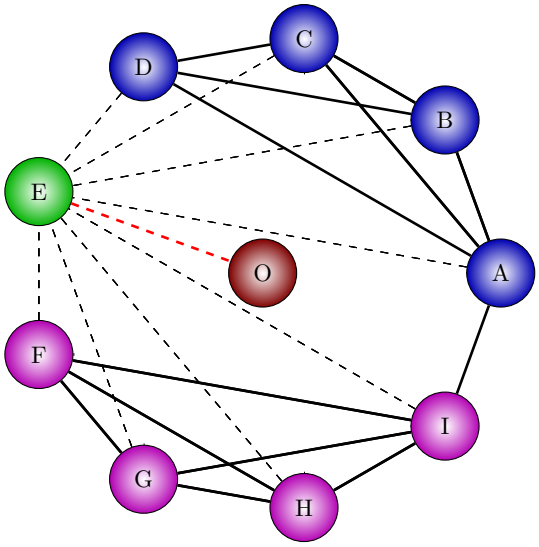

FIGURE 8.6: A sparse network

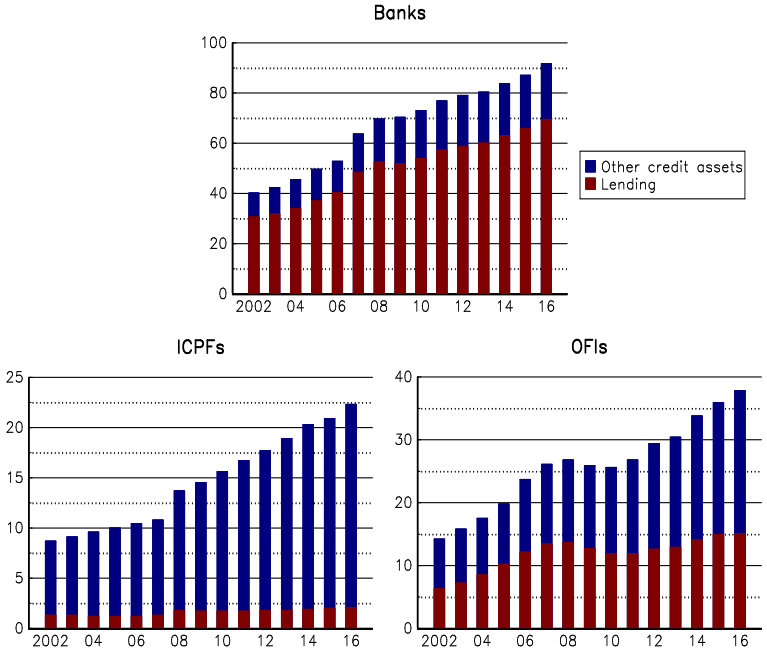

FIGURE 8.7: Credit assets (in $ tn)

Source: FSB (2018a) and author's calculations.

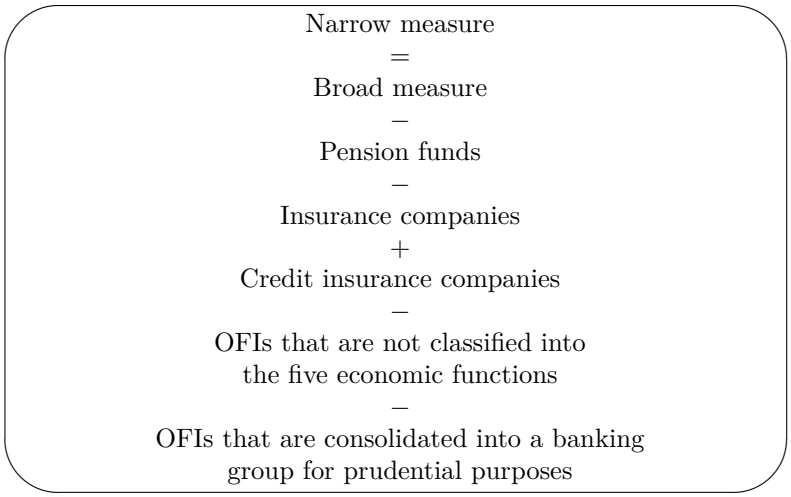

FIGURE 8.8: Calculation of the shadow banking narrow measure

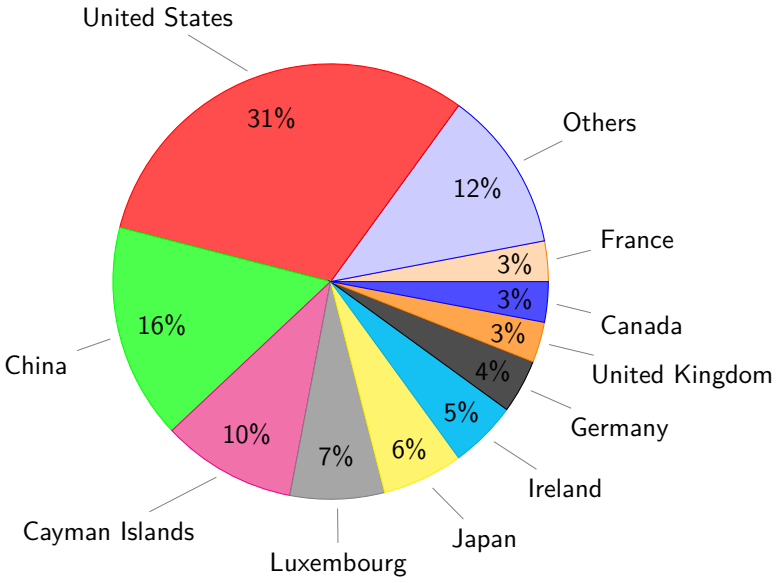

FIGURE 8.9: Breakdown by country of shadow banking assets (2016)

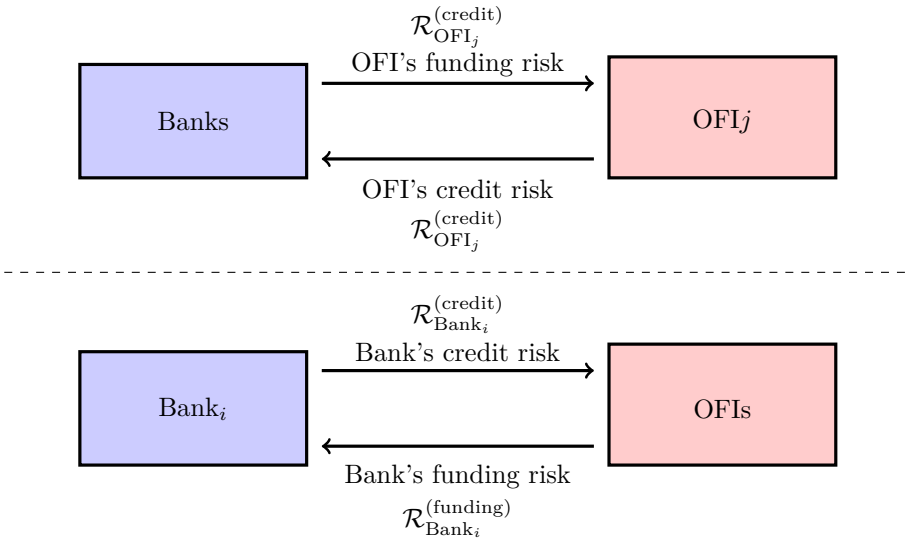

FIGURE 8.10: Interconnectedness between banks and OFIs

Part II

Mathematical and Statistical Tools

Chapter 9

Model Risk of Exotic Derivatives

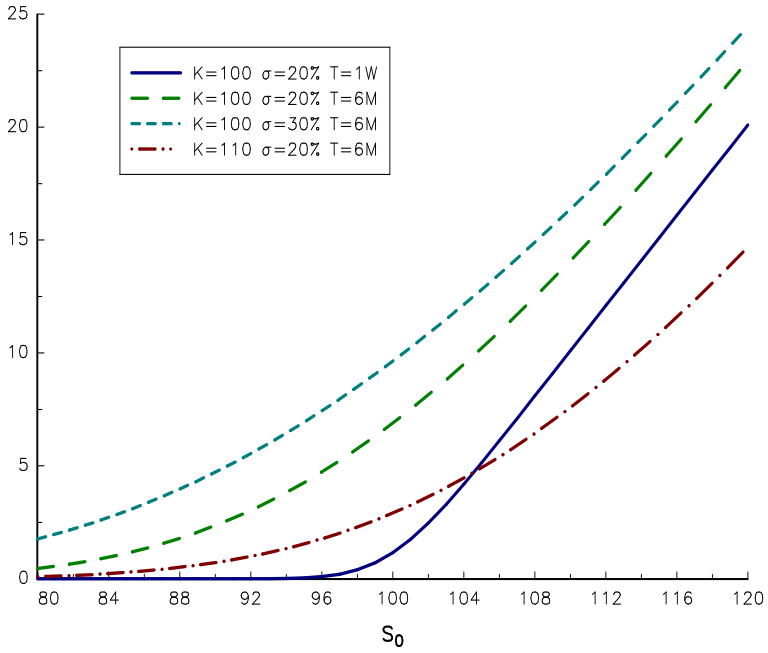

FIGURE 9.1: Price of the call option

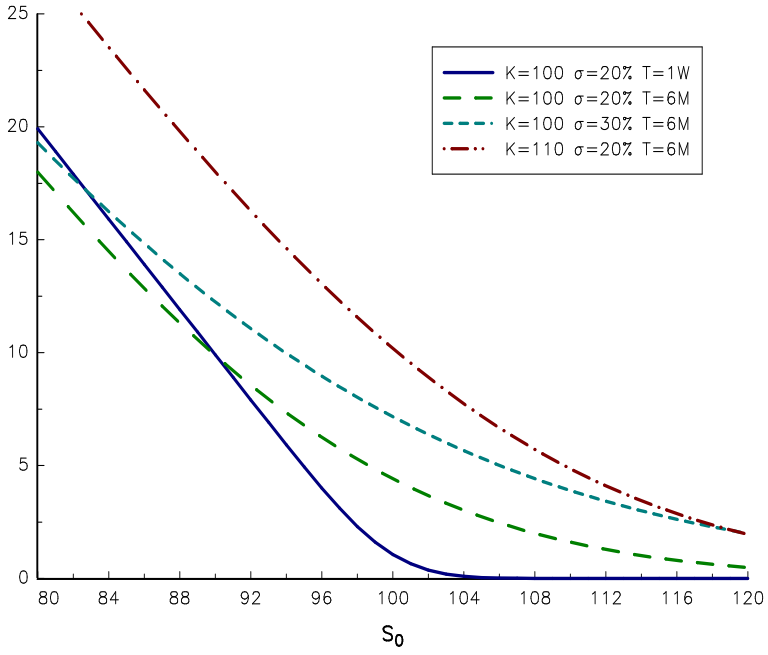

FIGURE 9.2: Price of the put option

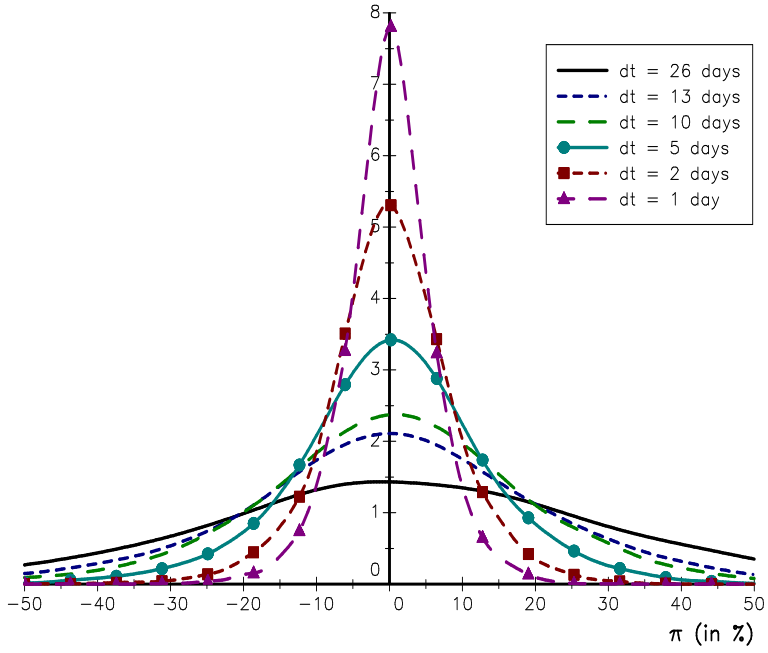

FIGURE 9.3: Probability density function of the hedging ratio π

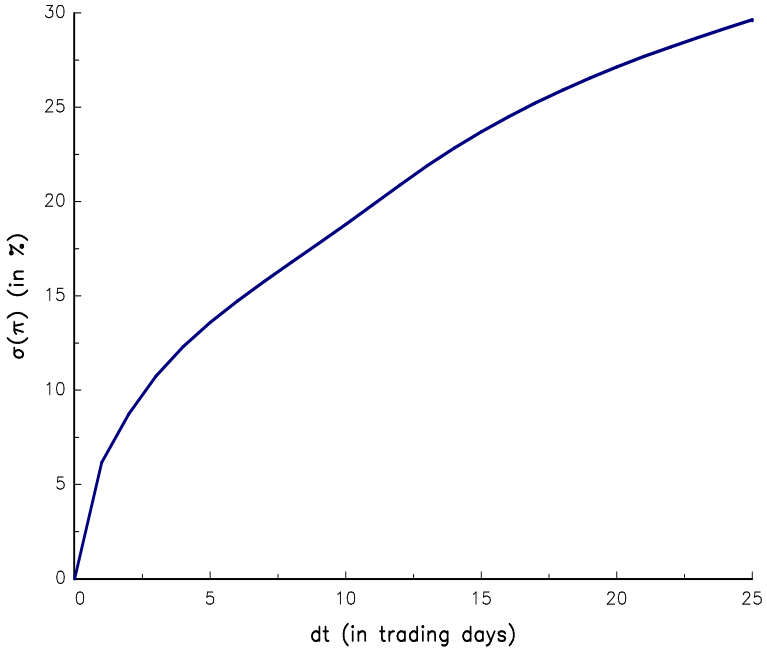

FIGURE 9.4: Relationship between the hedging efficiency $\sigma(\pi)$ and the hedging frequency

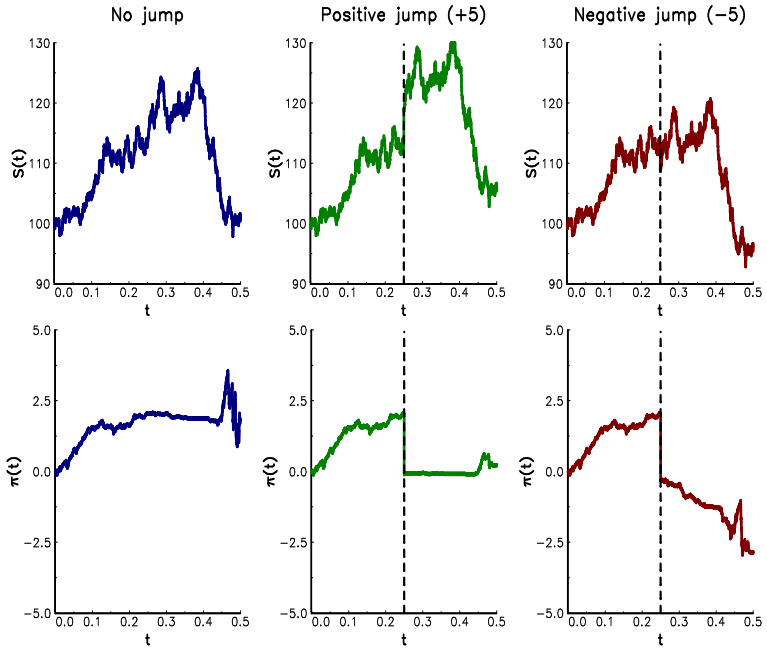

FIGURE 9.5: Impact of a jump on the hedging ratio $\pi(t)$

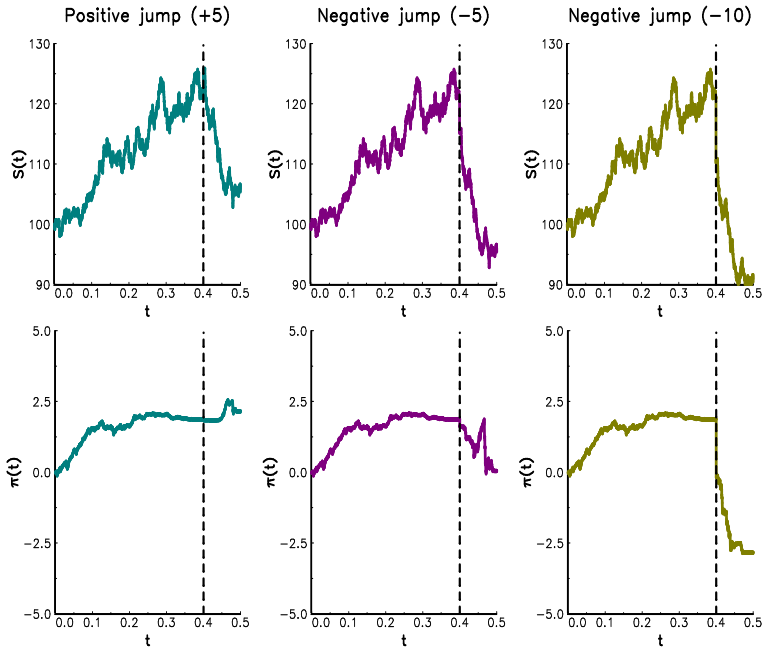

FIGURE 9.6: Impact of a jump on the hedging ratio $\pi(t)$

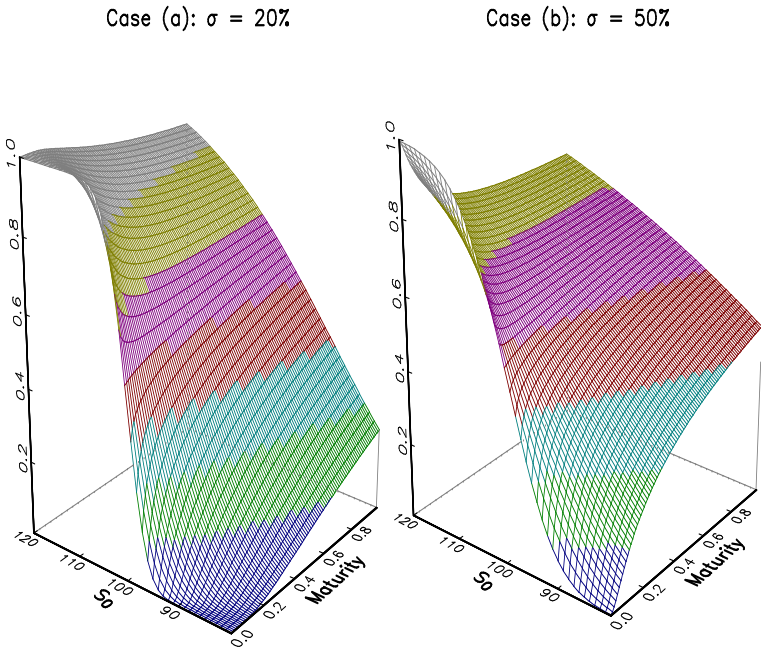

FIGURE 9.7: Delta coefficient of the call option

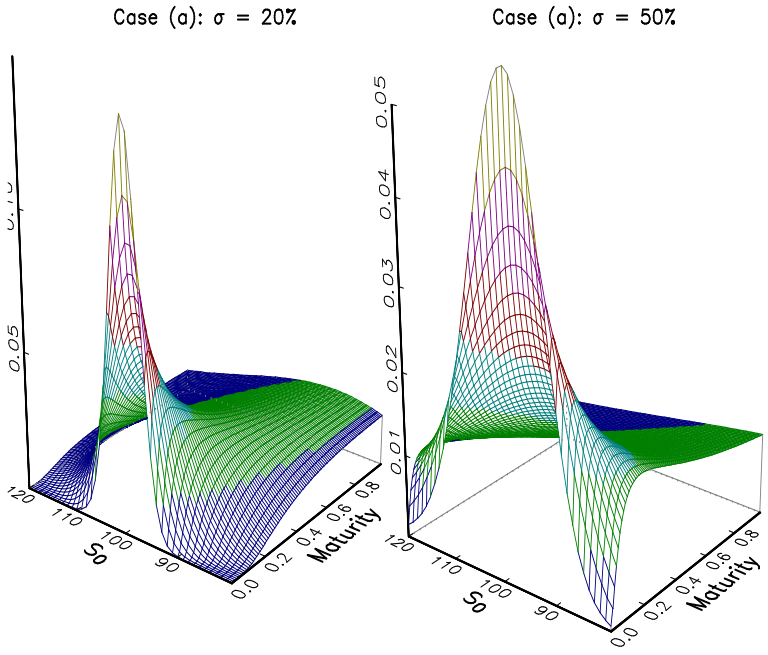

FIGURE 9.8: Gamma coefficient of the call option

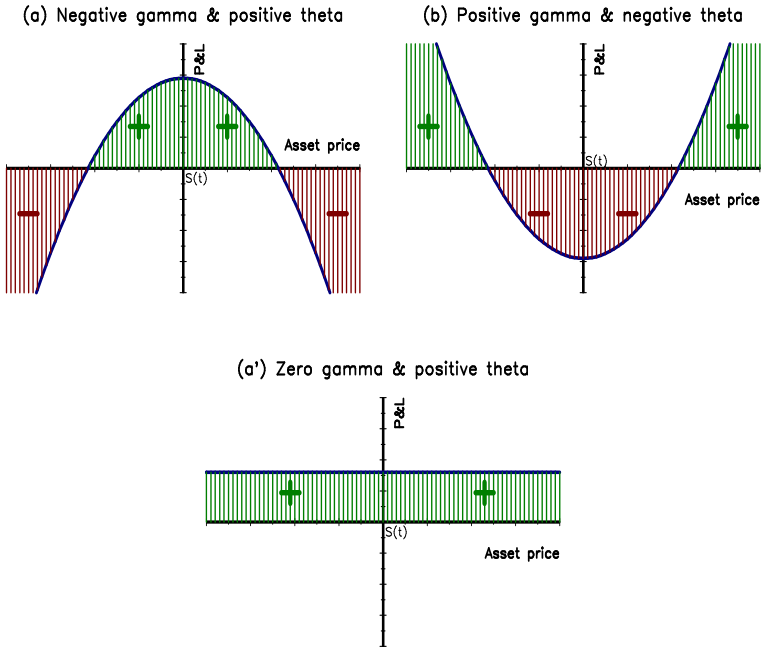

FIGURE 9.9: P&L of the delta neutral hedging portfolio

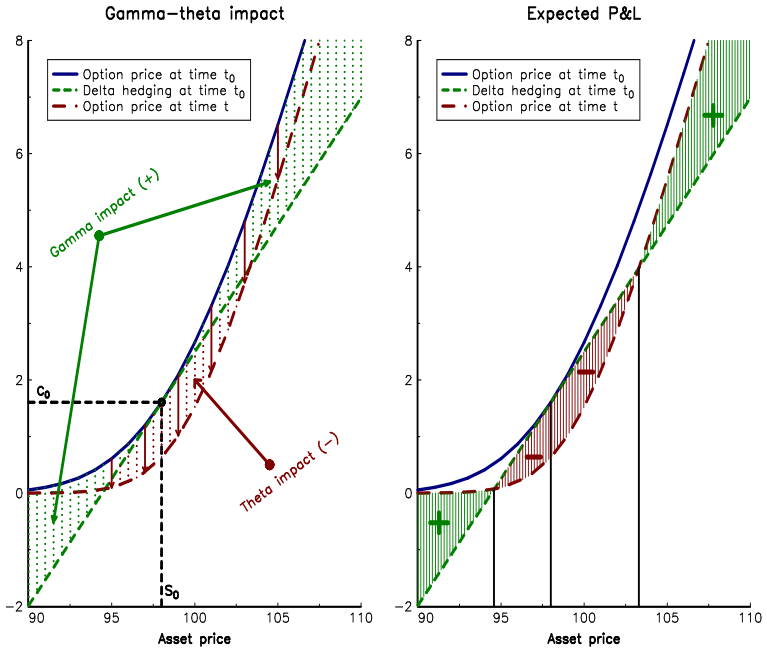

FIGURE 9.10: Illustration of the configuration ($\mathbf{\Gamma} > 0, \mathbf{\Theta} < 0$)

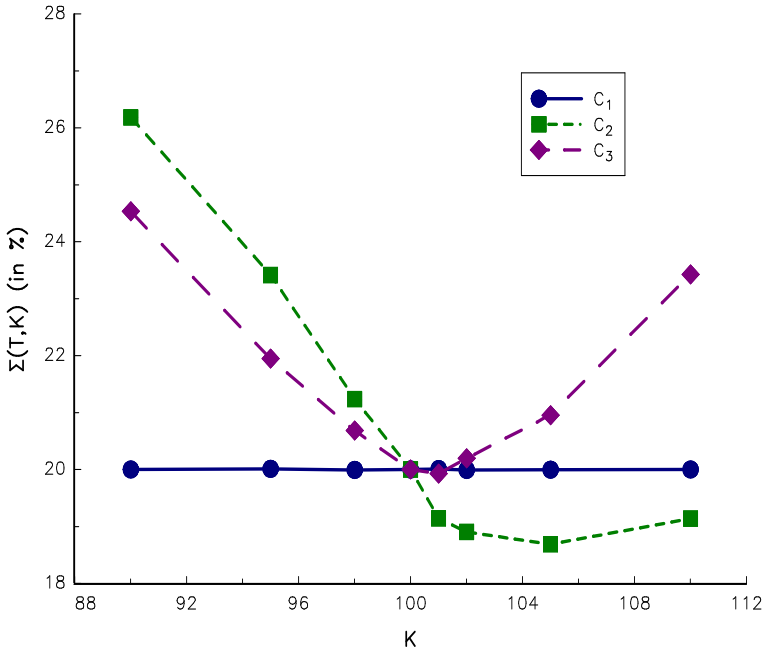

FIGURE 9.11: Volatility smile

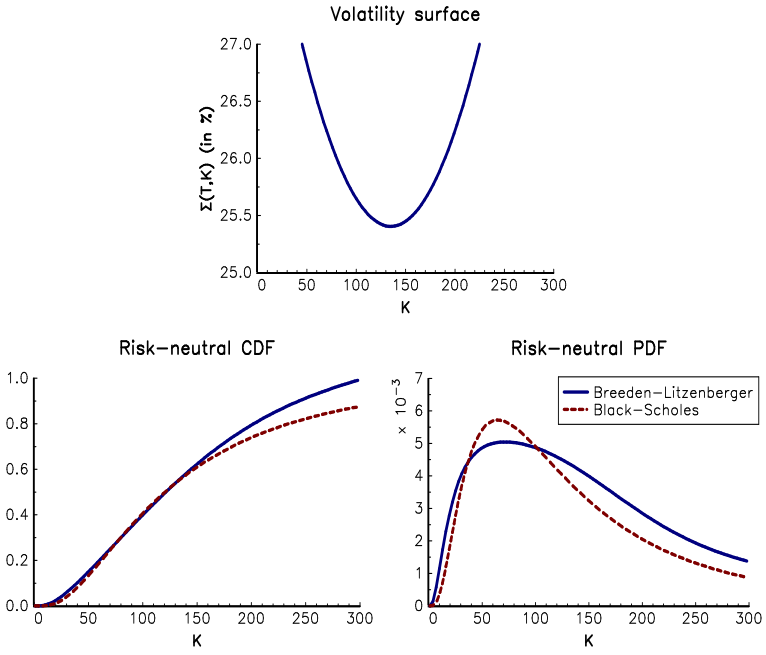

FIGURE 9.12: Risk-neutral probability density function

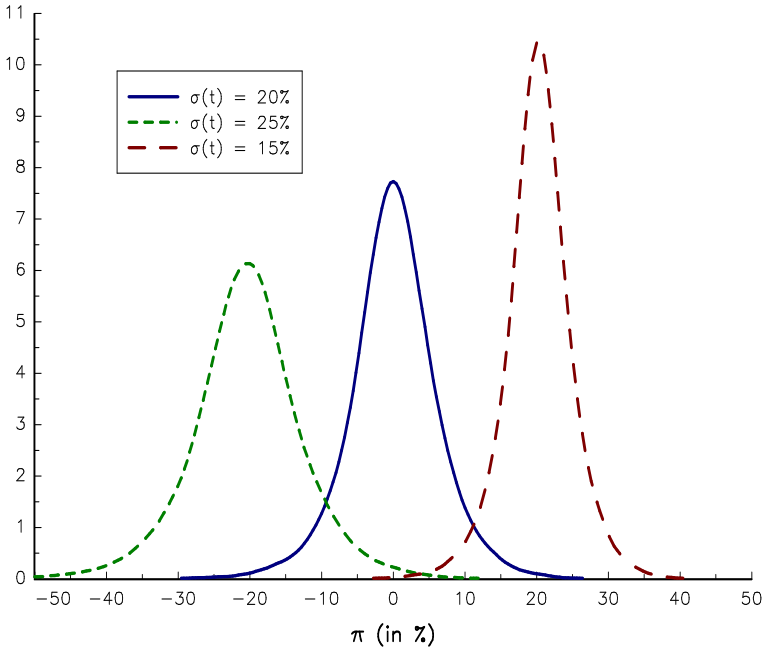

FIGURE 9.13: Hedging error when the implied volatility is 20%

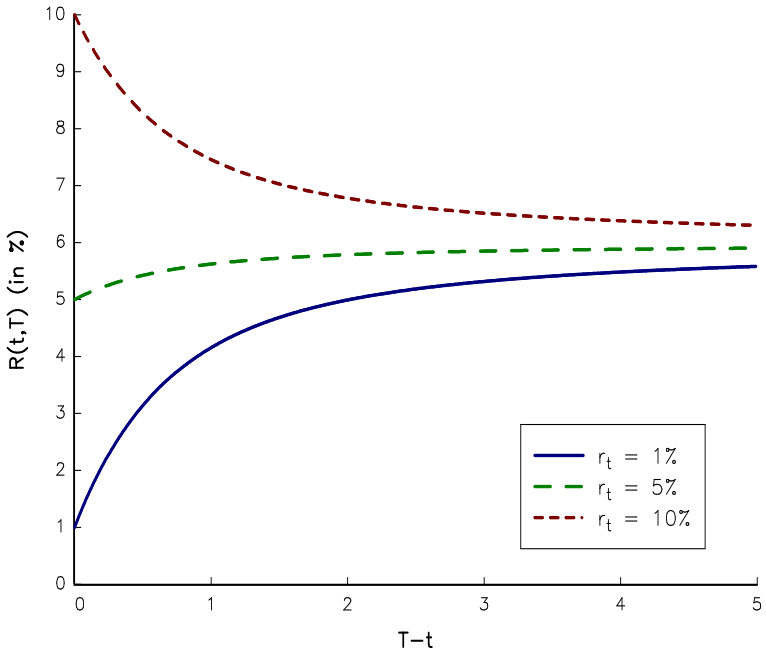

FIGURE 9.14: Vasicek model ($a = 2.5$, $b = 6\%$ and $\sigma = 5\%$)

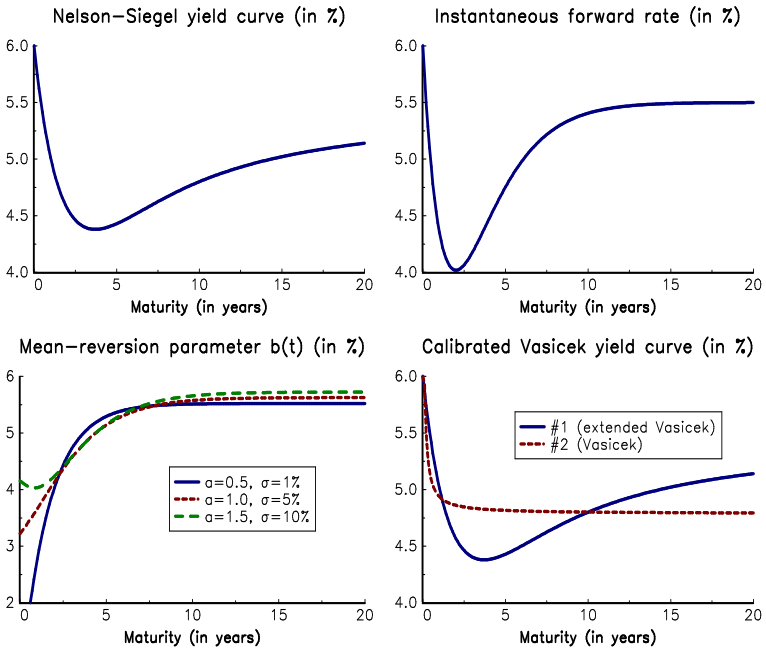

FIGURE 9.15: Calibration of the Vasicek model

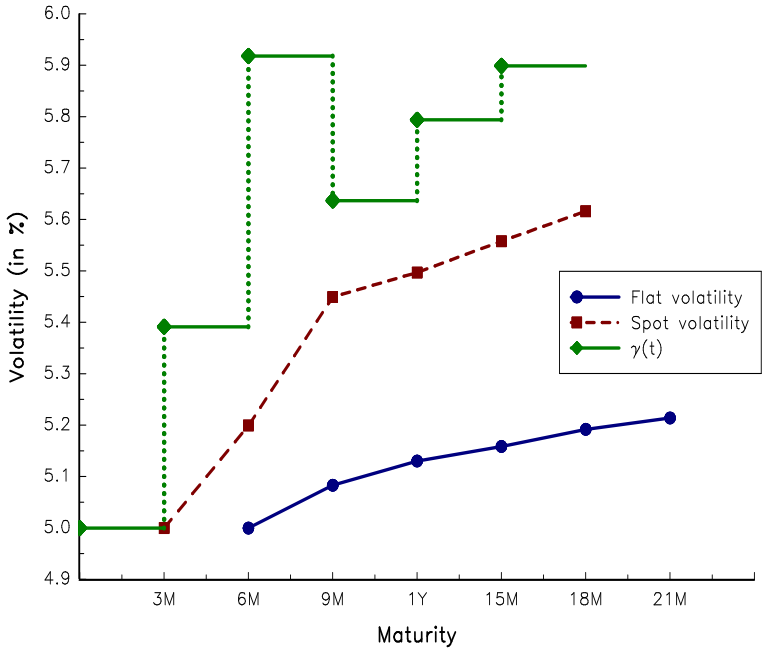

FIGURE 9.16: Flat and spot implied volatilities

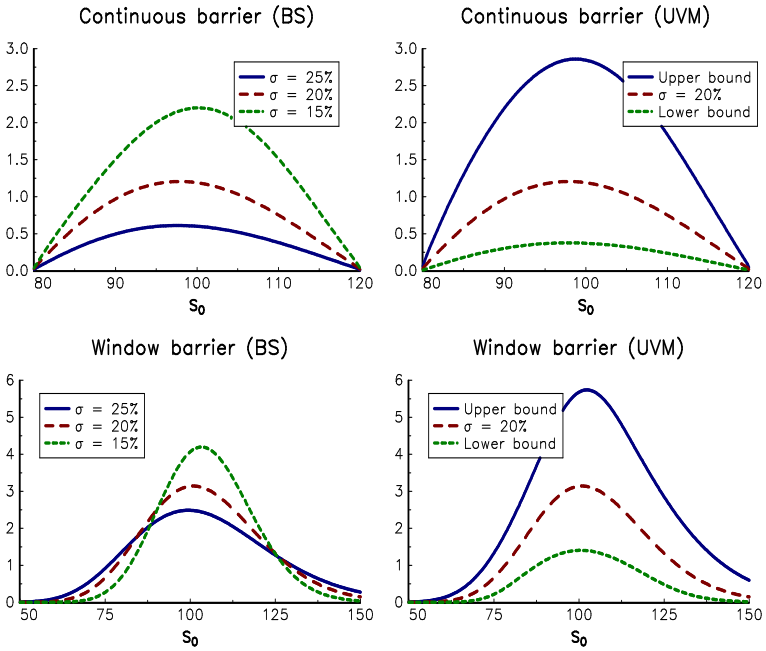

FIGURE 9.17: Comparing BS and UMV prices of the double KOC barrier option

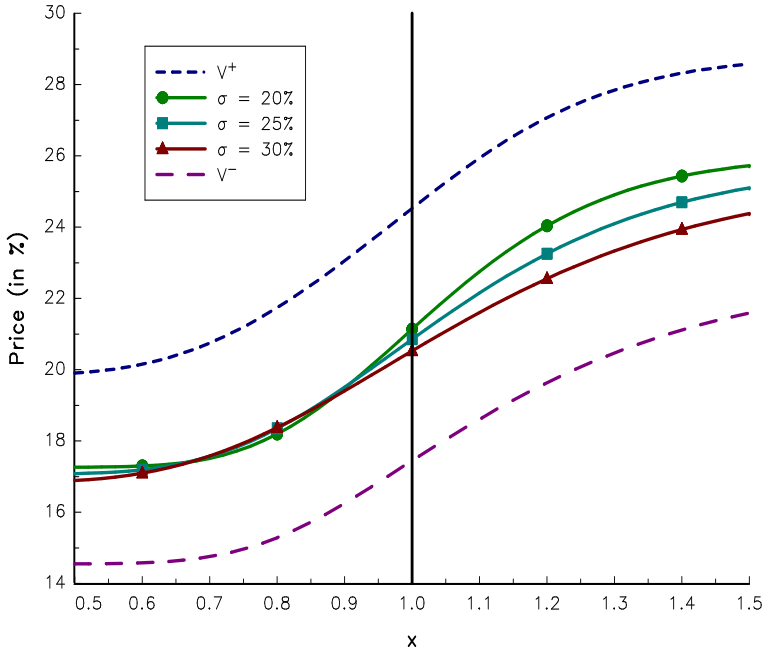

FIGURE 9.18: Comparing BS and UMV prices of the cliquet option

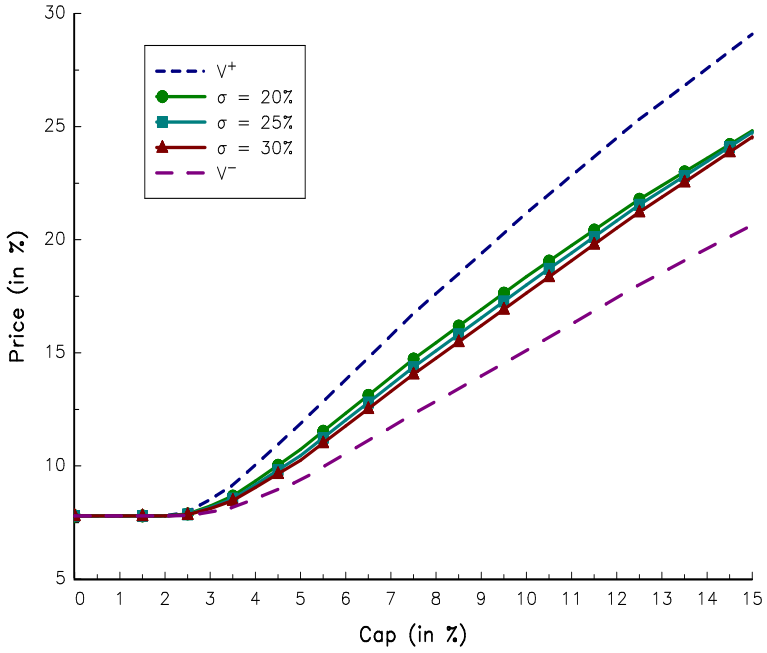

FIGURE 9.19: Influence of the local cap on the cliquet option price

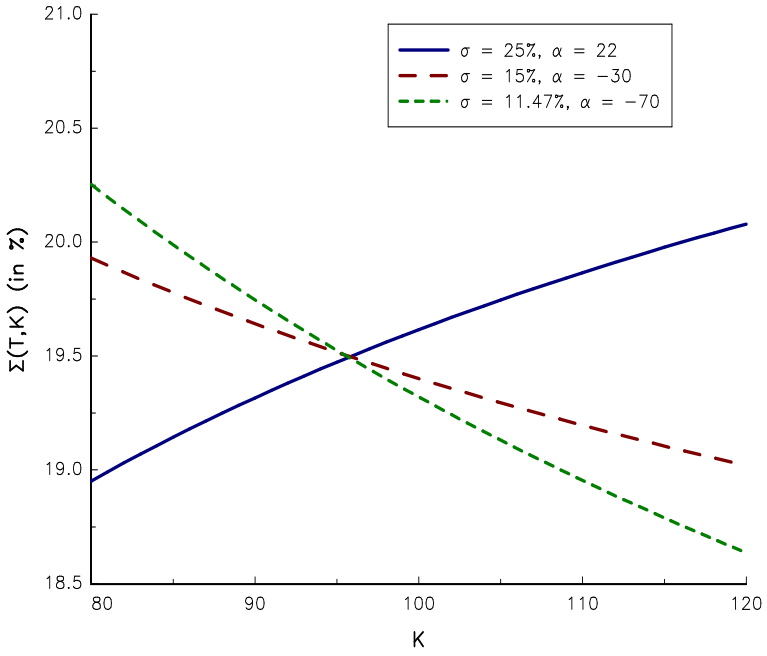

FIGURE 9.20: Volatility skew generated by the SLN model (fixed-strike parametrization)

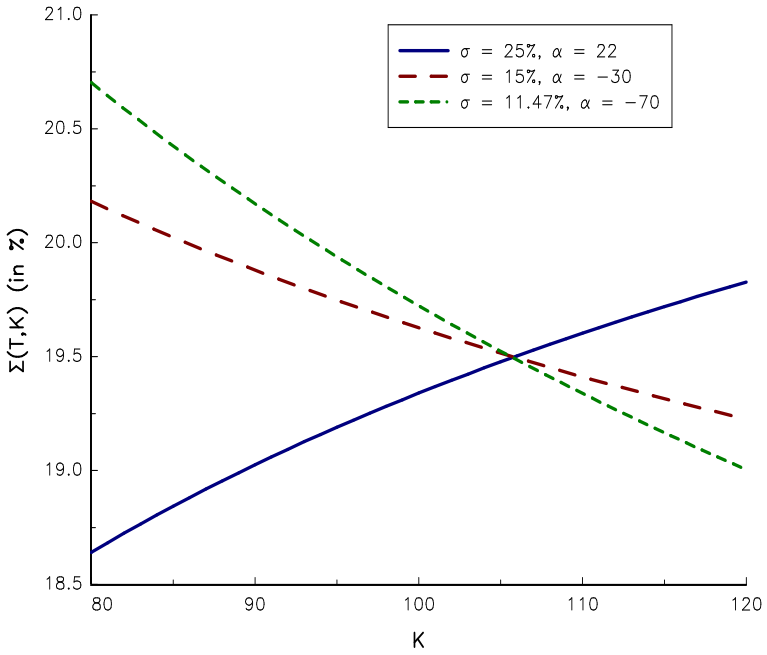

FIGURE 9.21: Volatility skew generated by the SLN model (floating-strike parametrization)

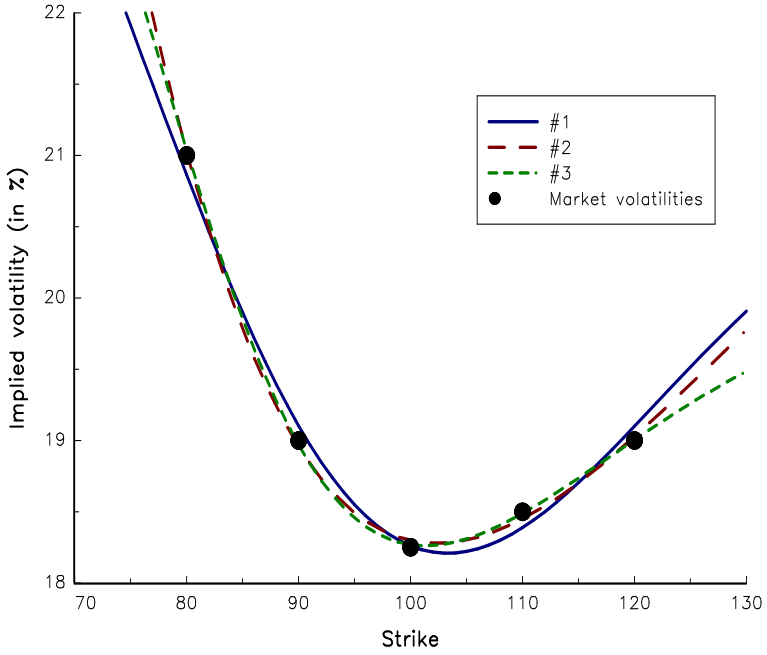

FIGURE 9.22: Implied volatility (in %) of calibrated mixed SLN models

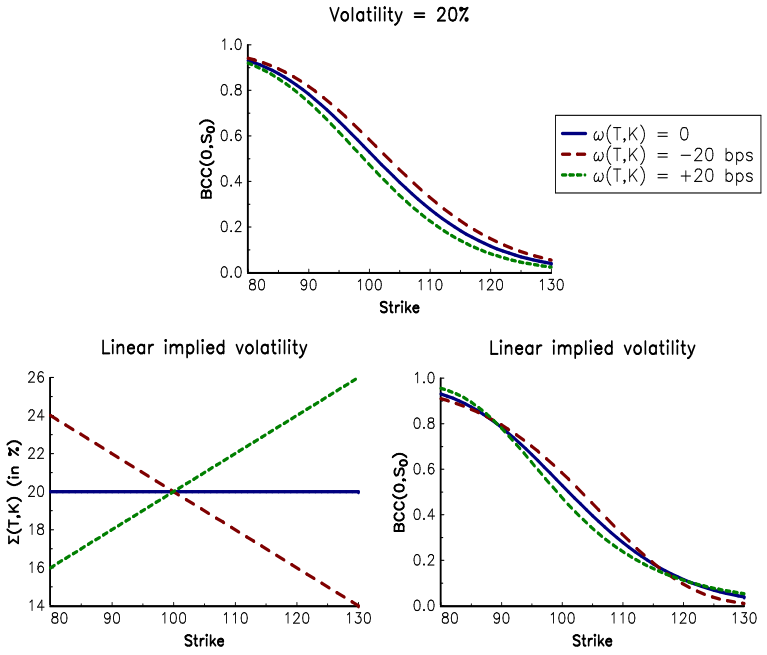

FIGURE 9.23: Impact of the implied volatility skew on the binary option price

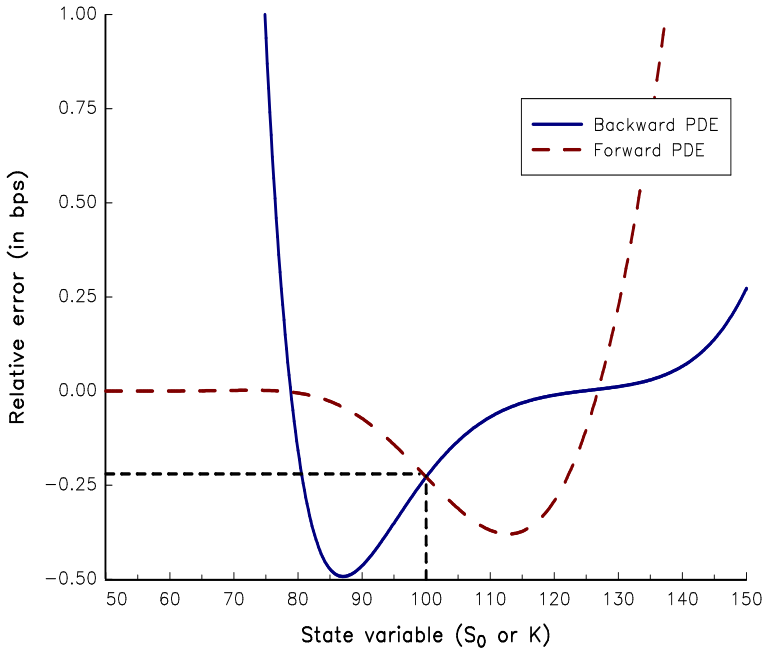

FIGURE 9.24: Relative error of backward and forward PDE numerical solutions

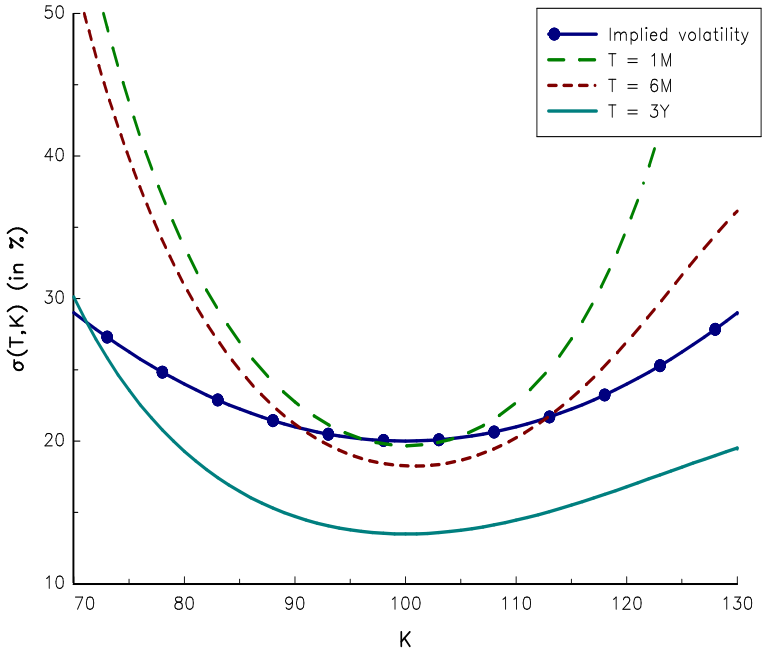

FIGURE 9.25: Calibrated local volatility $\sigma(T, S)$ (in %)

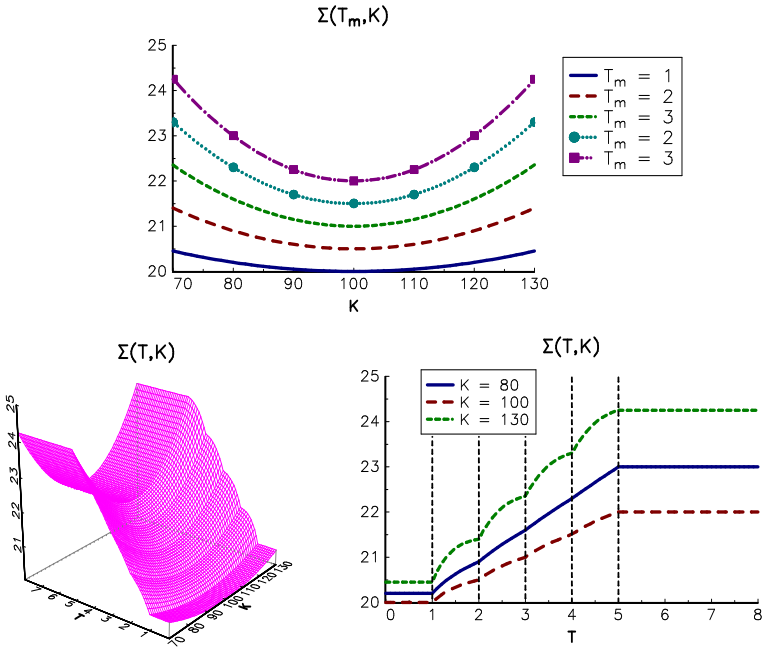

FIGURE 9.26: Time interpolation of the implied volatility

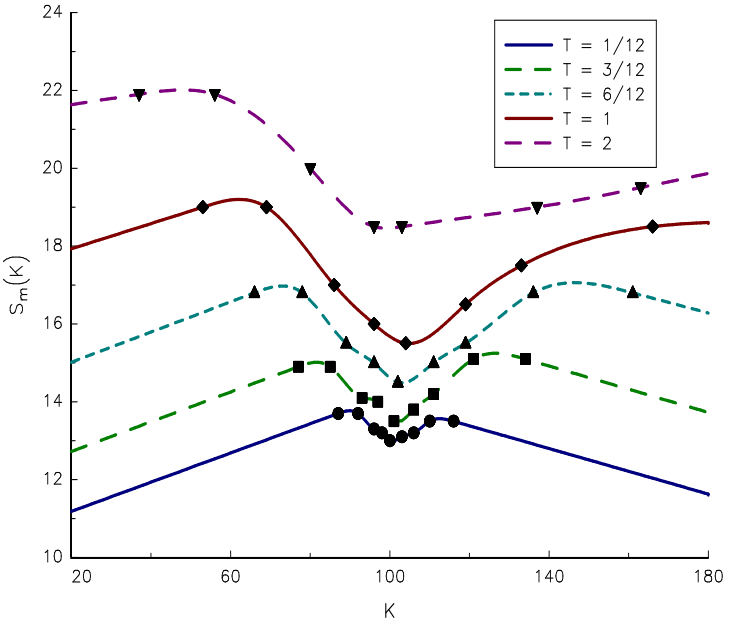

FIGURE 9.27: Cubic spline interpolation $\mathcal{S}_m(K)$ (in %)

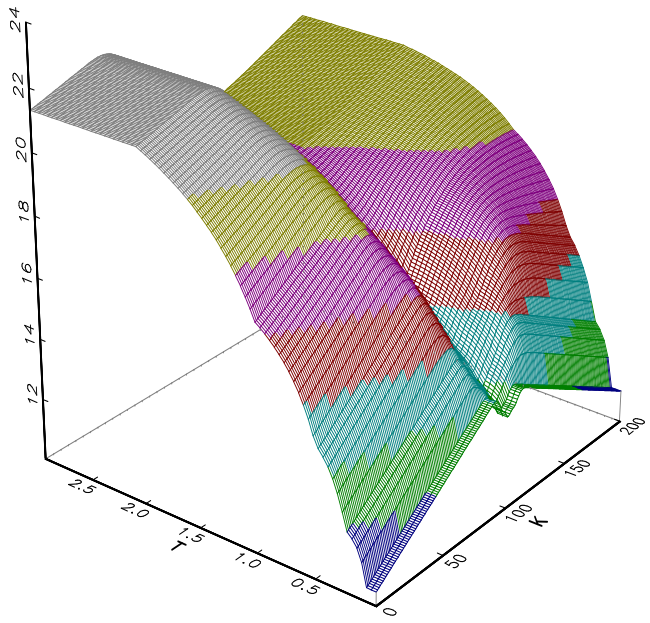

FIGURE 9.28: Implied volatility surface $\Sigma(T, K)$ (in %)

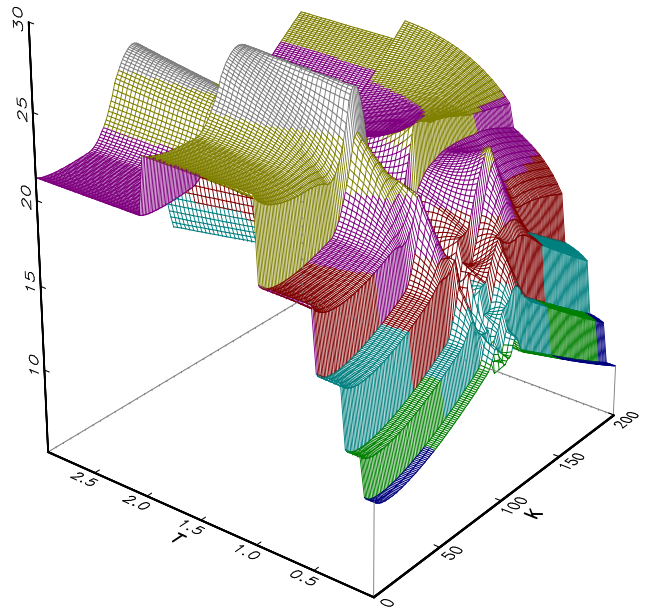

FIGURE 9.29: Local volatility surface $\sigma(T, K)$ (in %)

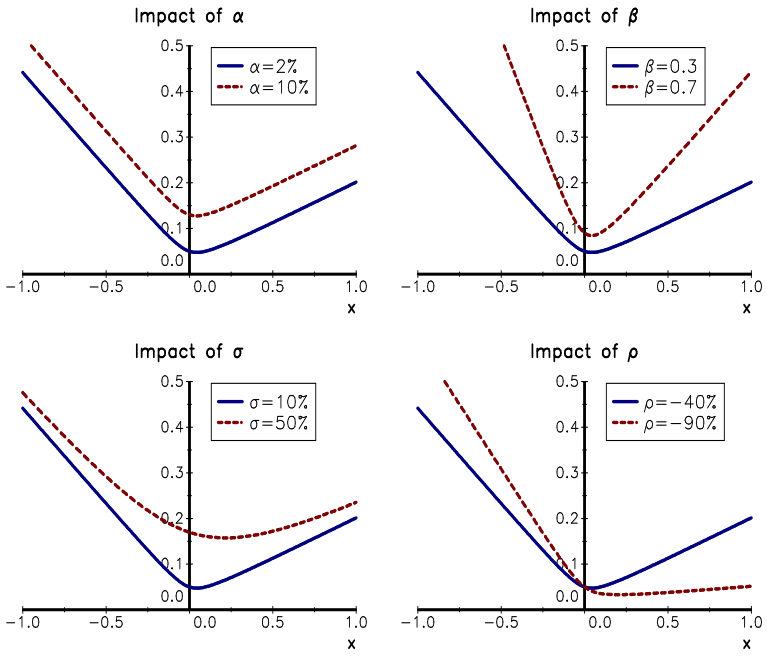

FIGURE 9.30: Impact of SVI parameters on the total variance $\tilde{v}_T(x)$

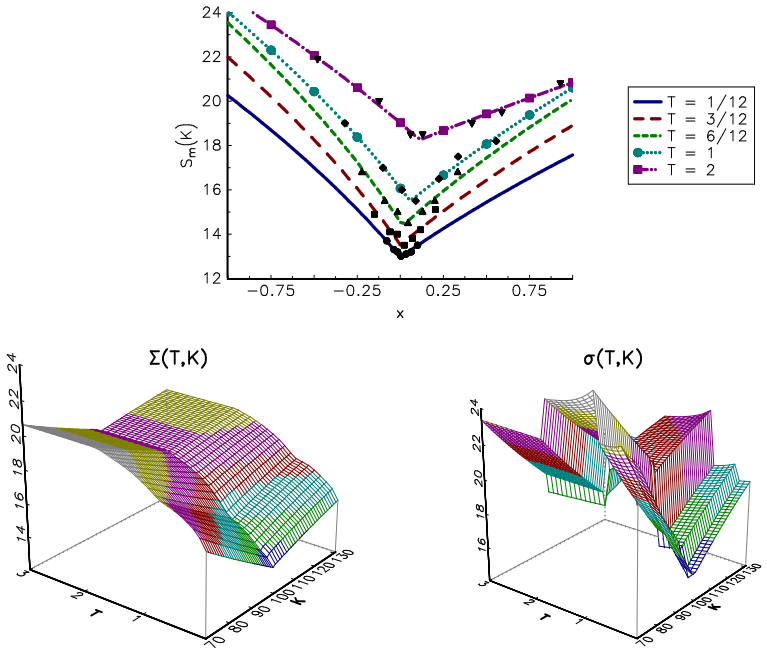

FIGURE 9.31: SVI parametrization, implied volatility $\Sigma(T,K)$ and local volatility $\sigma(T,K)$ (in %)

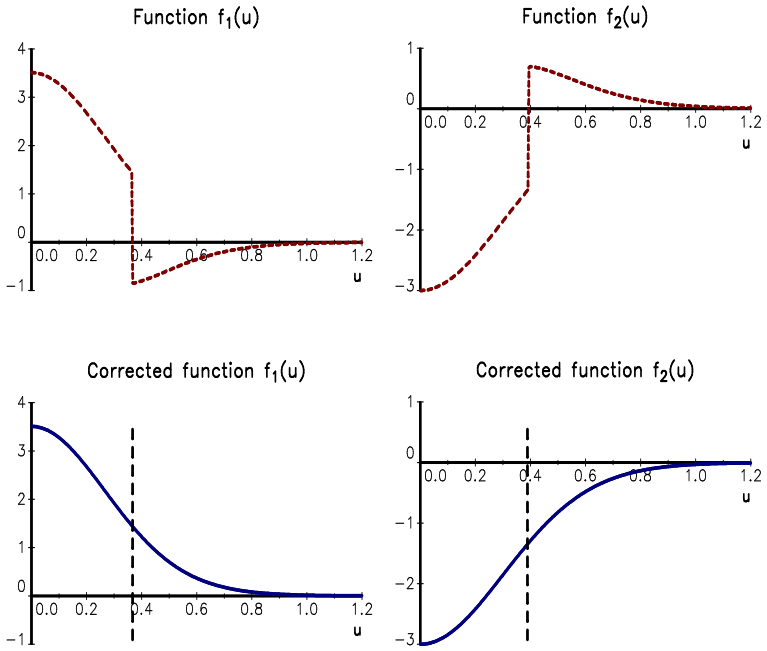

FIGURE 9.32: Functions $f_1(u)$ and $f_2(u)$ $(\kappa = 1)$

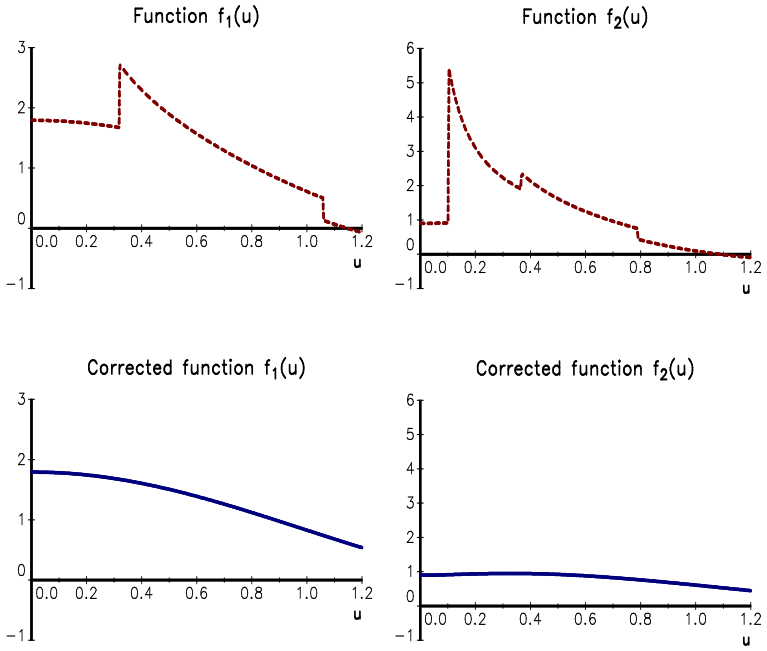

FIGURE 9.33: Functions $f_1(u)$ and $f_2(u)$ $(\kappa = 0.5)$

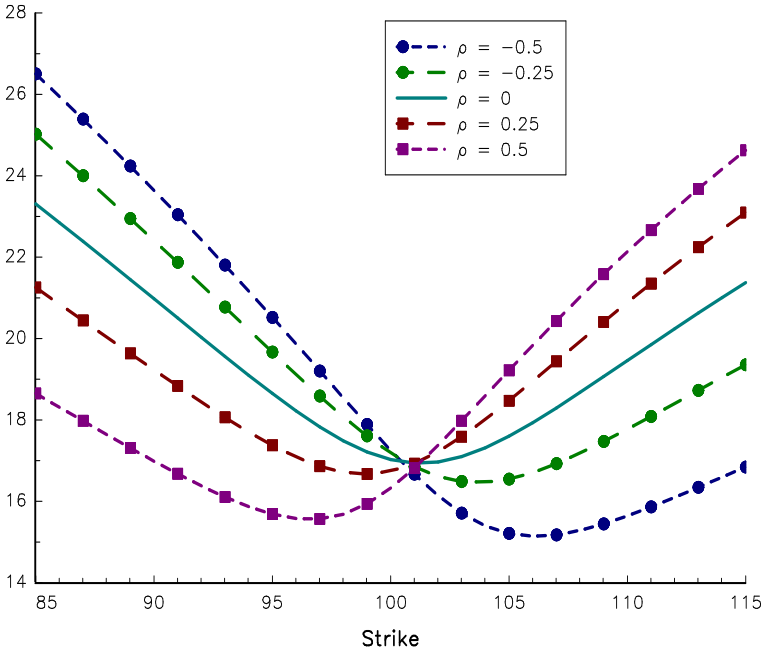

FIGURE 9.34: Implied volatility of the Heston model (in %)

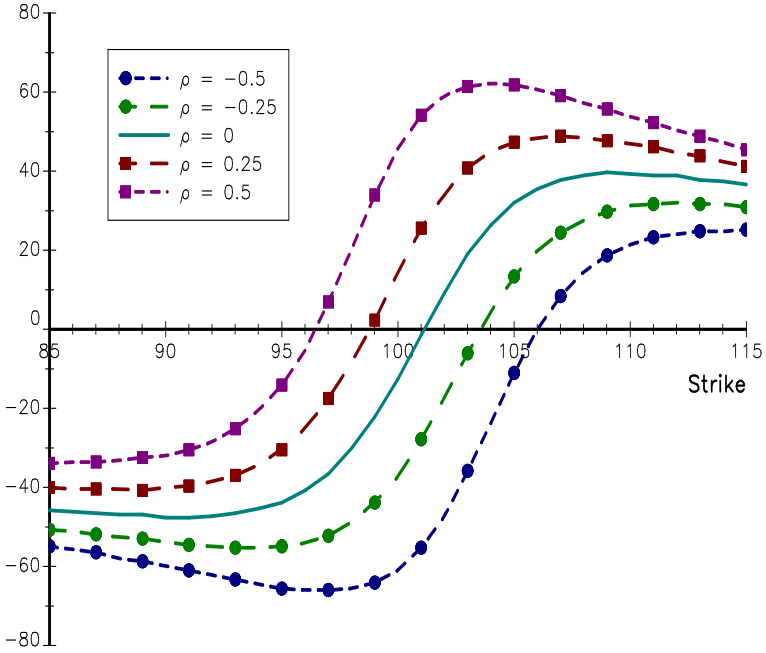

FIGURE 9.35: Skew of the Heston model (in bps)

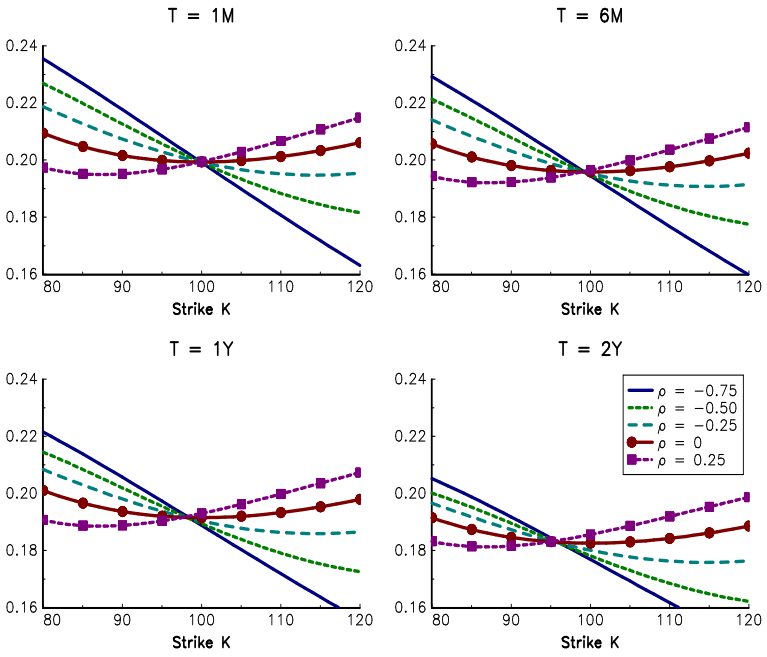

FIGURE 9.36: Implied volatility of the Durrleman formula (in %)

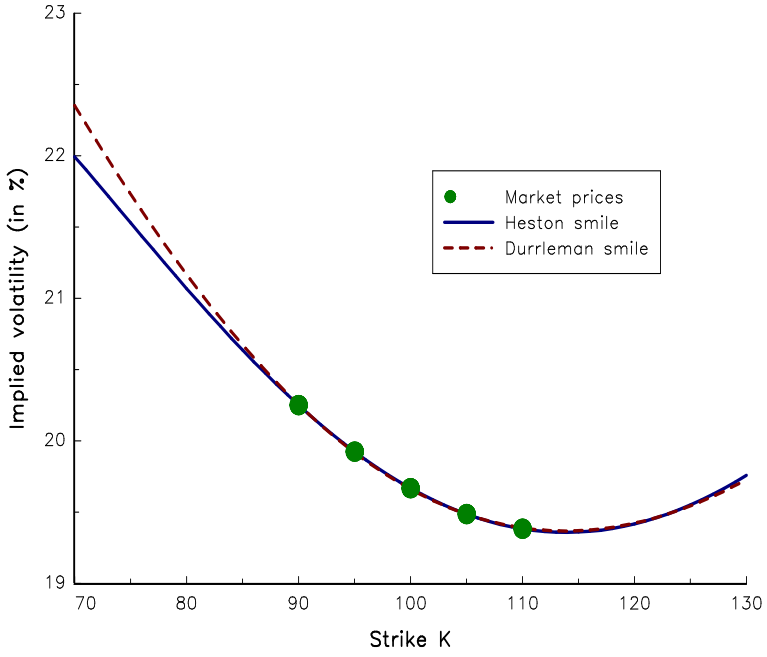

FIGURE 9.37: Calibration of the smile by the Heston model and the Durrleman formula

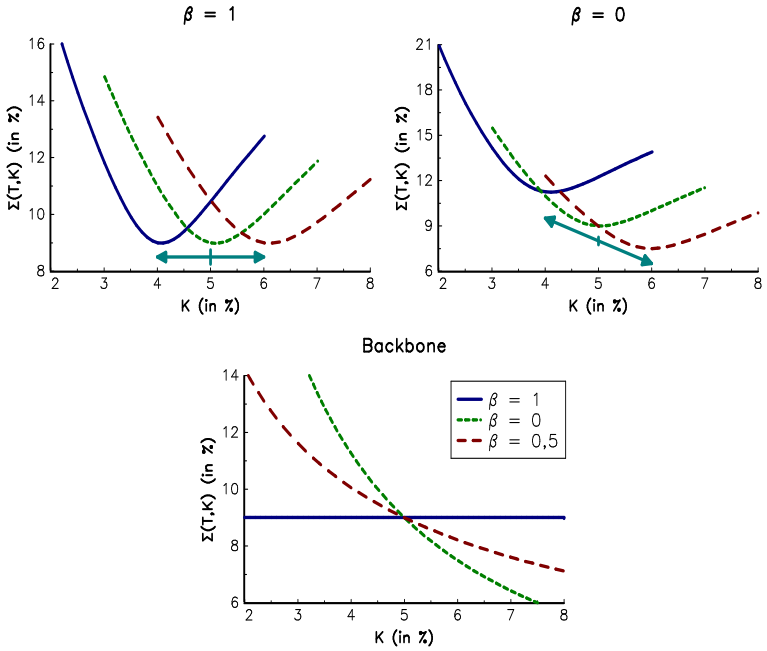

FIGURE 9.38: Impact of the parameter β

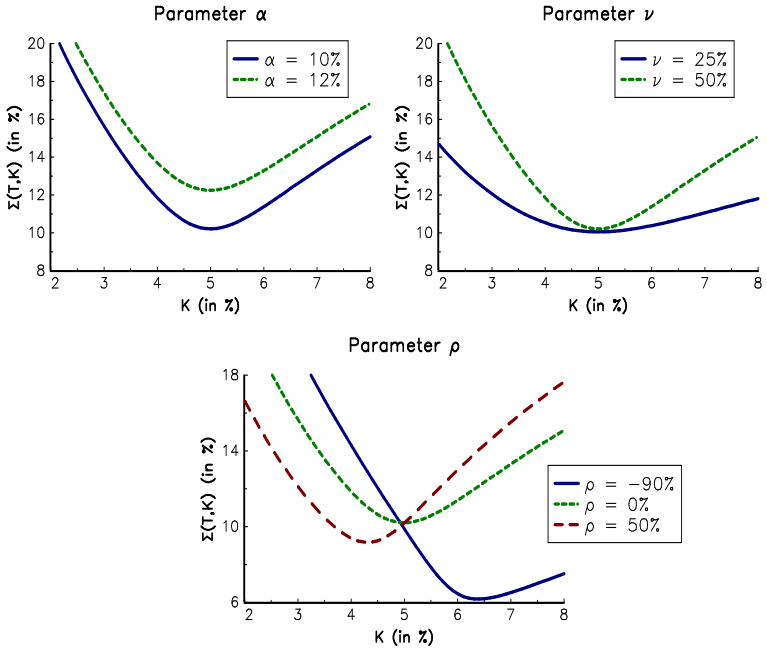

FIGURE 9.39: Impact of the parameters α, ν and ρ

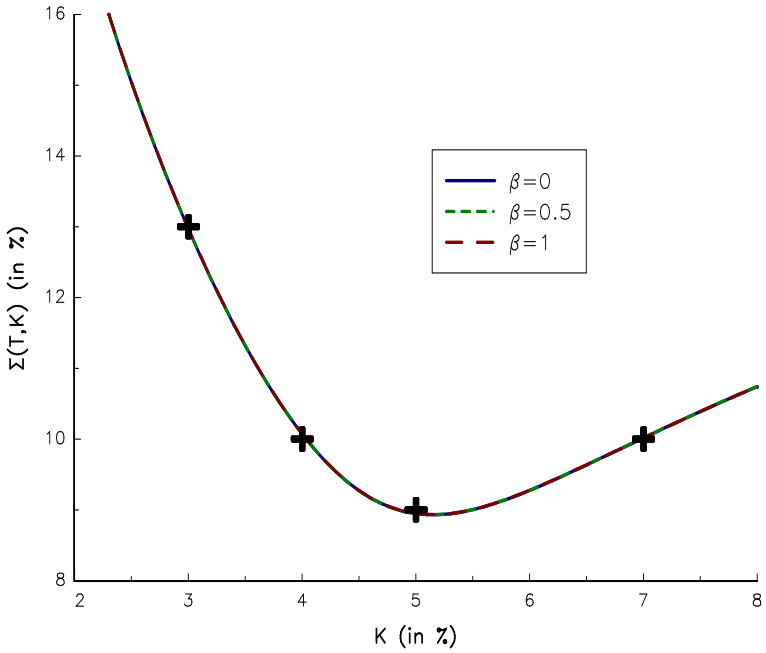

FIGURE 9.40: Implied volatility for different parameter sets (β, ρ)

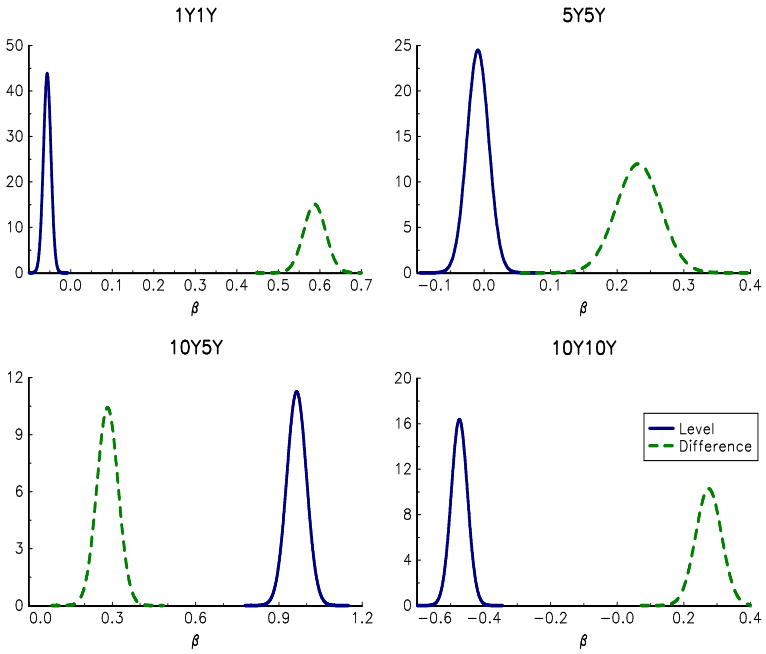

FIGURE 9.41: Probability density function of the estimate $\hat{\beta}$ (SABR model)

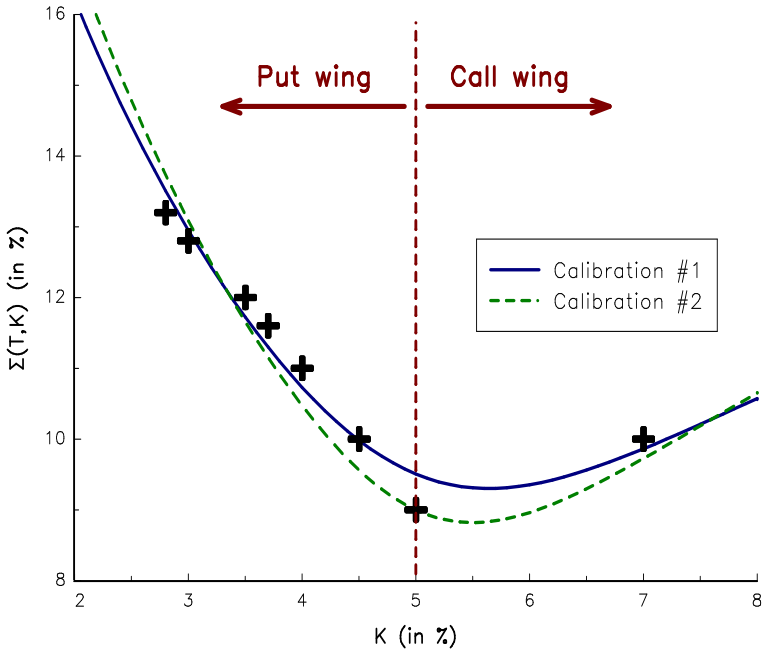

FIGURE 9.42: Calibration of the SABR model

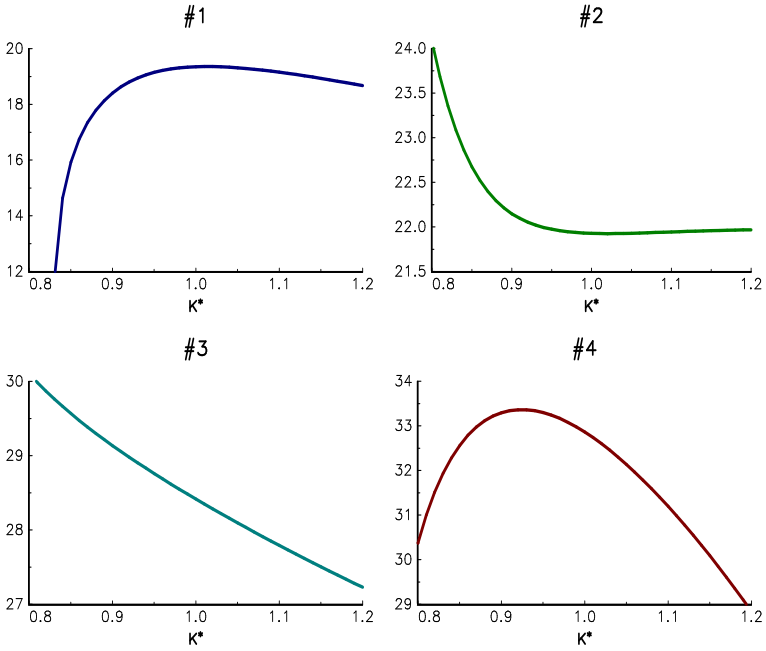

FIGURE 9.43: Volatility smiles generated by the quadratic Gaussian model

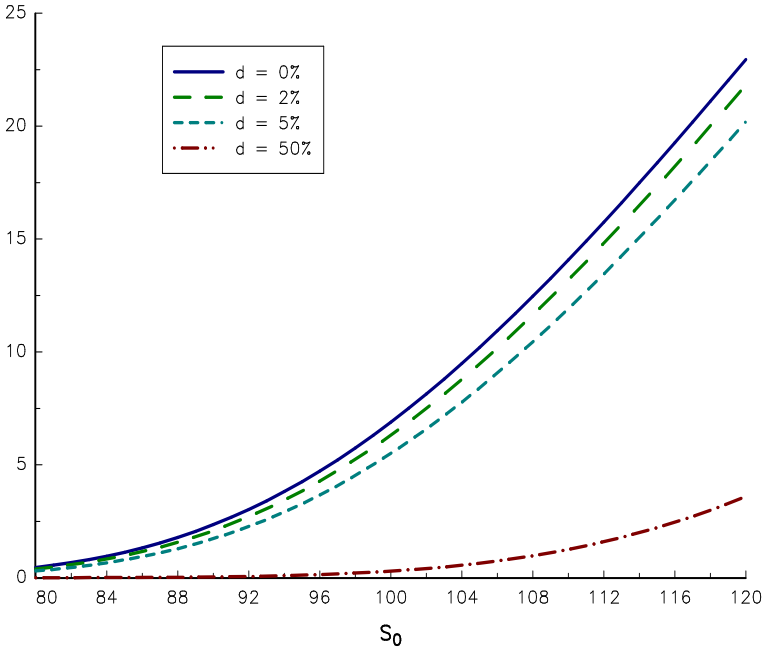

FIGURE 9.44: Impact of dividends on the call option price

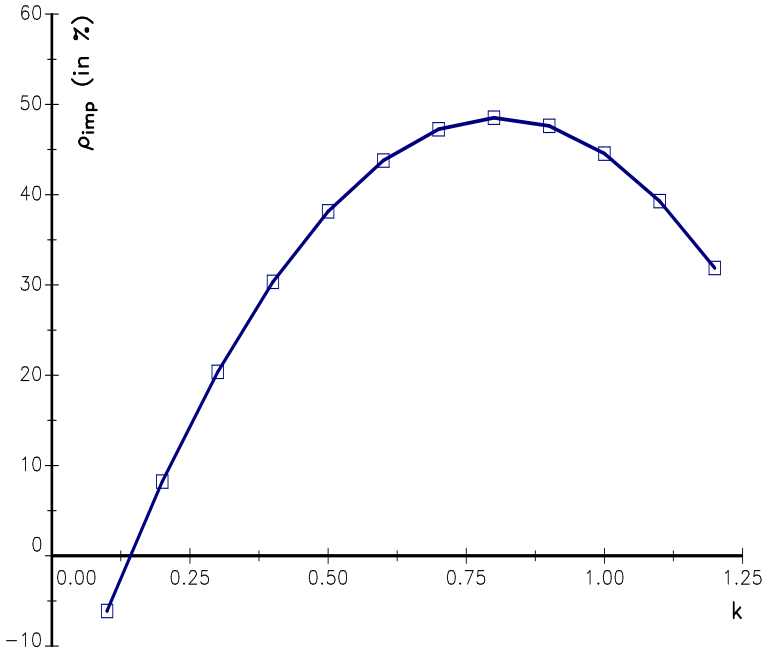

FIGURE 9.45: Correlation smile

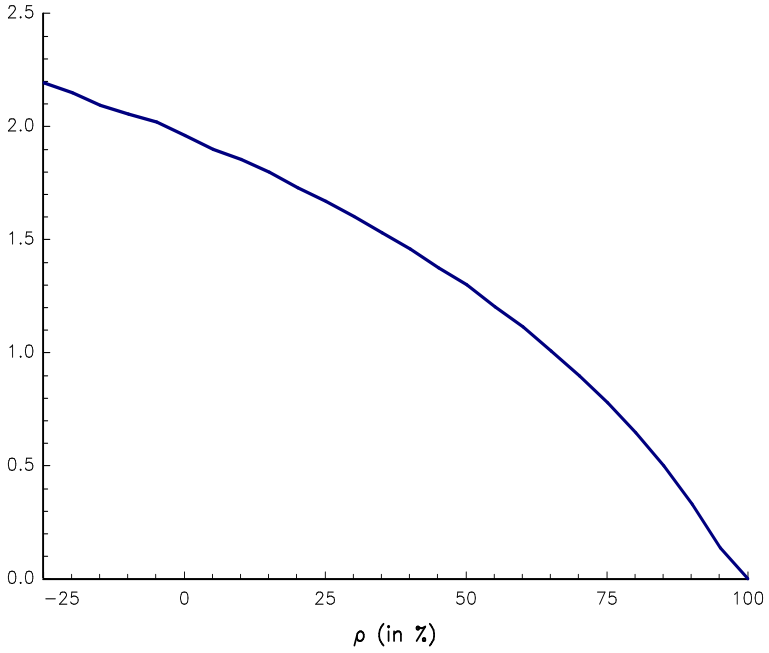

FIGURE 9.46: Price of the basket option with respect to the constant correlation

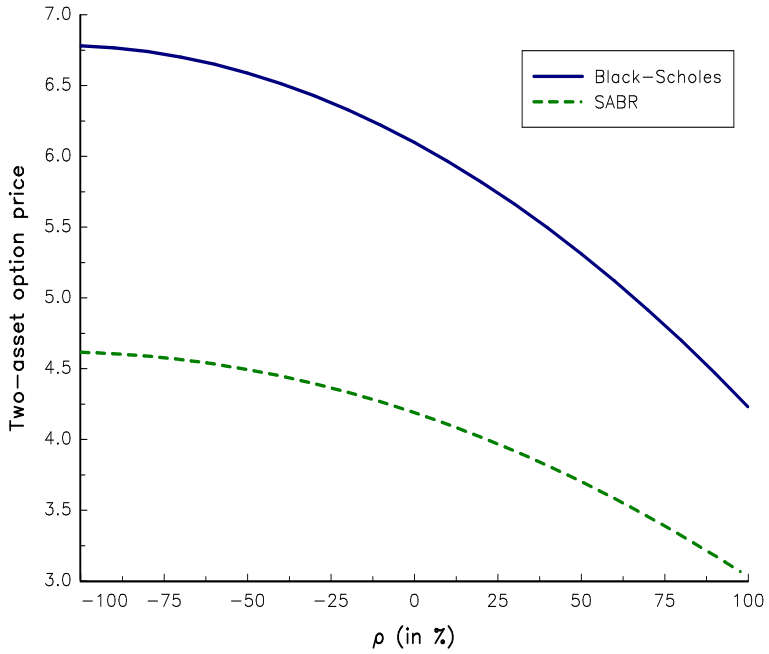

FIGURE 9.47: Comparison of the option price obtained with Black-Scholes and copula-SABR models

Chapter 10

Statistical Inference and Model Estimation

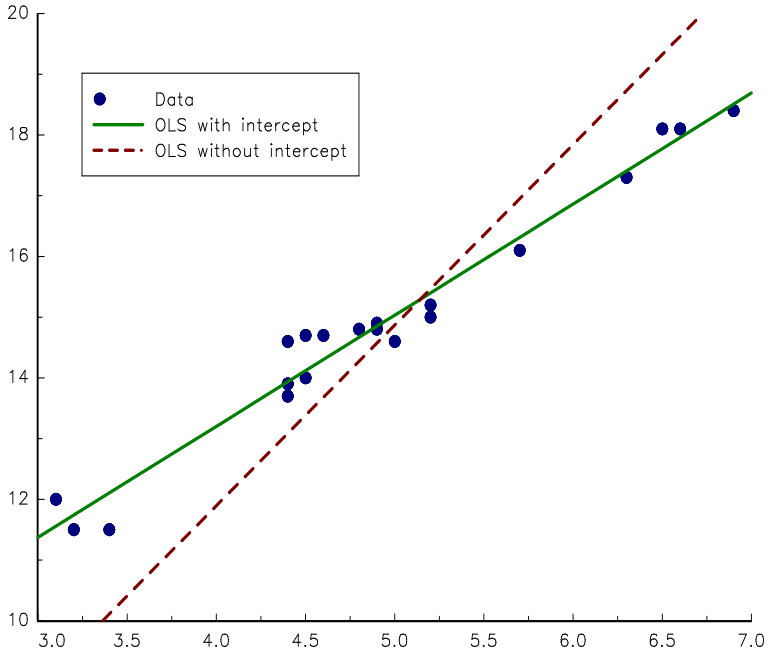

FIGURE 10.1: Illustration of the intercept problem

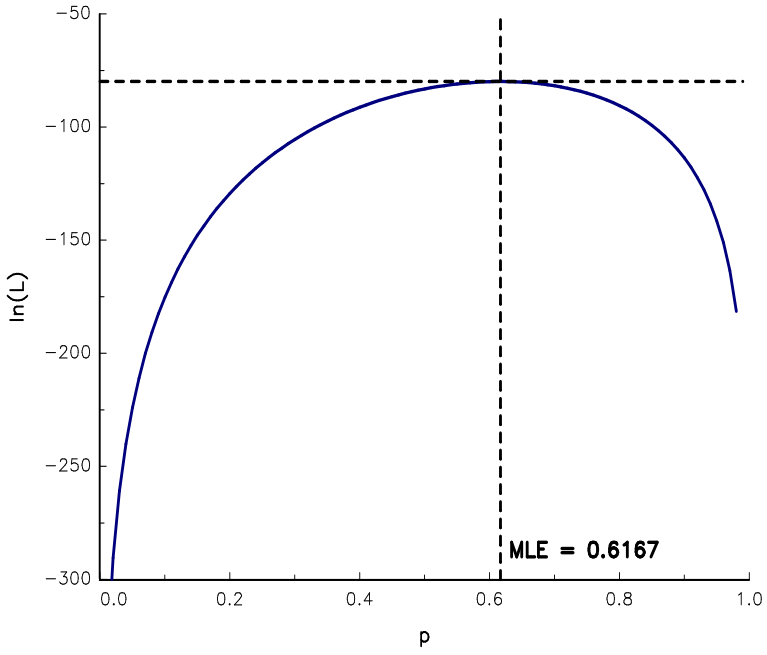

FIGURE 10.2: Log-likelihood function of the Bernoulli distribution

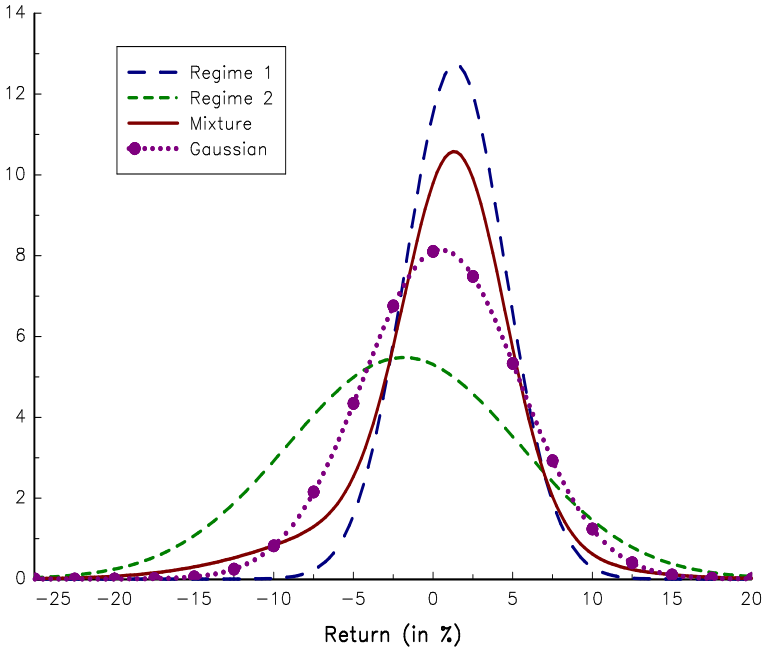

FIGURE 10.3: Probability density function of the monthly returns of the S&P 500 index

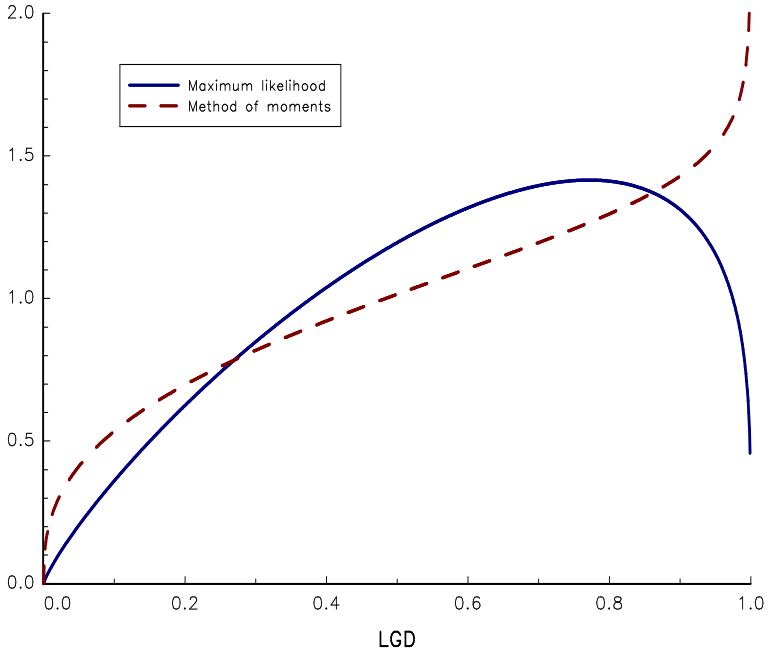

FIGURE 10.4: Calibrated density function of the loss given default

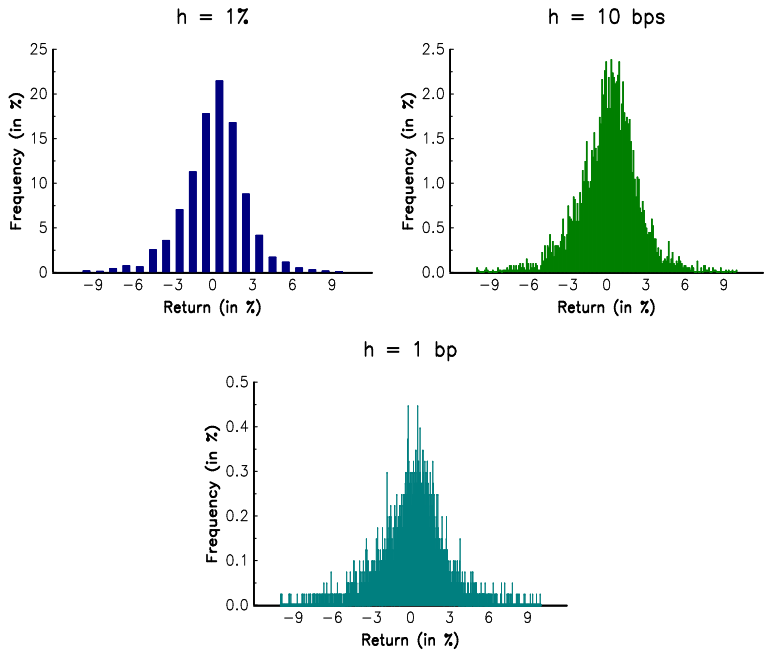

FIGURE 10.5: Histogram of the weekly returns of the S&P 500 index

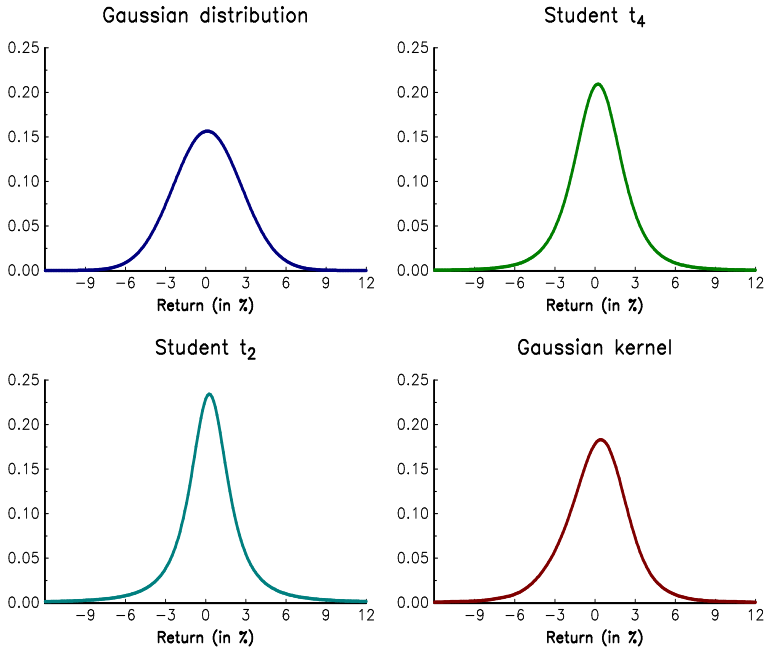

FIGURE 10.6: Density estimation of the weekly returns of the S&P 500 index

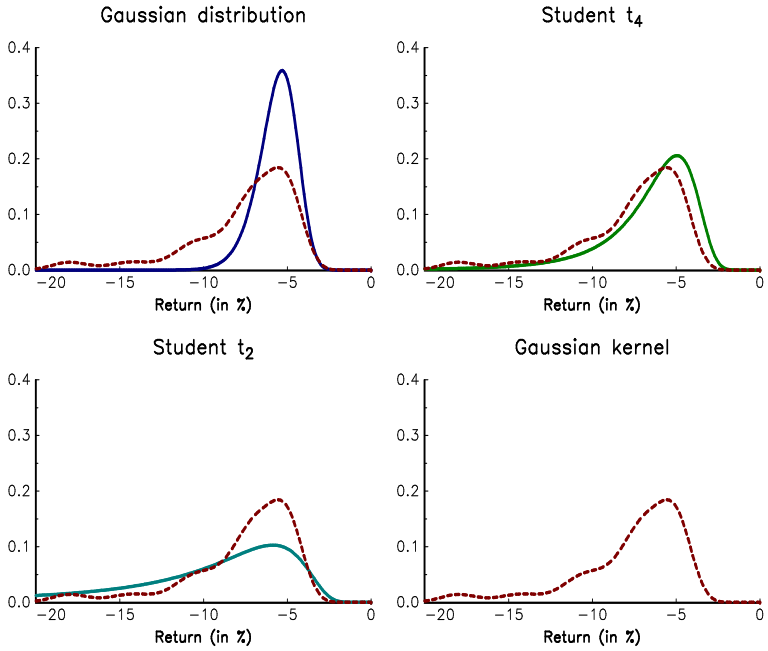

FIGURE 10.7: Density estimation of the worst weekly return of a year

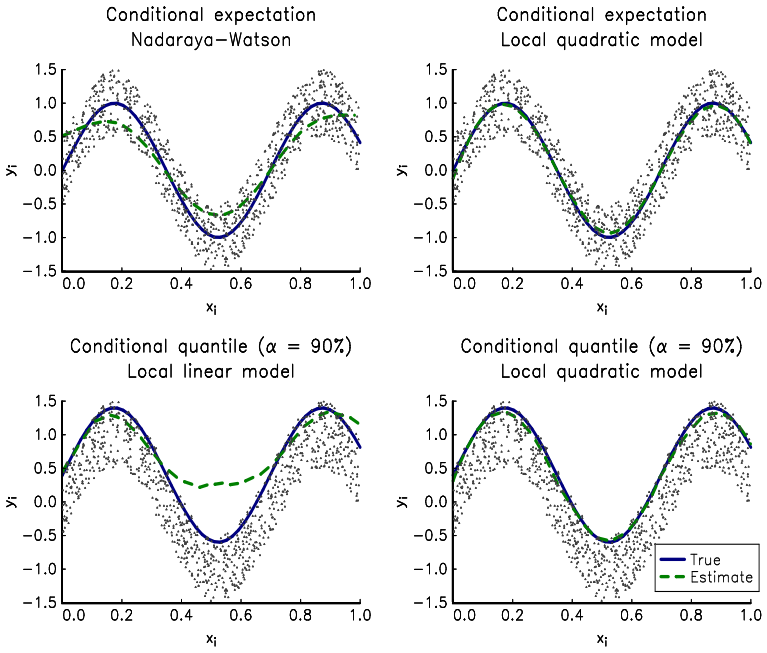

FIGURE 10.8: Non-parametric regression of the additive model

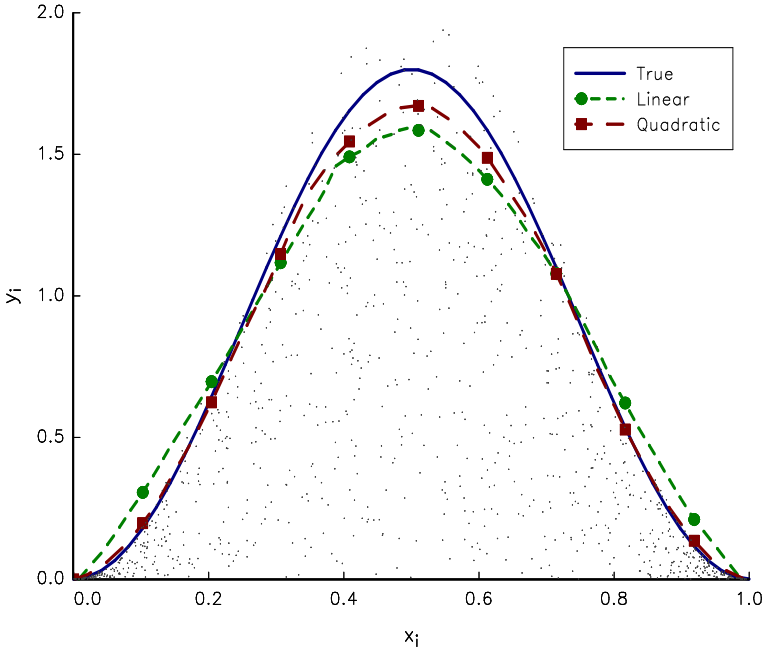

FIGURE 10.9: Non-parametric regression of the multiplicative model

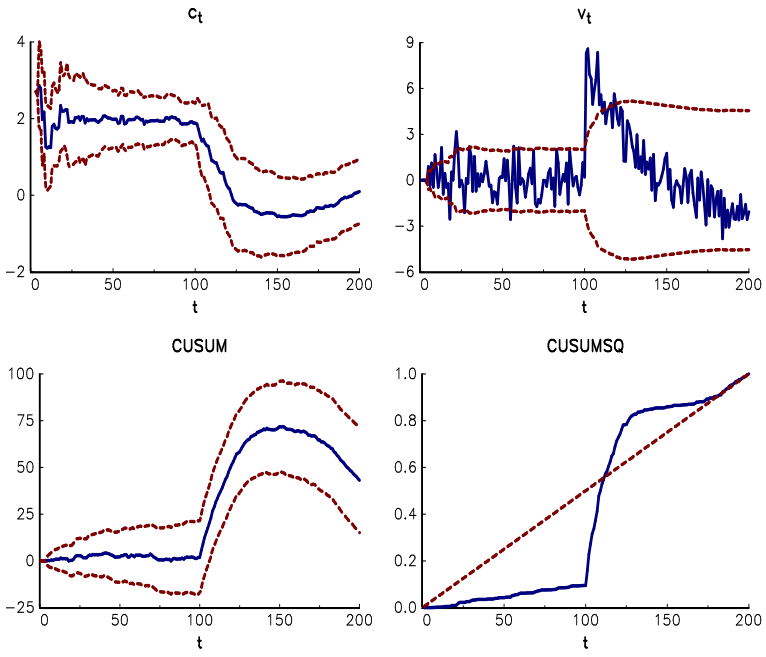

FIGURE 10.10: CUMSUM test and recursive least squares

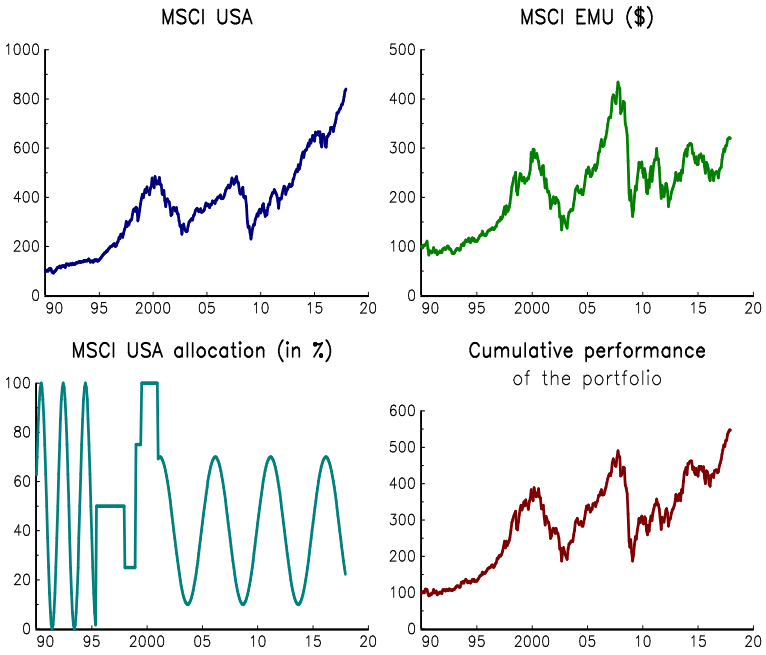

FIGURE 10.11: The tracking problem

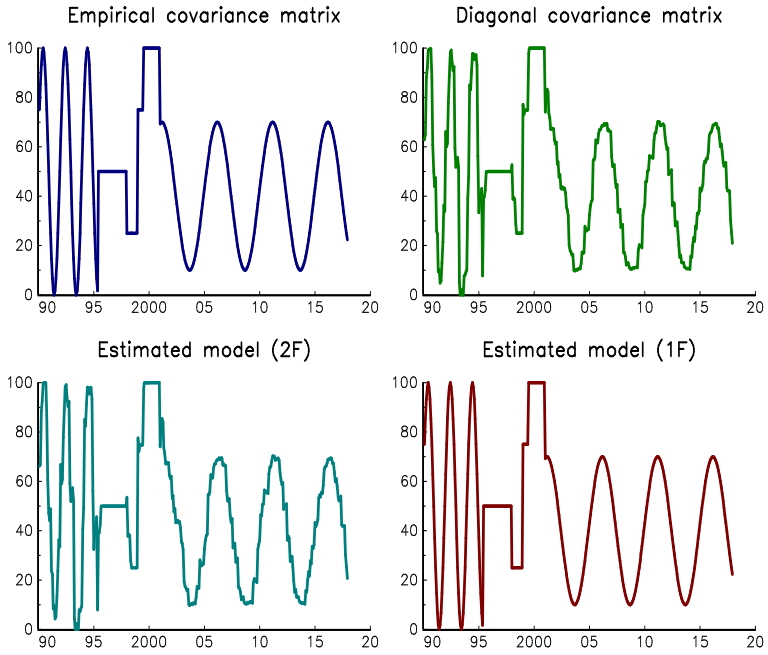

FIGURE 10.12: Estimation of the dynamic allocation by Kalman filtering

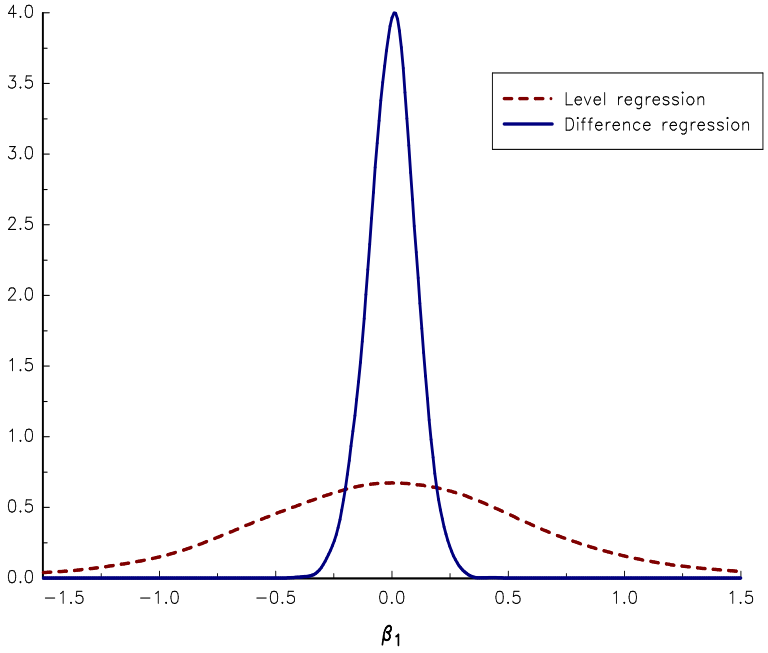

FIGURE 10.13: Probability density function of $\hat{\beta}_1$ in the case of a spurious regression

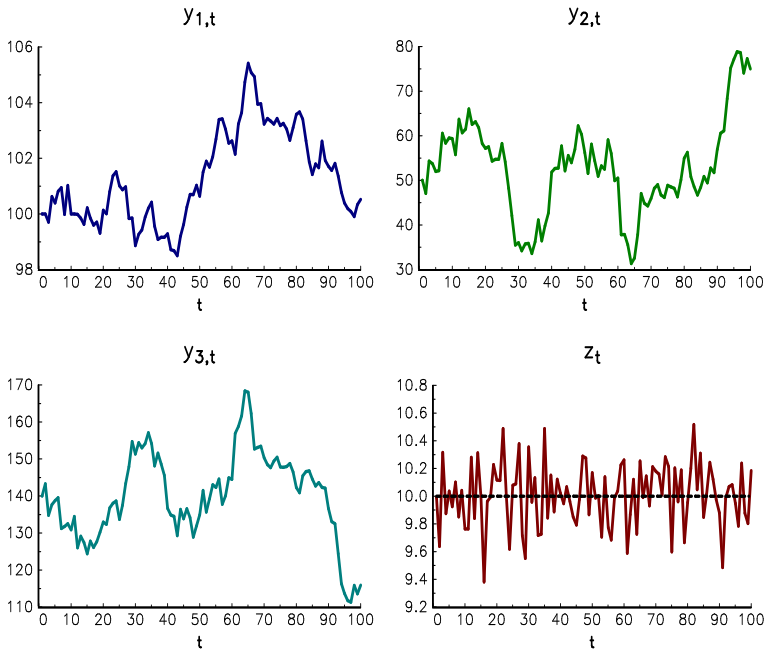

FIGURE 10.14: Illustration of the cointegration

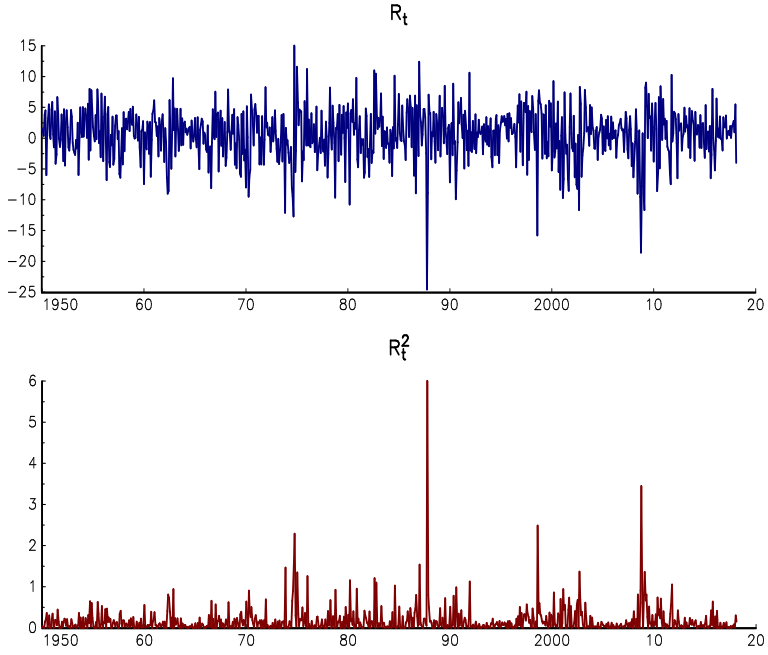

FIGURE 10.15: Monthly returns of the S&P 500 index (in %)

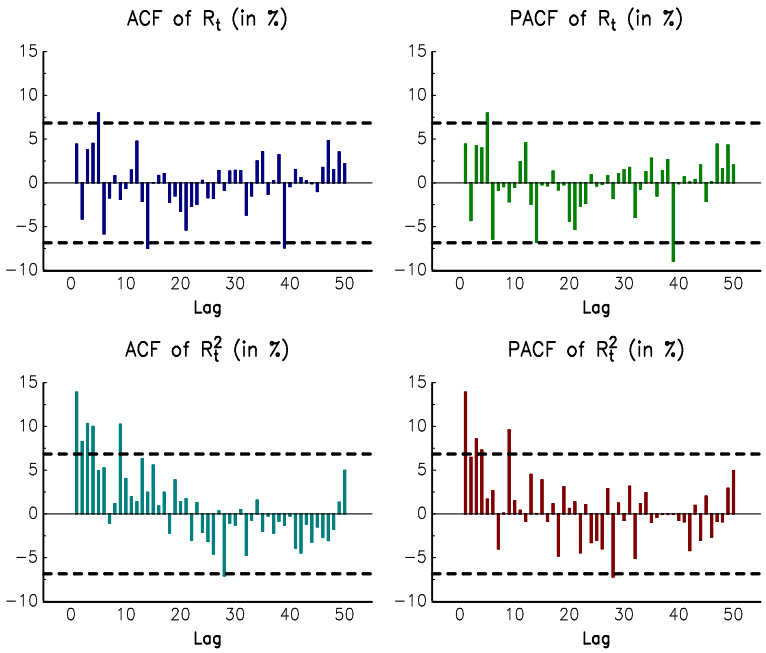

FIGURE 10.16: ACF and PACF of R_t and R_t^2

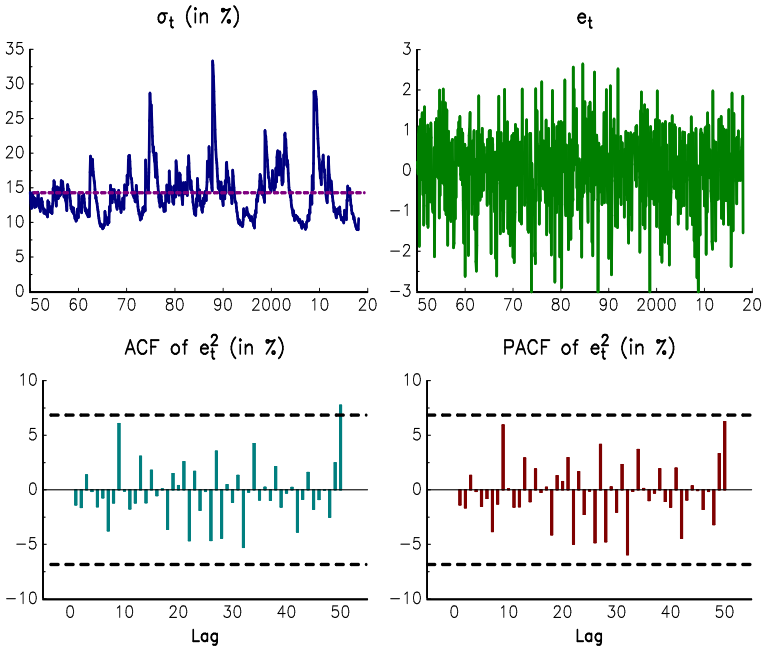

FIGURE 10.17: Diagnostic checking of the GARCH(1,1) model

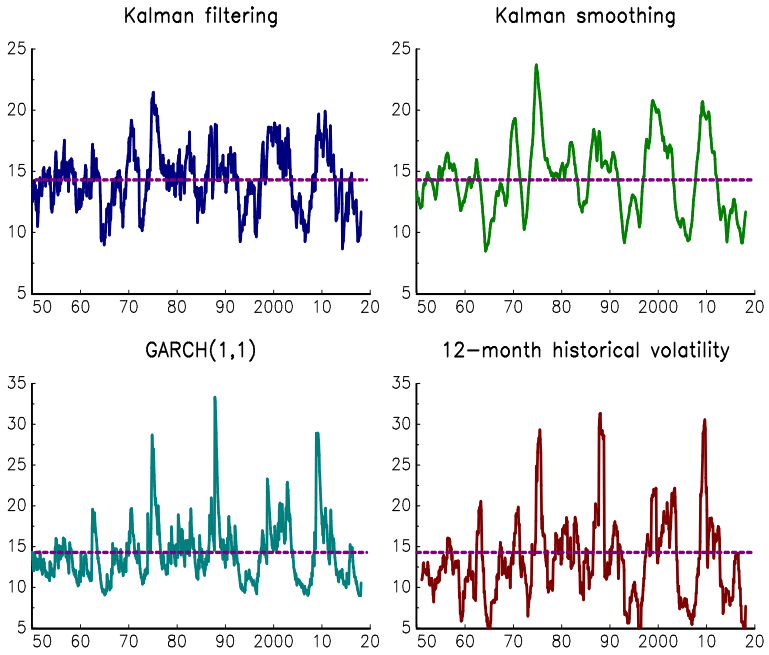

FIGURE 10.18: Estimation of the stochastic volatility model

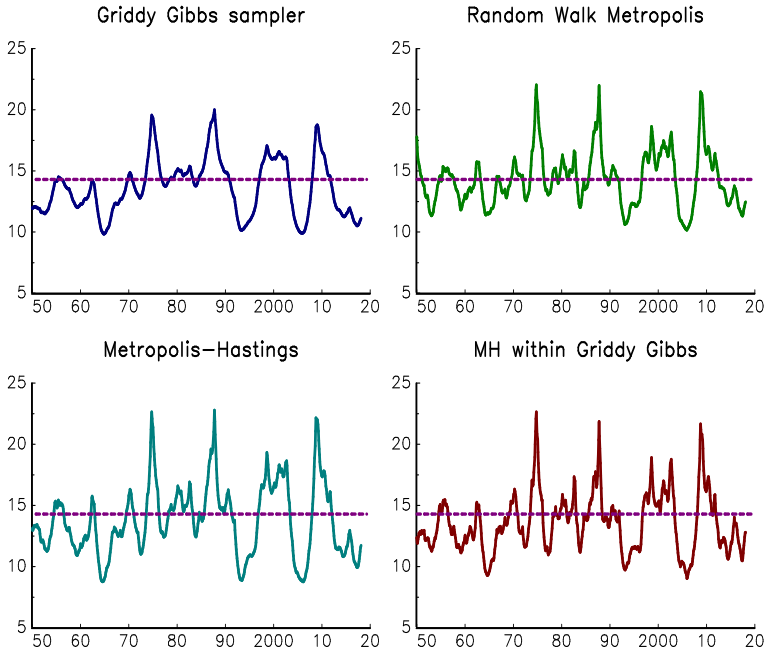

FIGURE 10.19: MCMC estimates of the stochastic volatility model

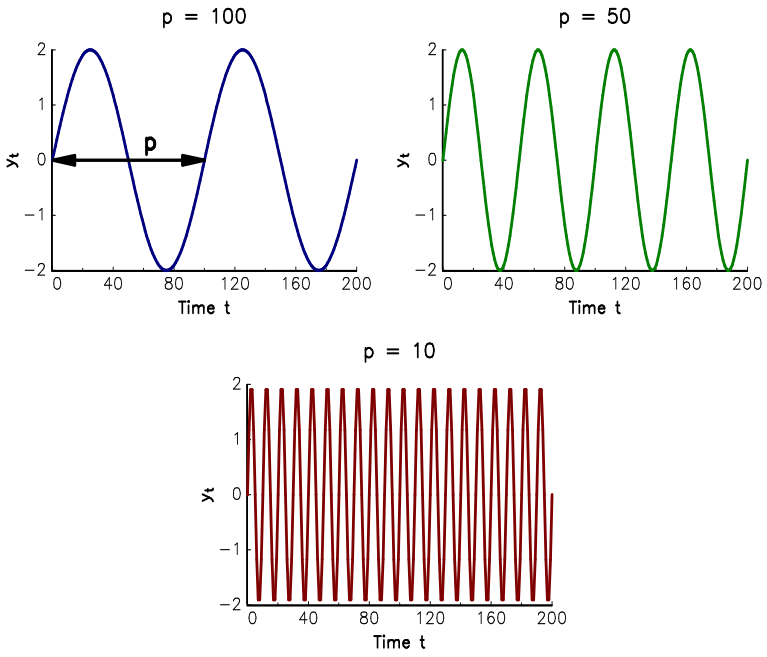

FIGURE 10.20: Time representation of the process x_t

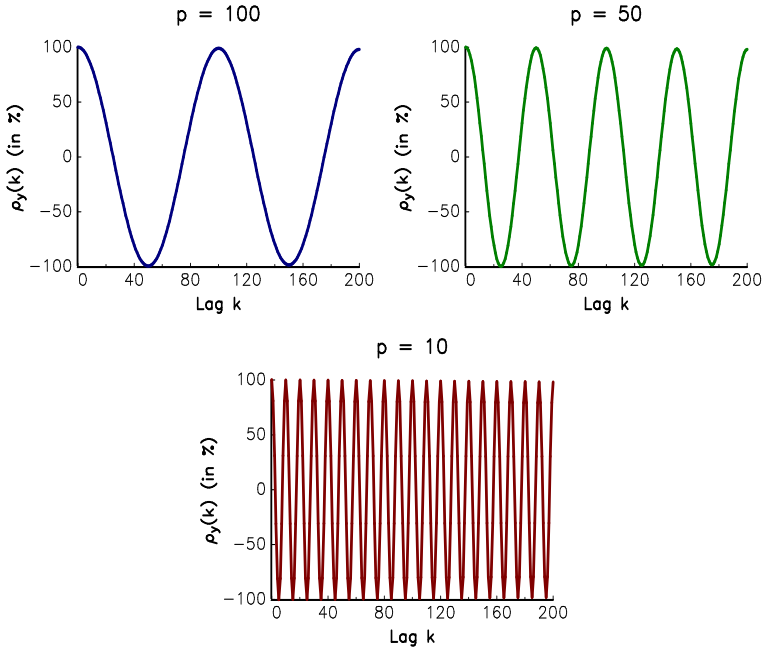

FIGURE 10.21: Autocorrelation representation of the process x_t

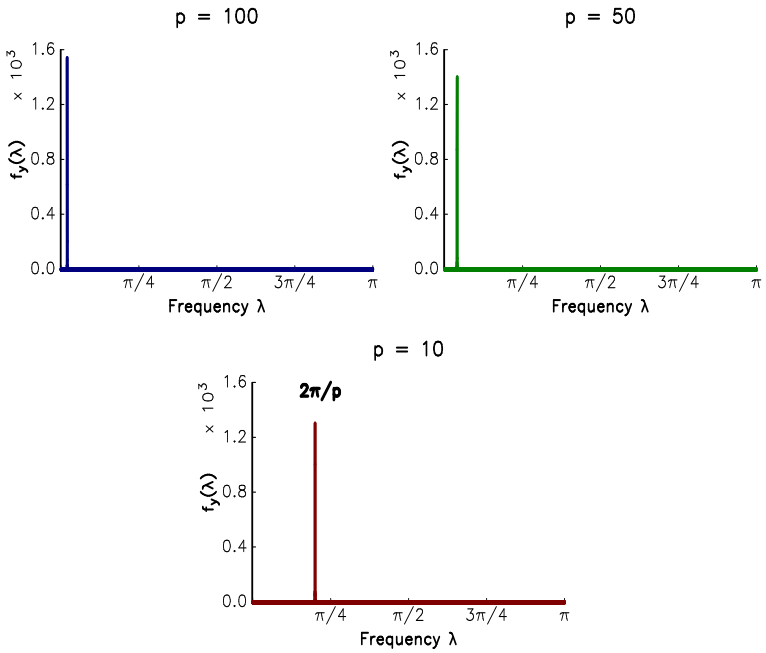

FIGURE 10.22: Spectral representation of the process x_t

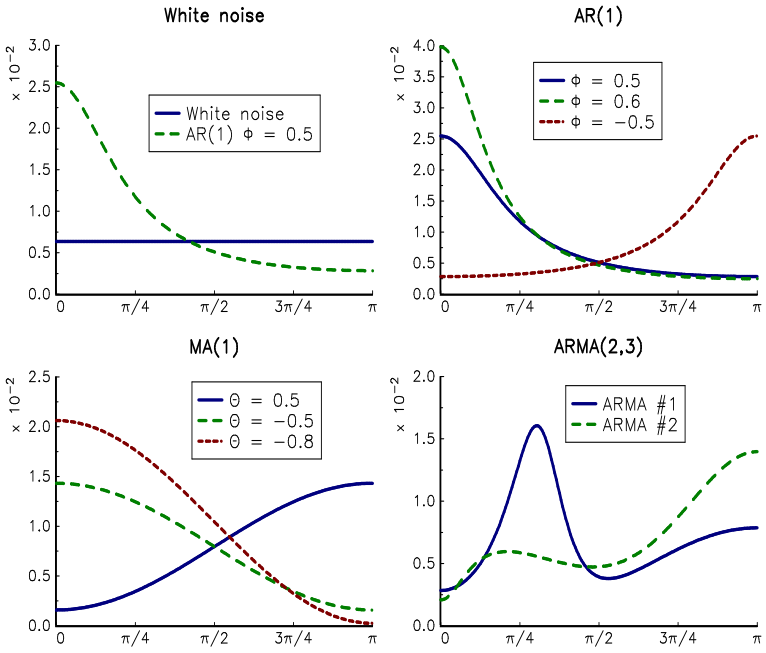

FIGURE 10.23: Spectral density function of ARMA processes

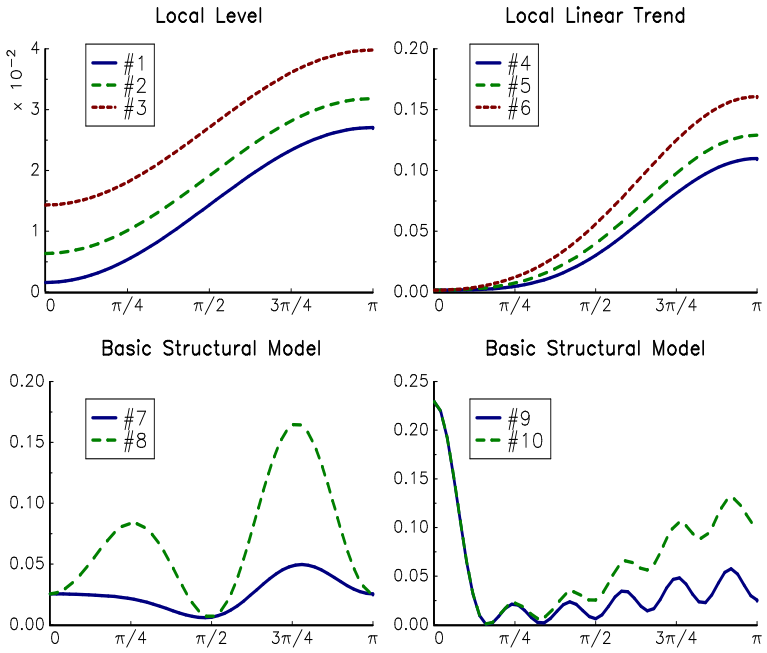

FIGURE 10.24: Spectral density function of LL, LLT and BSM

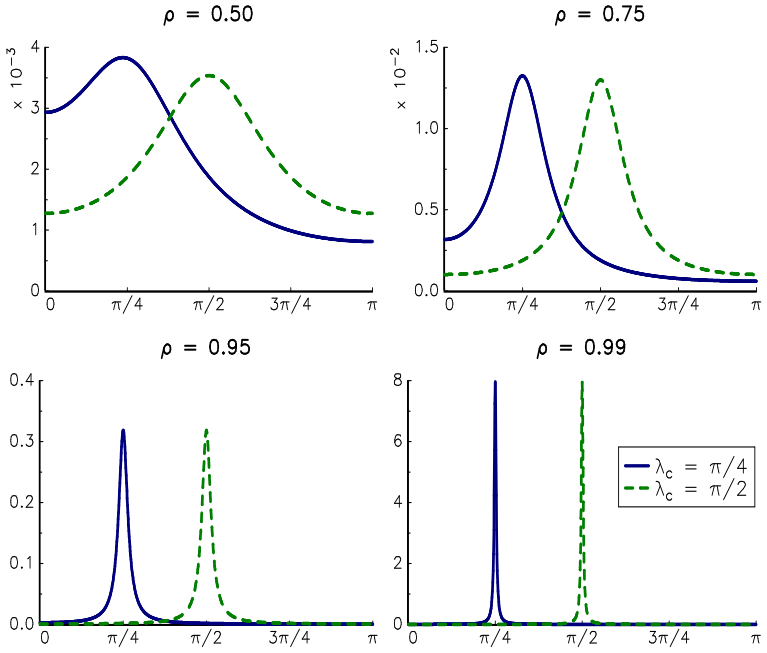

FIGURE 10.25: Spectral density function of the stochastic cycle model

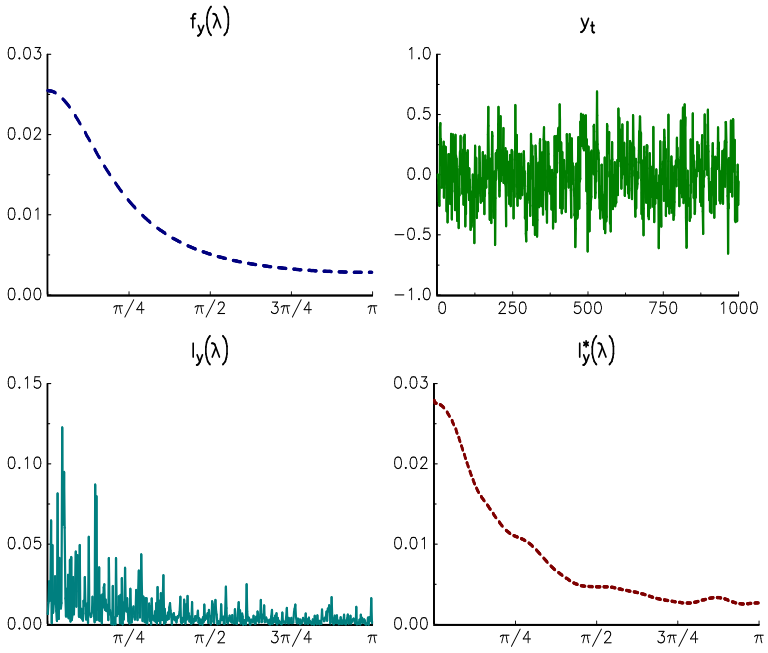

FIGURE 10.26: Estimation of the spectral density function

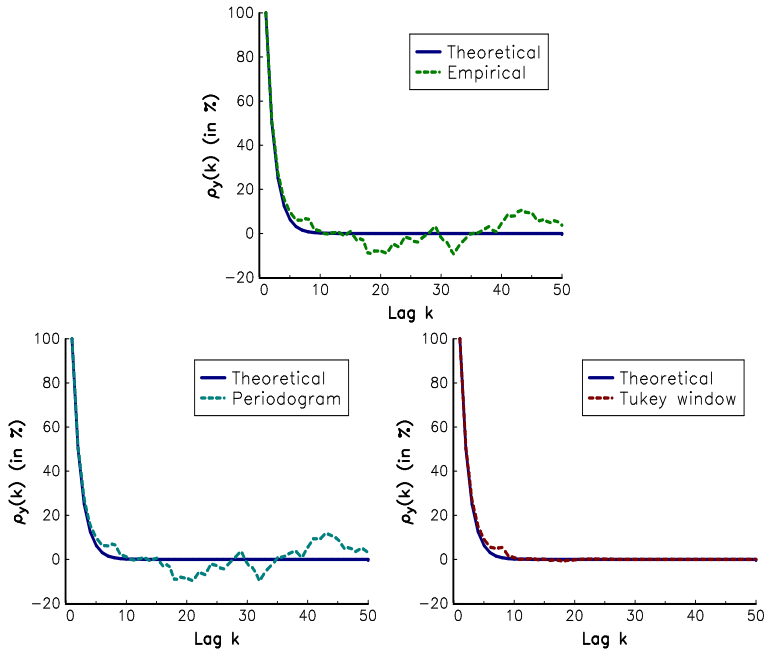

FIGURE 10.27: Estimation of the autocorrelation function

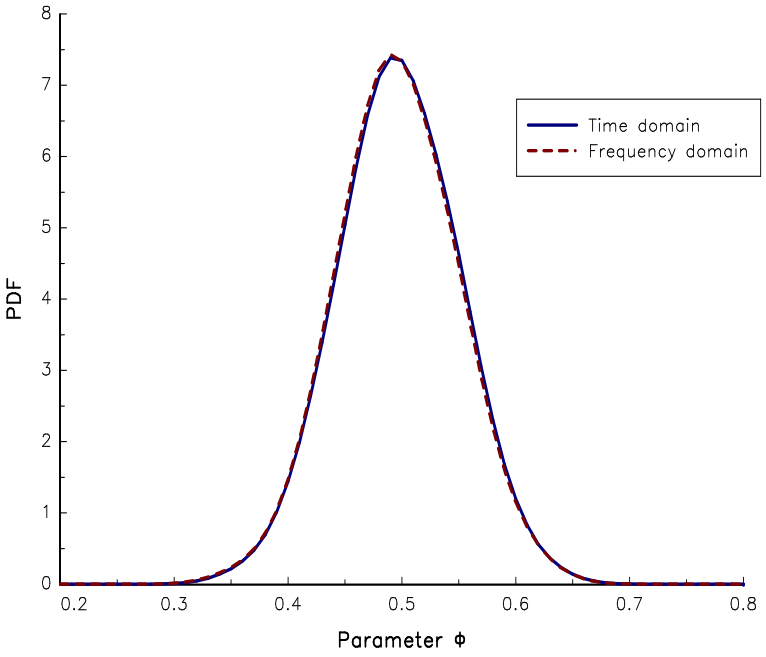

FIGURE 10.28: PDF of TDML and FDML estimators

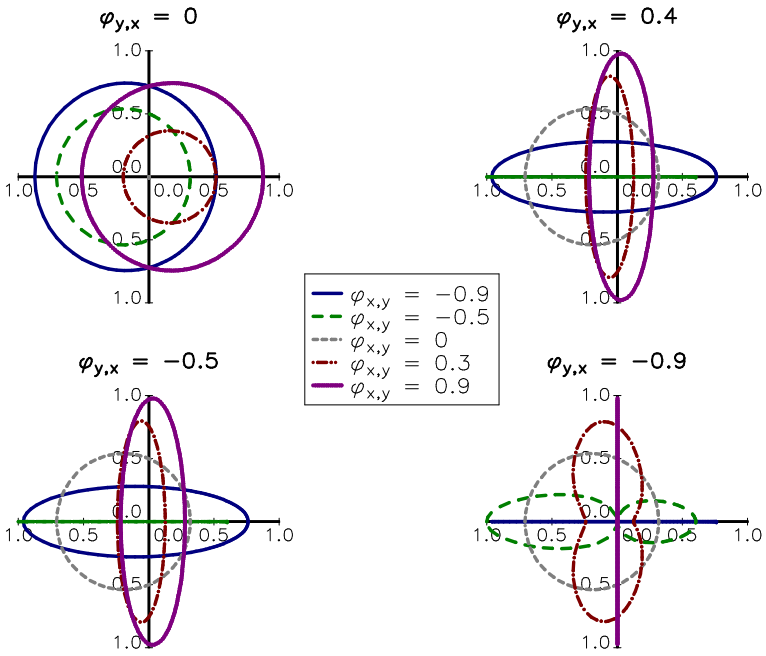

FIGURE 10.29: Coherency function $c_{y,x}(\lambda)$

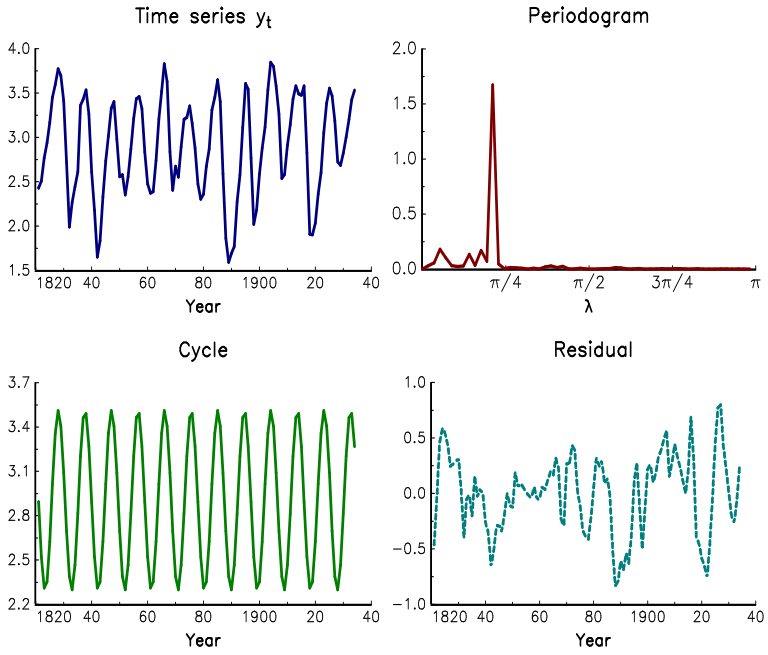

FIGURE 10.30: Detection of the cycle in the Canadian lynx data set

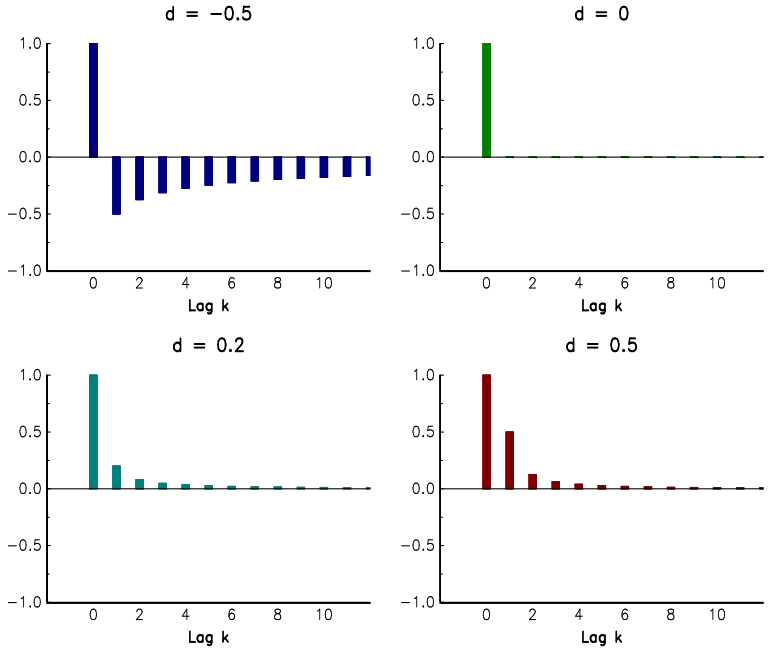

FIGURE 10.31: AR representation of the fractional process

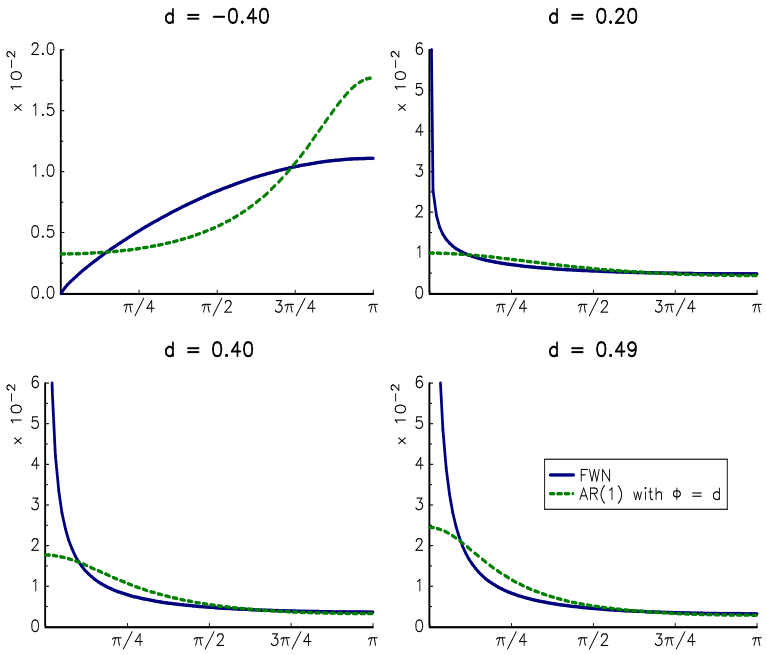

FIGURE 10.32: Spectral density function of the FWN process

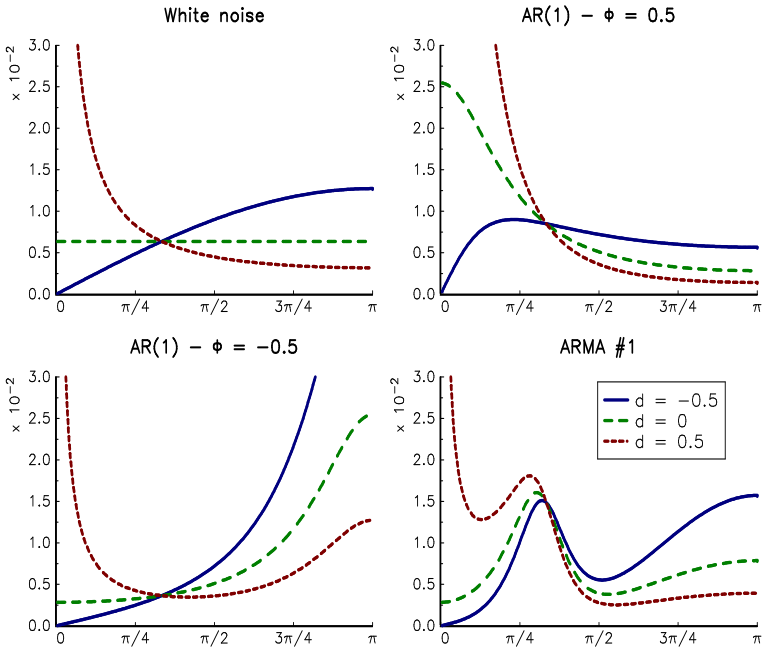

FIGURE 10.33: Spectral density function of the ARFIMA process

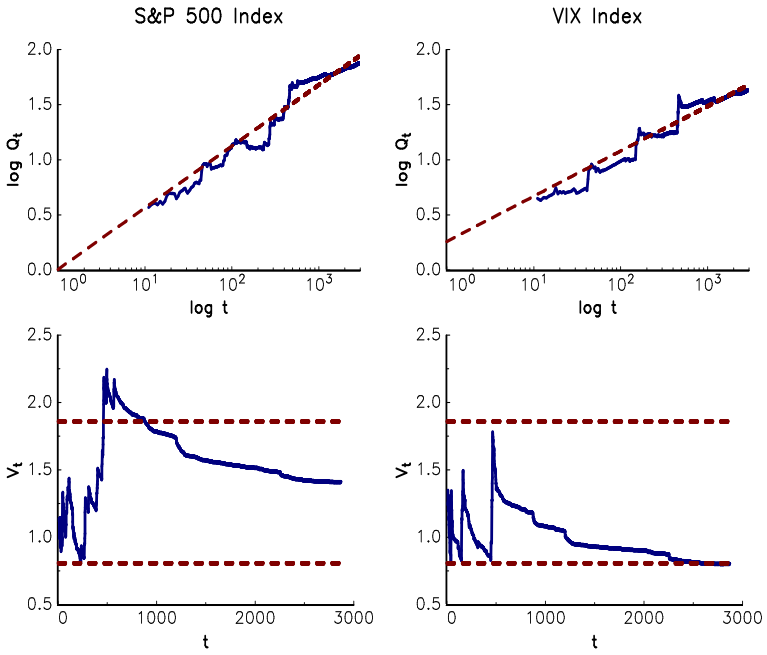

FIGURE 10.34: R/S analysis and estimation of the Hurst exponent

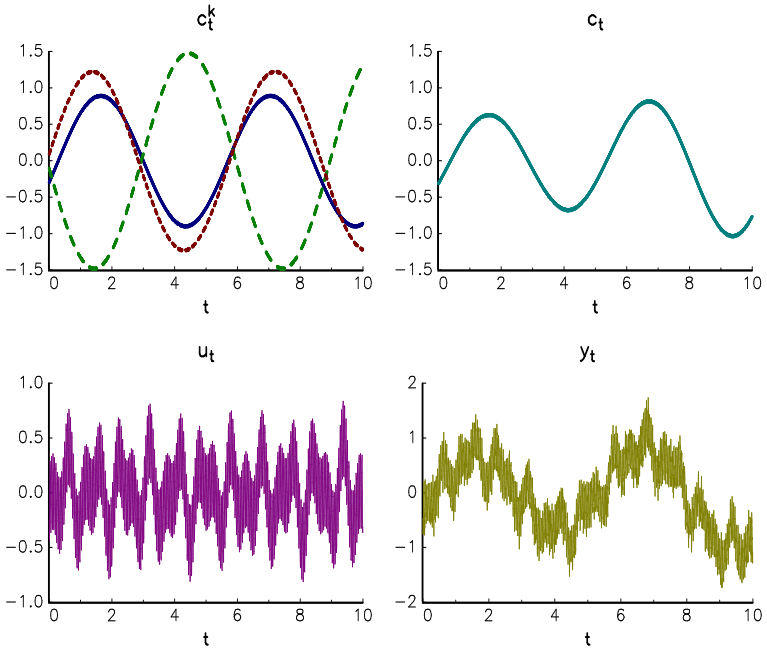

FIGURE 10.35: Spectral decomposition of the signal y_t

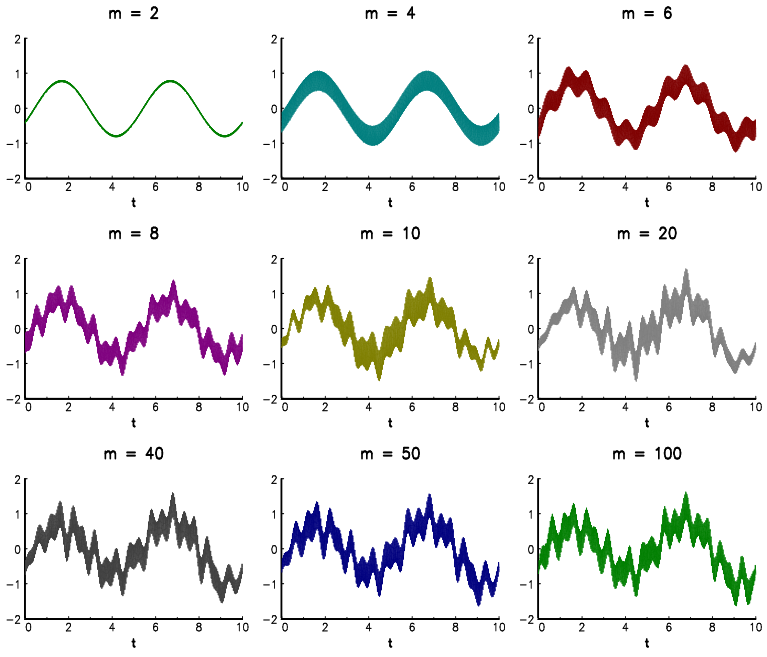

FIGURE 10.36: Reconstructed signal y_t^m

Chapter 11

Copulas and Dependence Modeling

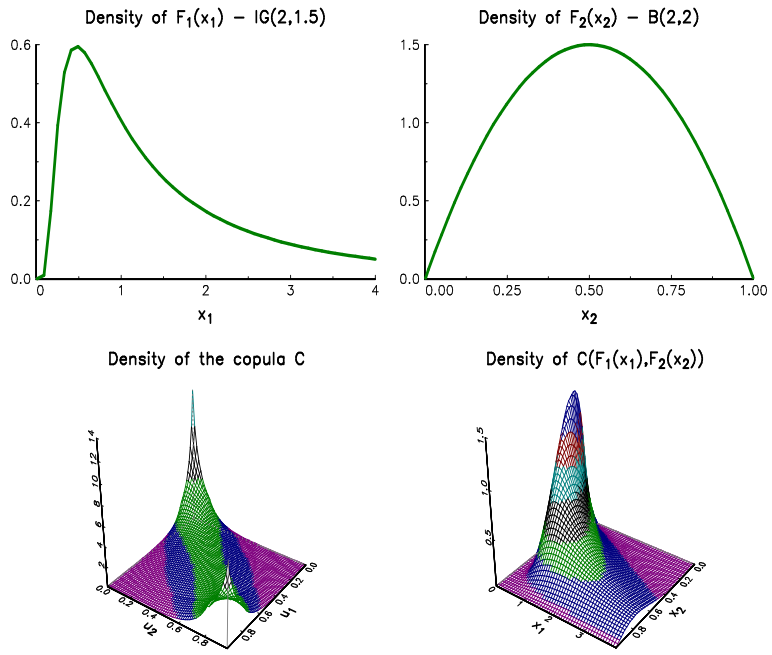

FIGURE 11.1: Example of a bivariate probability distribution with given marginals

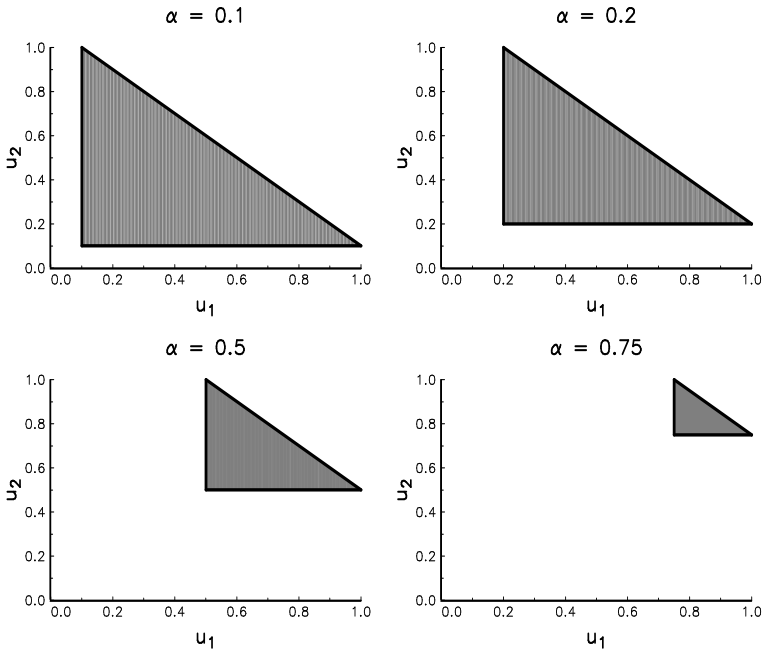

FIGURE 11.2: The triangle region of the contour lines $\mathbf{C}(u_1, u_2) = \alpha$

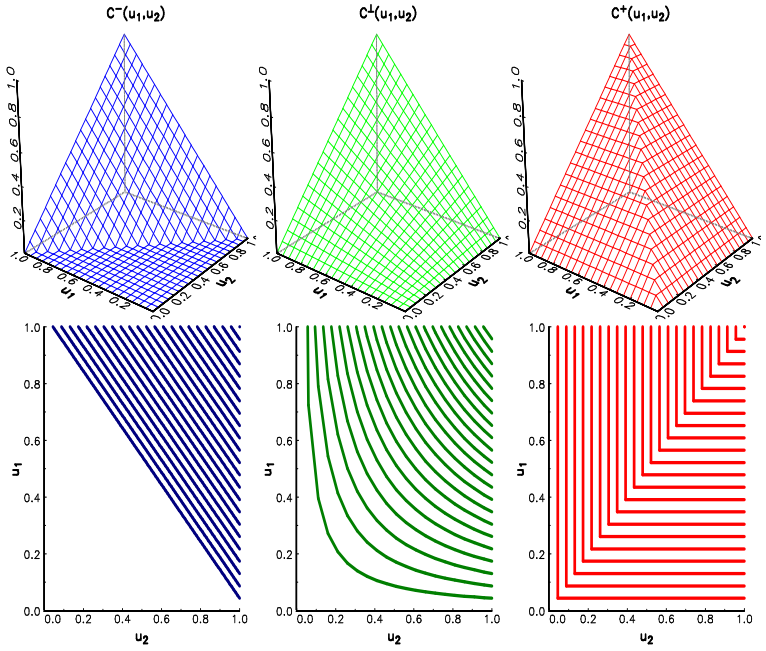

FIGURE 11.3: The three copula functions $\mathbf{C}^-$, $\mathbf{C}^\perp$ and $\mathbf{C}^+$

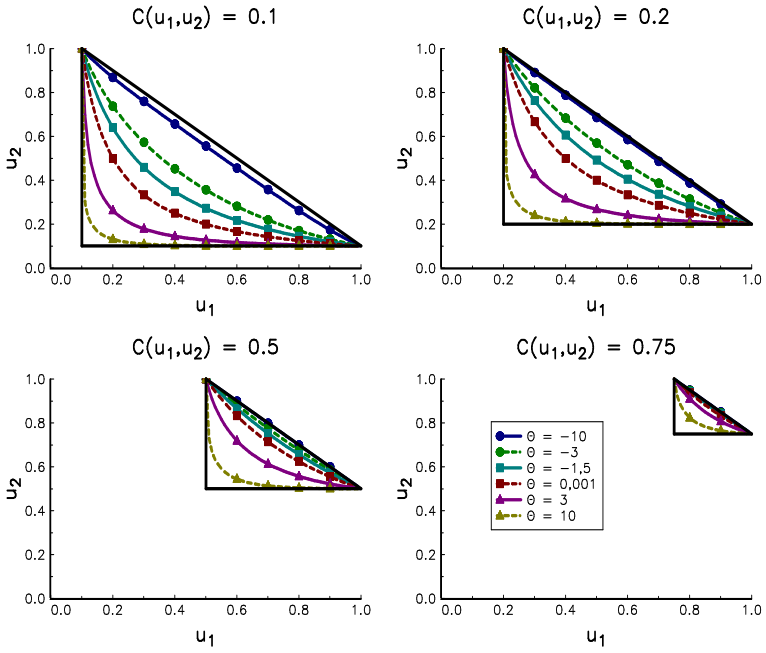

FIGURE 11.4: Concordance ordering of the Frank copula

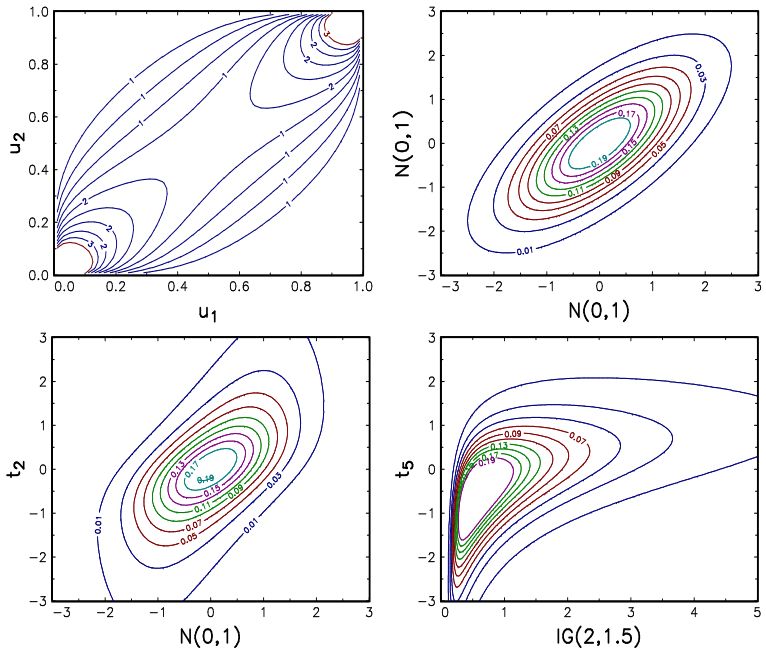

FIGURE 11.5: Contour lines of bivariate densities (Normal copula)

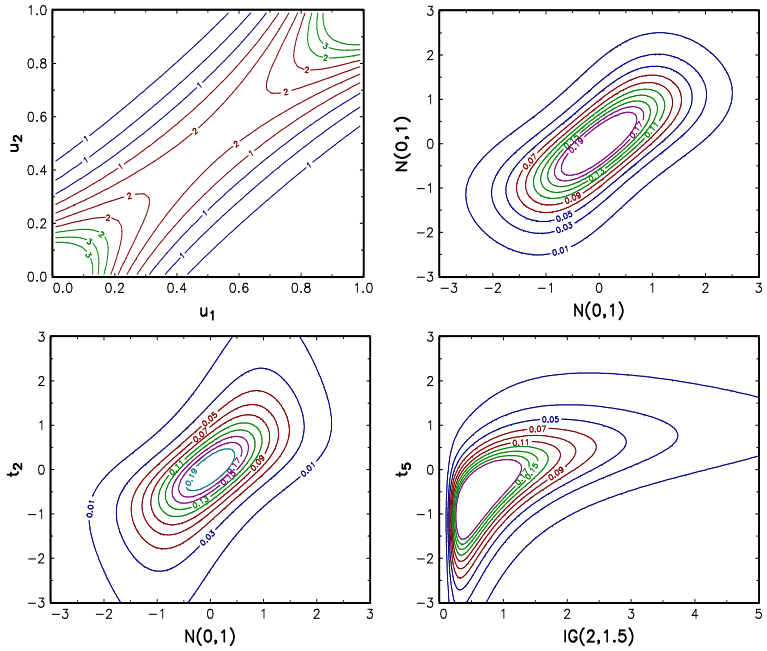

FIGURE 11.6: Contour lines of bivariate densities (Frank copula)

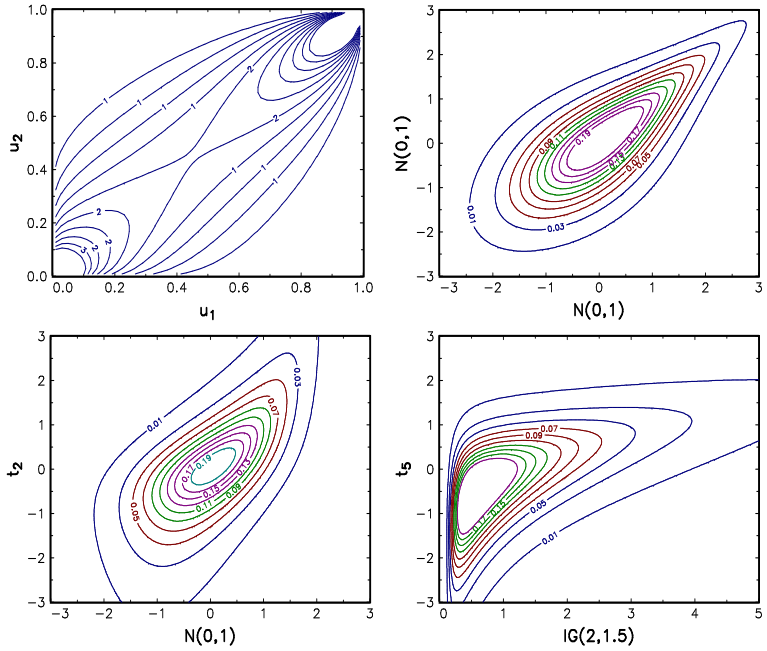

FIGURE 11.7: Contour lines of bivariate densities (Gumbel copula)

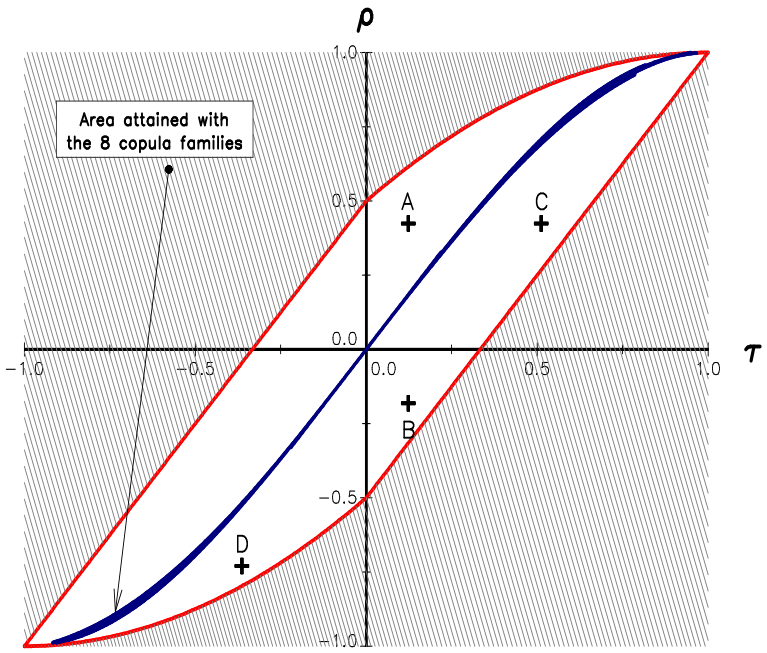

FIGURE 11.8: Bounds of (τ, ϱ) statistics

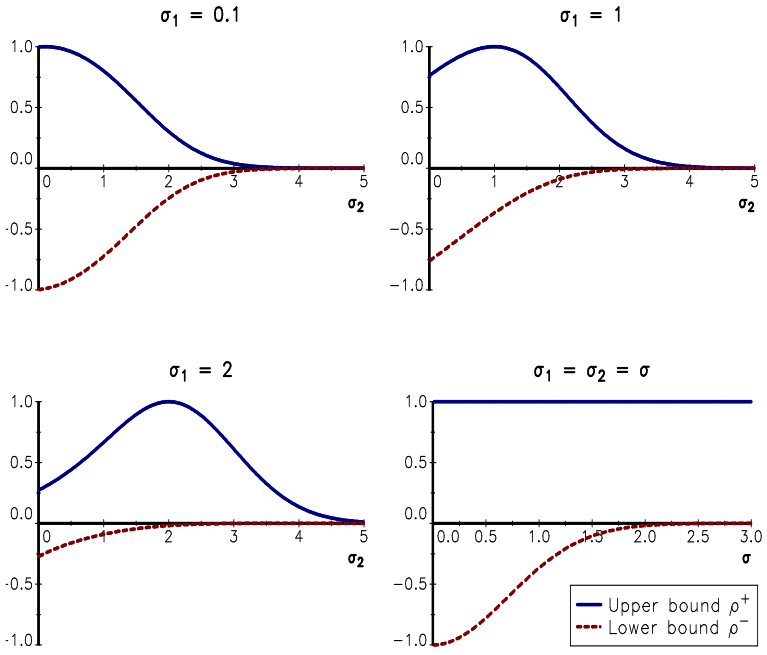

FIGURE 11.9: Bounds of the linear correlation between two log-normal random variables

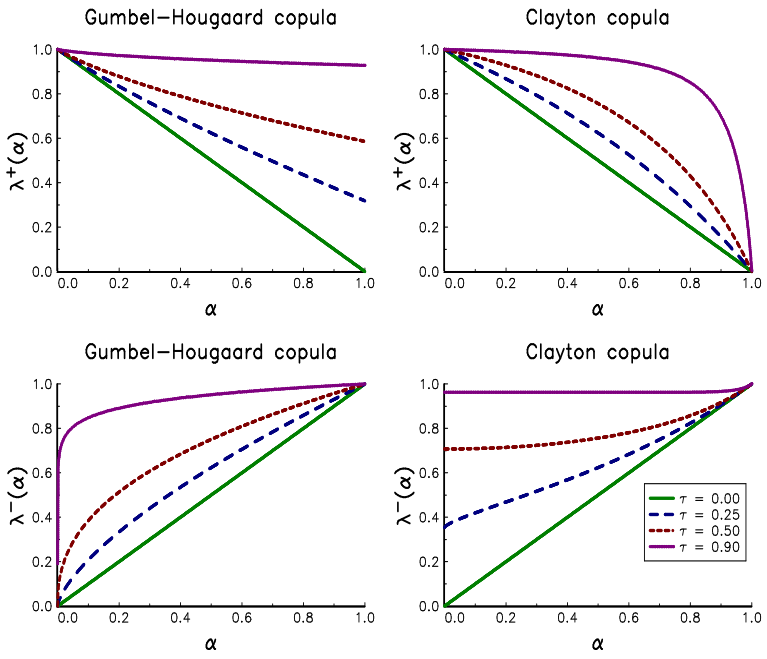

FIGURE 11.10: Quantile-quantile dependence measures $\lambda^{+}(\alpha)$ and $\lambda^{-}(\alpha)$

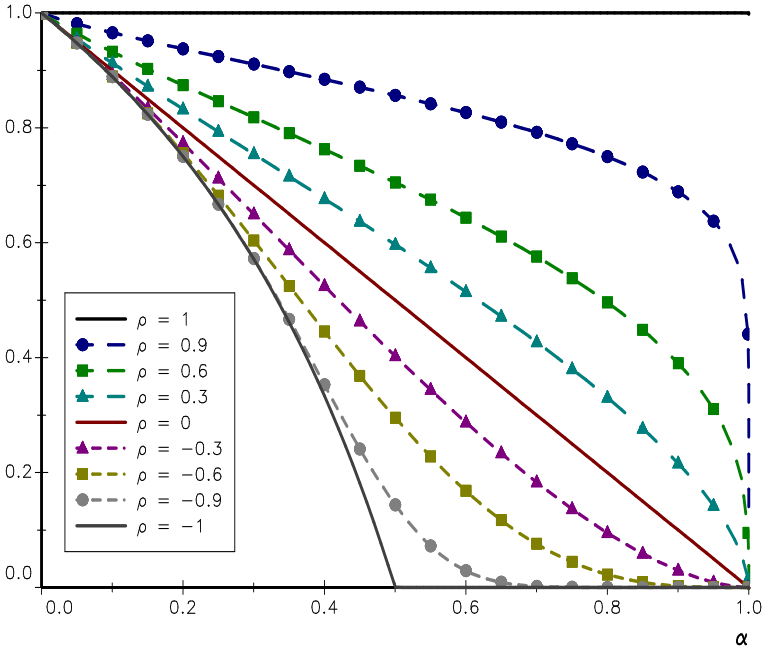

FIGURE 11.11: Tail dependence $\lambda^{+}(\alpha)$ for the Normal copula

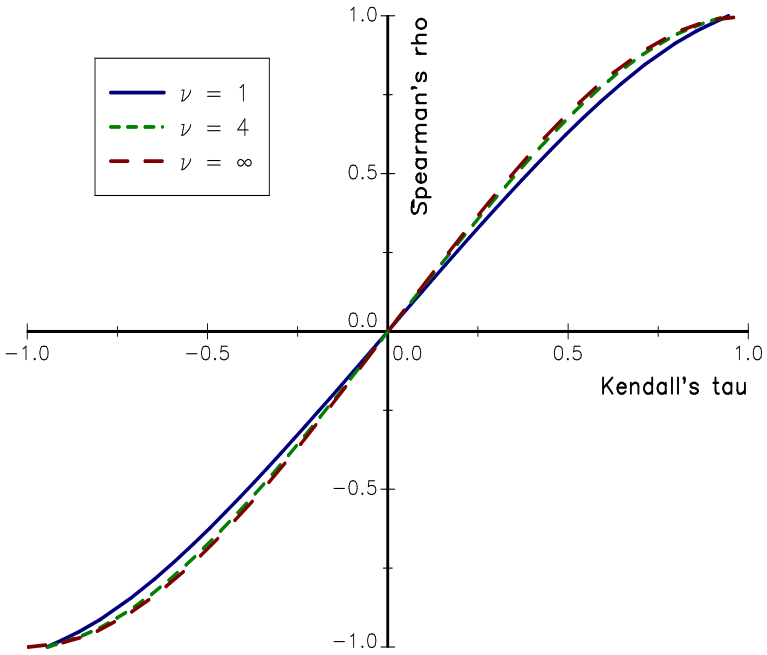

FIGURE 11.12: Relationship between τ and ϱ of the Student's t copula

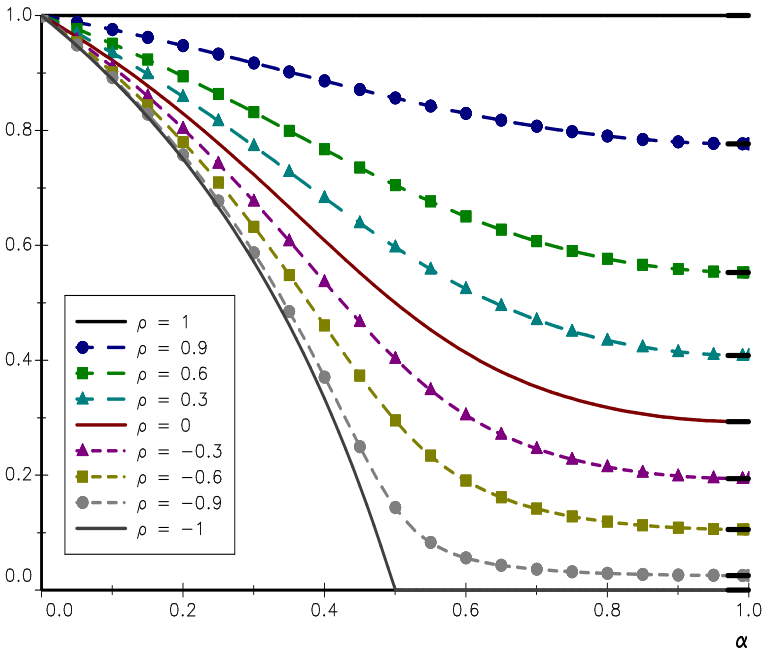

FIGURE 11.13: Tail dependence $\lambda^{+}(\alpha)$ for the Student's t copula ($\nu = 1$)

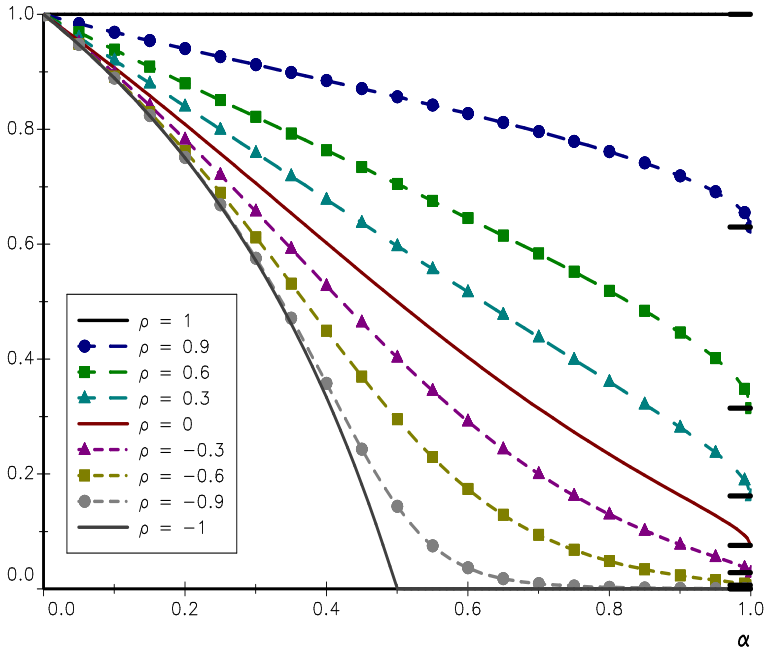

FIGURE 11.14: Tail dependence $\lambda^{+}(\alpha)$ for the Student's t copula ($\nu = 4$)

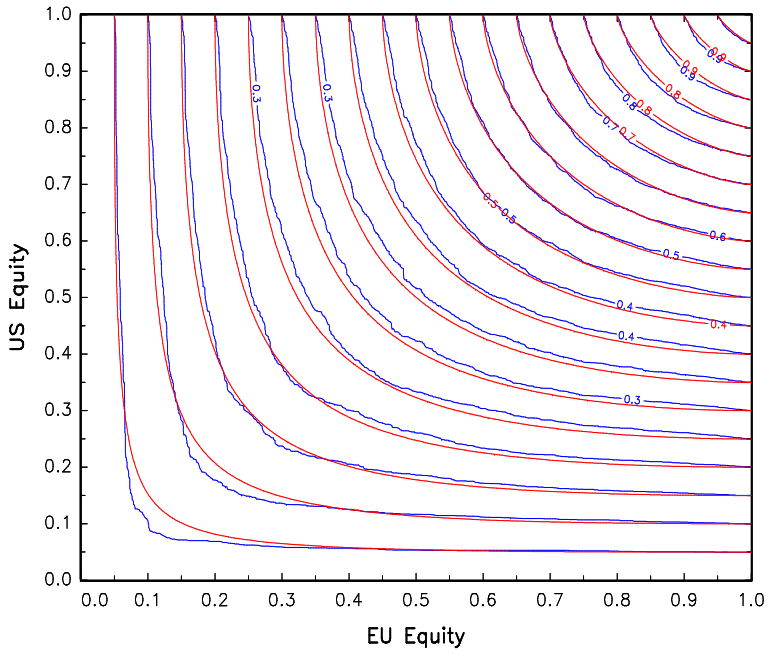

FIGURE 11.15: Comparison of the empirical copula (blue line) and the Normal copula (red line)

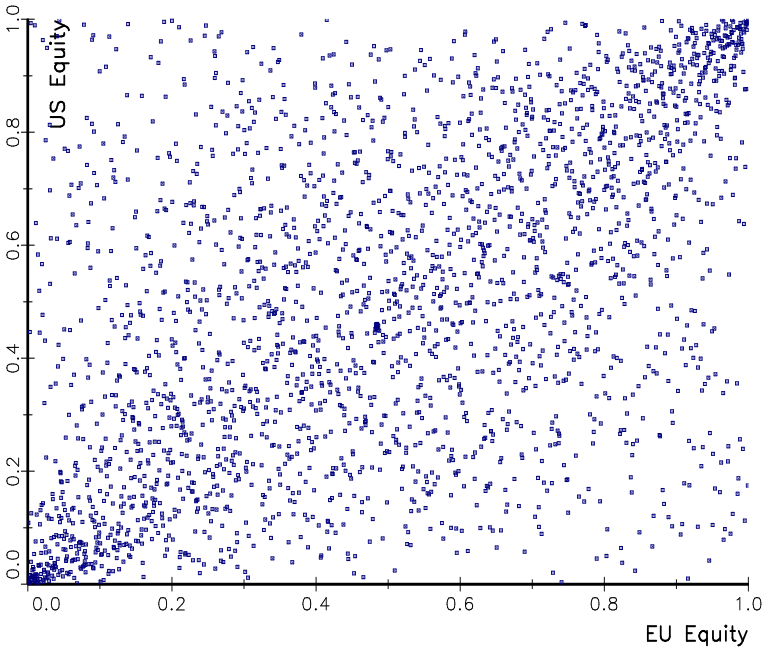

FIGURE 11.16: Dependogram of EU and US equity returns

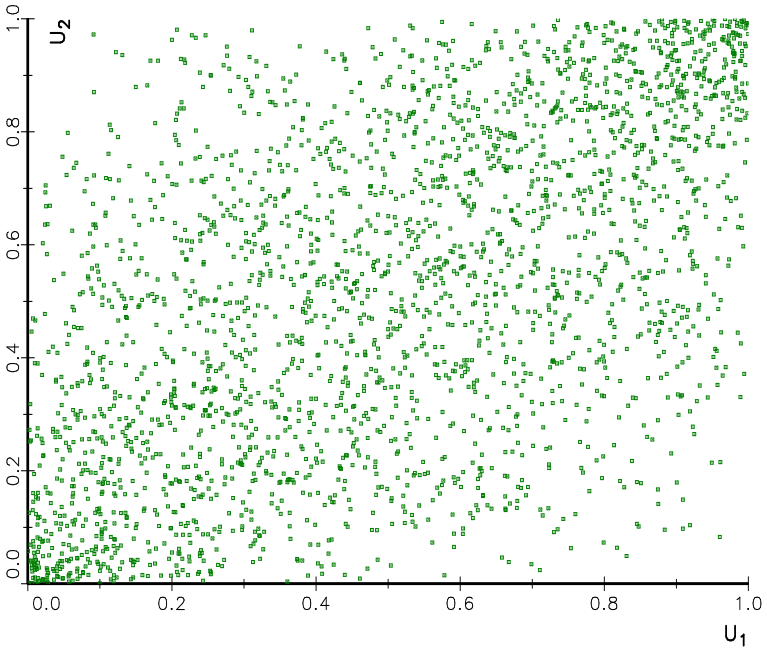

FIGURE 11.17: Dependogram of simulated Gaussian returns

Chapter 12

Extreme Value Theory

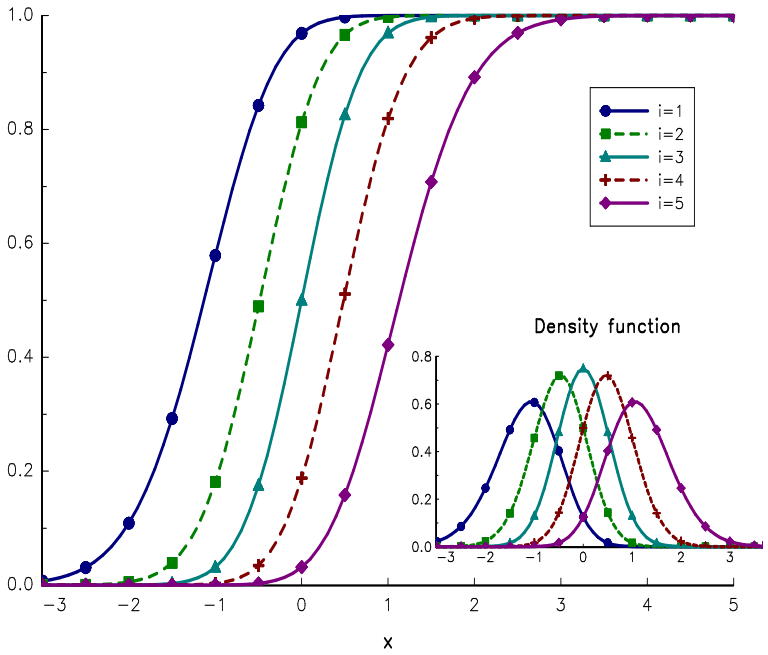

FIGURE 12.1: Distribution function $\mathbf{F}_{i:n}$ when the random variables $X_1, \ldots, X_n$ are Gaussian

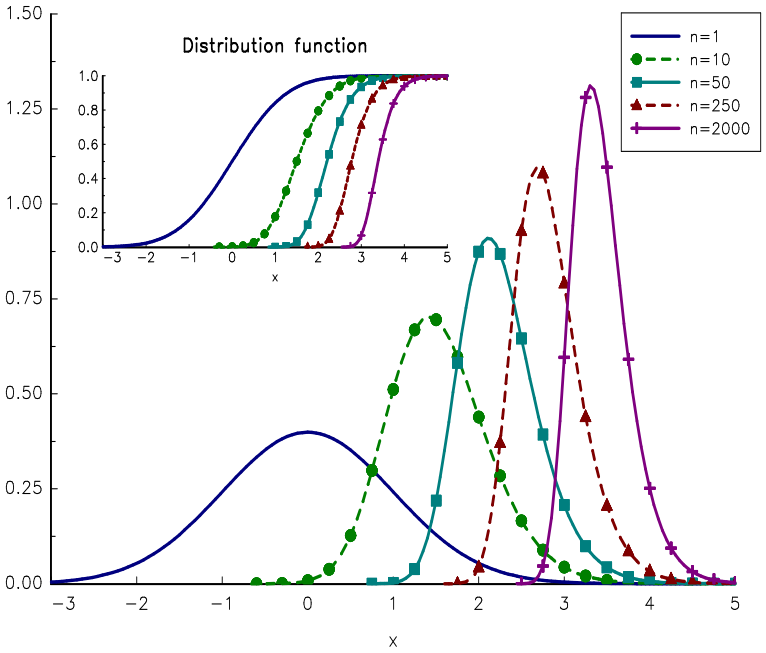

FIGURE 12.2: Density function $f_{n:n}$ of the Gaussian random variable $\mathcal{N}(0,1)$

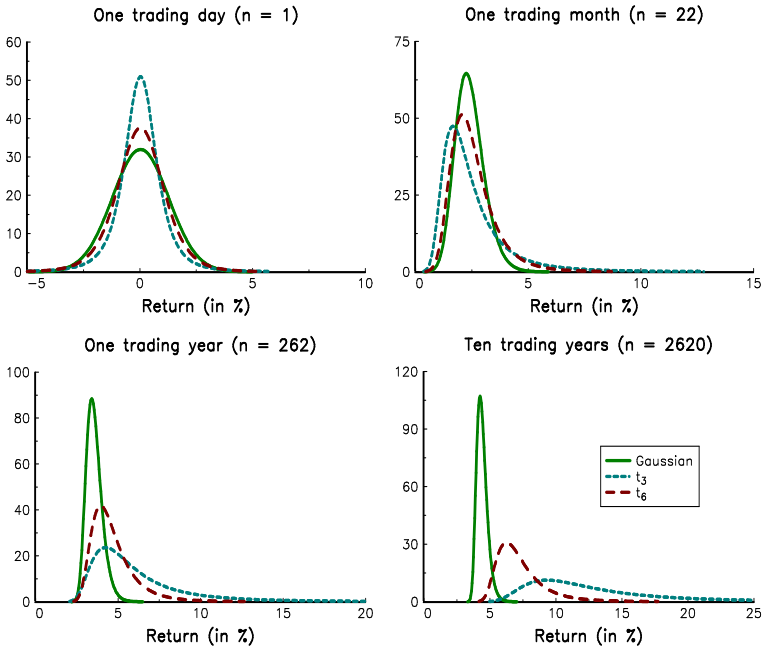

FIGURE 12.3: Density function of the maximum order statistic (daily return of the MSCI USA index, 1995-2015)

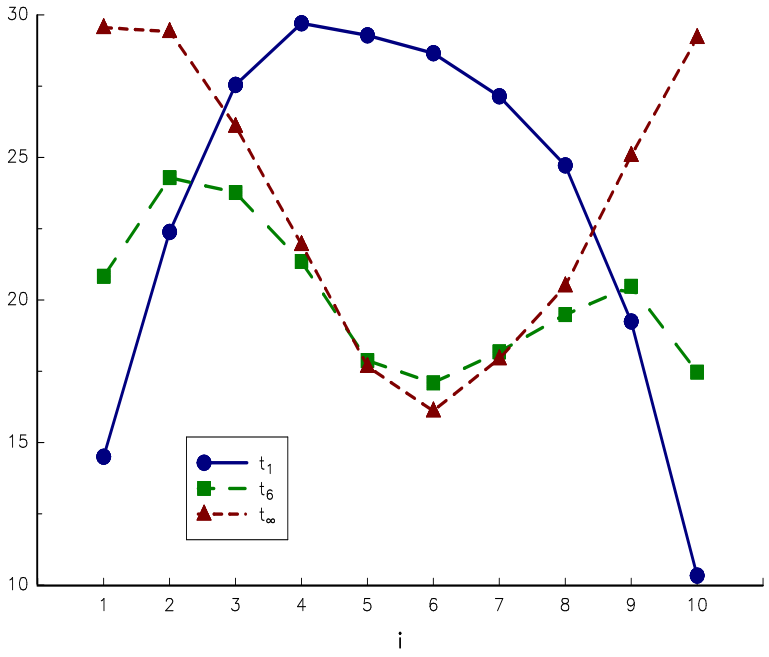

FIGURE 12.4: Annualized volatility (in %) calculated from the order statistics $R_{i:10}$

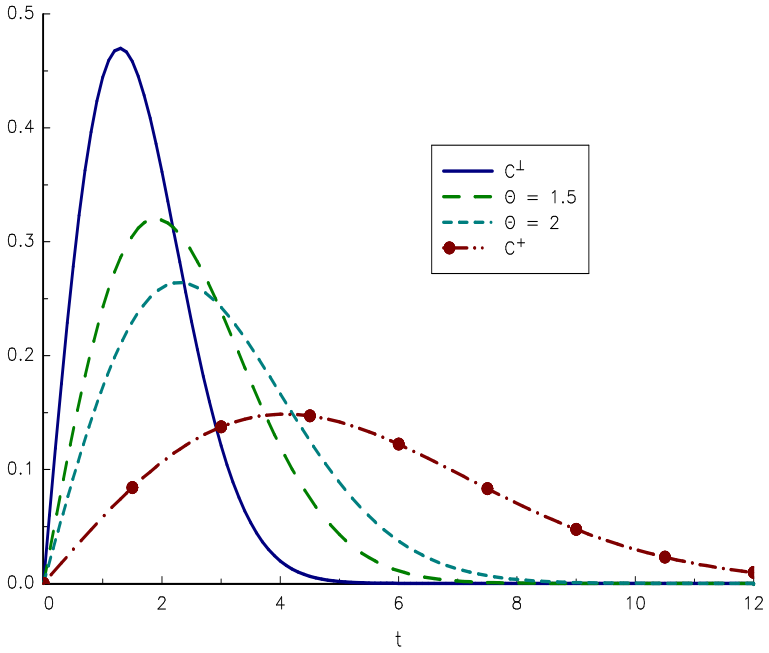

FIGURE 12.5: Density function of the first-to-default time $\boldsymbol{\tau}_{1:10}$

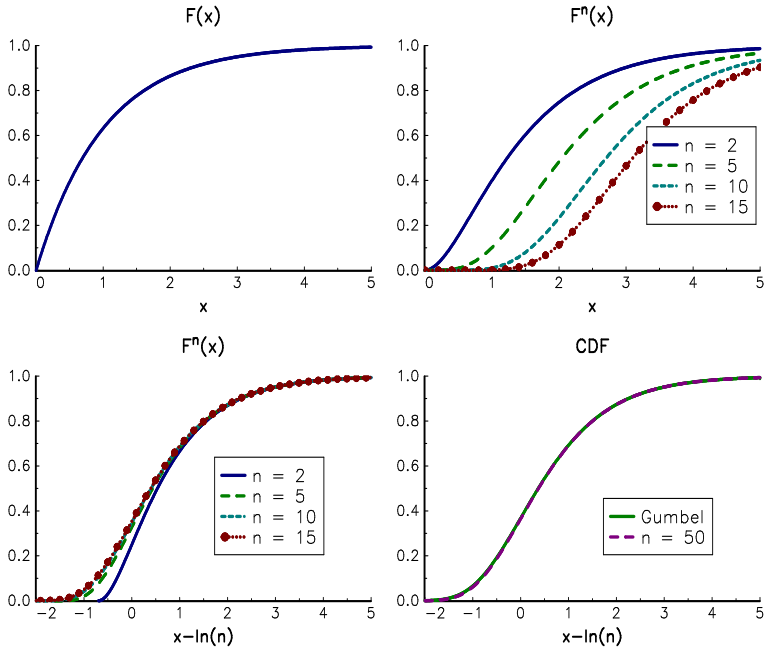

FIGURE 12.6: Max-convergence of the exponential distribution $\mathcal{E}(1)$ to the Gumbel distribution

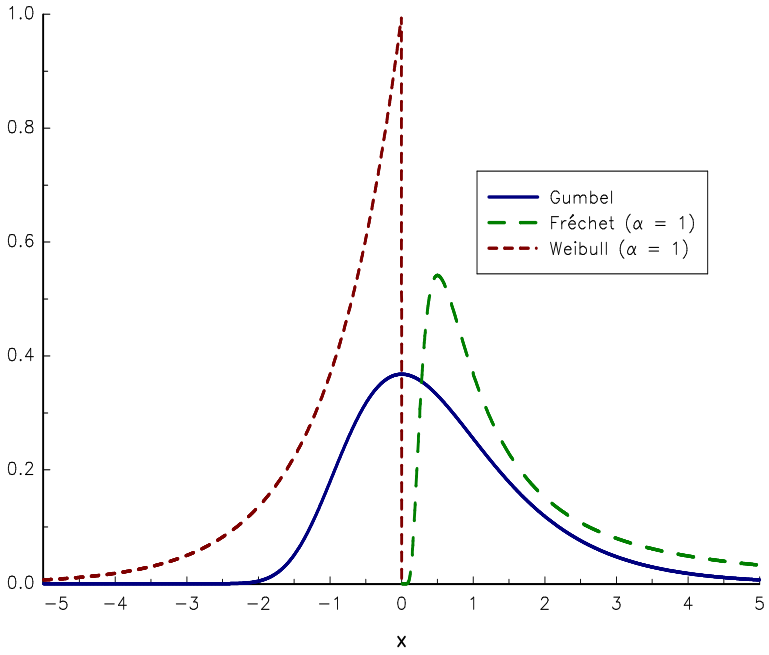

FIGURE 12.7: Density function of $\mathbf{\Lambda}$, $\mathbf{\Phi}_1$ and $\mathbf{\Psi}_1$

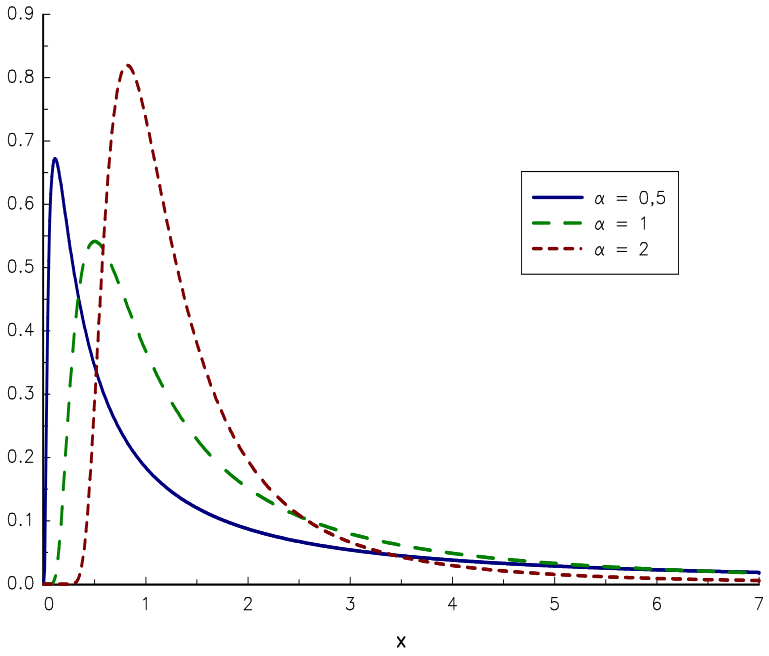

FIGURE 12.8: Density function of the Fréchet probability distribution

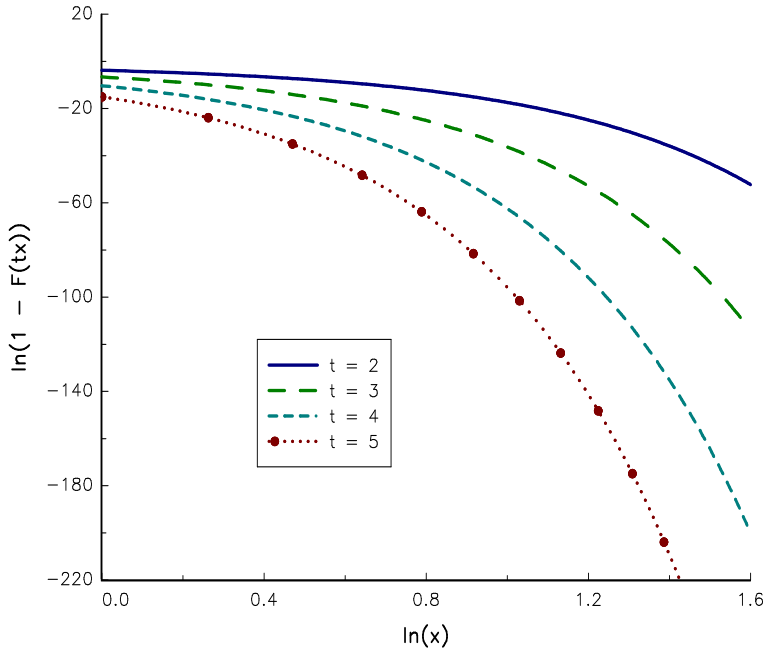

FIGURE 12.9: Graphical validation of the regular variation property for the normal distribution $\mathcal{N}(0,1)$

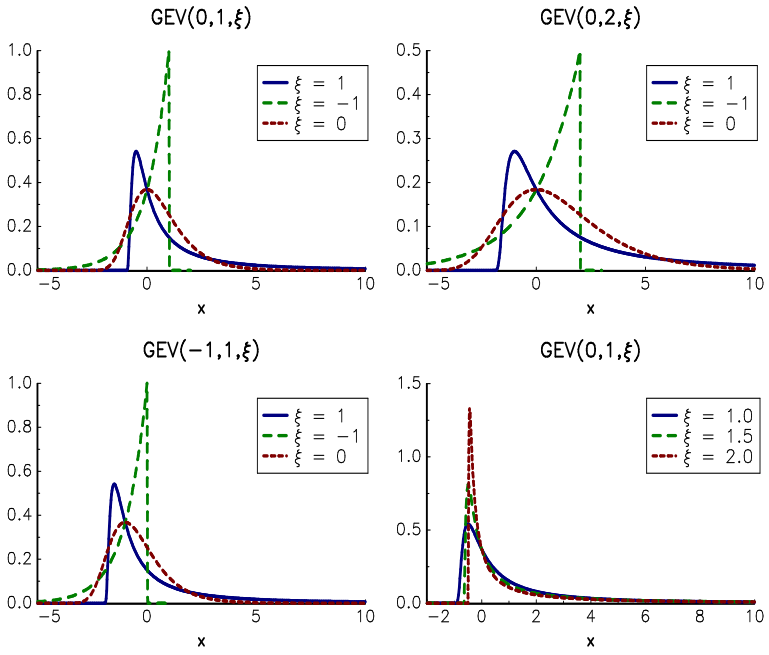

FIGURE 12.10: Probability density function of the GEV distribution

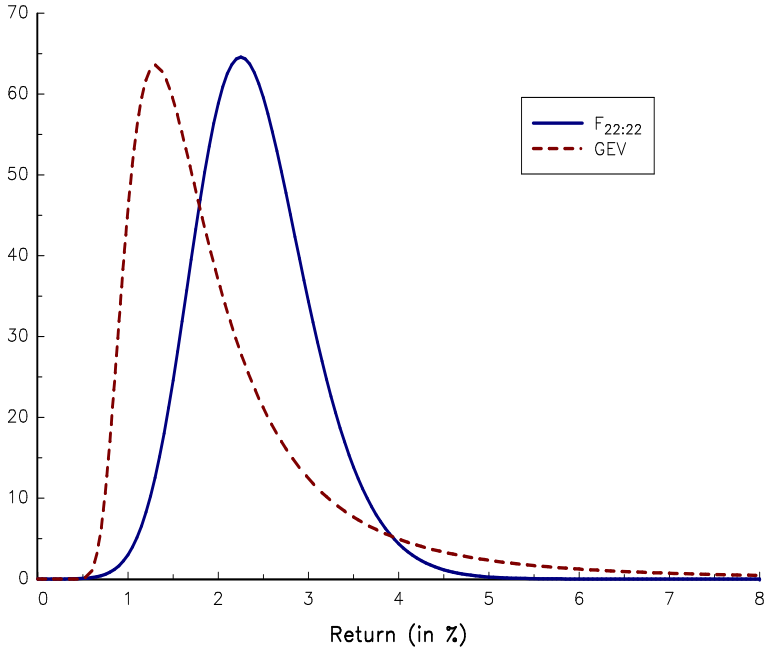

FIGURE 12.11: Probability density function of the maximum return $R_{22:22}$

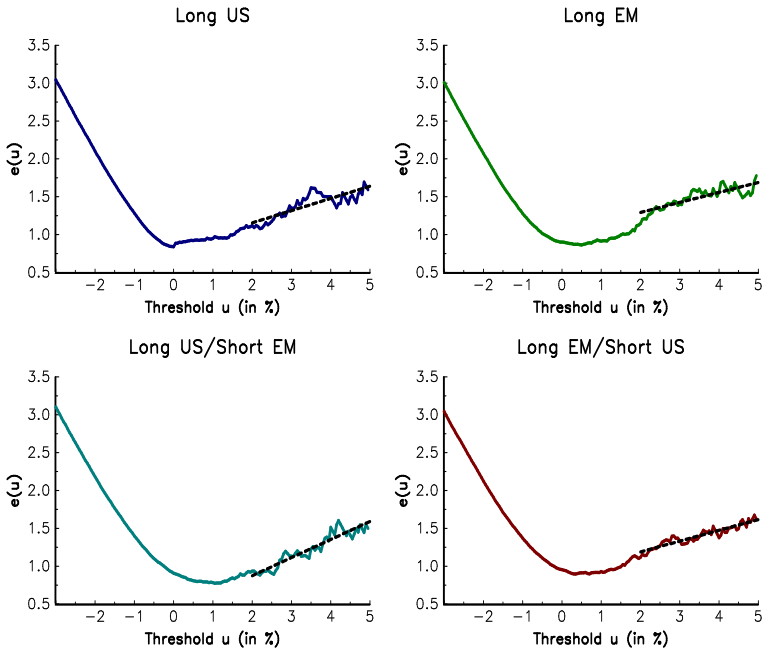

FIGURE 12.12: Mean residual life plot

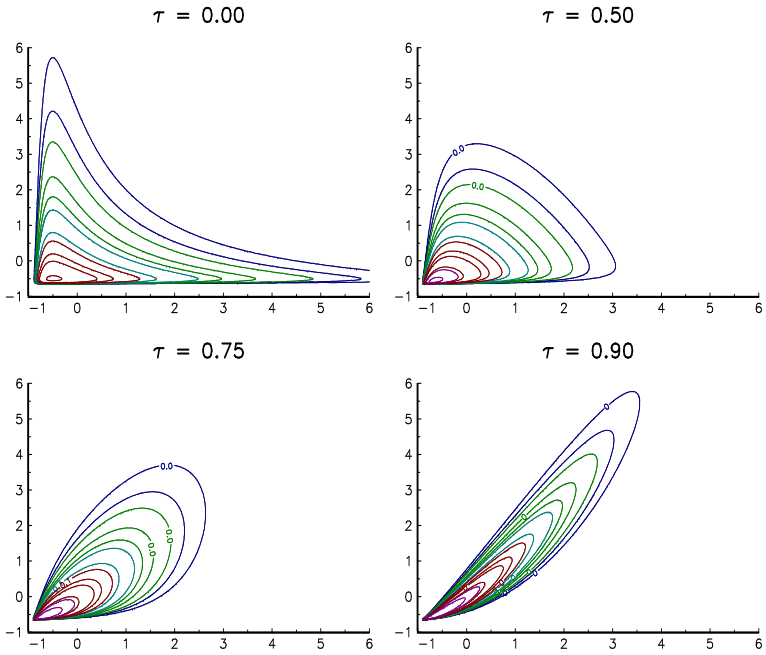

FIGURE 12.13: Multivariate extreme value distributions

Chapter 13

Monte Carlo Simulation Methods

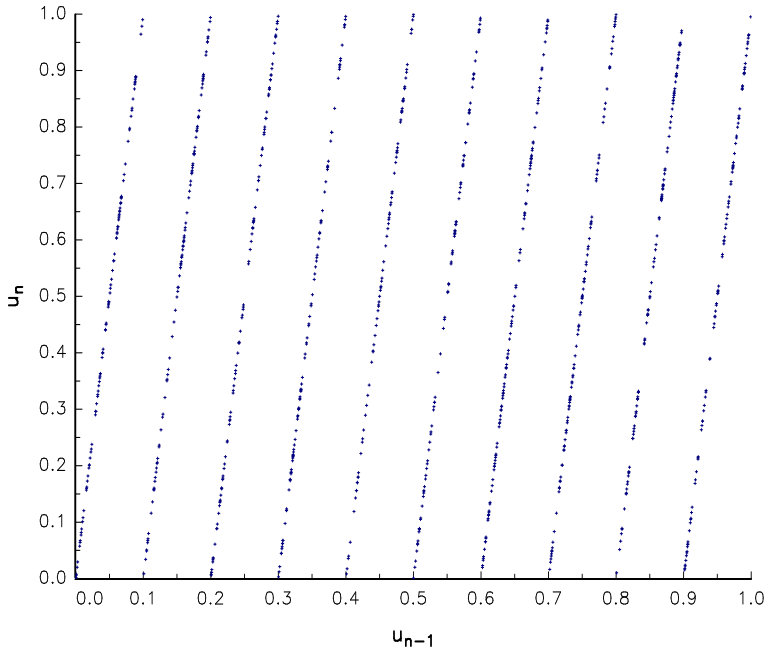

FIGURE 13.1: Lattice structure of the linear congruential generator

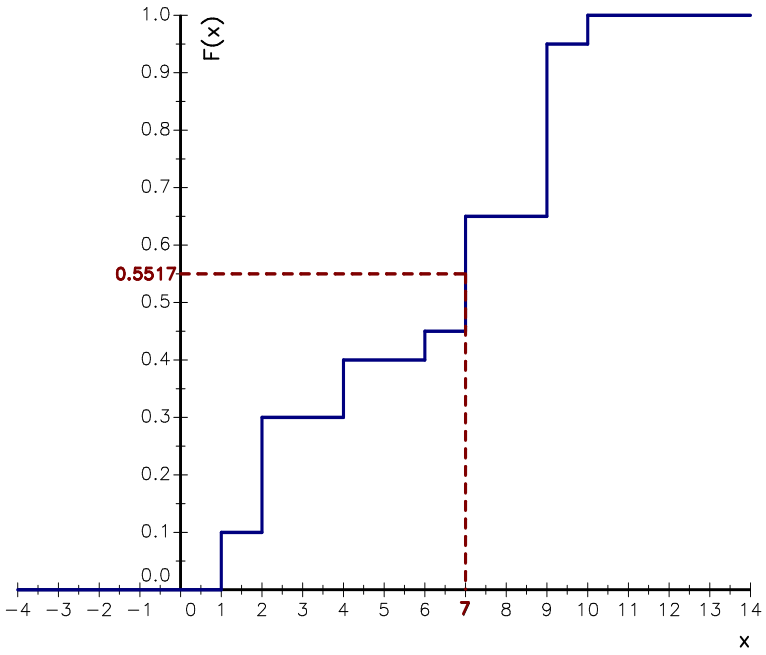

FIGURE 13.2: Inversion method when X is a discrete random variable

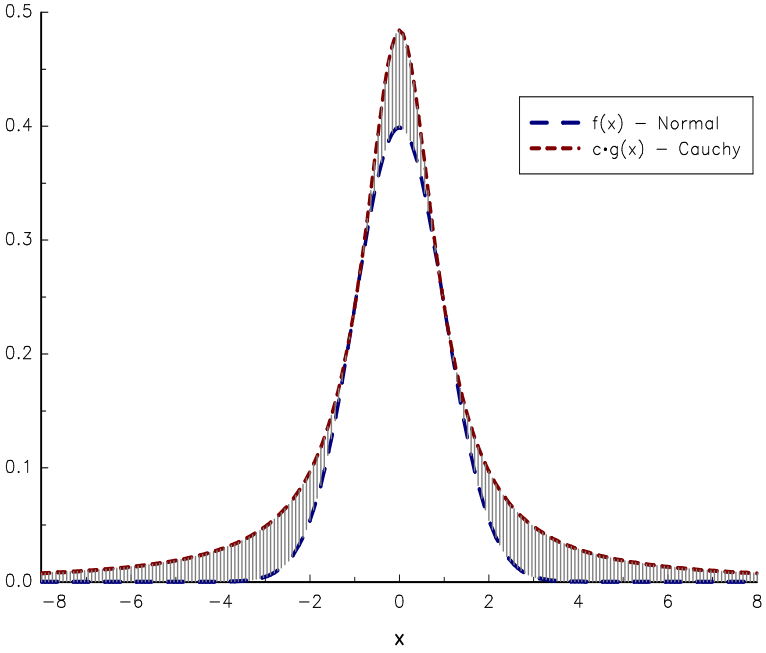

FIGURE 13.3: Rejection sampling applied to the normal distribution

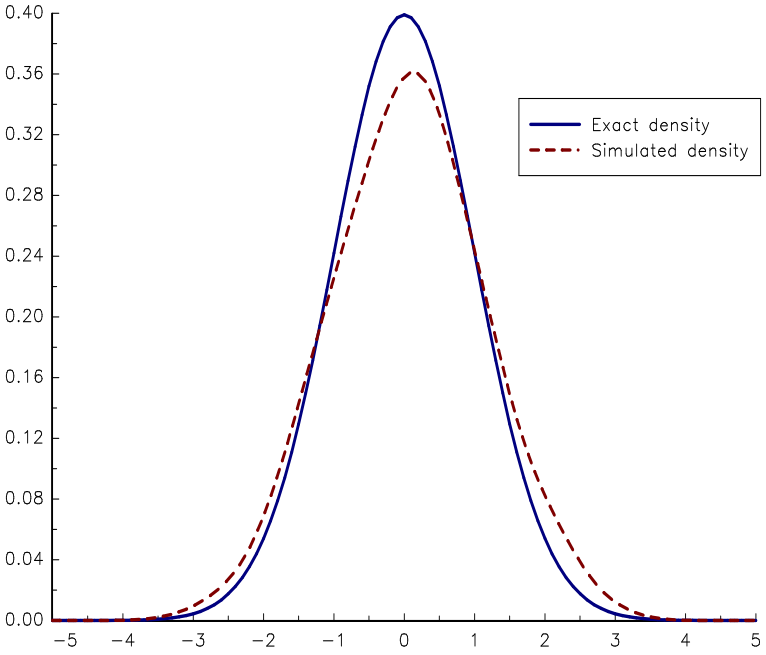

FIGURE 13.4: Comparison of the exact and simulated densities

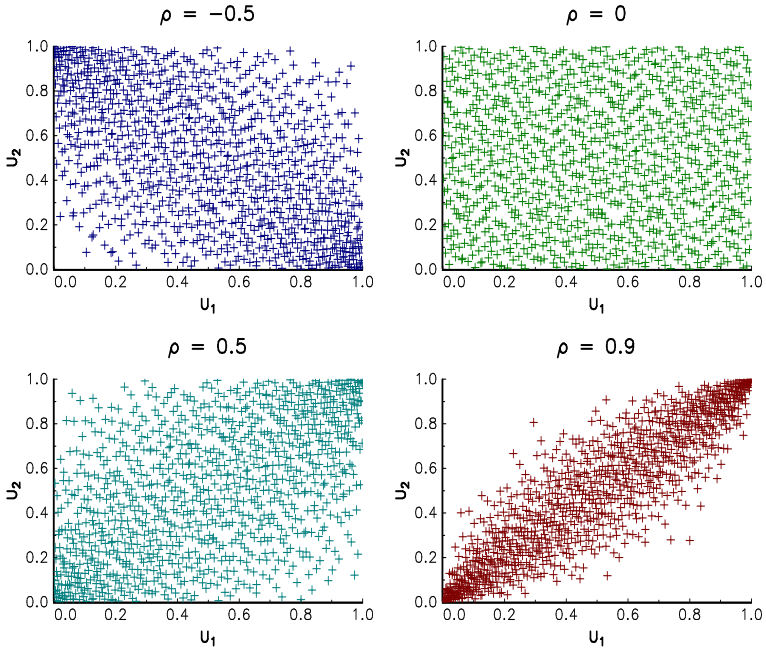

FIGURE 13.5: Simulation of the Normal copula

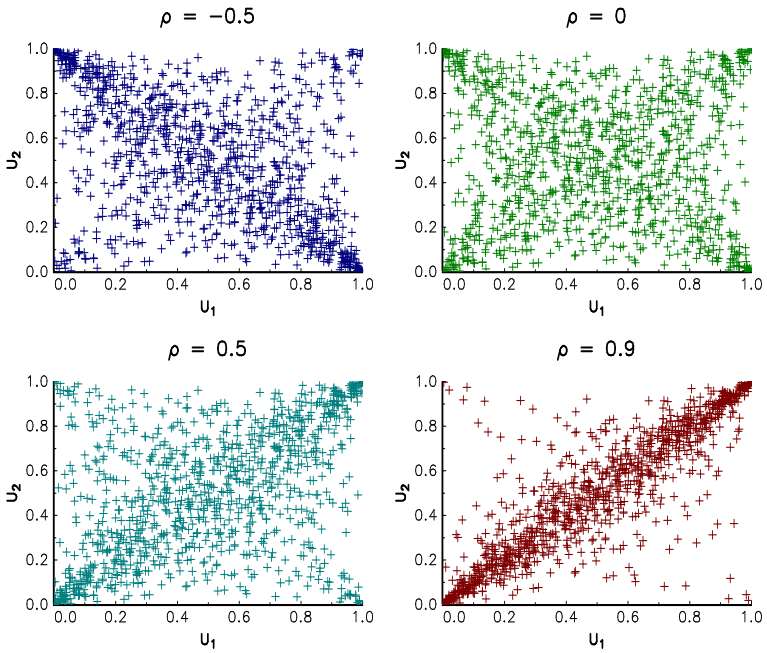

FIGURE 13.6: Simulation of the t_1 copula

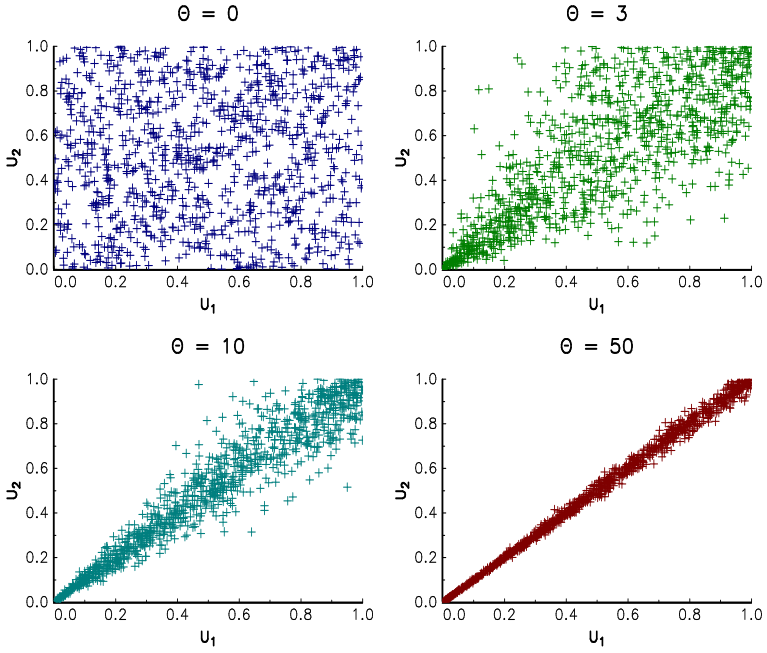

FIGURE 13.7: Simulation of the Clayton copula

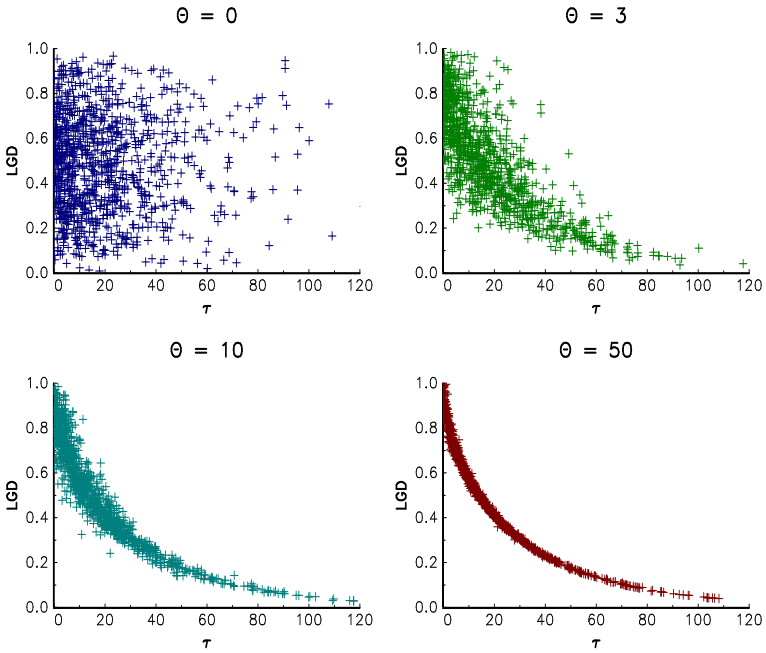

FIGURE 13.8: Simulation of the correlated random vector $(\boldsymbol{\tau}, \text{LGD})$

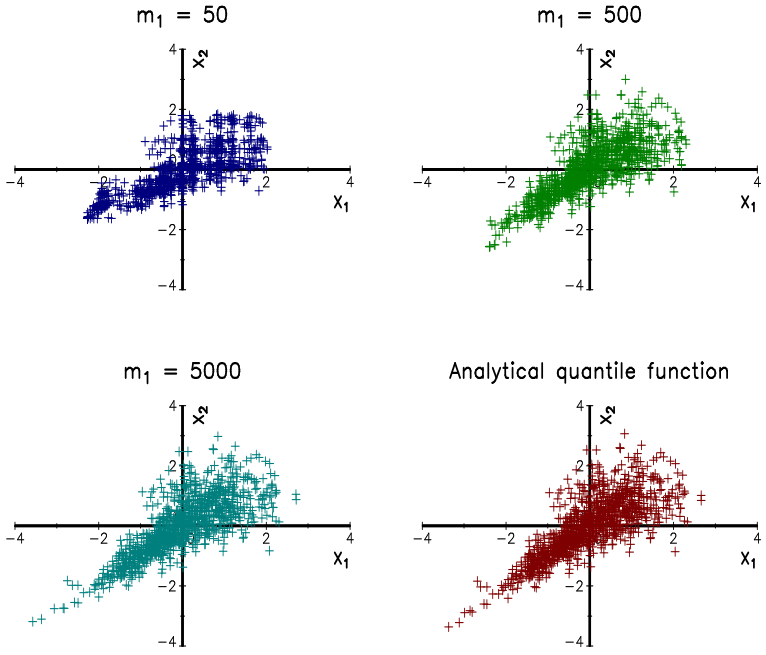

FIGURE 13.9: Convergence of the method of the empirical quantile function

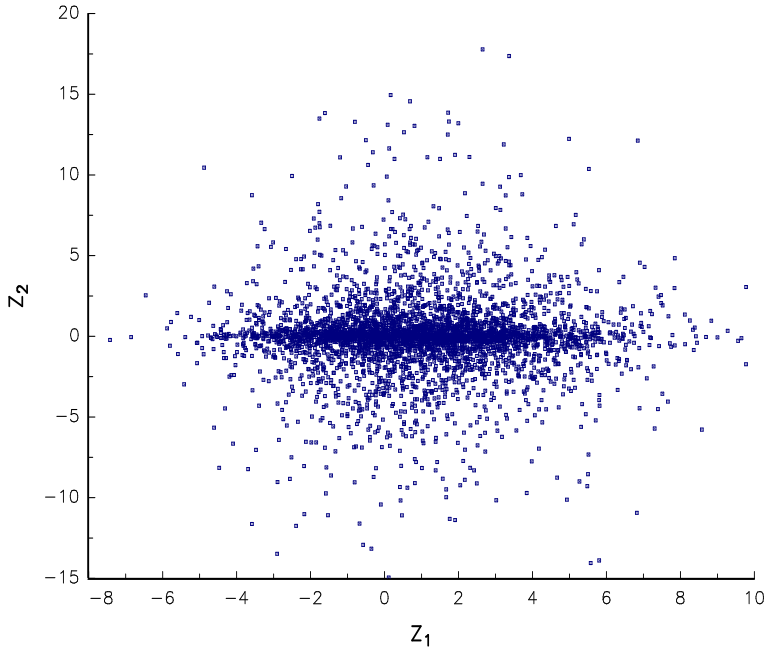

FIGURE 13.10: Simulation of the random variables Z_1 and Z_2

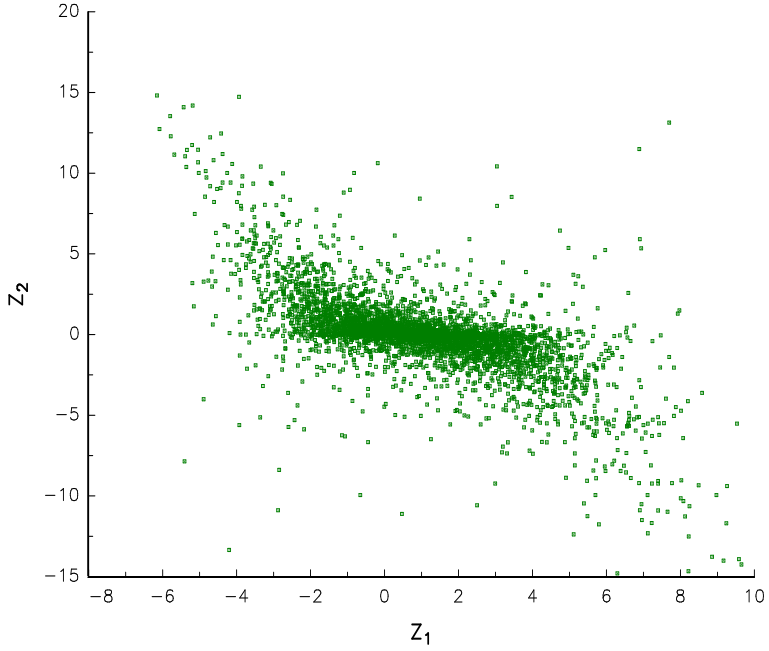

FIGURE 13.11: Simulation of the random vector (Z_1, Z_2)

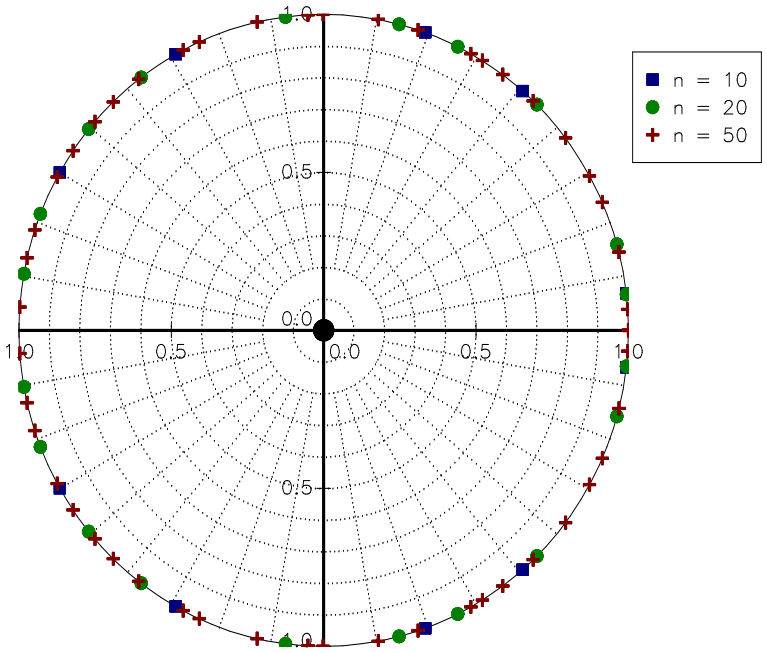

FIGURE 13.12: Distribution of the eigenvalues of simulated random orthogonal matrices

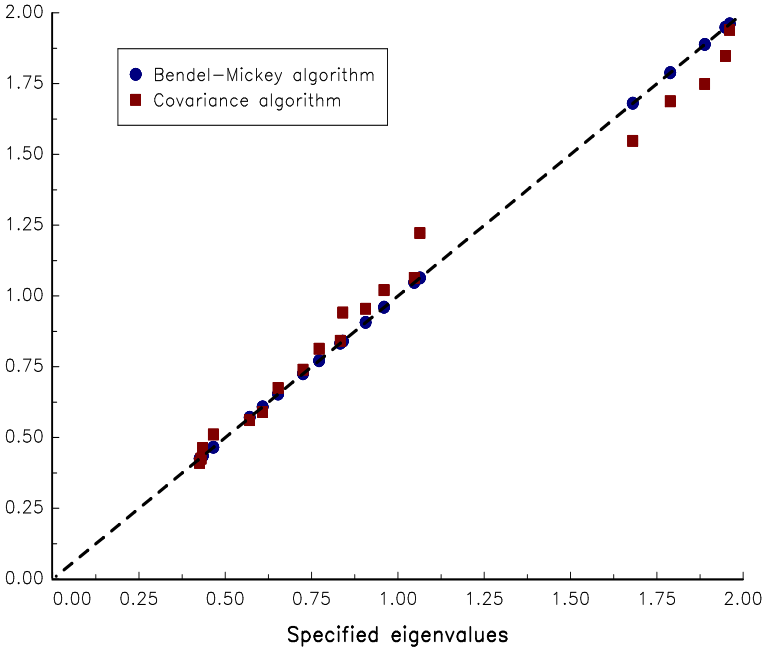

FIGURE 13.13: Comparison of the Bendel-Mickey and covariance algorithms

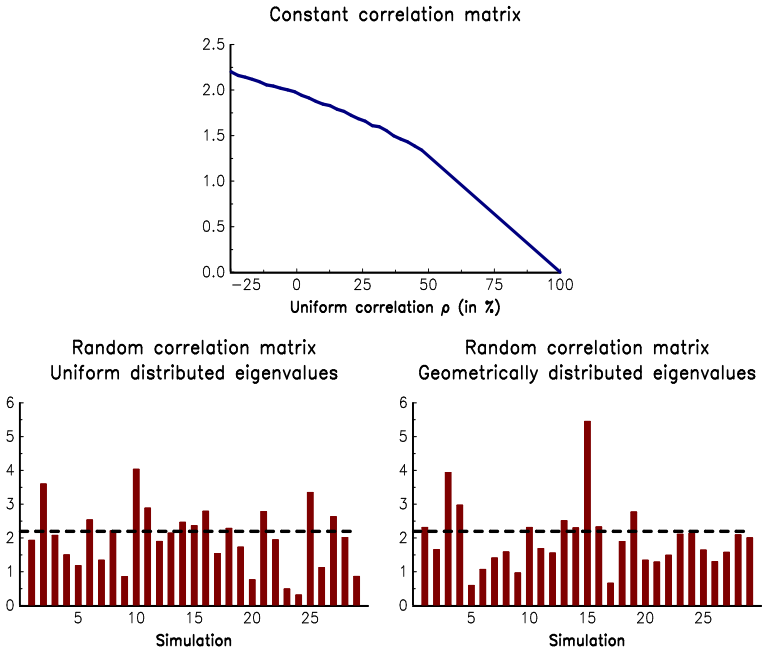

FIGURE 13.14: Price of the basket option

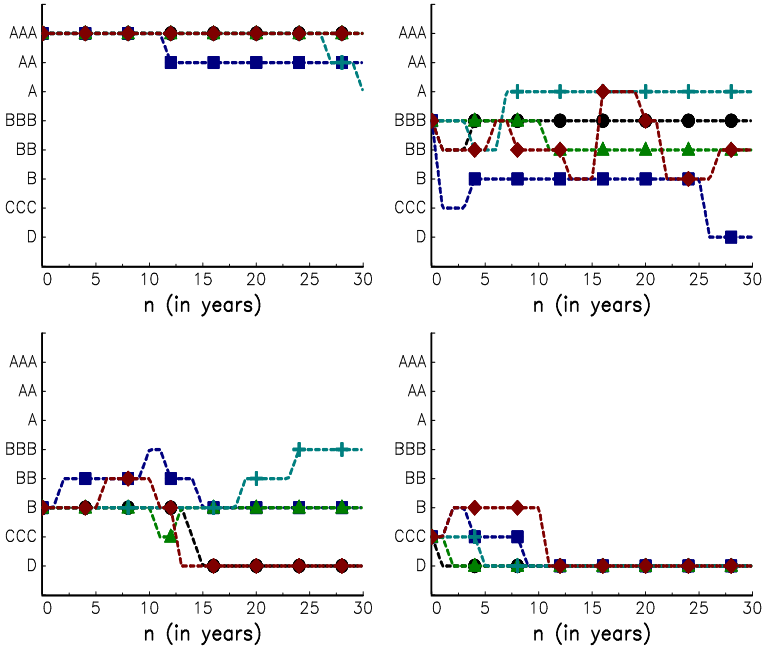

FIGURE 13.15: Simulation of rating dynamics (correlation matrix ρ_1)

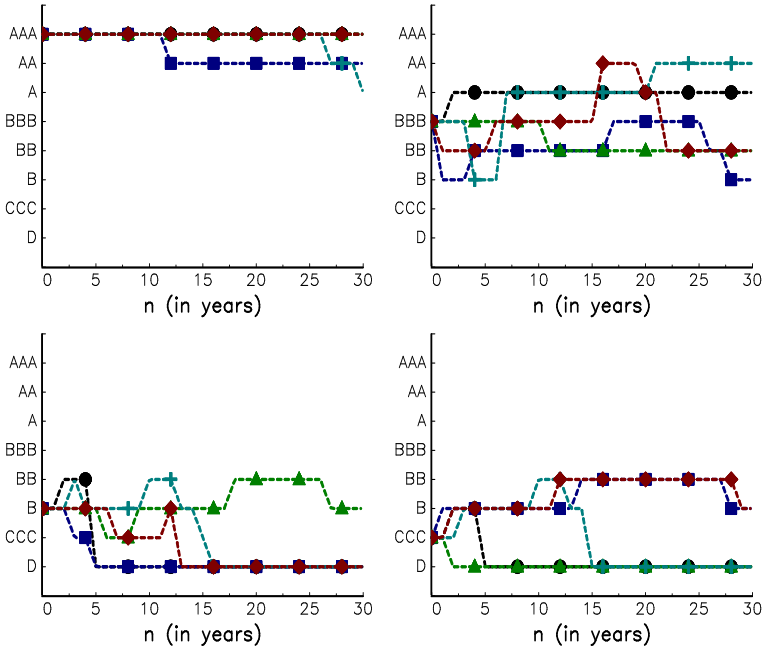

FIGURE 13.16: Simulation of rating dynamics (correlation matrix ρ_2)

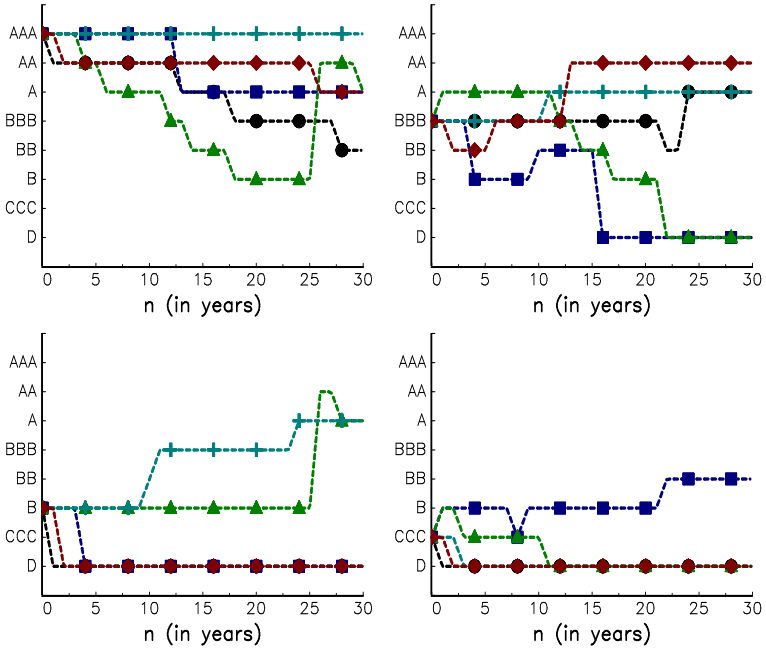

FIGURE 13.17: Simulation of rating dynamics (correlation matrix ρ_1)

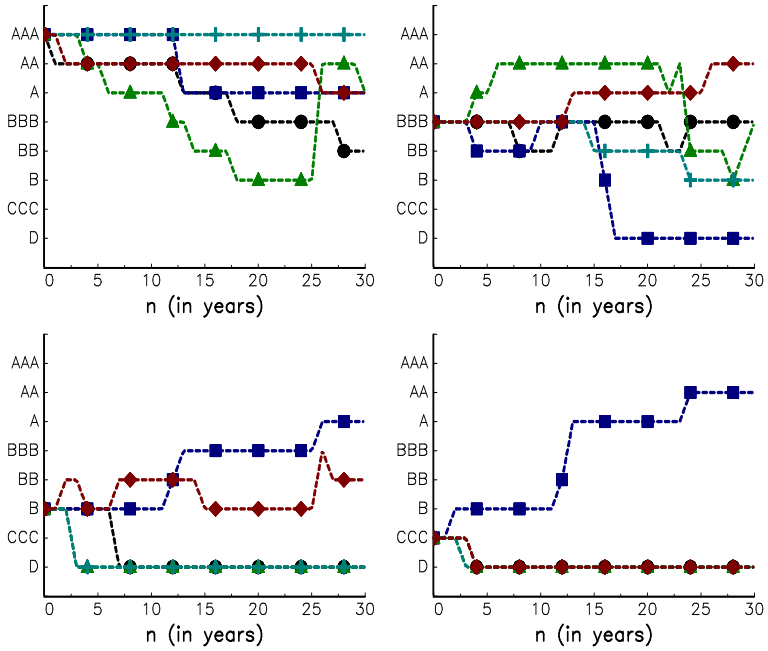

FIGURE 13.18: Simulation of rating dynamics (correlation matrix ρ_2)

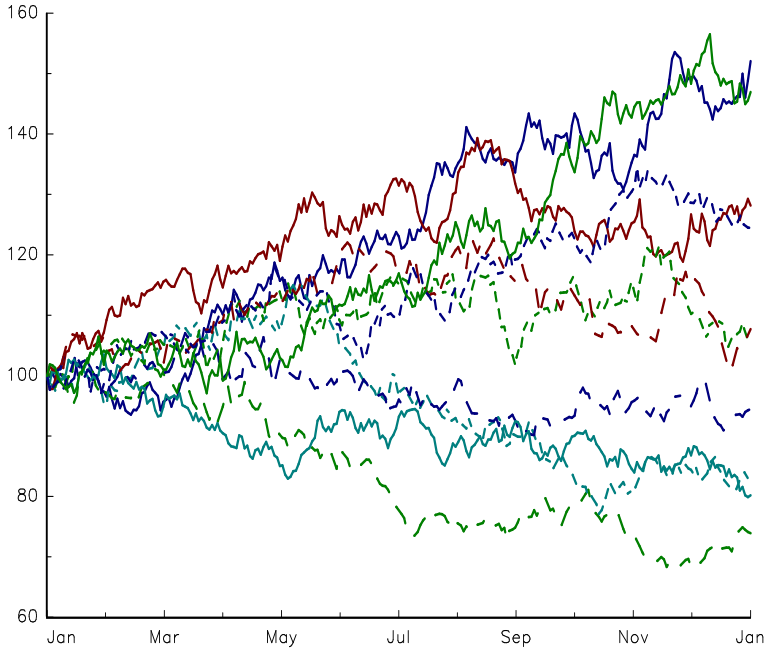

FIGURE 13.19: Simulation of the geometric Brownian motion

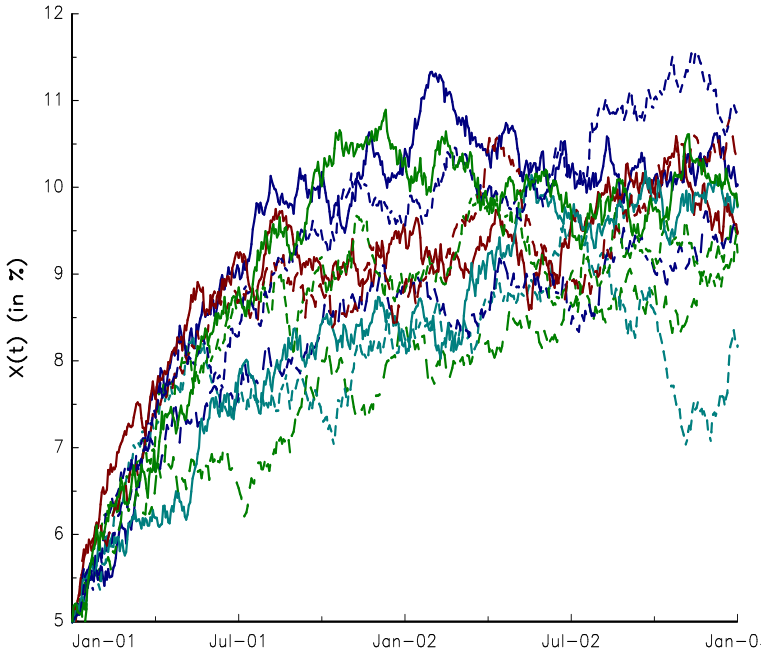

FIGURE 13.20: Simulation of the Ornstein-Uhlenbeck process

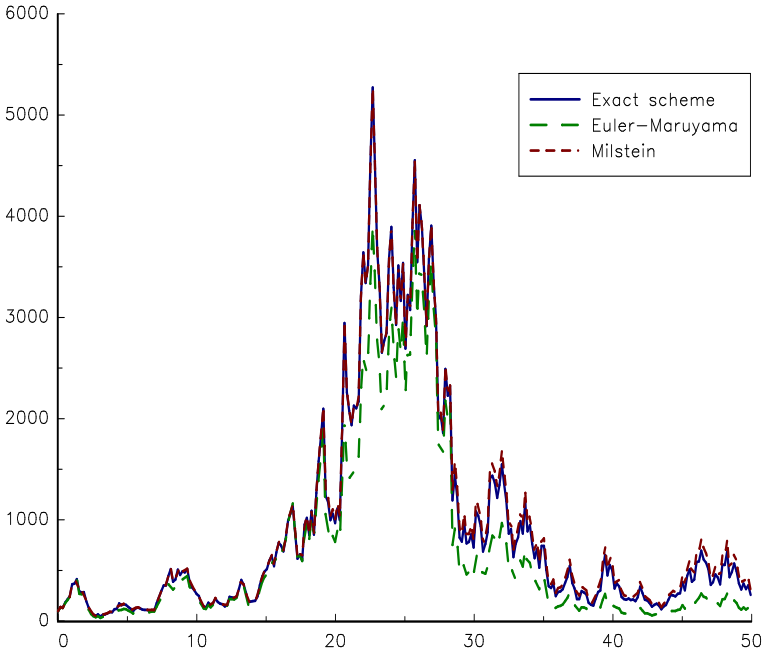

FIGURE 13.21: Comparison of exact, Euler-Maruyama and Milstein schemes (monthly discretization)

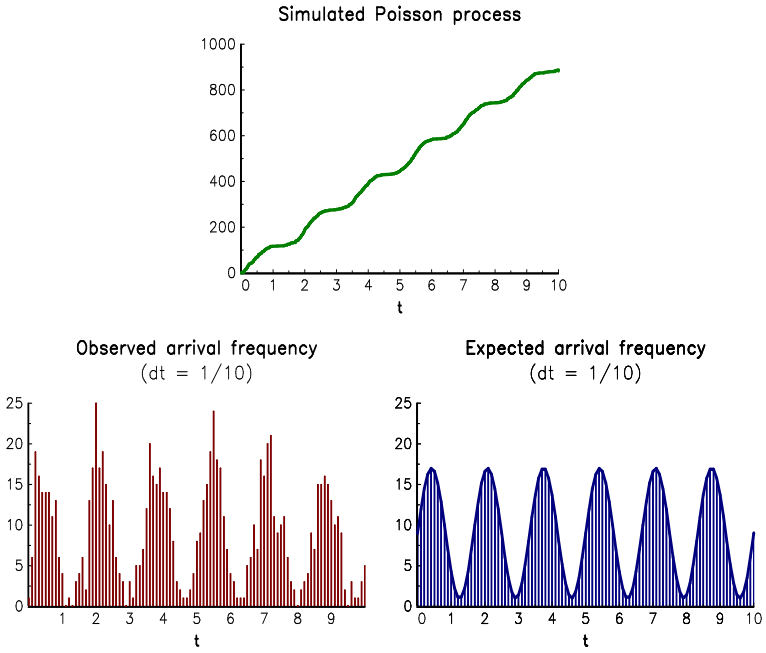

FIGURE 13.22: Simulation of a non-homogenous Poisson process with cyclical intensity

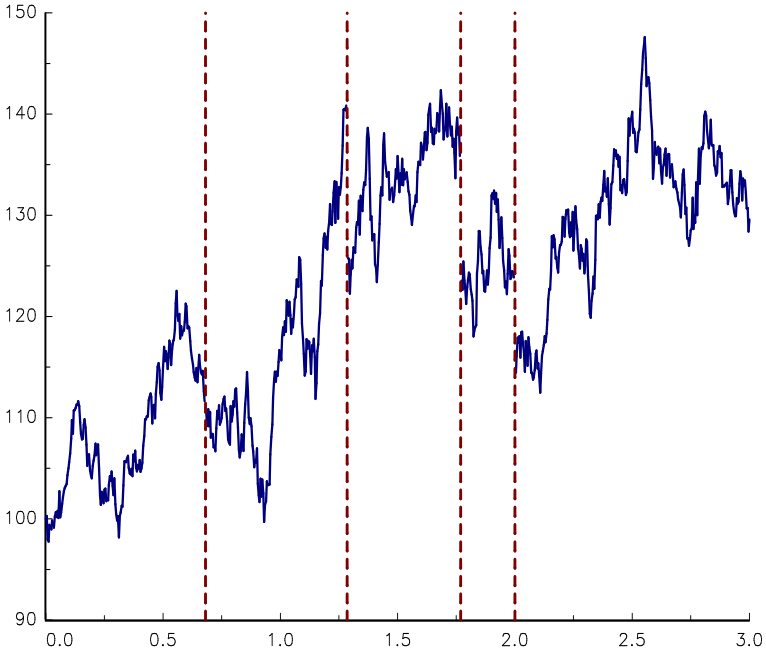

FIGURE 13.23: Simulation of a jump-diffusion process

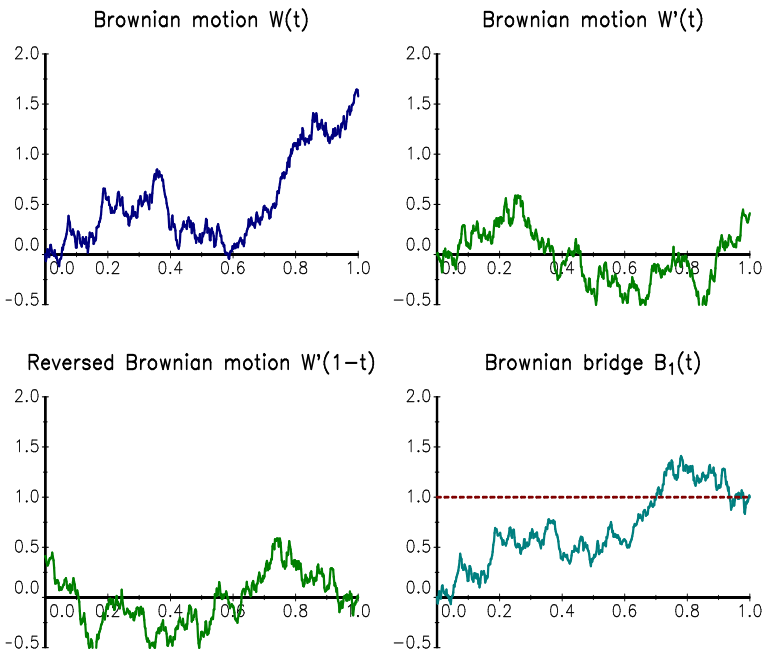

FIGURE 13.24: Simulation of the Brownian bridge $B_1(t)$ using the time reversibility property

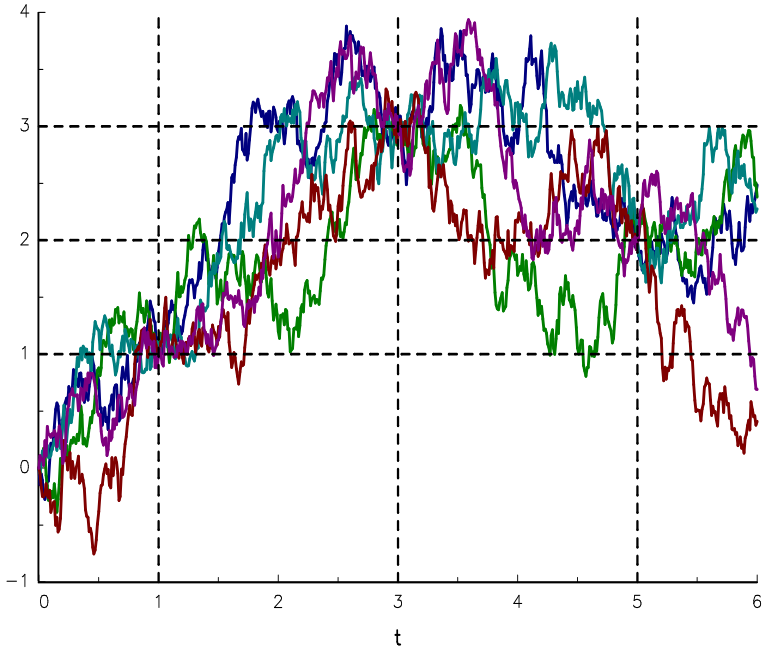

FIGURE 13.25: Simulation of the Brownian bridge $B(t)$

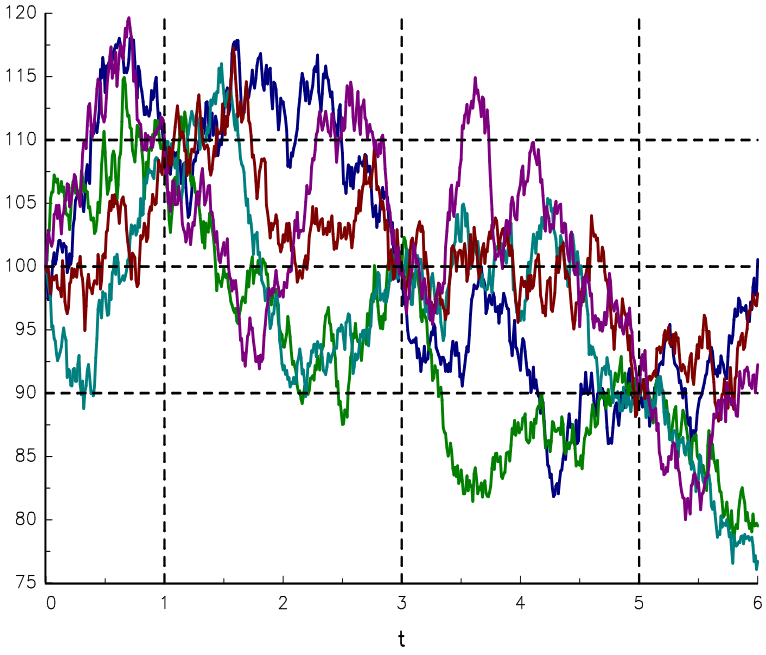

FIGURE 13.26: Simulation of the diffusion bridge $X(t)$

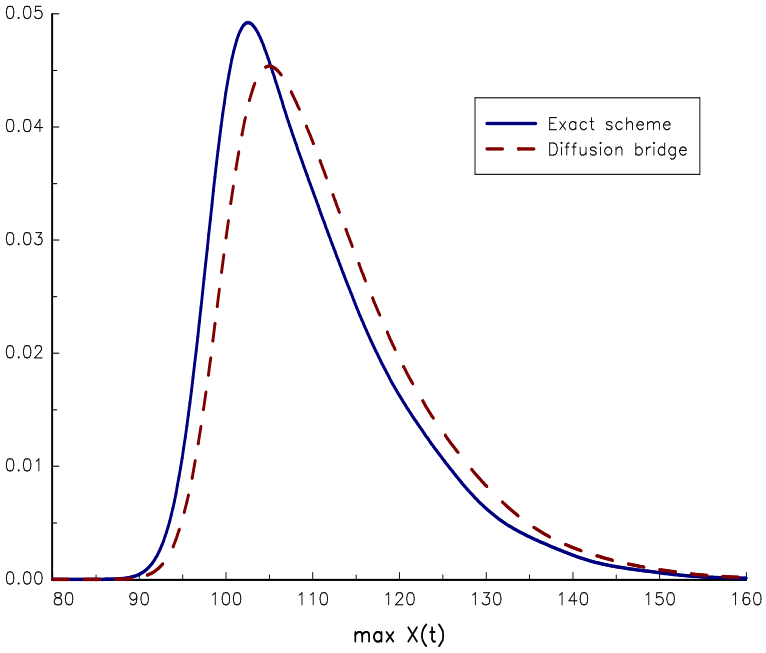

FIGURE 13.27: Density of the maximum estimators $\hat{M}$ and $\tilde{M}$

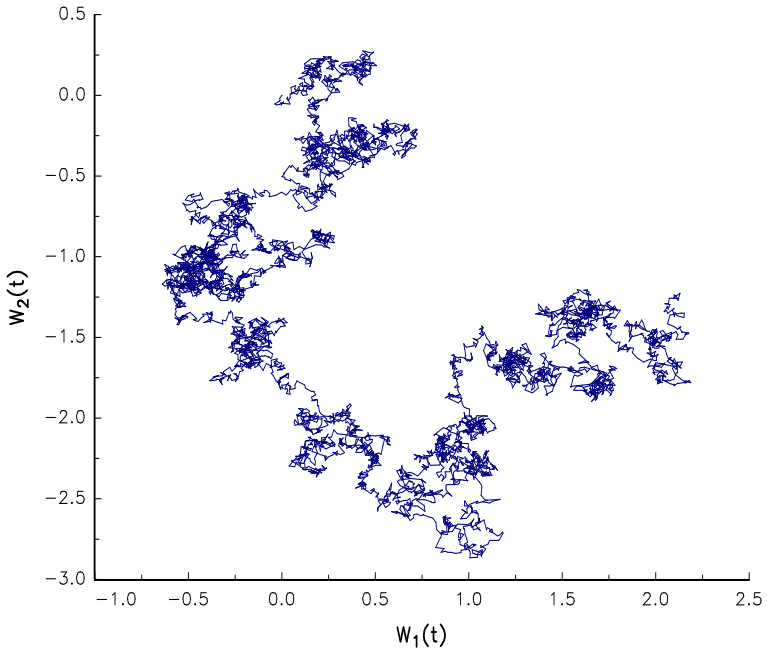

FIGURE 13.28: Brownian motion in the plane (independent case)

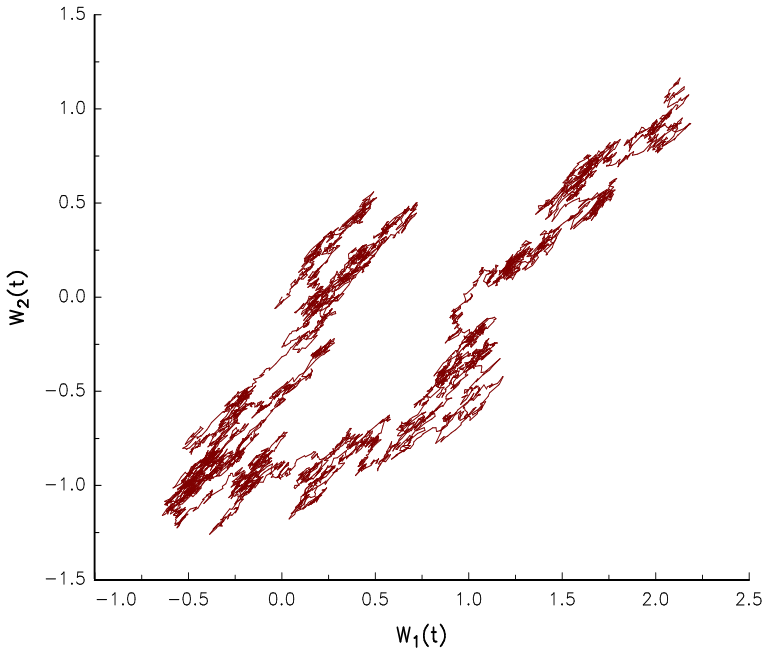

FIGURE 13.29: Brownian motion in the plane ($\rho_{1,2} = 85\%$)

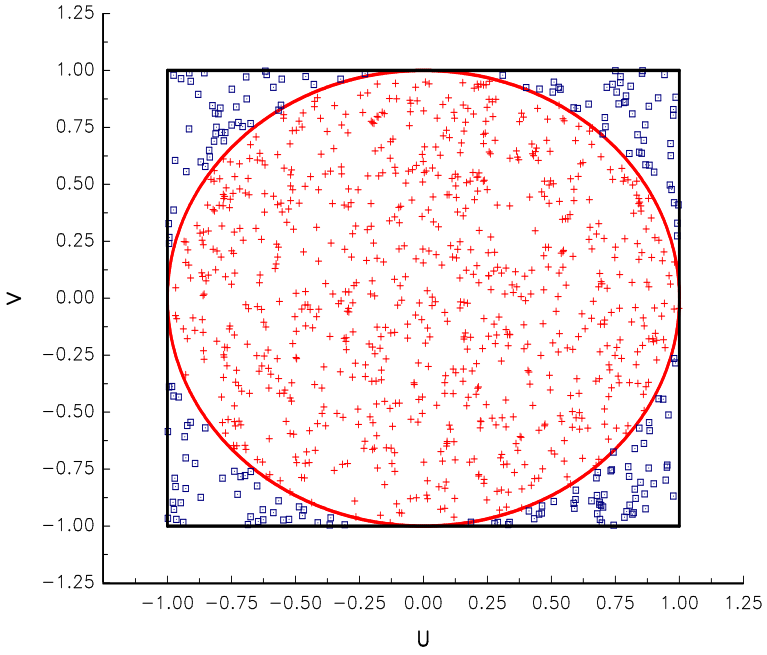

FIGURE 13.30: Computing π with 1 000 simulations

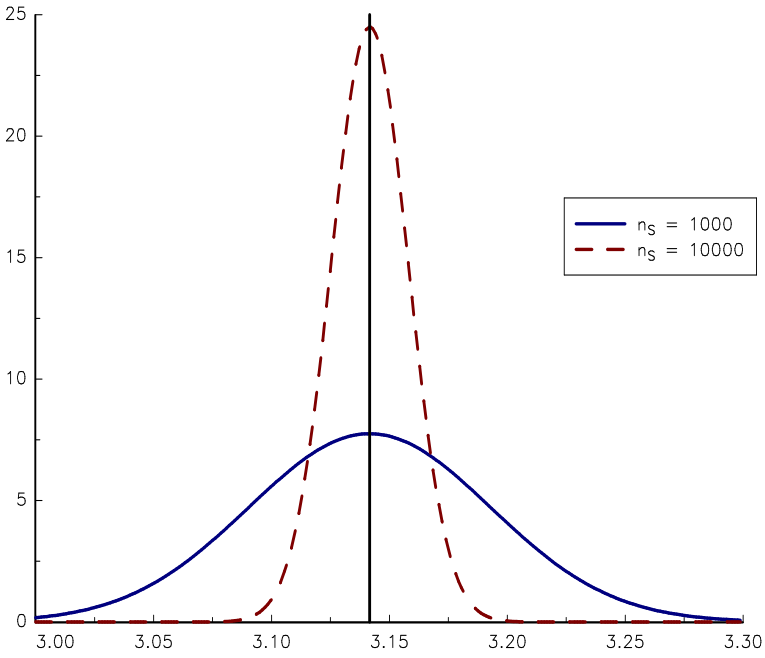

FIGURE 13.31: Density function of $\hat{\pi}_{n_S}$

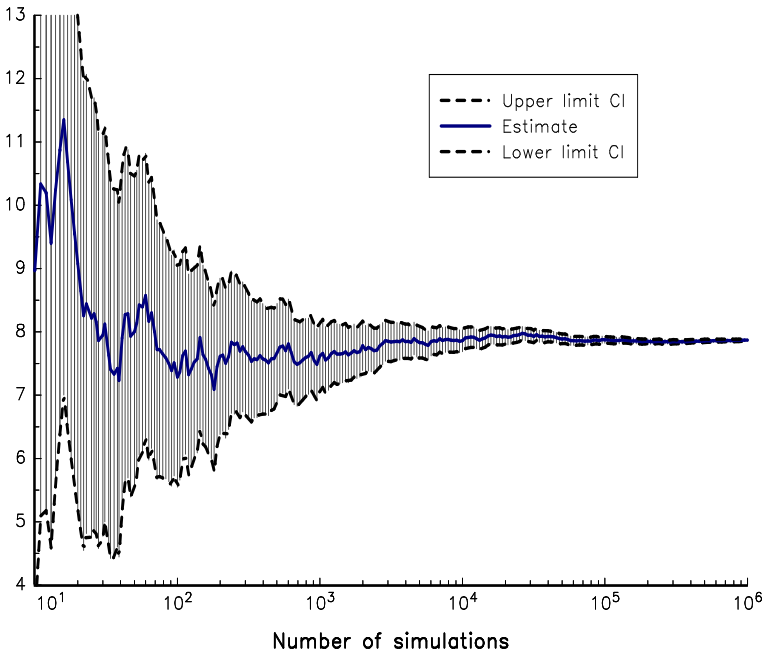

FIGURE 13.32: Convergence of the estimator $\hat{I}_{n_S}$

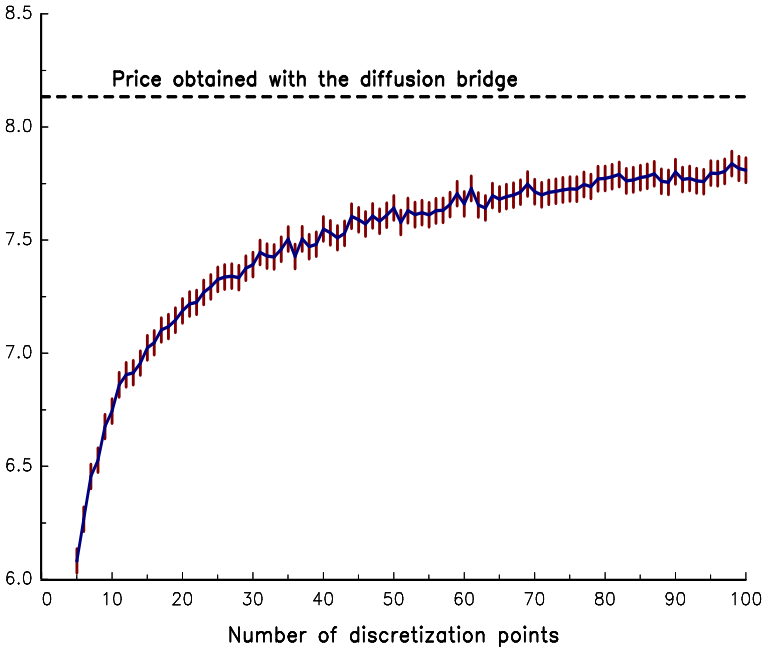

FIGURE 13.33: Computing the look-back option price

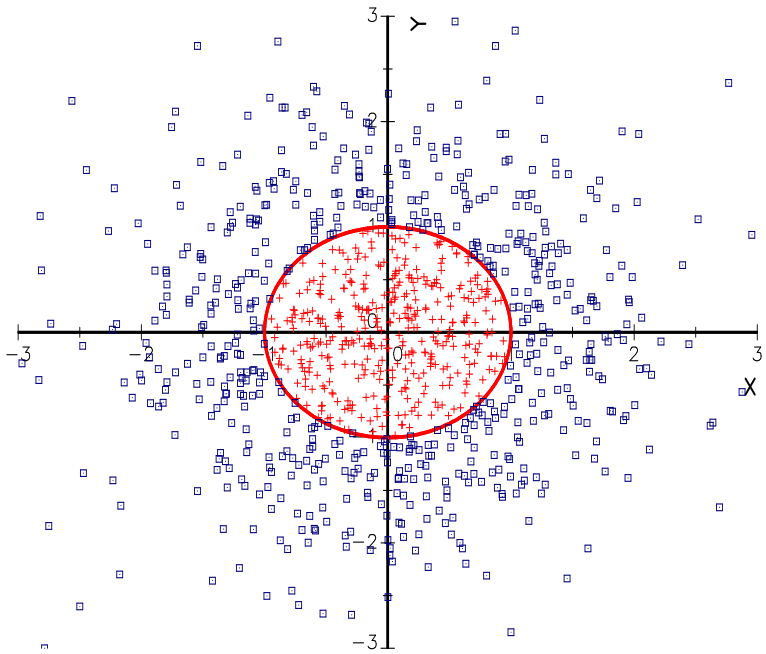

FIGURE 13.34: Computing π with normal random numbers

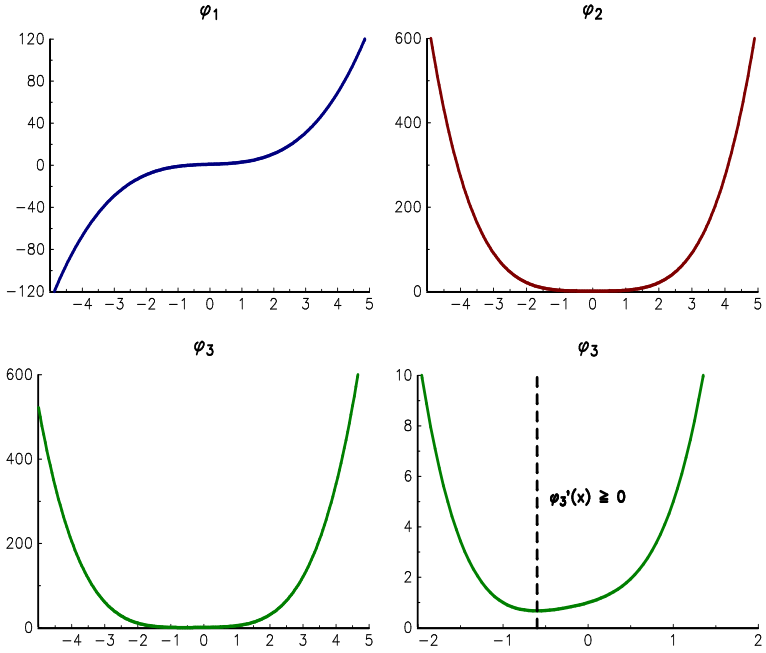

FIGURE 13.35: Functions $\varphi_1(x)$, $\varphi_2(x)$ and $\varphi_3(x)$

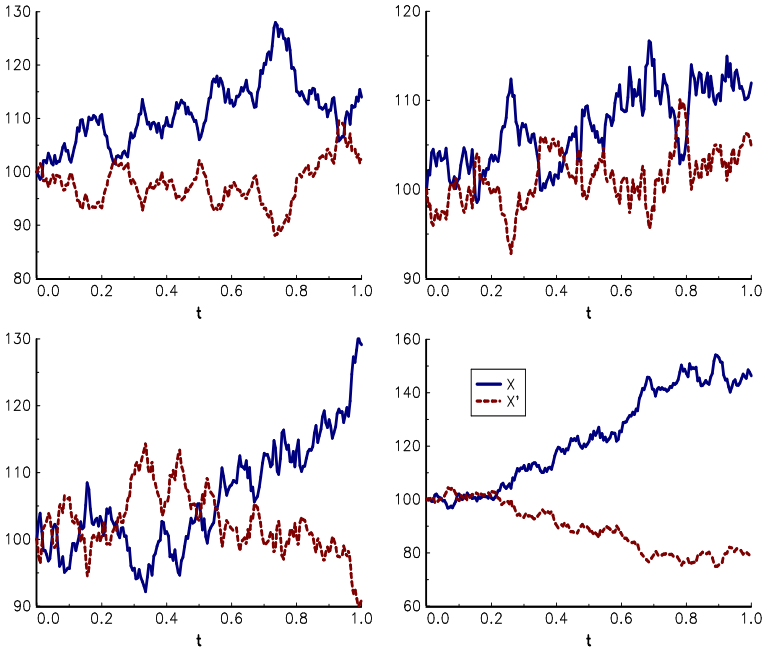

FIGURE 13.36: Antithetic simulation of the GBM process

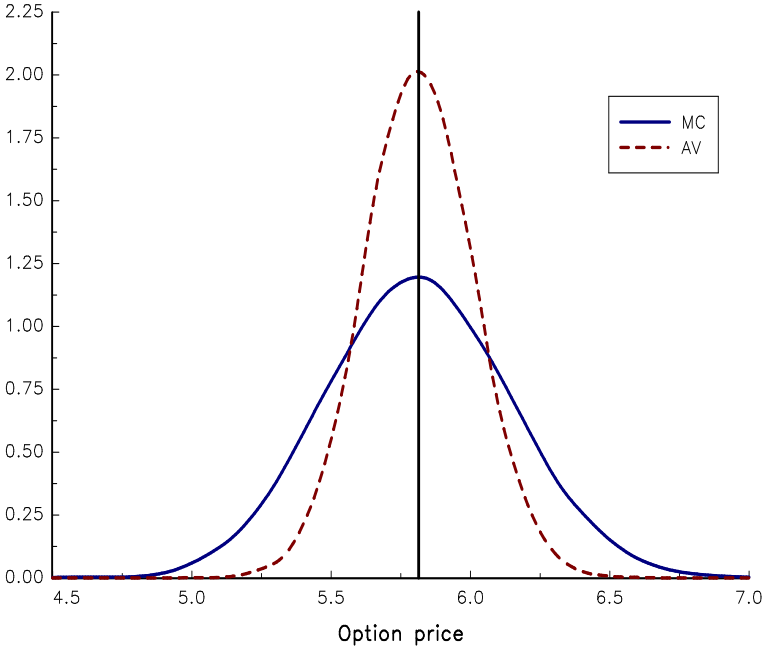

FIGURE 13.37: Probability density function of $\widehat{\mathcal{C}}_{\mathrm{MC}}$ and $\widehat{\mathcal{C}}_{\mathrm{AV}}$ ($n_S = 1\,000$)

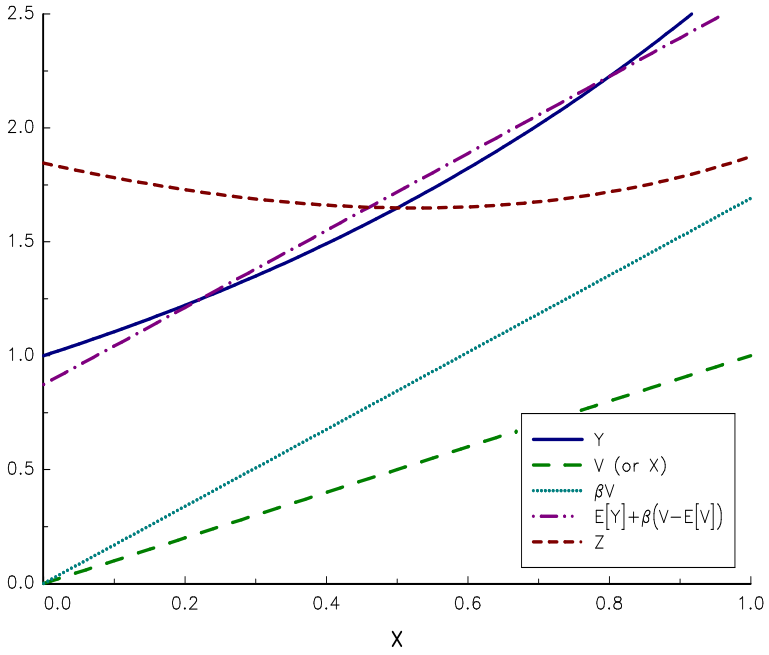

FIGURE 13.38: Understanding the variance reduction in control variates

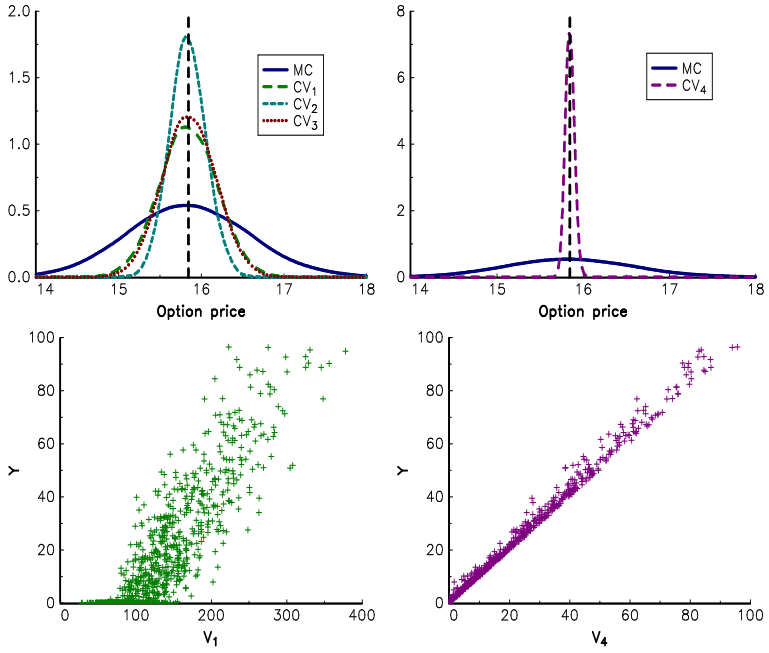

FIGURE 13.39: CV estimator of the arithmetic Asian call option

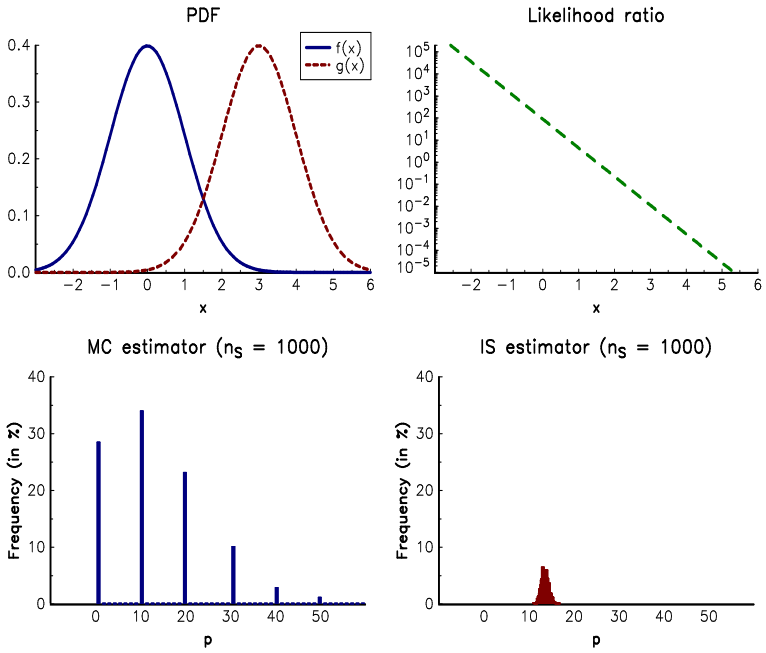

FIGURE 13.40: Histogram of the MC and IS estimators ($n_S = 1\,000$)

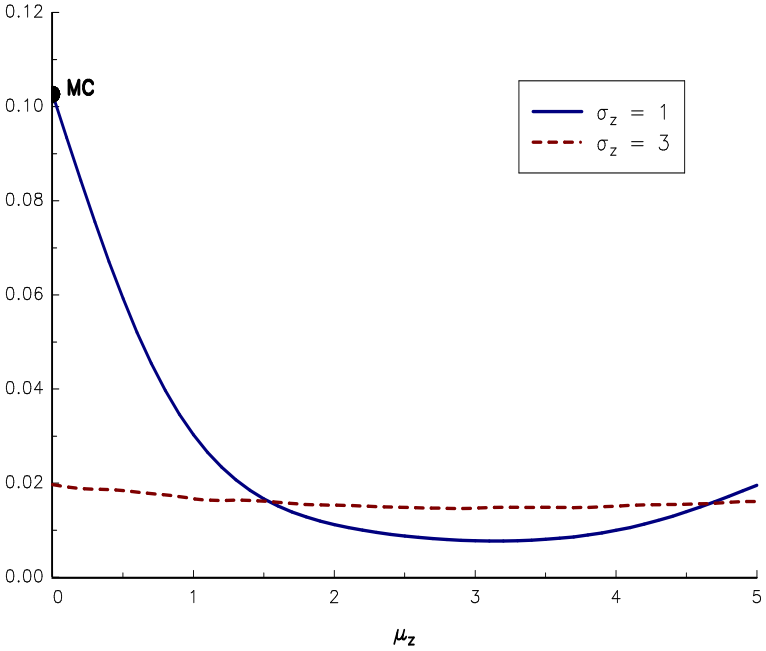

FIGURE 13.41: Standard deviation (in %) of the estimator $\hat{p}_{\text{IS}}$ ($n_S = 1\,000$)

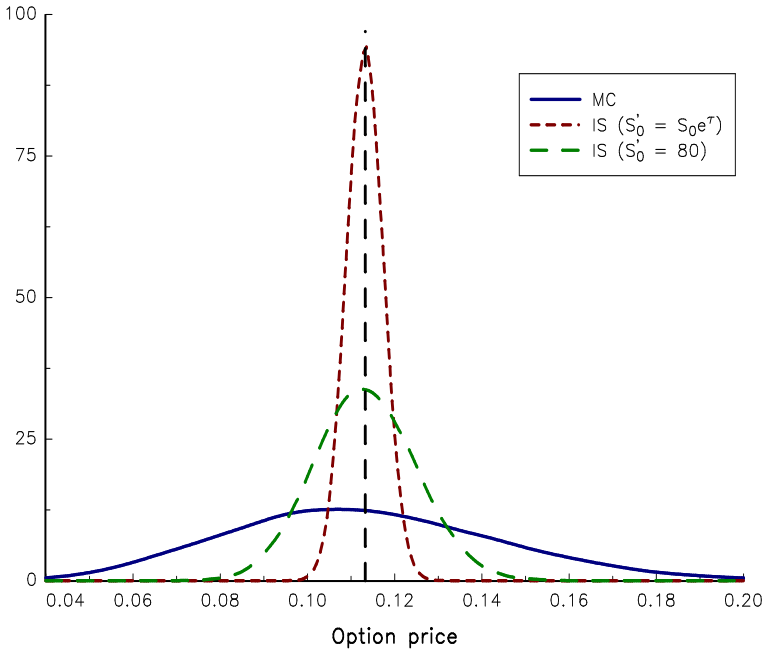

FIGURE 13.42: Density function of the estimators $\hat{\mathcal{P}}_{\text{MC}}$ and $\hat{\mathcal{P}}_{\text{IS}}$ $(n_S = 1\,000)$

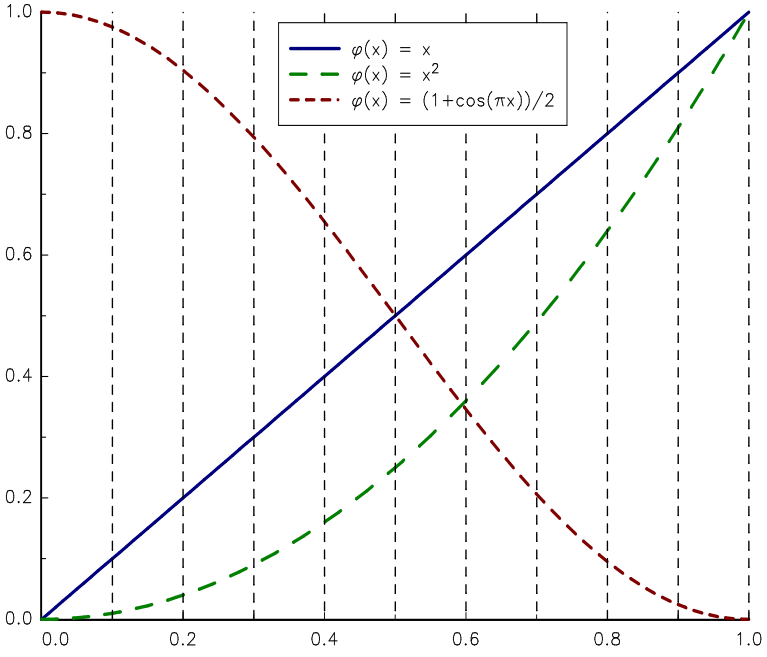

FIGURE 13.43: Function $\psi\,(x)$

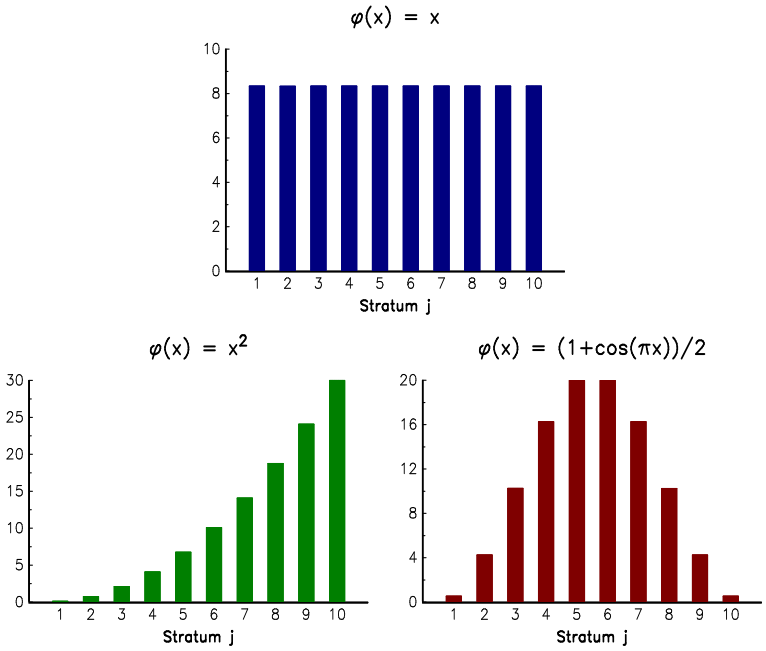

FIGURE 13.44: Intra-strata variance $\sigma^2(j)$ (in bps)

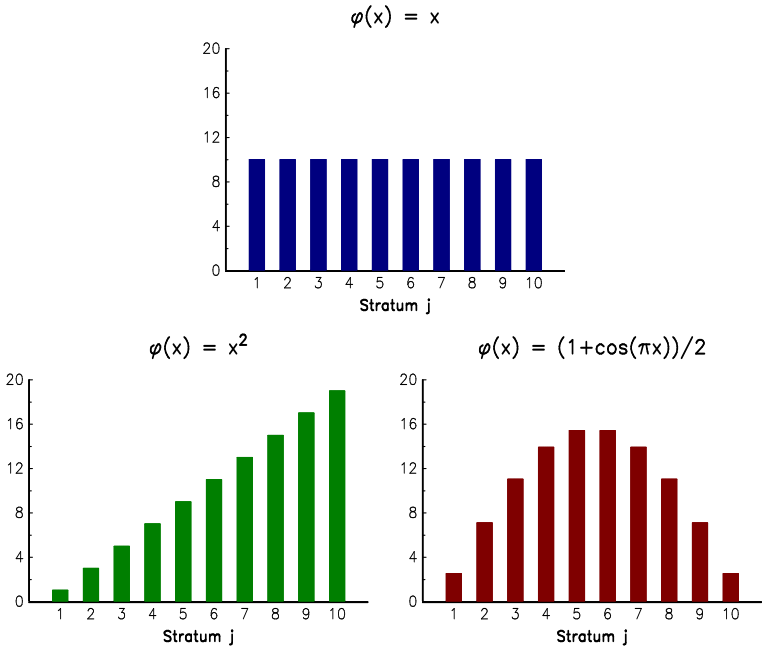

FIGURE 13.45: Optimal allocation $q^{\star}(j)$ (in %)

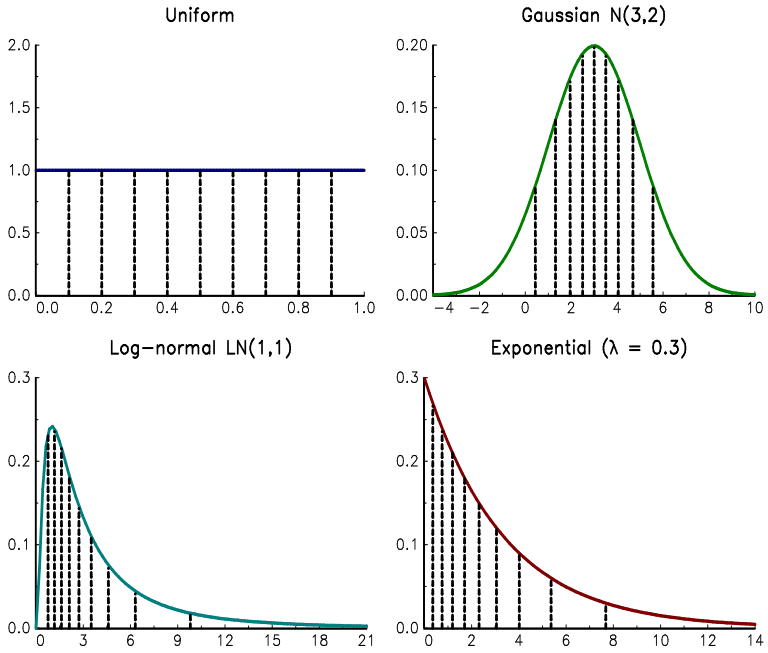

FIGURE 13.46: Strata for different random variables

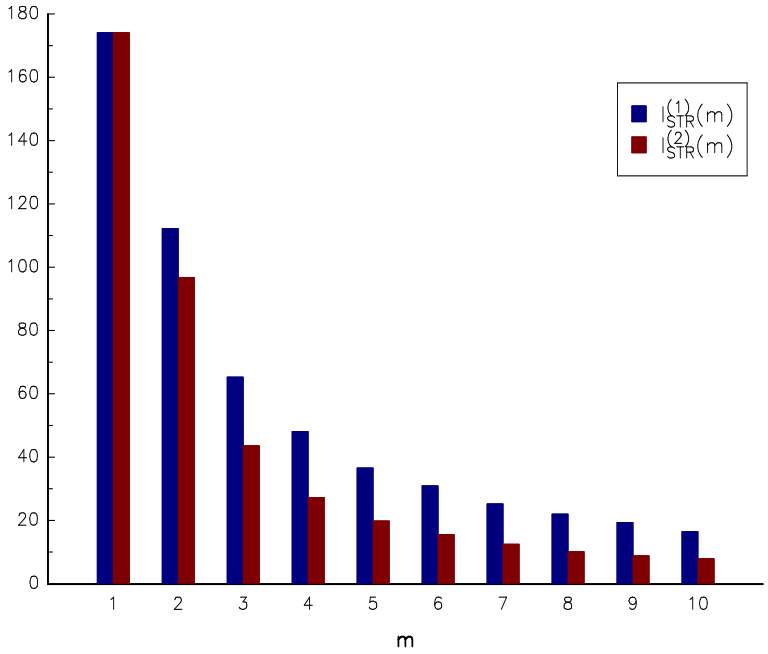

FIGURE 13.47: Variance of the two estimators $\hat{I}^{(1)}_{\text{STR}}(m)$ and $\hat{I}^{(2)}_{\text{STR}}(m)$ for different values of m

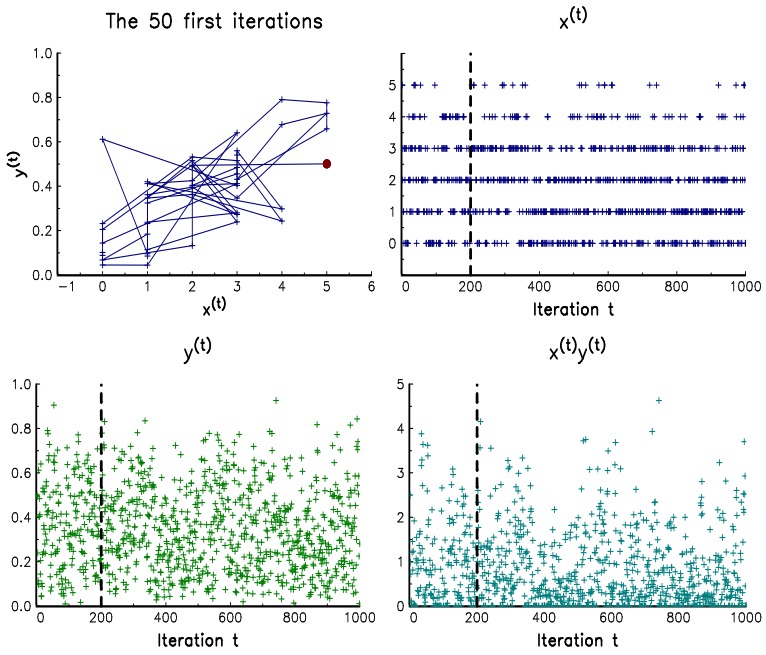

FIGURE 13.48: Illustration of the Gibbs sampler

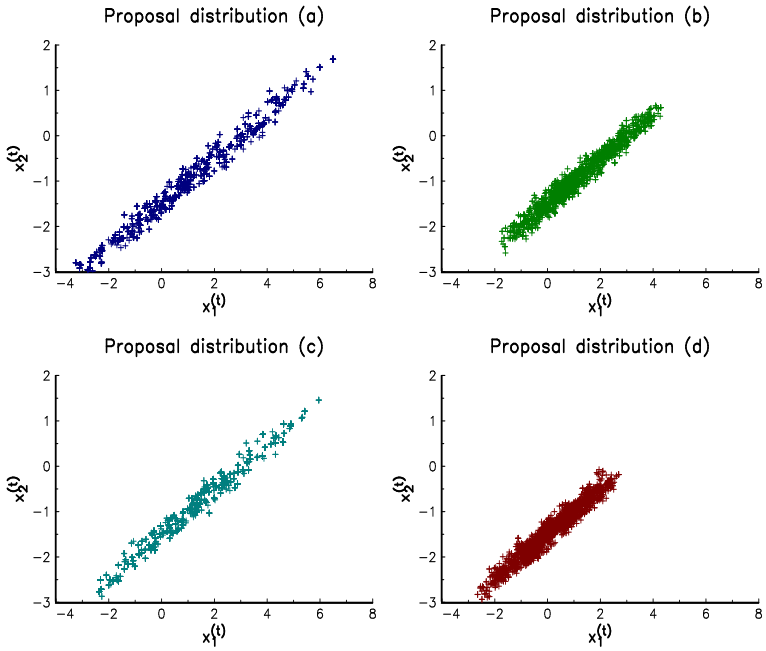

FIGURE 13.49: Illustration of the random walk sampler

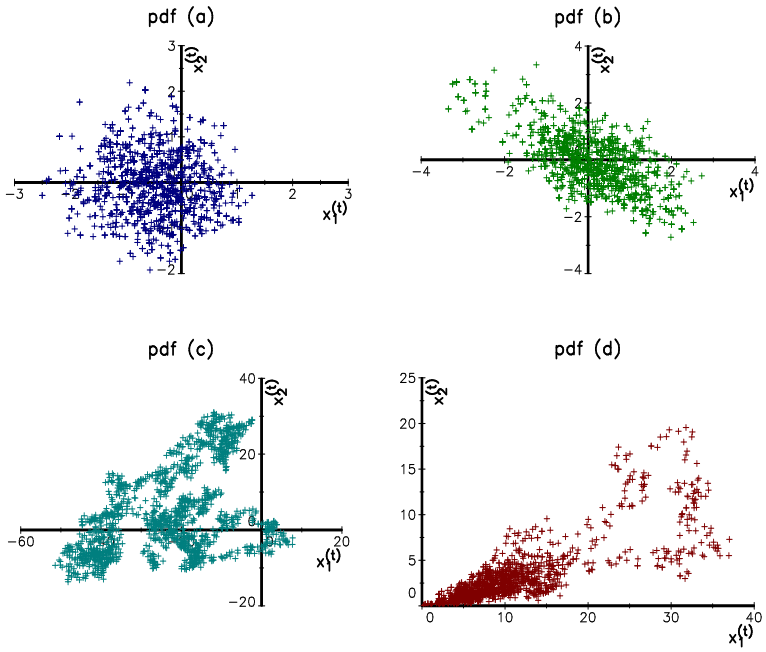

FIGURE 13.50: Simulating bivariate probability distributions with the MH algorithm

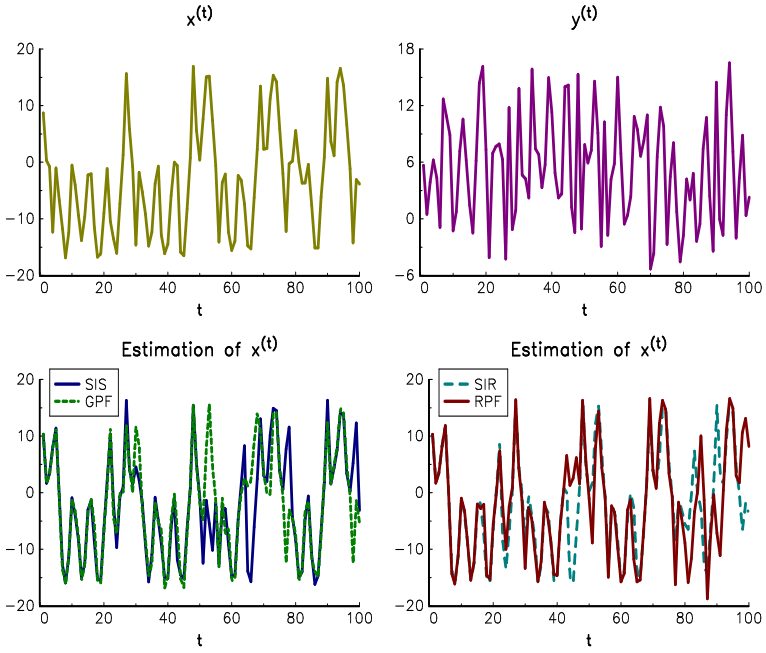

FIGURE 13.51: An example of a SMC run with 1 000 particles

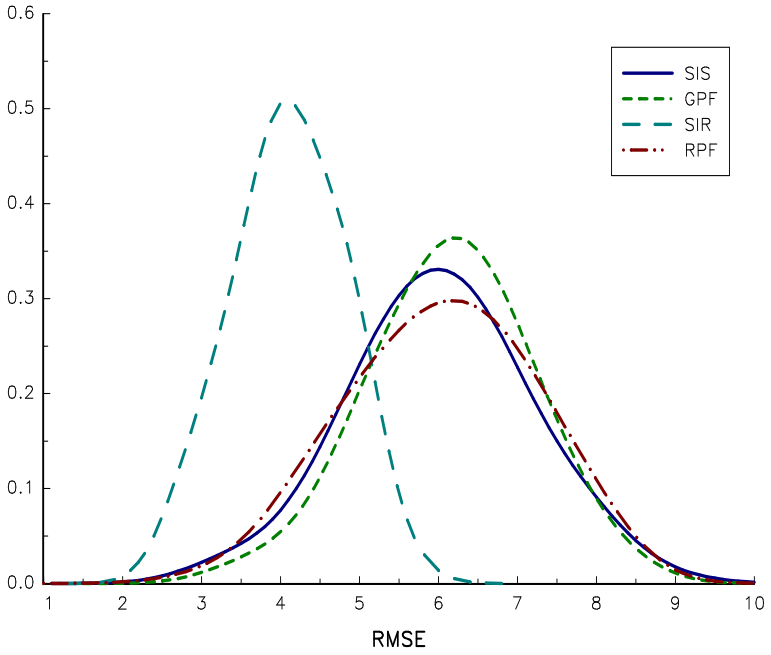

FIGURE 13.52: Density of the RMSE statistic for 1 000 particles

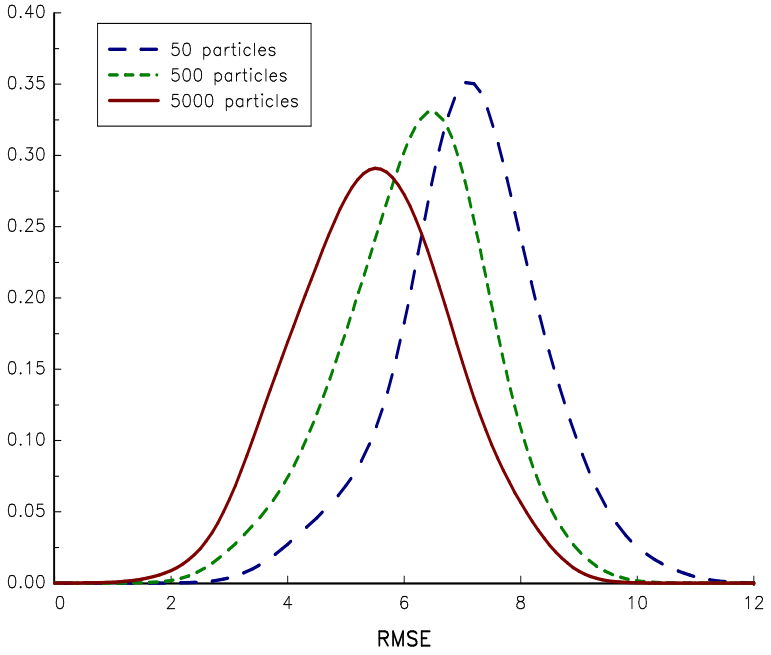

FIGURE 13.53: Density of the RMSE statistic for the SIS algorithm

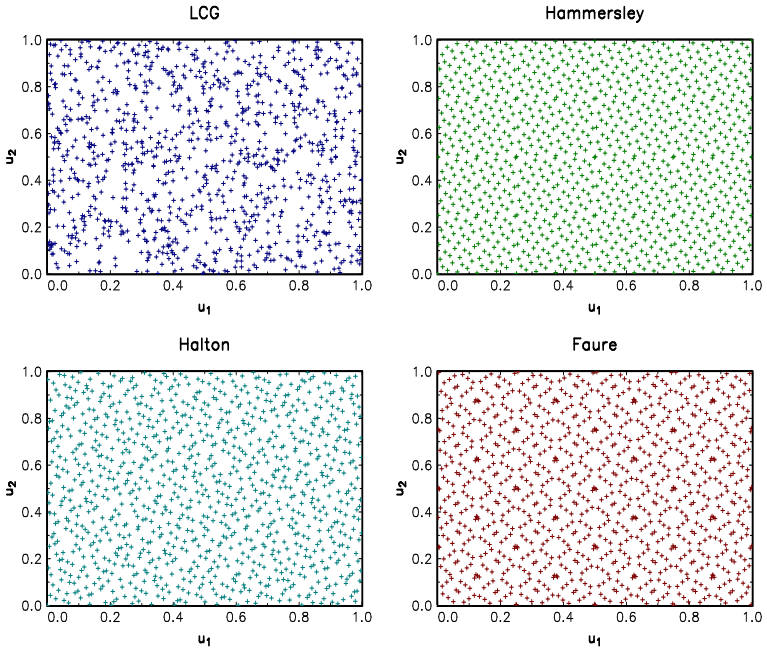

FIGURE 13.54: Comparison of different low discrepancy sequences

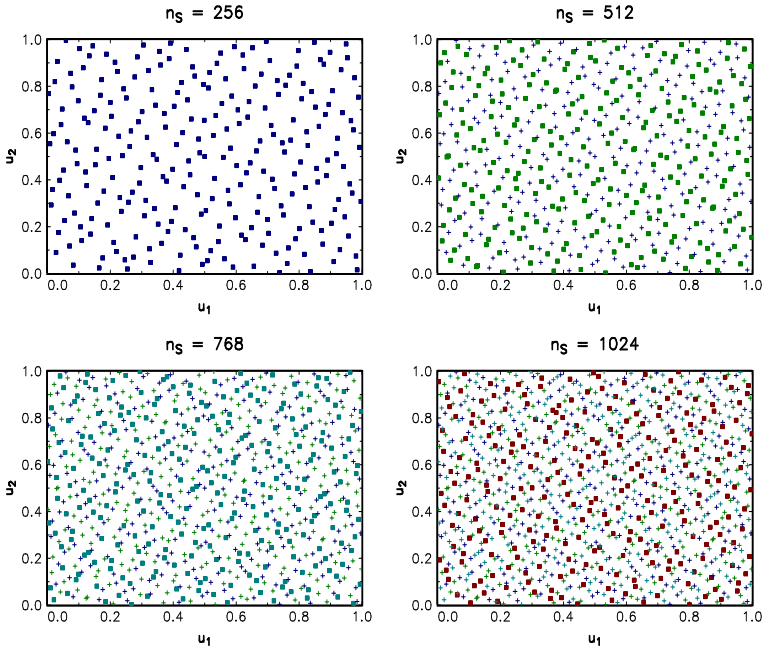

FIGURE 13.55: The Sobol generator

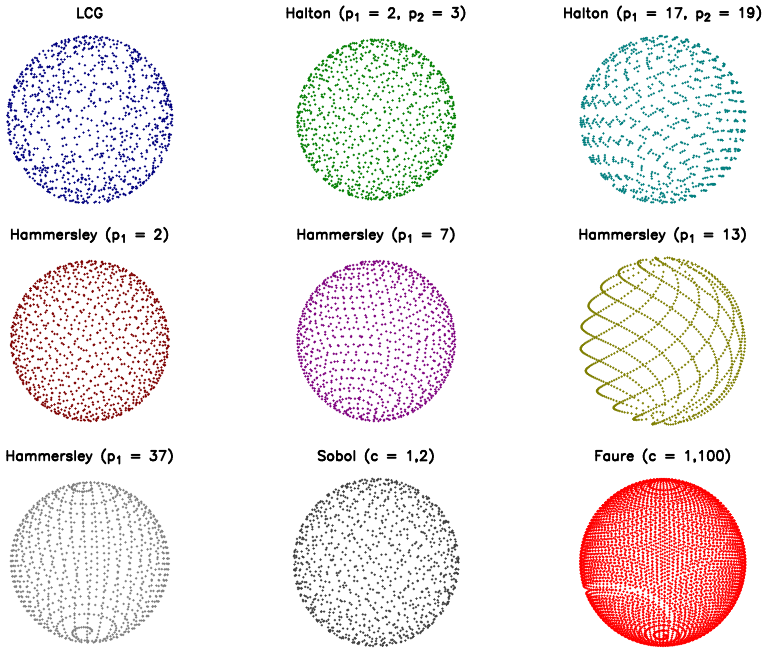

FIGURE 13.56: Quasi-random points on the unit sphere

Chapter 14

Stress Testing and Scenario Analysis

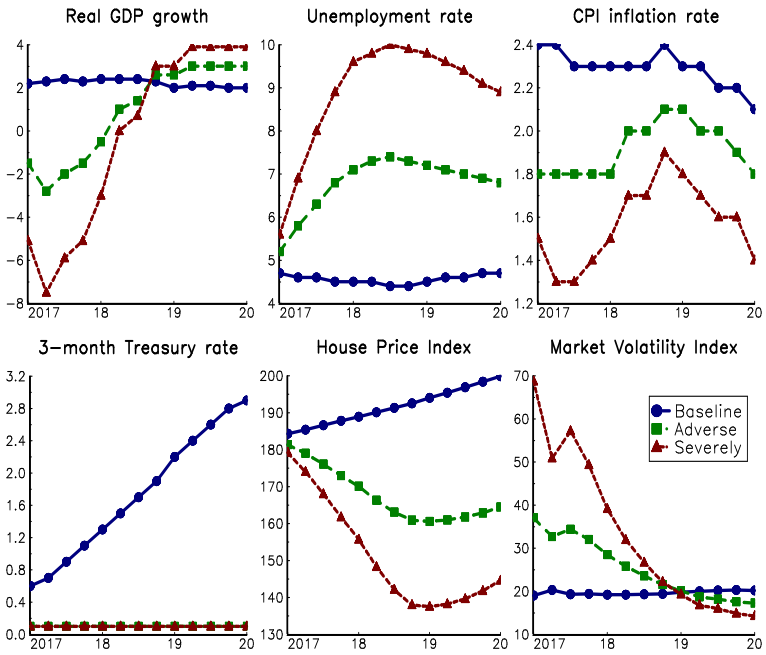

FIGURE 14.1: 2017 DFAST supervisory scenarios: Domestic variables

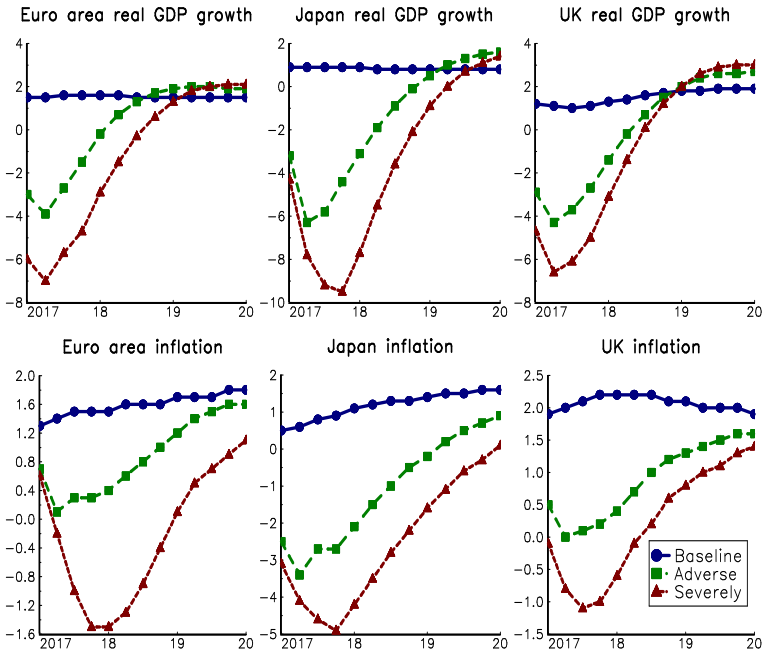

FIGURE 14.2: 2017 DFAST supervisory scenarios: International variables

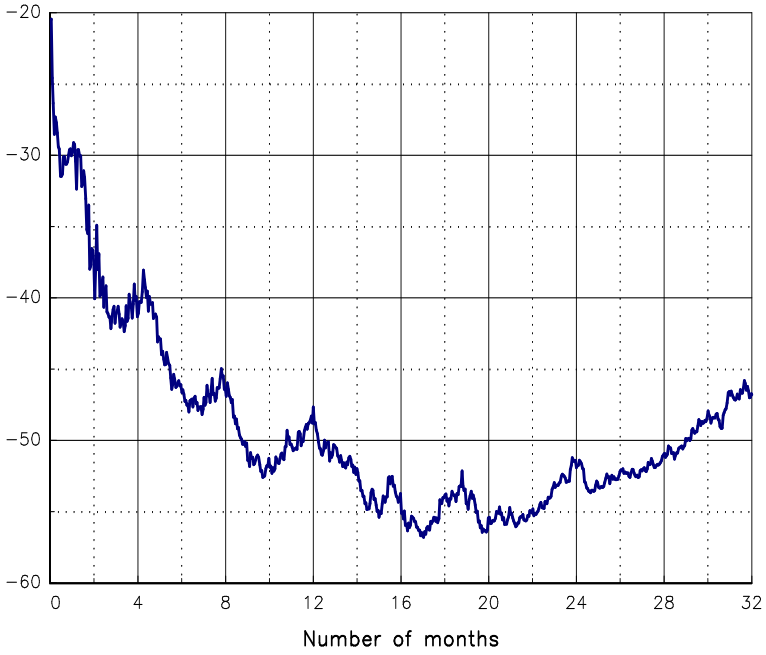

FIGURE 14.3: Loss function of the S&P 500 index

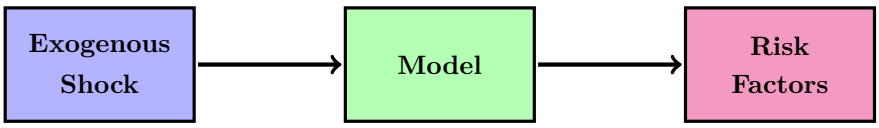

FIGURE 14.4: Macroeconomic approach of stress testing

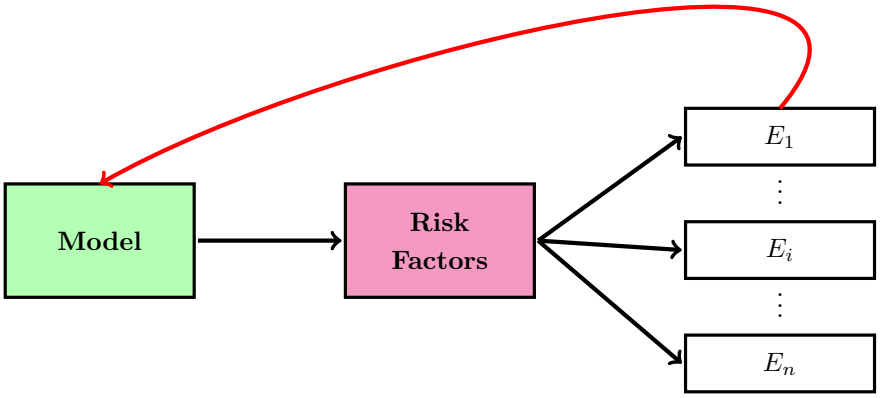

FIGURE 14.5: Feedback effects in stress testing models

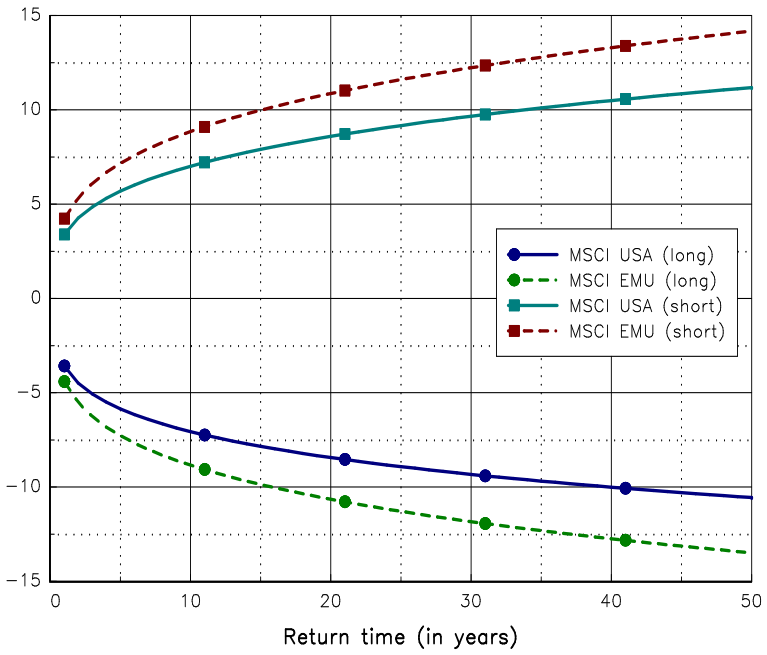

FIGURE 14.6: Stress scenarios (in %) of MSCI USA and MSCI EMU indices

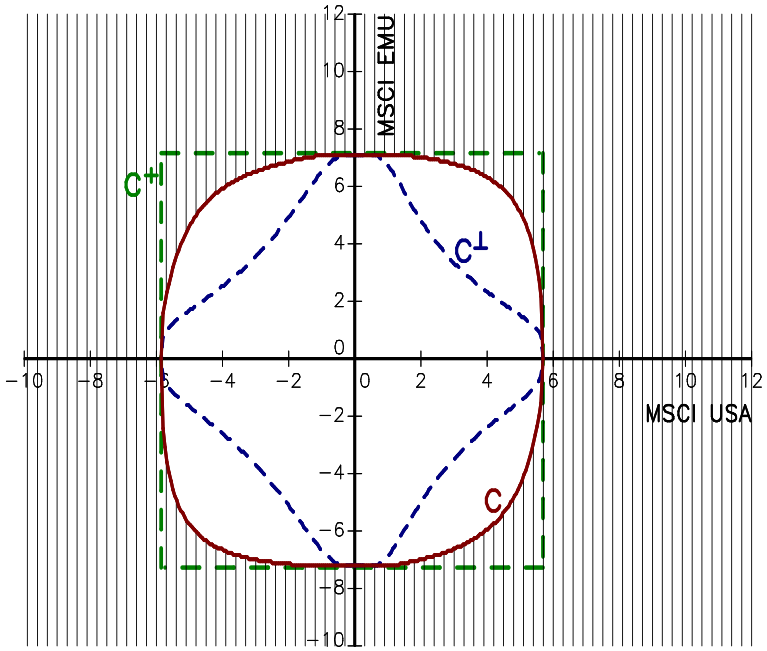

FIGURE 14.7: Failure area of MSCI USA and MSCI EMU indices (blockwise dependence)

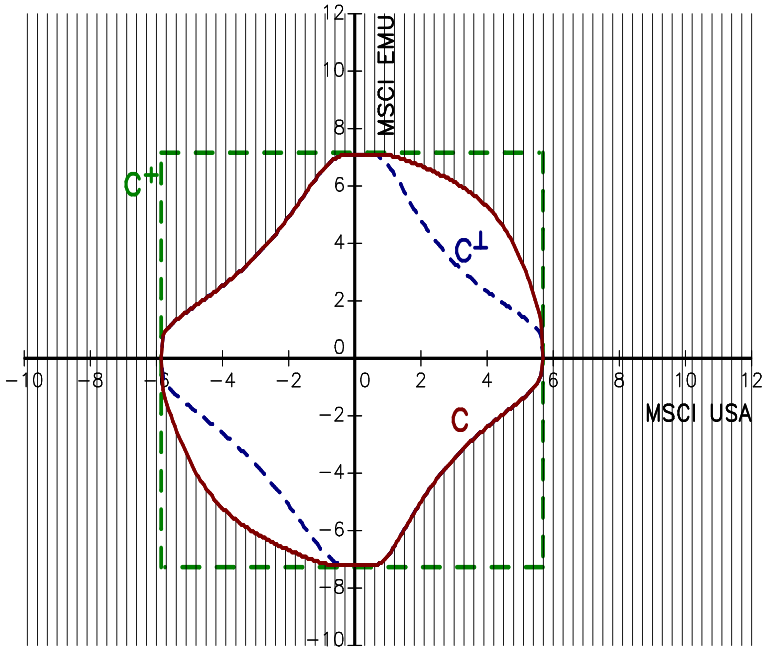

FIGURE 14.8: Failure area of MSCI USA and MSCI EMU indices (daily dependence)

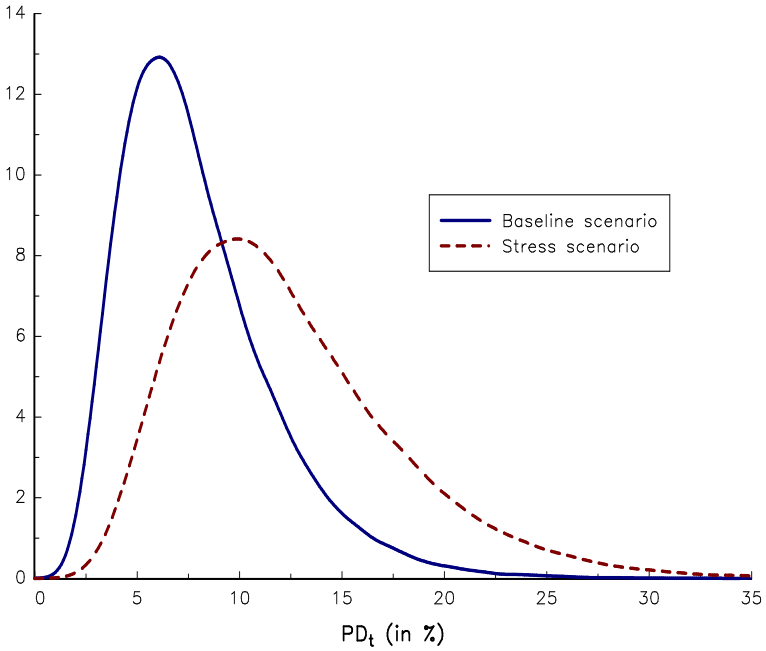

FIGURE 14.9: Probability density function of PD_t

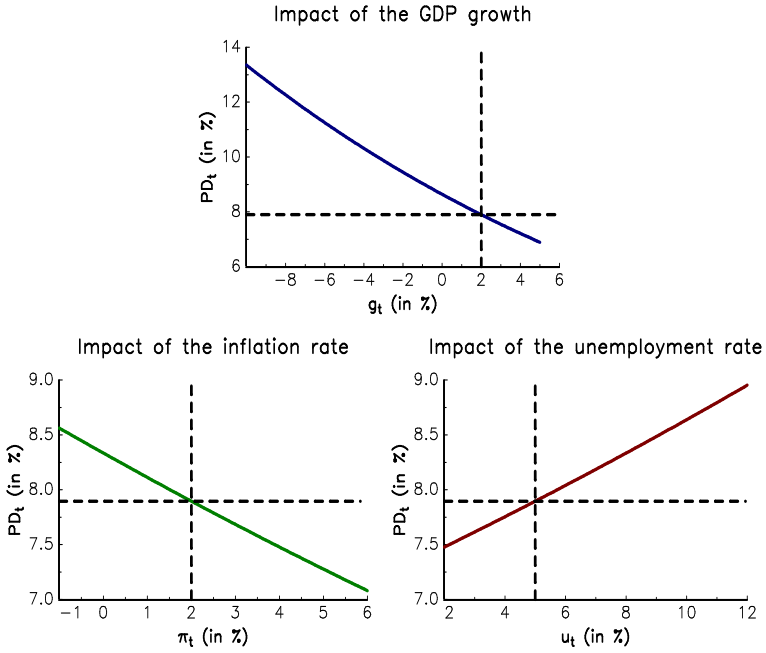

FIGURE 14.10: Relationship between the macroeconomic variables and PD_t

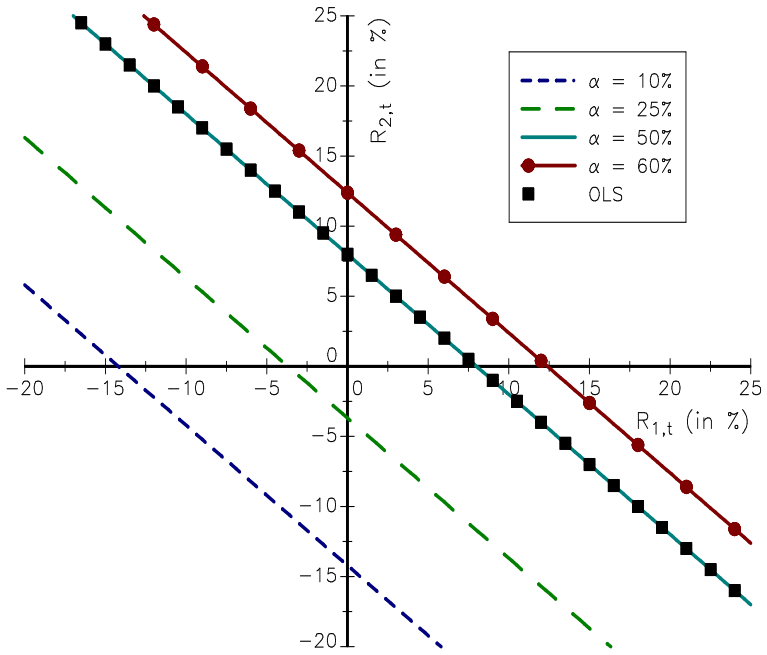

FIGURE 14.11: Conditional quantile (Gaussian distribution)

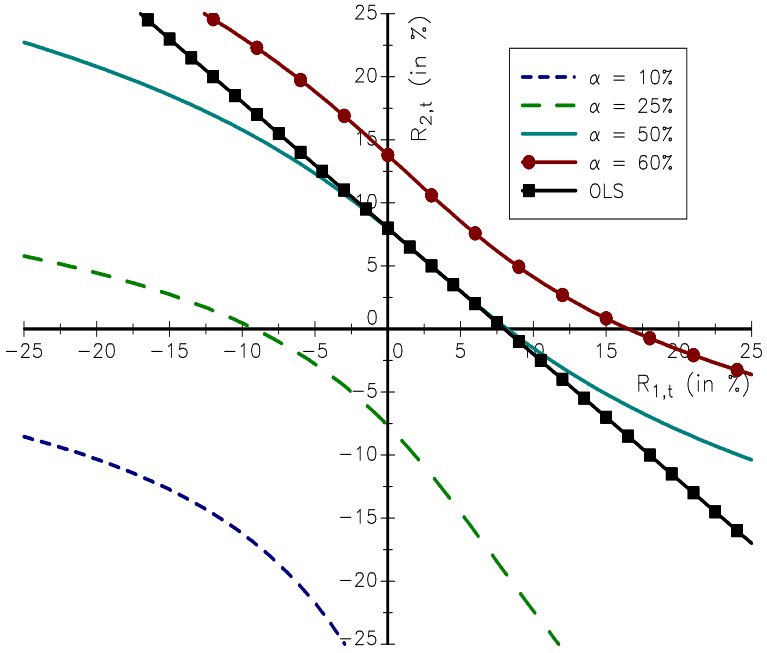

FIGURE 14.12: Conditional quantile (Normal copula & Student's t marginals)

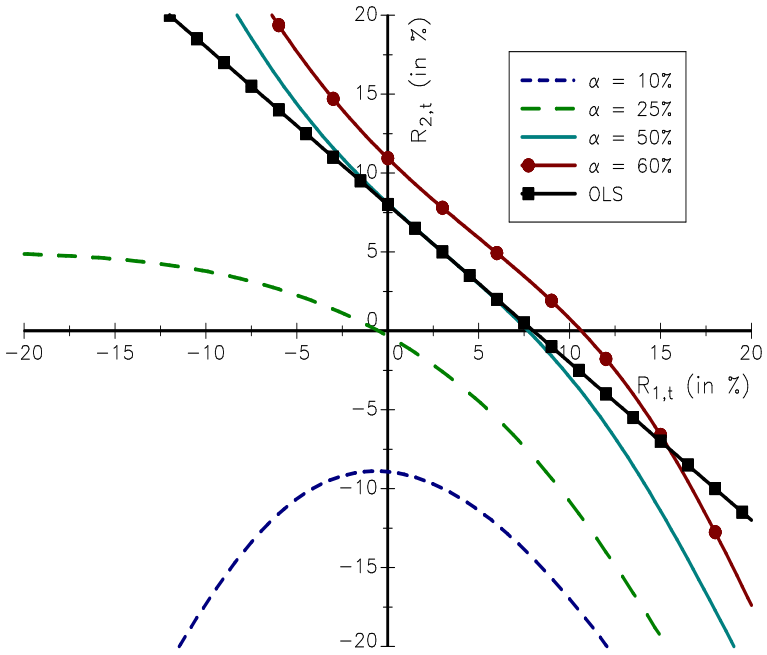

FIGURE 14.13: Conditional quantile (Student's t copula & Gaussian marginals)

Chapter 15

Credit Scoring Models

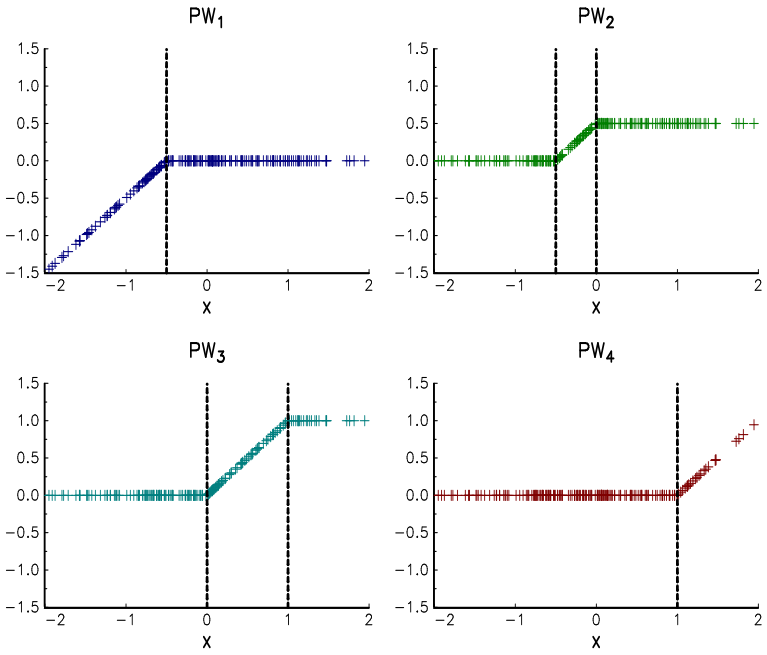

FIGURE 15.1: Piecewise variables

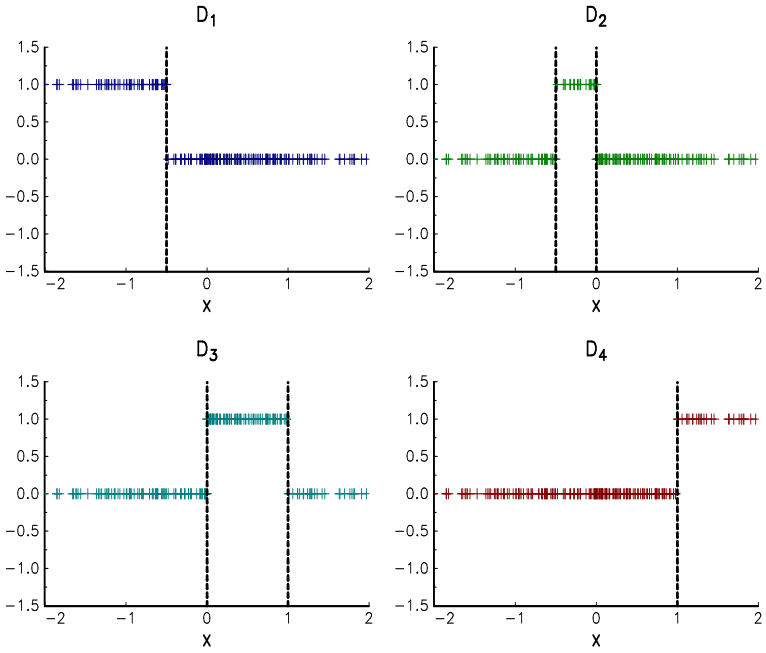

FIGURE 15.2: Dummy variables

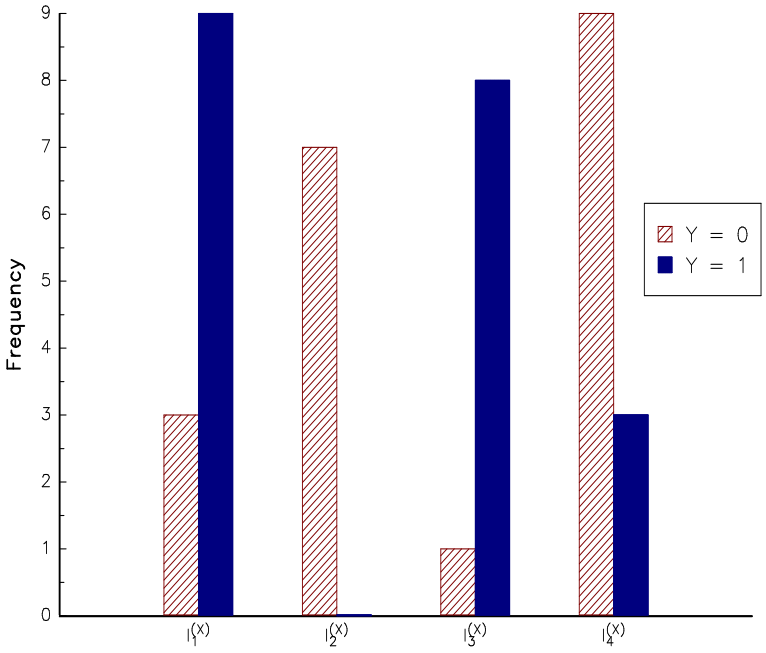

FIGURE 15.3: Optimal slicing with four classes

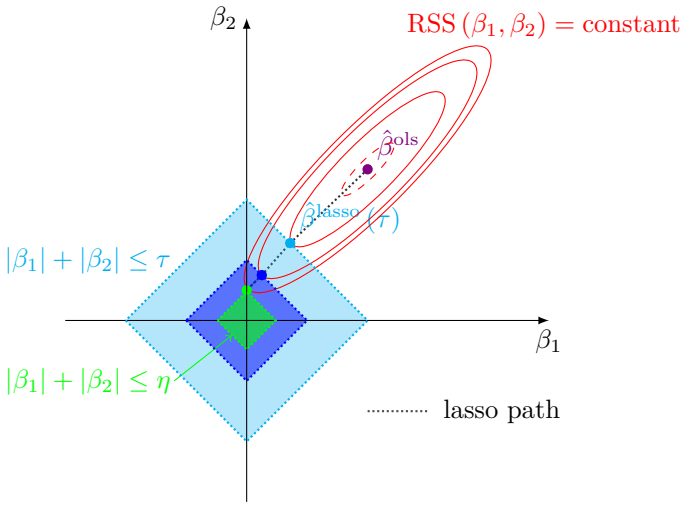

FIGURE 15.4: Interpretation of the lasso regression

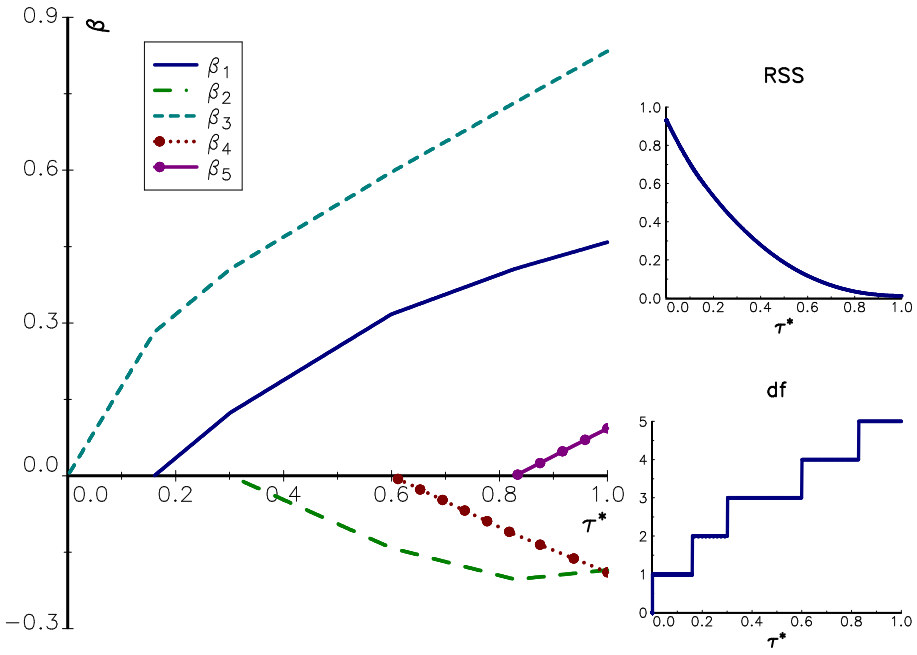

FIGURE 15.5: Variable selection with the lasso regression

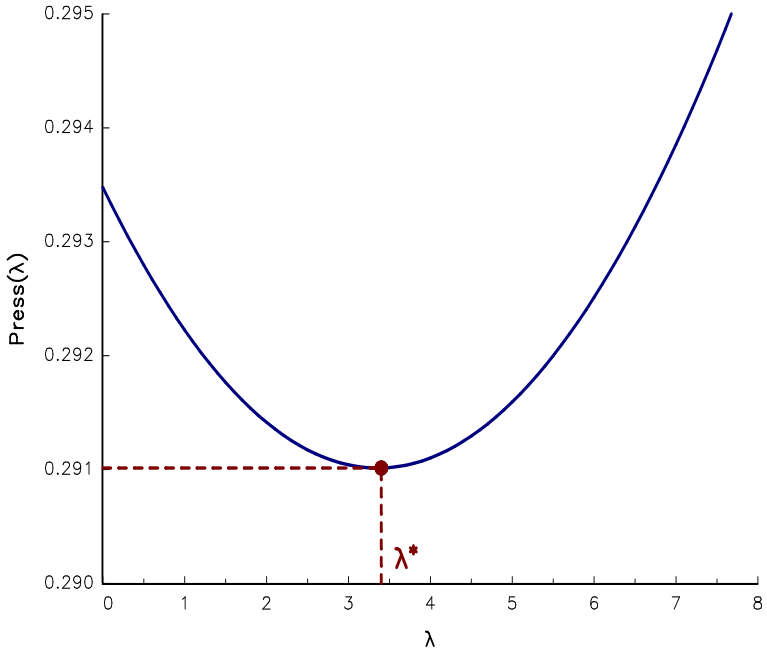

FIGURE 15.6: Selection of the ridge parameter using the PRESS statistic

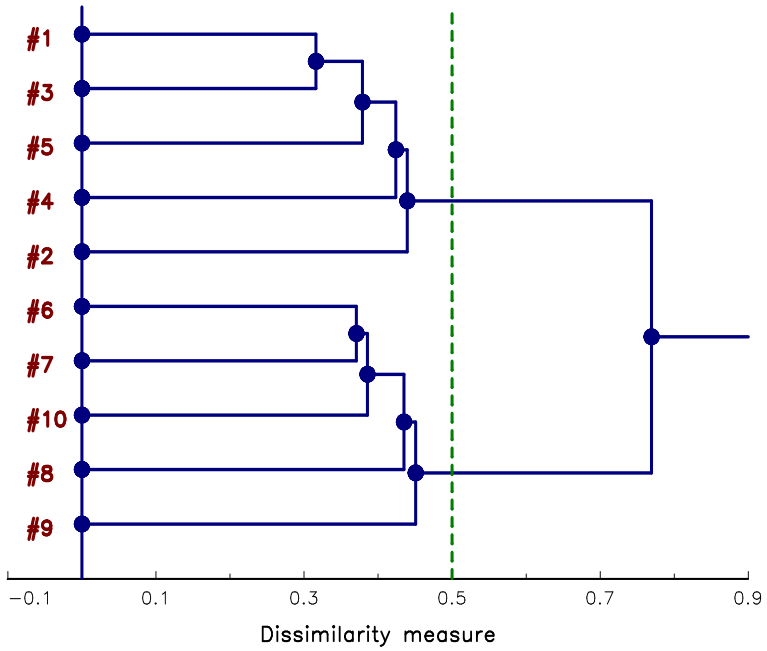

FIGURE 15.7: An example of dendrogram

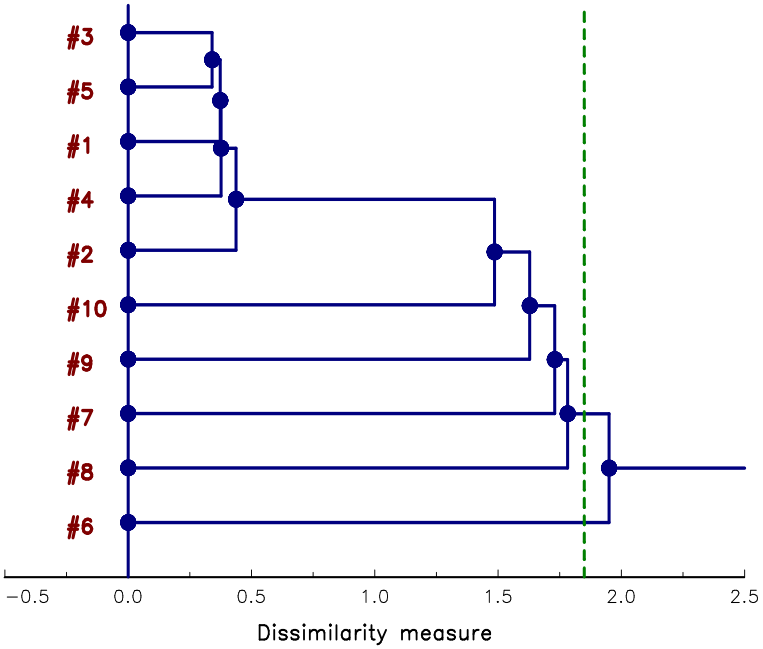

FIGURE 15.8: Unbalanced clustering

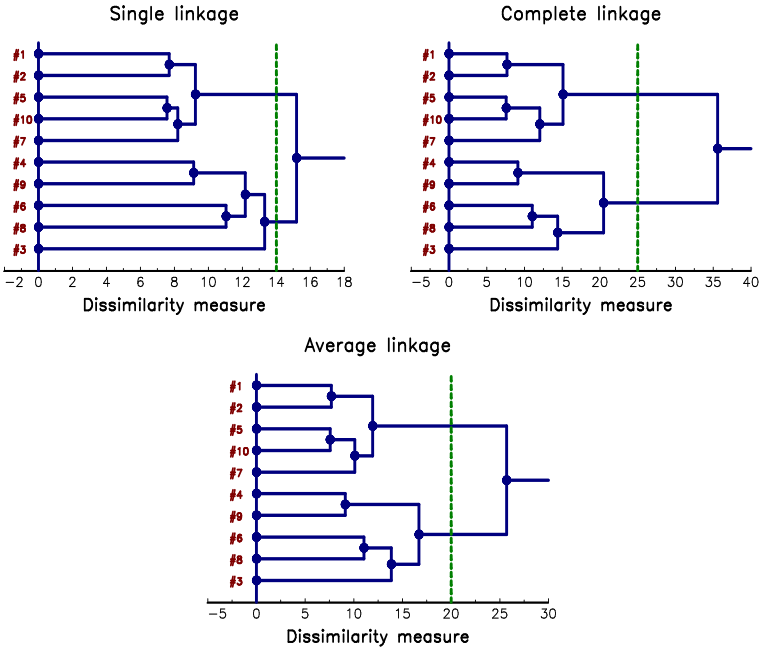

FIGURE 15.9: Comparison of the three dendrograms

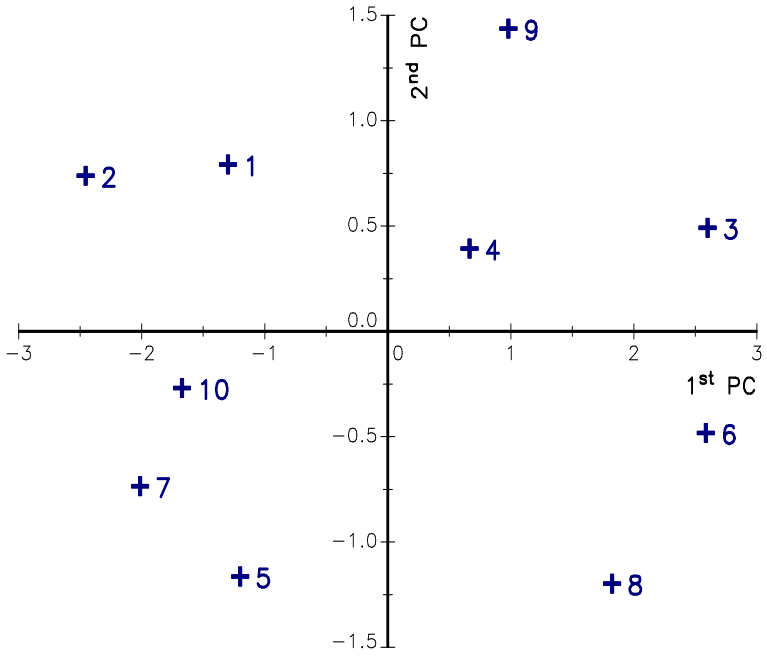

FIGURE 15.10: Scatterplot of the factor values $z_{i,1}$ and $z_{i,2}$

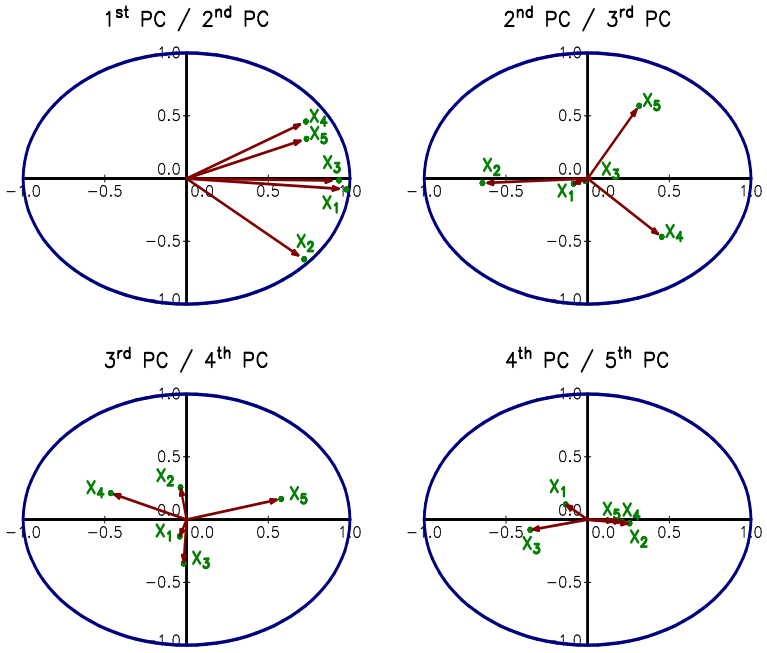

FIGURE 15.11: PCA correlation circle

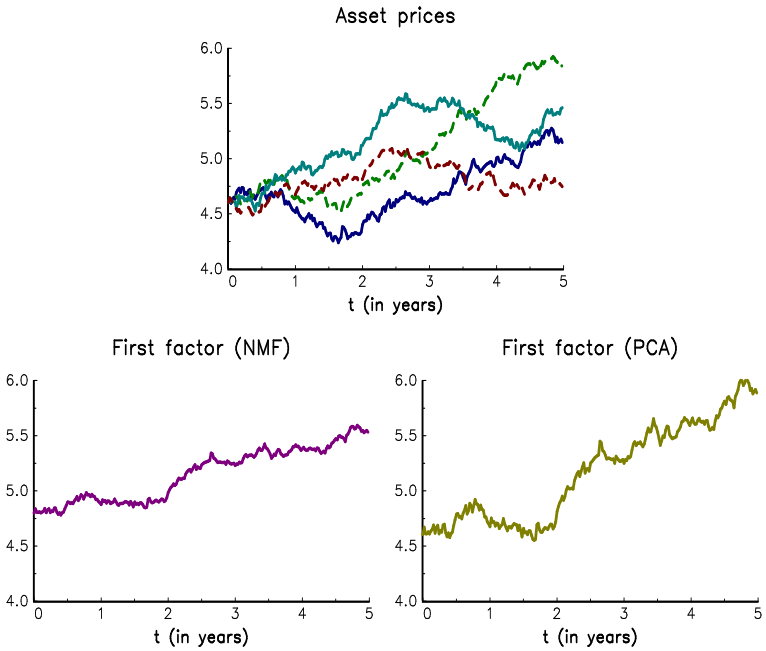

FIGURE 15.12: Estimating the first factor of a basket of financial assets

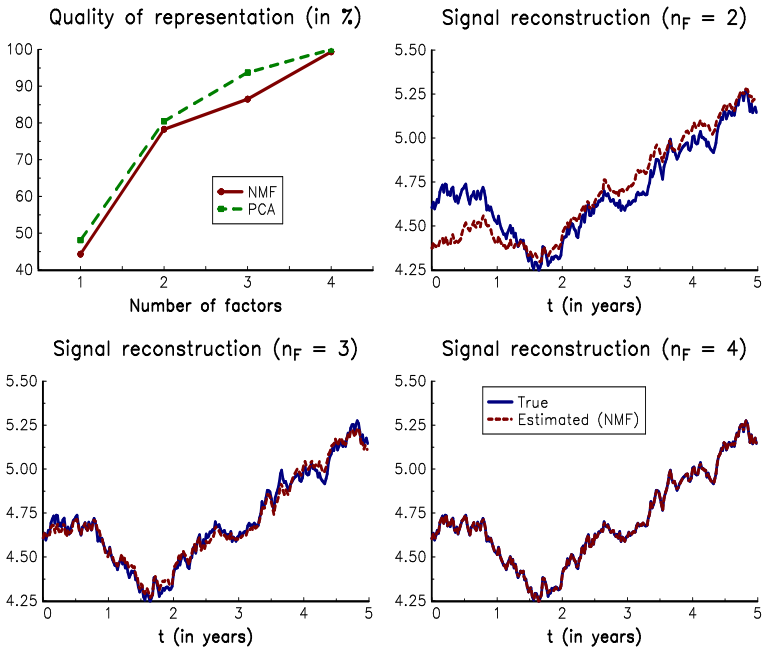

FIGURE 15.13: Variance decomposition and signal reconstruction

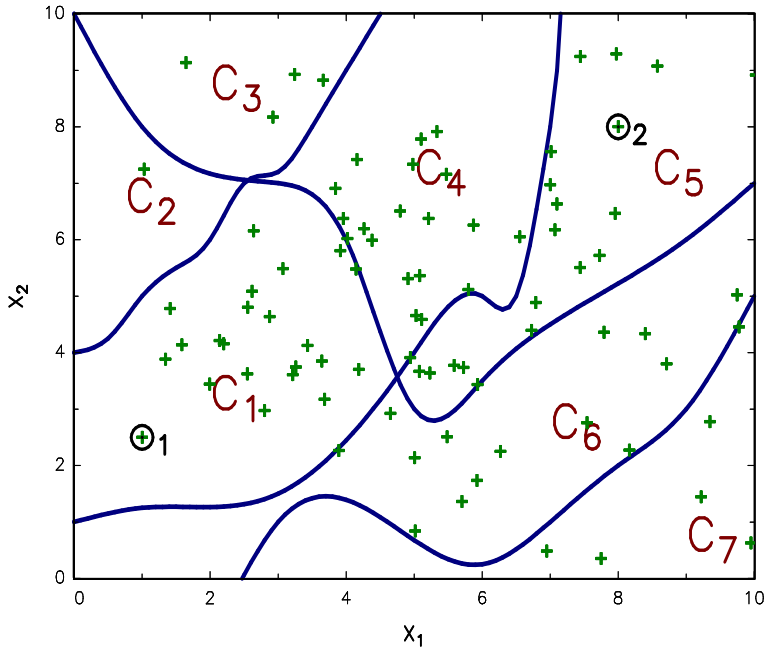

FIGURE 15.14: Classification statistical problem

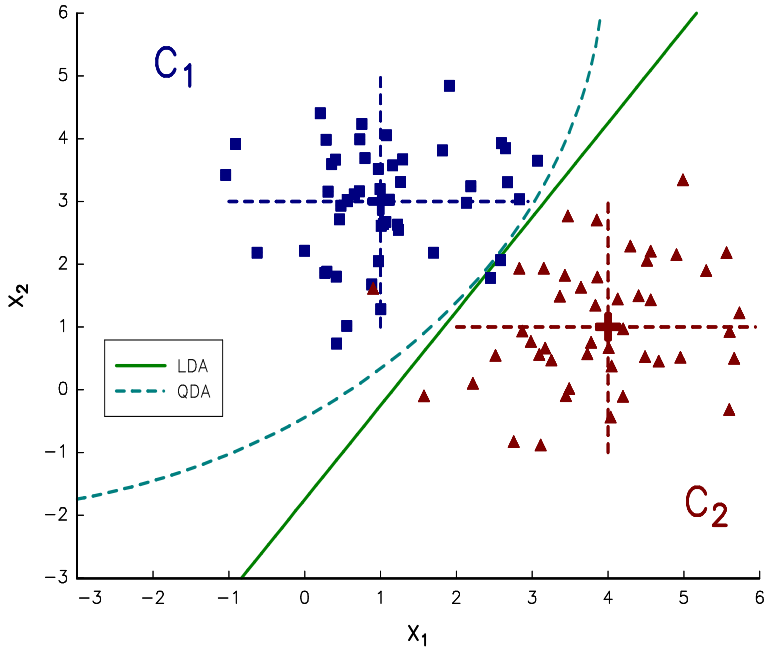

FIGURE 15.15: Boundary decision of discriminant analysis

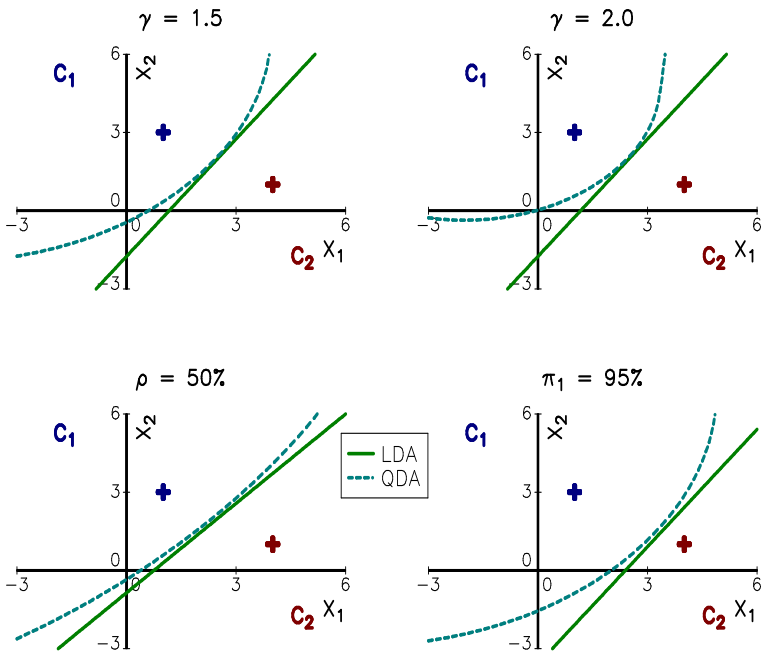

FIGURE 15.16: Impact of the parameters on LDA/QDA boundary decisions

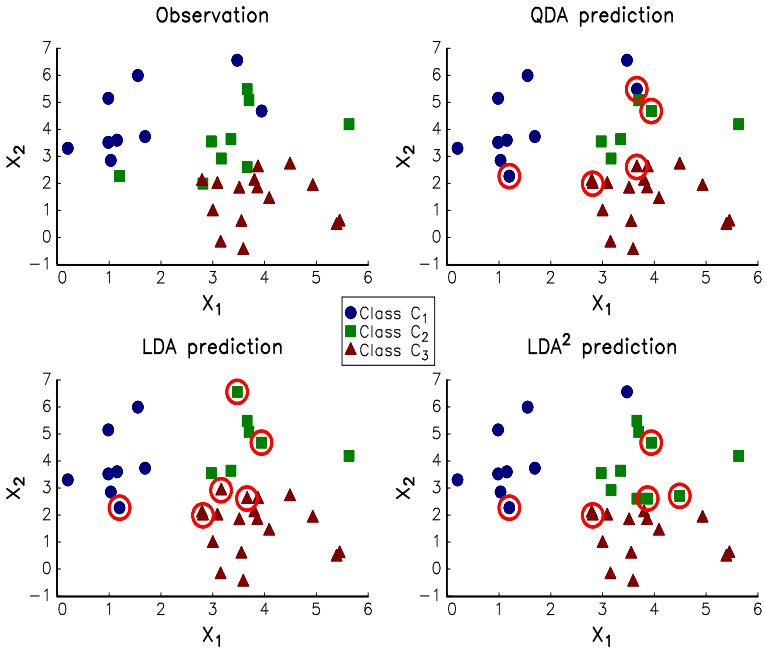

FIGURE 15.17: Comparing QDA, LDA and LDA^2 predictions

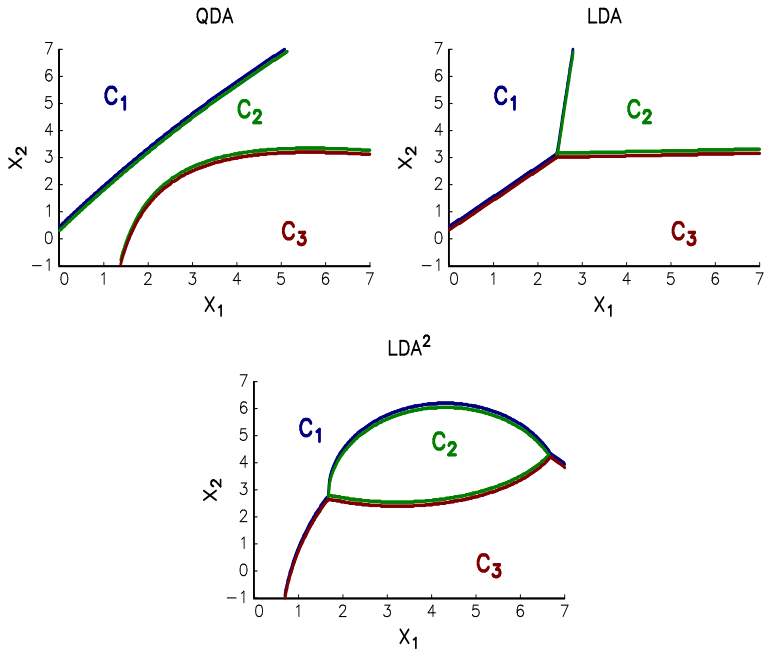

FIGURE 15.18: QDA, LDA and LDA^2 decision regions

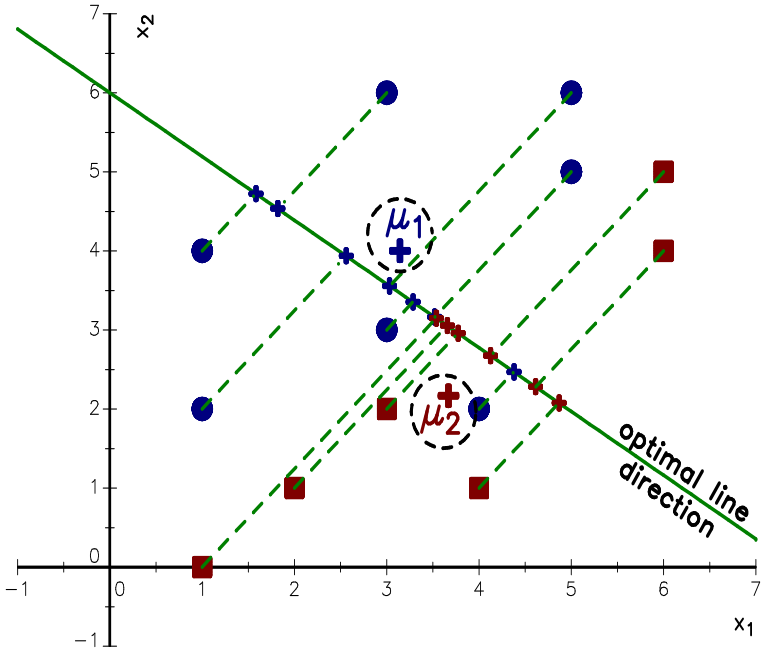

FIGURE 15.19: Linear projection and the Fisher solution

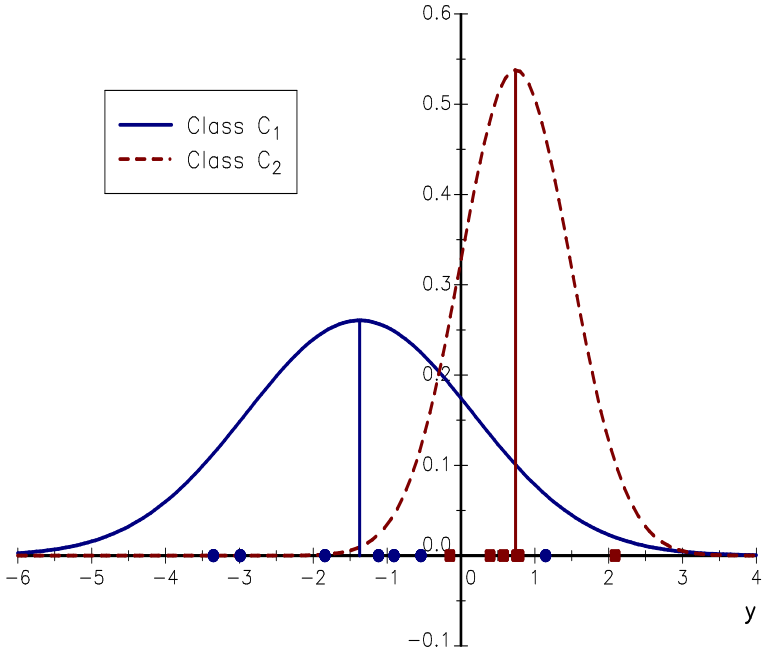

FIGURE 15.20: Class separation and the cut-off criterion

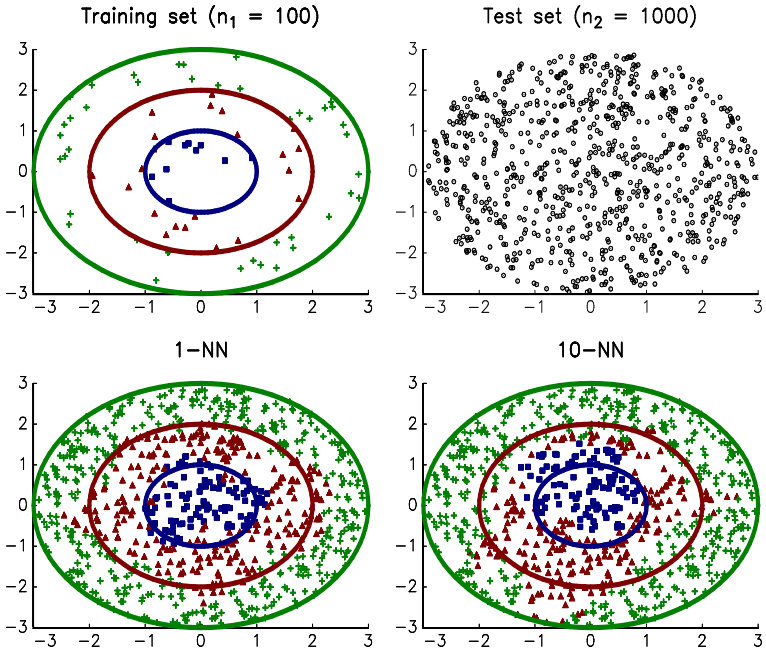

FIGURE 15.21: Illustration of the k-NN classifier

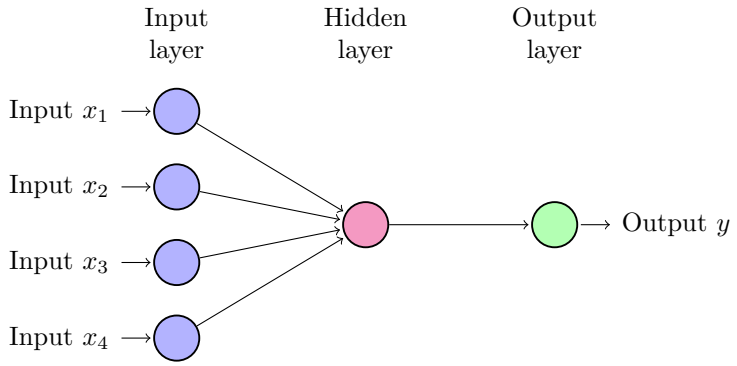

FIGURE 15.22: The perceptron

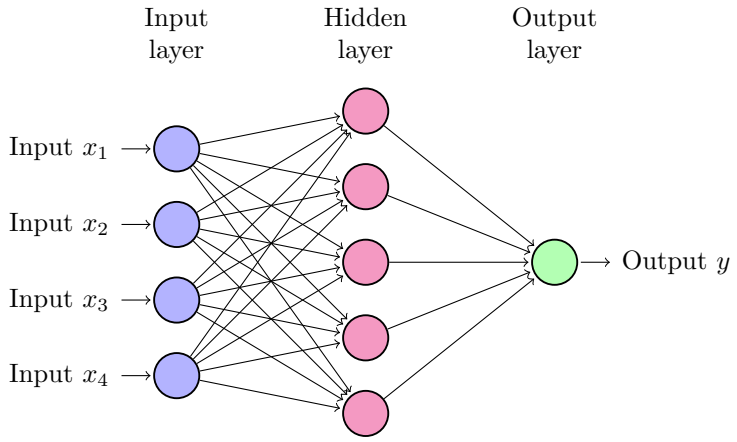

FIGURE 15.23: Feed-forward neural network with a single hidden layer

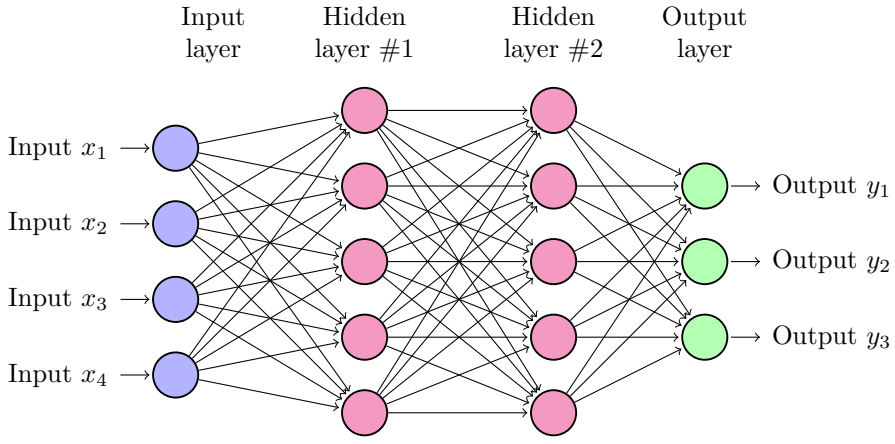

FIGURE 15.24: Feed-forward neural network with two hidden layers and three output units

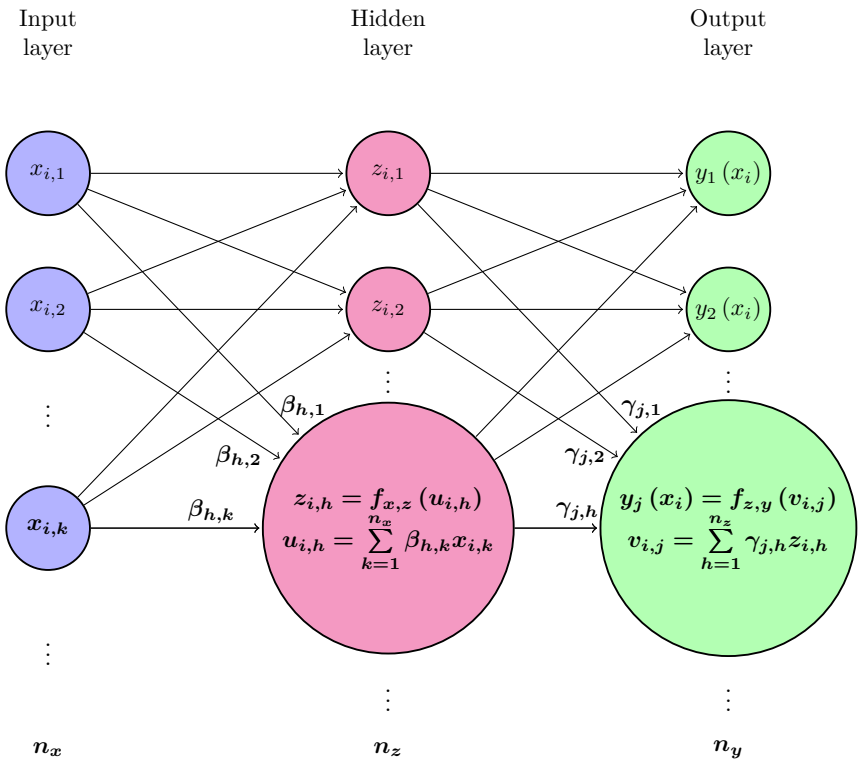

FIGURE 15.25: Canonical neural network

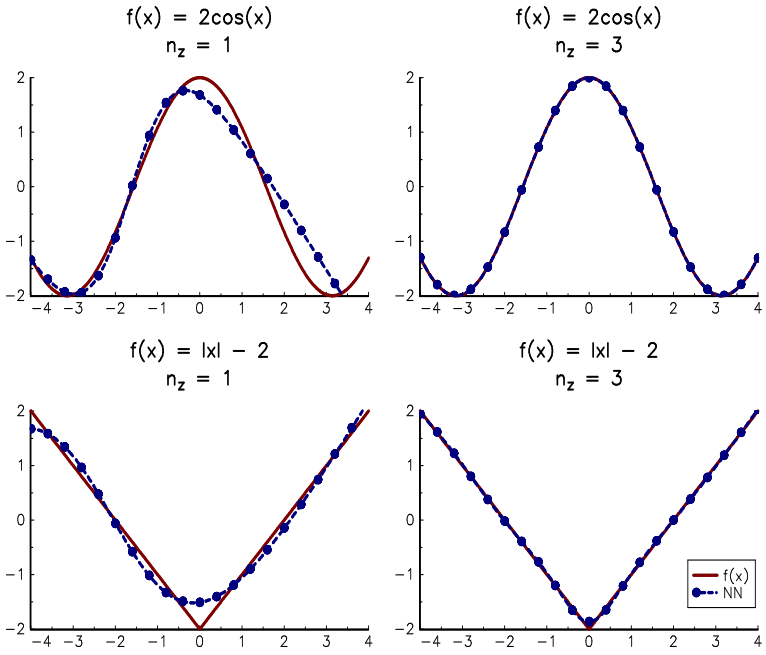

FIGURE 15.26: Neural networks as universal approximators

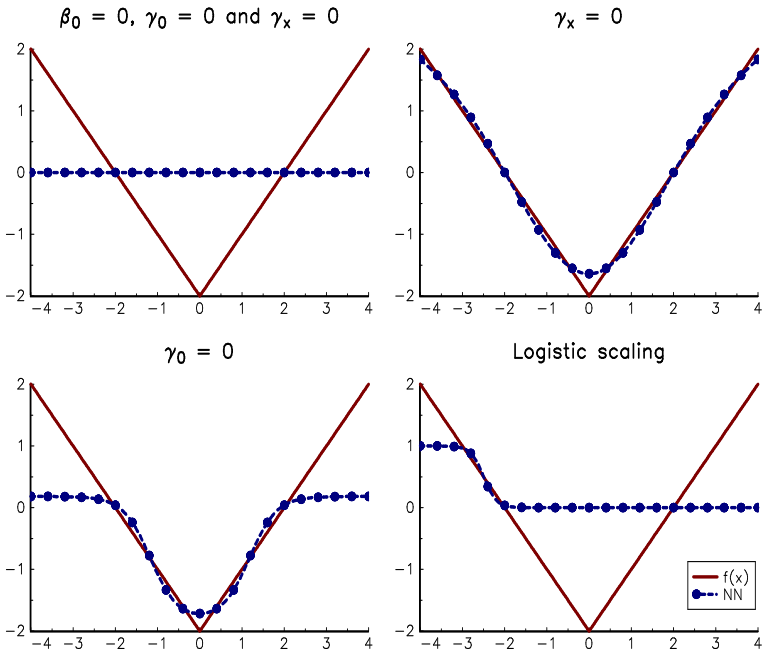

FIGURE 15.27: The scaling issue of neural networks ($f(x) = |x| - 2$)

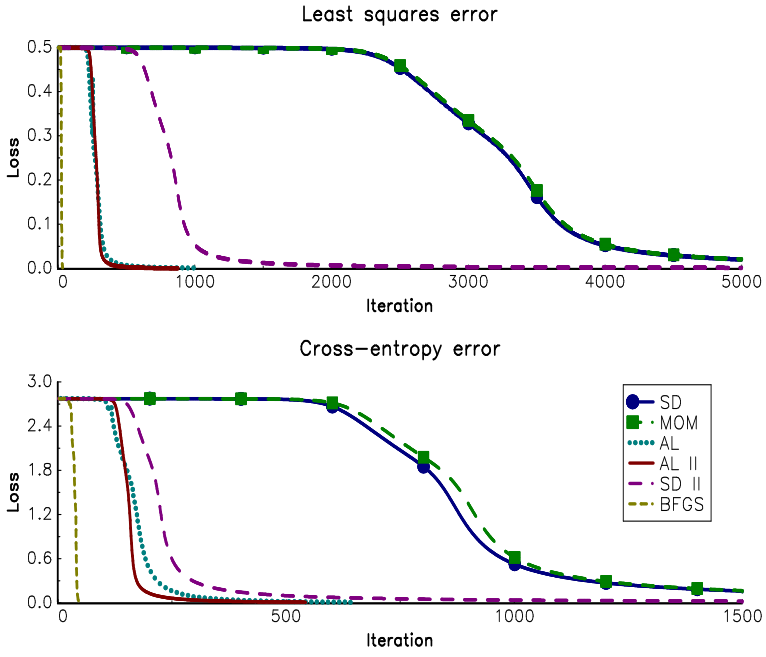

FIGURE 15.28: Convergence of the XOR problem

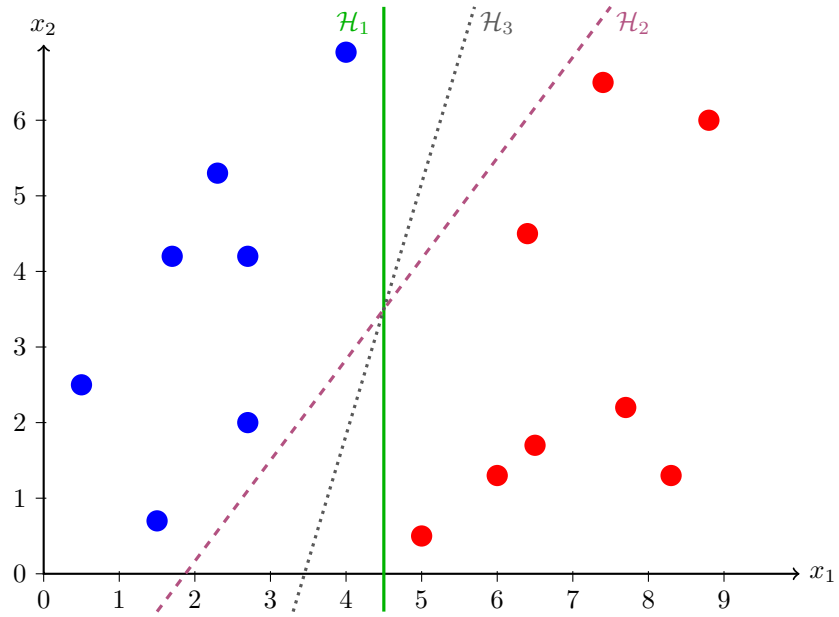

FIGURE 15.29: Separating hyperplane picking

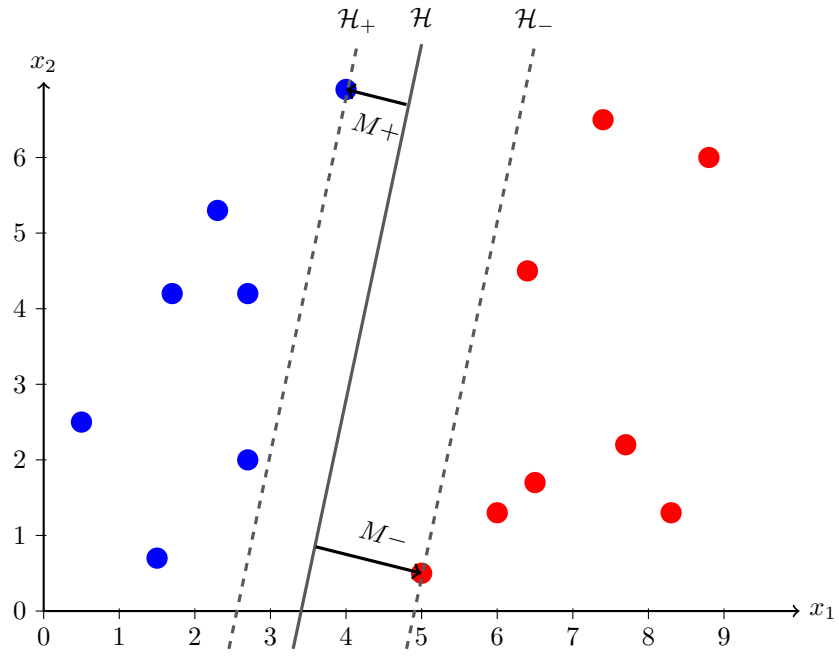

FIGURE 15.30: Margins of separation

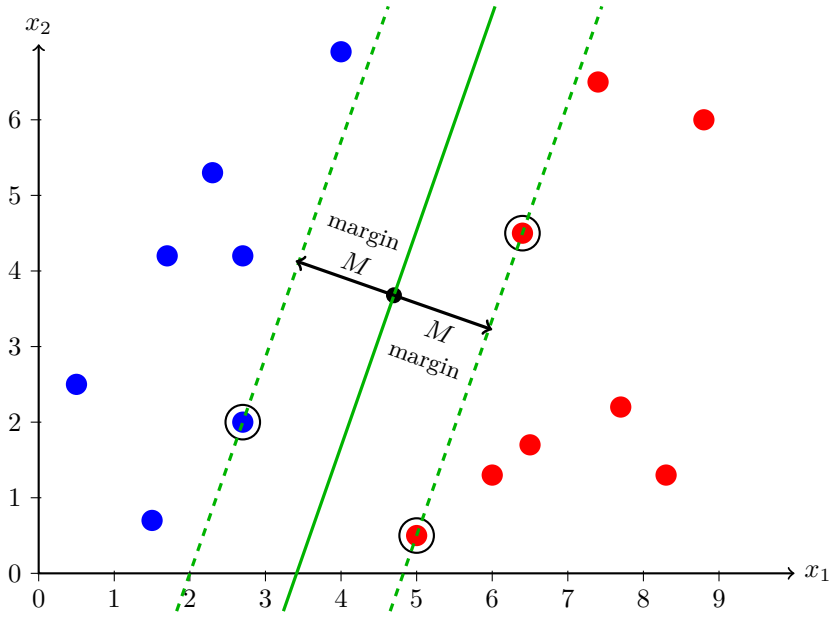

FIGURE 15.31: Optimal hyperplane

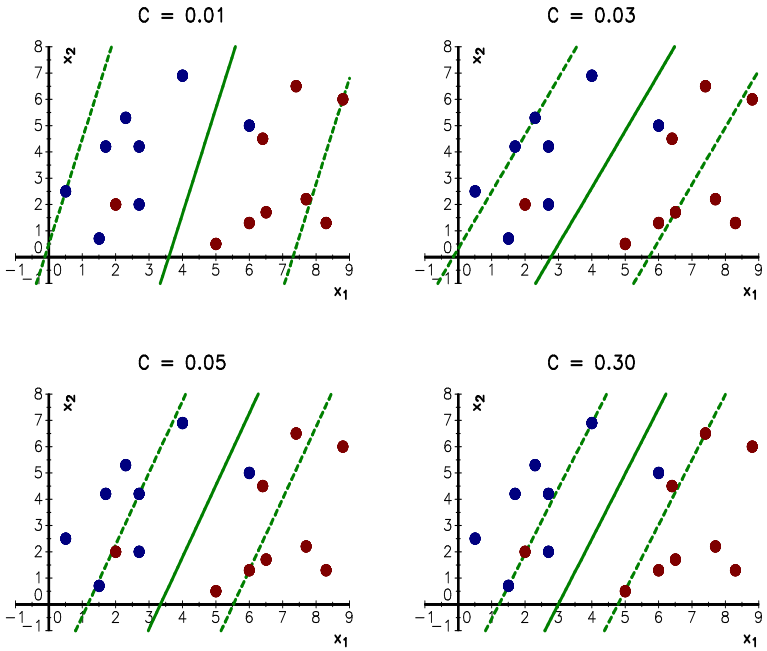

FIGURE 15.32: Soft margin SVM classifiers

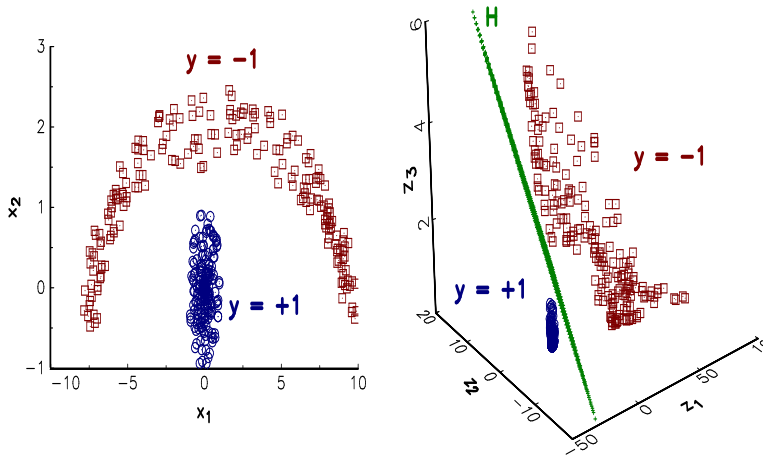

FIGURE 15.33: Transforming a non-linearly separable training set into a linearly separable training set

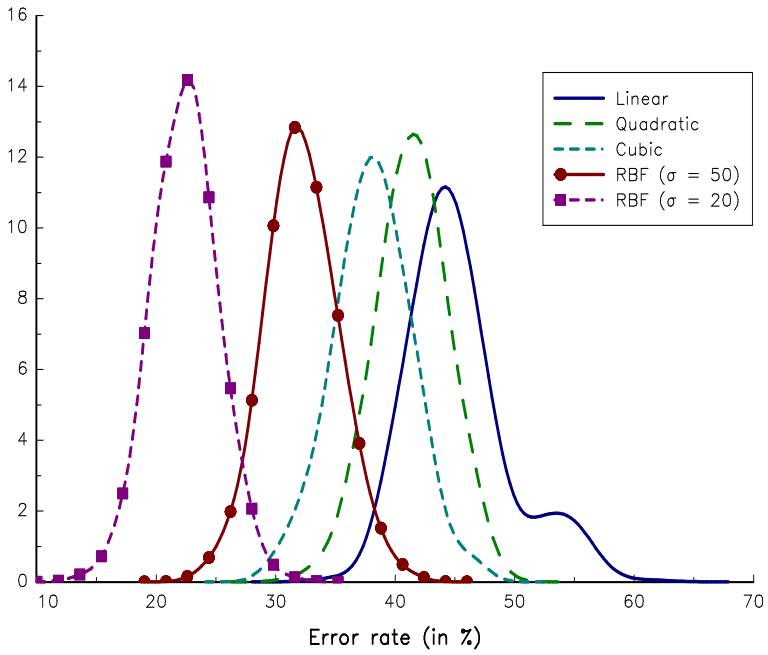

FIGURE 15.34: Probability density function of in-sample error rates

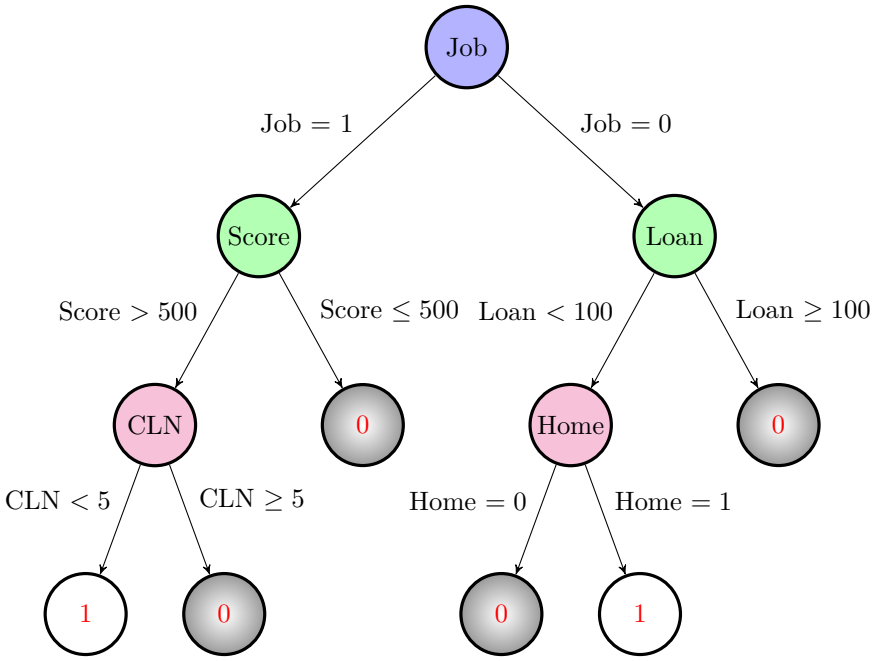

FIGURE 15.35: An example of decision tree

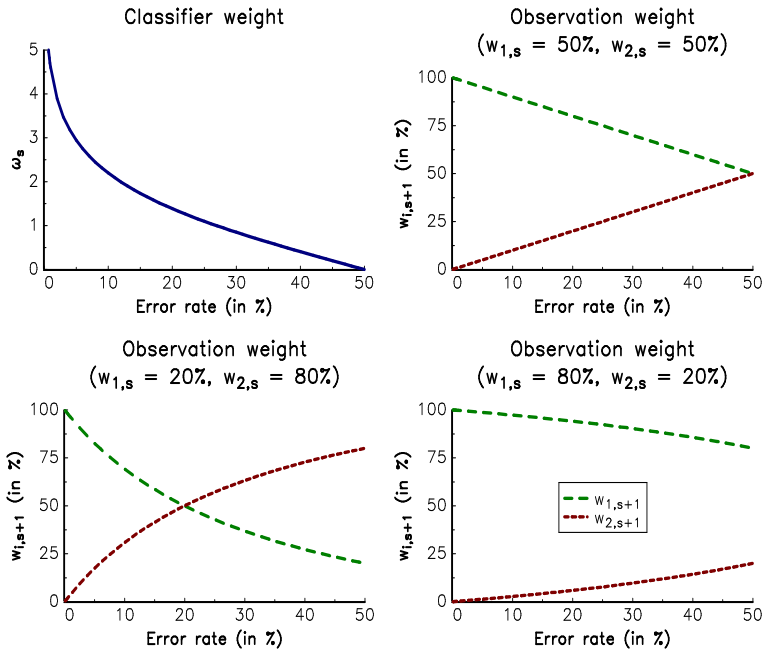

FIGURE 15.36: Weighting schemes of the boosting approach

1/36	1/36	1/36	1/36	1/36	1/36
1/36	1/36	1/36	1/36	1/36	1/36
1/36	1/36	1/36	1/36	1/36	1/36
1/36	1/36	1/36	1/36	1/36	1/36
1/36	1/36	1/36	1/36	1/36	1/36
1/36	1/36	1/36	1/36	1/36	1/36

$H(X) = H(Y) = 1.792$
$H(X,Y) = 3.584$
$I(X,Y) = 0$

1/6					
	1/6				
		1/6			
			1/6		
				1/6	
					1/6

$H(X) = H(Y) = 1.792$
$H(X,Y) = 1.792$
$I(X,Y) = 1.792$

1/24	1/24				
1/24	1/24	1/24	1/48		
	1/24	1/6	1/24	1/48	
	1/48	1/24	1/6	1/24	
		1/48	1/24	1/24	1/24
				1/24	1/24

$H(X) = H(Y) = 1.683$
$H(X,Y) = 2.774$
$I(X,Y) = 0.593$

					1/12
1/8			1/8		
	1/24				
5/24		1/24			
3/24				1/24	
3/24	1/24	1/24			

$H(X) = 1.658$
$H(Y) = 1.328$
$I(X,Y) = 0.750$

FIGURE 15.37: Examples of Shannon entropy calculation

	y_1	y_2	y_3	y_4	y_5
s_1	10	9			
s_2	7	9			
s_3	3		7	2	
s_4		2	10	4	5
s_5				10	2
s_6			3	4	13

$H(S_1) = 1.767$
$H(Y) = 1.609$
$H(S_1, Y) = 2.614$
$I(S_1, Y) = 0.763$

	y_1	y_2	y_3	y_4	y_5
s_1	7	10			
s_2	10	8			
s_3			5	4	3
s_4	3		10	6	4
s_5	2			5	8
s_6			5	5	5

$H(S_1) = 1.771$
$H(Y) = 1.609$
$H(S_1, Y) = 2.745$
$I(S_1, Y) = 0.636$

FIGURE 15.38: Scorecards S_1 and S_2

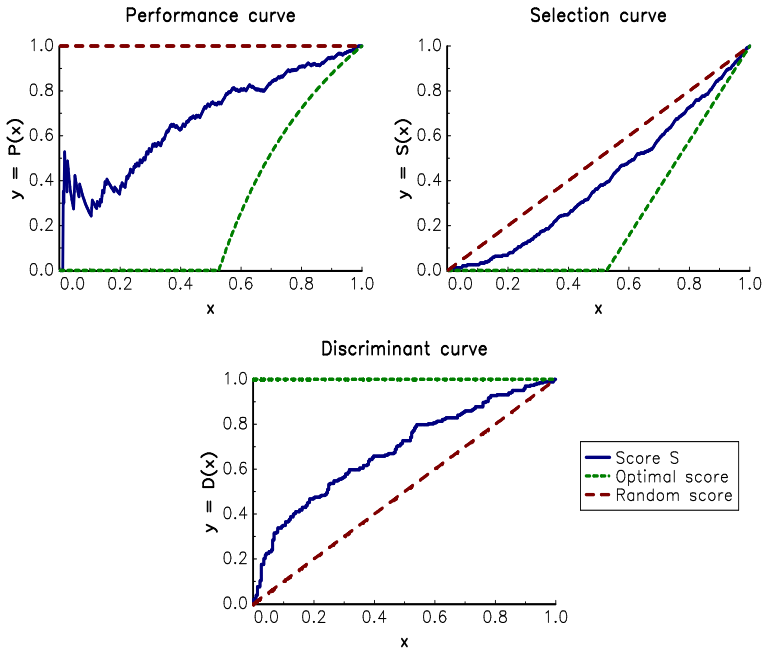

FIGURE 15.39: Performance, selection and discriminant curves

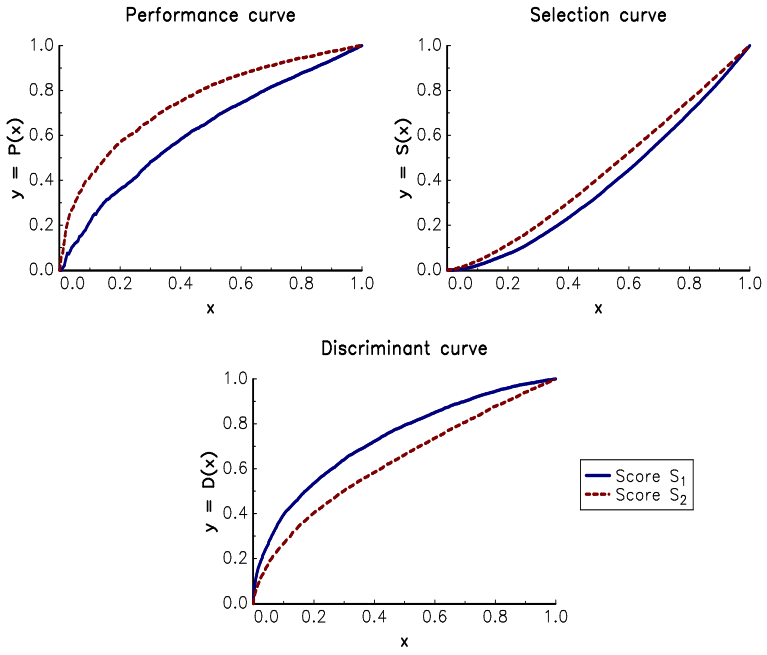

FIGURE 15.40: The score S_1 is better than the score S_2

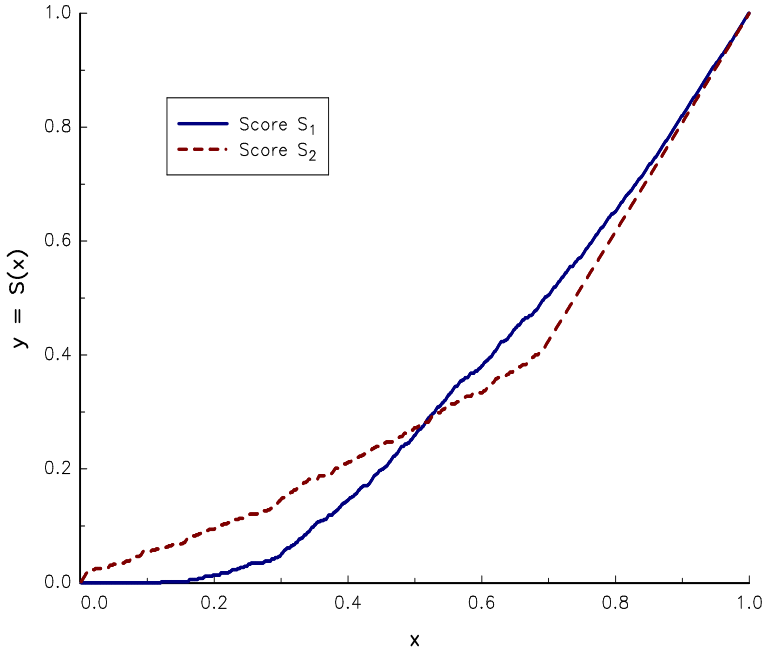

FIGURE 15.41: Illustration of the partial ordering between two scores

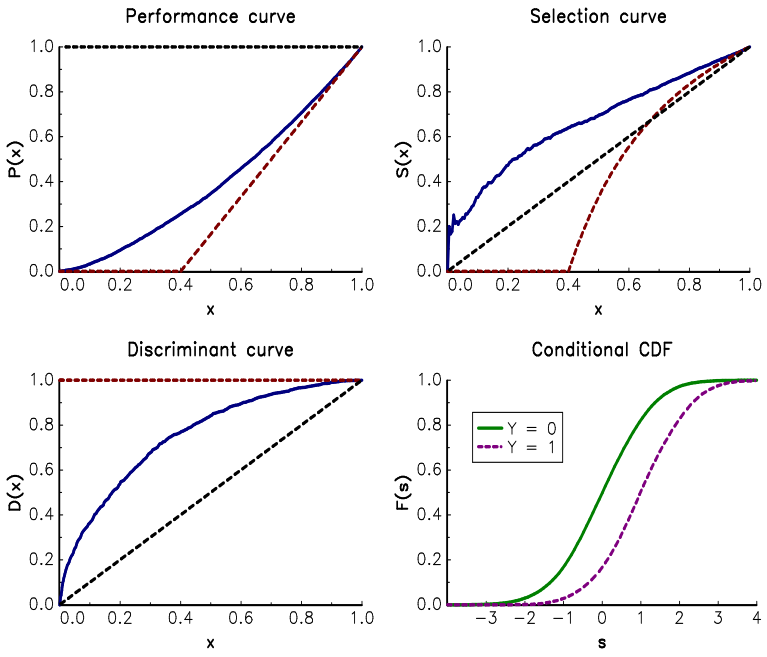

FIGURE 15.42: Comparison of the distributions $\mathbf{F}_0(s)$ and $\mathbf{F}_1(s)$

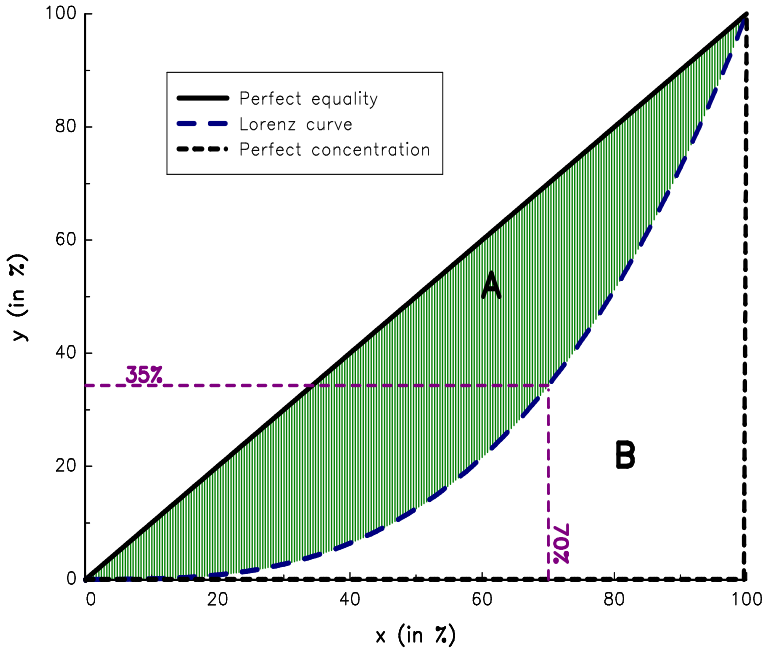

FIGURE 15.43: An example of Lorenz curve

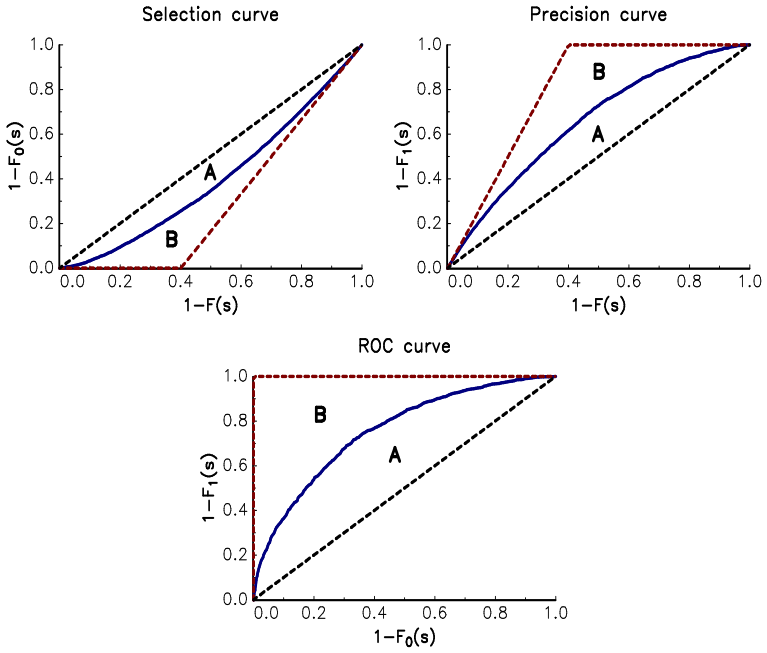

FIGURE 15.44: Selection, precision and ROC curves

Conclusion

Appendix A

Technical Appendix

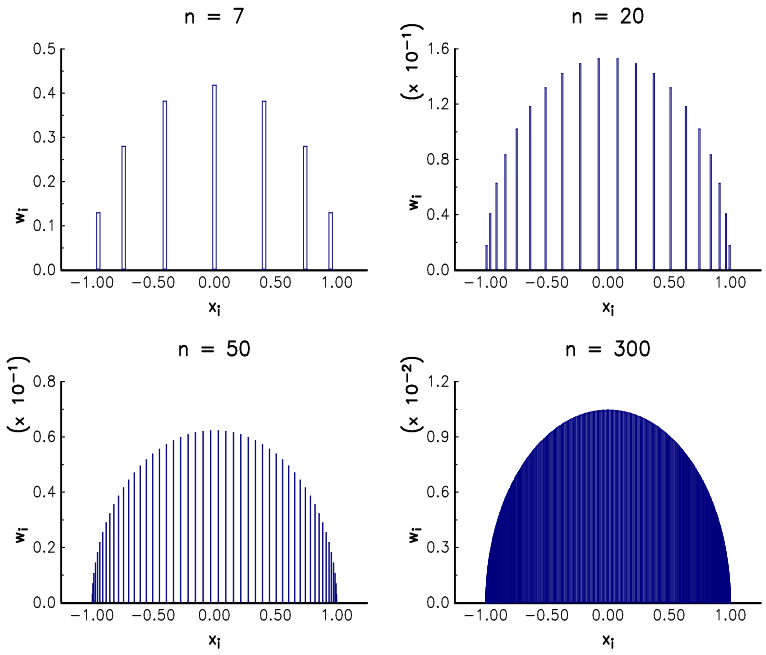

FIGURE A.1: Weights and knots of the Gauss-Legendre quadrature

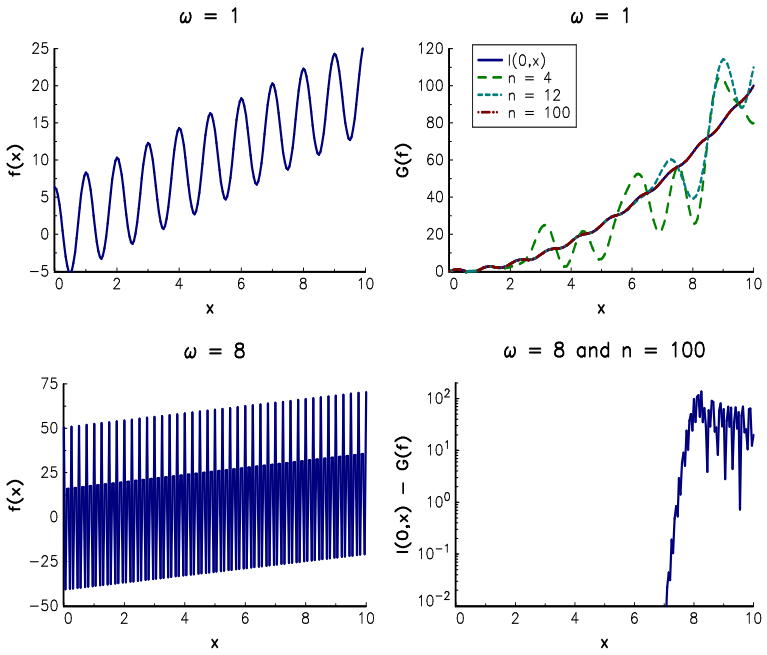

FIGURE A.2: Gauss-Legendre numerical integration

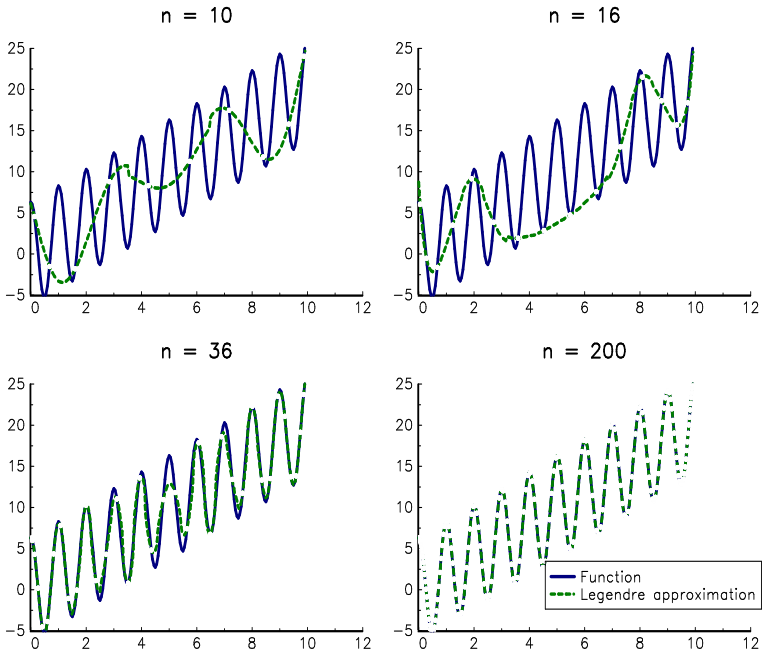

FIGURE A.3: Legendre approximation of $f(x) = 2\pi\cos(2\pi x) + 2x$